



Evaluation of oxidative stress induction in rats following exposure to silver nanorods

Harikiran Lingabathula & Narsimhareddy Yellu

To cite this article: Harikiran Lingabathula & Narsimhareddy Yellu (2017) Evaluation of oxidative stress induction in rats following exposure to silver nanorods, Toxicology Mechanisms and Methods, 27:4, 272-278, DOI: [10.1080/15376516.2016.1274351](https://doi.org/10.1080/15376516.2016.1274351)

To link to this article: <http://dx.doi.org/10.1080/15376516.2016.1274351>



Accepted author version posted online: 28 Dec 2016.
Published online: 25 Jan 2017.



[Submit your article to this journal](#)



Article views: 7



[View related articles](#)



[View Crossmark data](#)

RESEARCH ARTICLE

Evaluation of oxidative stress induction in rats following exposure to silver nanorods

Harikiran Lingabathula  and Narsimhareddy Yellu

Department of Pharmacology and Toxicology, University College of Pharmaceutical Sciences, Kakatiya University, Warangal, Telangana, India

ABSTRACT

The study investigated the oxidative stress induction by the 10 and 25 nm silver nanorods (SNRs) following intra-tracheal instillation in rats after 1 day, 1 week, 1 month and 3 months post instillation periods at 1 and 5 mg/kg b.w. doses. The blood was withdrawn by retro orbital plexus method after exposure periods and different oxidative stress markers were estimated. The results showed that the both sizes of SNRs induced increased levels of malondialdehyde (MDA) and depleted glutathione (GSH) levels after 1 day and 1 week post exposure periods. The 10 and 25 nm SNRs at both doses displayed that significantly reduced levels of superoxide dismutase (SOD) and catalase following 1 day and 1 week post exposure periods. Also, the results have shown that decrease in total antioxidant capacity (TAC) of both sizes of SNRs significantly following 1 day and 1 week post exposure periods, indicating the oxidative stress induction by SNRs. In spite, there were no significant changes in oxidative stress markers following 1 month and 3 months post exposure periods may be due to recovery. The increased levels of MDA and decreased levels of GSH, SOD, catalase and TAC activity are strongly associated to ROS production and lipid peroxidation, suggesting the induction of oxidative stress in rats. The 10 nm SNRs at 5 mg/kg b.w. dose exposures in rats have shown greater changes in all oxidative stress parameters, indicating the greater induction of oxidative stress when compared with the 25 nm SNRs, representing the size–dose–dependent induction of oxidative stress of SNRs.

ARTICLE HISTORY

Received 5 November 2016
Revised 27 November 2016
Accepted 15 December 2016

KEYWORDS

Lipid peroxidation; oxidative stress; silver nanorods; superoxide dismutase; toxicity

Introduction

Nanomaterials (NMs) are structures that have one of its dimensions should be in the range of 1–100 nm. The production and utilization of NMs were rapidly growing due to its wide range of commercial applications can be attributed to its small size, high specific surface area, attractive physico-chemical properties, high reactivity and unique mechanical properties (Wan-Seob et al., 2009; Yah et al., 2011). These NMs are used in various applications like material engineering, energy production, environment remediation, microelectronics, biosensing and biomedicine (Rosella et al., 2013; Saunders, 2012). Recently, the manufactured NMs are utilized extensively in modern technology, there is a limited availability of data in relation to toxicities concerning to human health and environment (Alicia et al., 2014).

The recent study evaluated the toxicity of gold nanorods following 48 h exposure in human Hep G2 liver cells *in vitro*. Results revealed that the gold nanorods induced cytotoxicity, inflammation and oxidative stress in liver cells *via* decrease in cell viability, increased lactate dehydrogenase (LDH) leakage, depleted glutathione (GSH) levels, and elevated lipid peroxidation, caspase-3 and interleukin-8 levels (Harikiran & Narsimhareddy, 2016). The pulmonary toxicity of magnesium oxide NMs and multi-walled carbon NMs were investigated after intra-tracheal instillation in rats and evaluated

bronchoalveolar lavage fluid tissue damage markers. Alkaline phosphatase and LDH leakage were enhanced at 1 day, 1 week and 1 month post-exposure intervals and also the histological studies of rat lungs revealed the pulmonary toxicity of magnesium oxide and multi-walled carbon NMs (Kiranmai et al., 2013; Reddy et al., 2012).

The silver nanoparticles (SNPs) are having great potentials in future industrial applications (Coradeghini et al., 2013). SNPs are utilized in medical devices, surgical instruments, biosensors, textiles, refrigerators, cosmetics, deodorants and packaging materials for food (Chen & Schluesener, 2008; Marin et al., 2015; Wijnhoven et al., 2009). The silver nanorods (SNRs) are finding applications in different areas such as textile, painting and food industries, cosmetics, sunscreens, bio-sensing, antimicrobial activities, medical devices and imaging applications (Animesh et al., 2013; Dubas & Pimpan, 2008; Maqusood et al., 2010). Recently, SNRs also having great potentials in the determination of trace chloropropanol (Li et al., 2015) and used as high brightness photocathode material (Subramanian et al., 2013).

Because of these huge applications of SNPs, the occupational exposure for these materials also increased enormously. One of the recent study conducted by Alicia et al. (2014) evaluated the 4.7 and 42 nm SNPs toxicities upon two different cell lines and concluded that the SNPs induced

cytotoxicity *via* reactive oxygen species (ROS) generation, GSH depletion and oxidative stress induction. Recently, some of the studies were conducted on SNPs *in vitro* and *in vivo* and reported the toxicities induced by the SNPs in different human cell lines and animals (Jennifer et al., 2016; Marin et al., 2015; Susann et al., 2013; Xiaomei et al., 2015). Most of the studies evaluated the toxicities of SNPs, but there is a little availability of toxicity data related to SNRs, because the size, shape and surface coating of the SNPs can affect the level of toxicity (Lankveld et al., 2010; Rothen et al., 2010; Sur et al., 2010). Some of the studies evaluated the toxicity of SNRs by using different human cell lines and reported the SNRs induced cytotoxicity towards different cell lines *in vitro* (Favi et al., 2015; Harikiran et al., 2015). The present study goal was to investigate the oxidative stress induction by poly ethylene glycol (PEG) coated, 10 and 25 nm SNRs following intra-tracheal instillation in rats and the results were compared against the control and a positive control, quartz (QTZ).

Materials and methods

Chemicals

The 10 and 25 nm SNRs were purchased from Sigma-Aldrich, St. Louis, MO. QTZ particles (58–68 μm ; 99.95% purity) were procured from Berkely Springs, Morgan County, WV. Phosphate buffer saline (PBS) and PEG were acquired from Himedia, India. All the biochemical assay kits were procured from Cayman Chemicals, Ann Arbor, MI.

Animals and treatment

Male Wistar rats of six-week-old were purchased from Sainath agencies, Hyderabad, India and before starting the experiments kept one week for acclimatization. The rats were housed in polypropylene cages in a room; water and feed were available *ad libitum* with controlled temperature ($25 \pm 2^\circ\text{C}$), humidity ($55 \pm 5\%$) and a 12-h light/dark cycle throughout the acclimatization and experimental periods. The rats, weighed approximately 220 g were selected and randomly divided into seven groups (6 rats in each group). The different groups of rats were exposed with a single dose of 1 mg/kg and 5 mg/kg b.w. of 10 nm SNRs, 25 nm SNRs, QTZ and control (PBS + 1% PEG) by intra-tracheal instillation method as described by Warheit et al. (2007). The experiment was approved by the Animal ethics committee, Kakatiya University.

Collection of blood

The blood was collected from the control, SNRs and QTZ exposed rats by means of retro orbital plexus at 1 day, 1 week, 1 month and 3 months after instillation periods. The serum was obtained by immediate centrifugation of blood samples at 3000 rpm for 10 min at room temperature. The serum was used for the estimation of the oxidative stress parameters using following biochemical assays.

Oxidative stress assessment

Lipid peroxides are unstable indicators of oxidative stress in cells that decompose to generate more complex and reactive compound such as malondialdehyde (MDA), natural byproduct of lipid peroxidation. Thiobarbituric acid reactive substance (TBARS) is a well-established assay for screening and monitoring lipid peroxidation (Anreddy et al., 2010). MDA forms a 1:2 adduct with thiobarbituric acid (TBA). The MDA–TBA complex formed from the reaction of MDA in samples with TBA can be measured colorimetrically. GSH is an important intracellular tripeptide thiol composed of glutamic acid, cysteine and glycine. GSH helps to protect cells from free radical damage through acting as an antioxidant. The GSH assay measuring the total concentration of GSH, which includes both oxidized and reduced GSH. GSH reductase reduces oxidized GSH (GSSG) to reduced GSH. Subsequently, the chromogen reacts with the thiol group of GSH to generate a colored complex that absorbs at 405 nm (Mytilineou et al., 2002).

Superoxide dismutase (SOD) brings about the dismutation of superoxide anion into H_2O_2 and molecular oxygen, is one of the most important antioxidative enzymes (Lepock et al., 1990). Superoxide anions (O_2^-) are generated by a xanthine oxidase system and then detected with a chromagen solution. However, in the presence of SOD, the superoxide anion concentrations are declined, yielding less colorimetric signal (Zelko et al., 2002). Catalase is an antioxidant enzyme, which is present in mammalian and non-mammalian cells that destroy hydrogen peroxide by dismutation (Votyakova & Reynolds, 2004). The method is based on the enzyme with methanol in the presence of hydrogen peroxide and the formaldehyde produced was quantified spectrophotometrically with 4-amino-3-hydrazino-5-mercapto-1,2,4-triazole as the chromogen (Wheeler et al., 1990). All these assays were performed by using respective diagnostic kits as per the manufacturer's protocol.

The TAC was estimated by using a stable free radical 2,2-diphenyl-1-picryl hydrazyl (DPPH), at the concentration of 0.2 mM in methanol. DPPH is a paramagnetic compound having an odd electron. It can accept an electron (or) hydrogen radical to become a stable, diamagnetic molecule. It shows a strong absorption band at 517 nm in methanol and its solution appears in deep violet color (Reddy et al., 2011). Ascorbic acid was used as a reference standard and the TAC was expressed in terms of nM of ascorbic acid.

Statistical analysis

Data were expressed as mean \pm SD (standard deviation). Statistical analysis was performed for all the biochemical assays using ANOVA followed by Bonferroni posttests and the statistical significances were indicated by $\$p < .05$, $\#p < .01$, $*p < .001$ versus control (PBS + 1% PEG).

Results

The MDA levels were increased following intra-tracheal instillation of SNRs, QTZ and control treated rats at 1 day and

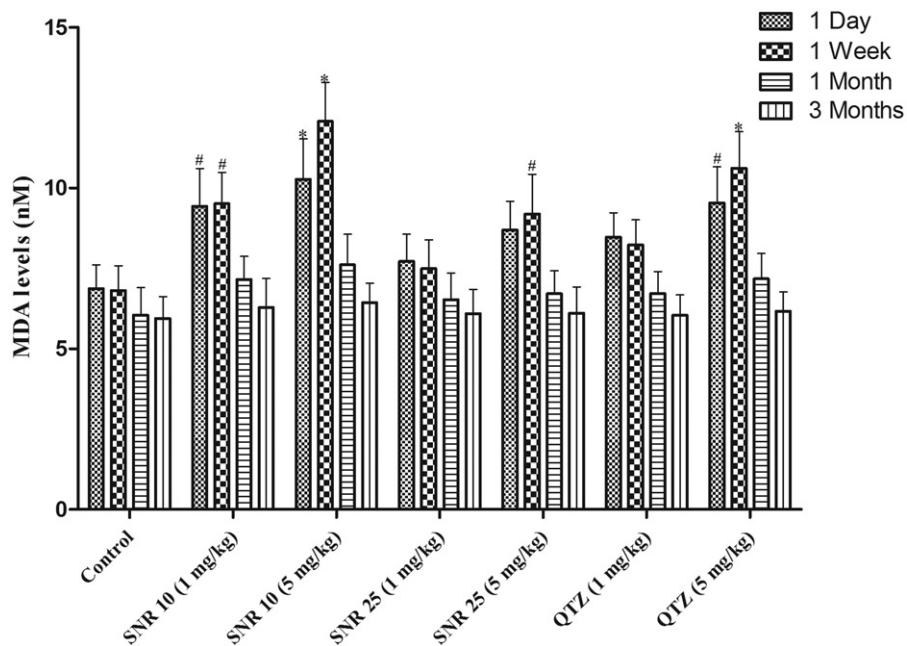


Figure 1. MDA levels (nM) following intra-tracheal instillation of SNRs in rats; Data were expressed as mean \pm SD ($n=6$); $\$p < .05$, $\#p < .01$, $*p < .001$ versus control treated rats.

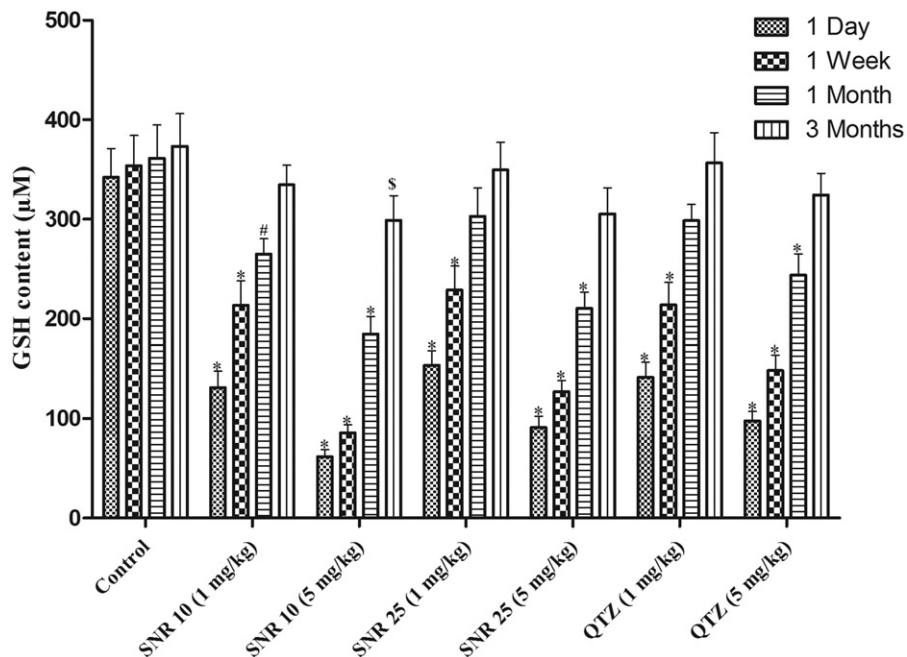


Figure 2. GSH levels (μM) following intra-tracheal instillation of SNRs in rats; Data were expressed as mean \pm SD ($n=6$); $\$p < .05$, $\#p < .01$, $*p < .001$ versus control treated rats.

1 week post exposure periods (Figure 1), indicating lipid peroxidation. The 10 nm SNRs have shown significant elevated lipid peroxidation following 1 day and 1 week post exposure periods at 1 mg/kg ($p < .01$) and 5 mg/kg ($p < .001$) b.w. doses. The 25 nm SNRs at 5 mg/kg b.w. dose significantly increased MDA levels following 1 week ($p < .01$) post exposure period. The 10 nm SNRs have shown significant depleted GSH levels following 1 day ($p < .001$), 1 week ($p < .001$) and 1 month ($p < .05$) post exposure periods at 1 mg/kg and 5 mg/kg b.w. doses versus control treated rats, whereas the 25 nm SNRs at 5 mg/kg b.w. dose only

significantly decreased the GSH content following 1 day ($p < .001$), 1 week ($p < .001$) and 1 month ($p < .01$) post exposure periods (Figure 2).

The SOD levels in rat blood following exposure of SNRs, QTZ and control were estimated at 1 day, 1 week, 1 month and 3 months post exposure periods were presented in Figure 3. The 10 and 25 nm SNRs at 5 mg/kg dose significantly ($p < .001$) depleted the SOD levels following 1 day and 1 week post exposure periods compared with control treated rats. The 10 nm SNRs at both doses and 25 nm SNRs at 5 mg/kg dose have shown significantly ($p < .001$) decreased levels

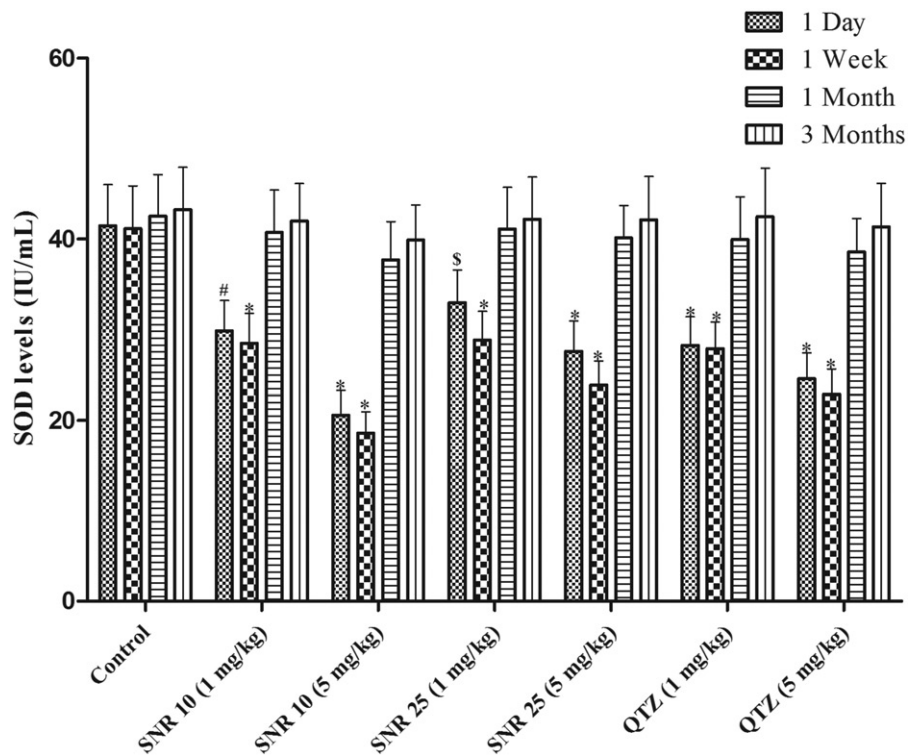


Figure 3. SOD levels (IU/mL) following intra-tracheal instillation of SNRs in rats; Data were expressed as mean \pm SD ($n = 6$); $\$p < .05$, $\#p < .01$, $*p < .001$ versus control treated rats.

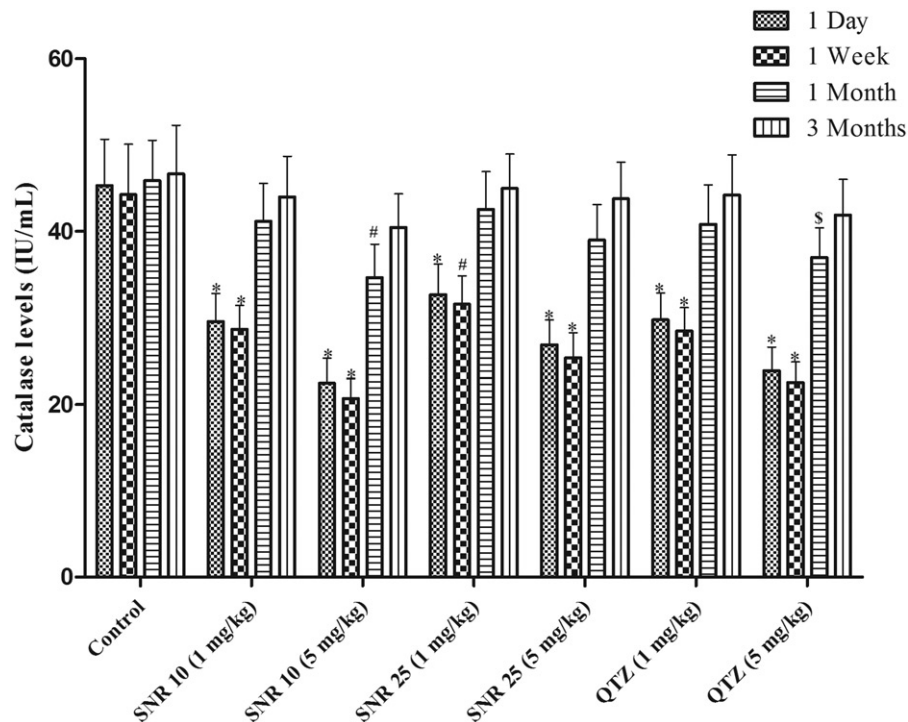


Figure 4. Catalase levels (IU/mL) following intra-tracheal instillation of SNRs in rats; Data were expressed as mean \pm SD ($n = 6$); $\$p < .05$, $\#p < .01$, $*p < .001$ versus control treated rats.

of catalase following 1 day and 1 week post exposure periods. The 10 nm SNRs at 5 mg/kg dose ($p < .01$) decreased the catalase levels following 1 month post exposure also. The 25 nm SNRs at 1 mg/kg dose has displayed decreased catalase levels following 1 day ($p < .001$) and 1 week ($p < .01$) post exposure periods (Figure 4).

The TAC levels in rat serum upon intra-tracheal instillation of SNRs, QTZ and control were estimated at 1 day, 1 week, 1 month and 3 months post exposure periods were presented in Figure 5. The 10 nm SNRs have displayed significantly decreased levels of TAC following 1 day and 1 week post exposure periods ($p < .001$) at both doses whereas at

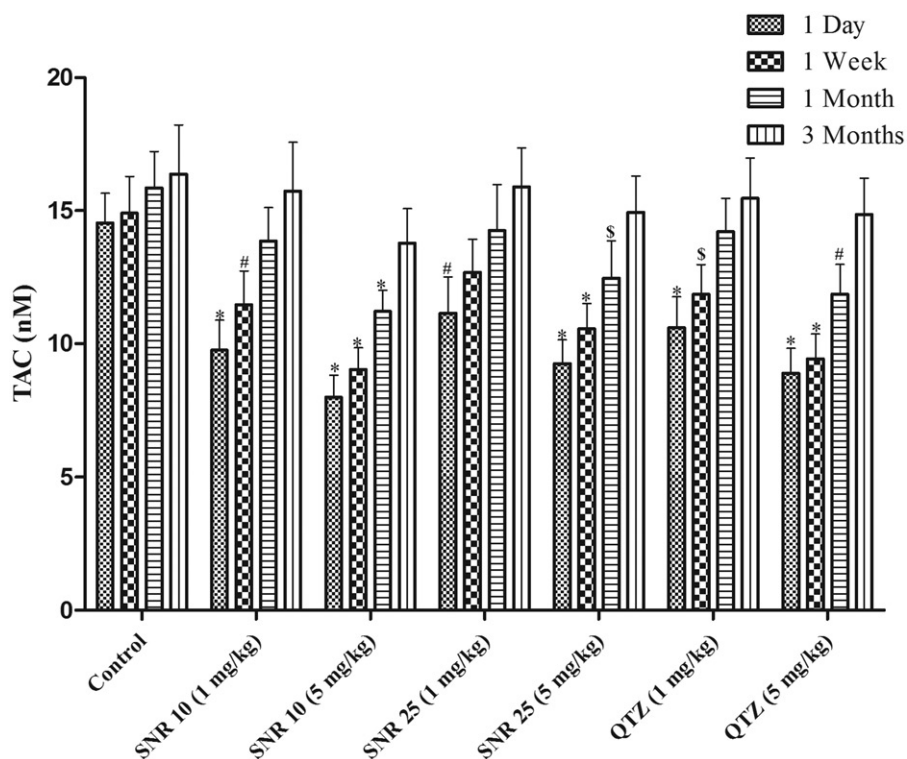


Figure 5. TAC (nM) following intra-tracheal instillation of SNRs in rats; Data were expressed as mean \pm SD ($n = 6$); \$ $p < .05$, # $p < .01$, * $p < .001$ versus control treated rats.

5 mg/kg dose has shown significantly decreased TAC levels following 1 month post exposure ($p < .001$). 25 nm SNRs have shown decreased levels of TAC following 1 day ($p < .001$), 1 week ($p < .001$) and 1 month ($p < .05$) post exposure periods at 5 mg/kg dose.

Discussion

The present investigation was to assess the oxidative stress and total antioxidant capacity (TAC) of 10 nm and 25 nm SNRs, QTZ and control (PBS +1% PEG) at 1 and 5 mg/kg b.w. doses following intra-tracheal instillation in rats using estimation of oxidative stress parameters such as MDA, GSH, SOD, catalase and TAC after 1 day, 1 week, 1 month and 3 months post exposure periods. Most of the previous investigations were suggested that the toxicity of NPs was mainly due to production of ROS and induction of oxidative stress (Alexandra et al., 2012; Abudayyak et al., 2016; Pengjuan et al., 2012).

One of the recent study conducted by Alicia et al. (2014) evaluated the 4.7 and 42 nm SNPs toxicities upon two different cell lines and concluded that the SNPs induced cytotoxicity via ROS generation, GSH depletion and oxidative stress induction. Igor et al. (2011) investigated the oxidative stress induced by different metallic NPs such as CdS and ZnO on human kidney cells (Glomerular and tubular). CdS and ZnO NPs significantly increased the cell mortality, generation of ROS and intracellular levels of GSH revealed that NPs induced stress. Generation of ROS and induction of oxidative stress clearly proposed that the metal NPs nephrotoxic potential. The previous studies were conducted mainly by using human

cells *in vitro* and no clear guidelines were available for toxicity testing of these NPs. We have made an attempt to evaluate the oxidative stress induction, *in vivo* in rats following exposure of SNRs.

The present investigation results were displayed that the intra-tracheal instillation of both sizes of SNRs revealed increased levels of MDA and depleted blood GSH levels following 1 day and 1 week post exposure periods at 5 mg/kg b.w. dose. In contrast, there were little or no increased levels of MDA and decreased levels of GSH were detected at 1 month and 3 months post exposure periods. The 10 nm SNRs at 1 mg/kg b.w. dose also displayed significant increased lipid peroxidation and depleted GSH content, whereas 25 nm SNRs were not significantly, representing the size-dependent toxicity.

Induction of oxidative stress can be expressed in terms of GSH estimation and is an important antioxidant that is oxidized during oxidative stress (Marquis et al., 2009). ROS production and subsequent oxidative stress induction was manifested by increased levels of MDA and reduction in GSH content. The SNRs might have resulted in ROS generation and oxidative stress induction via elevated MDA levels and depleted GSH content following instillation after 1 day and 1 week post exposure periods. Recently, Porntipa et al. (2013) examined the *in vitro* toxicity of SNPs in relation to the generation of ROS in A549 lung cells. SNPs exposure results in ROS formation, reduction in mitochondrial membrane potential, S phase arrest and increase in the proportion of cells in the sub-G1 (apoptosis) population in a concentration-time-dependent fashion. The study was supported our results related to ROS generation and subsequent induction of oxidative stress by SNRs.

Our results pertaining to enzymatic oxidative stress markers in rat blood after intra-tracheal instillation of both sizes of SNRs at 1 mg/kg and 5 mg/kg b.w. doses displayed that significantly decreased levels of SOD and catalase following 1 day and 1 week post exposure periods. Whereas, there was no significant fall in these enzymatic oxidative stress markers following 1 month and 3 months post exposure periods may be due to recovery. SOD is one of the most important anti-oxidative enzymes (Valentine & Hart, 2003). Catalase is one of the major antioxidant enzymes that destroy hydrogen peroxide by dismutation (Votyakova & Reynolds, 2004; Zhang et al., 2001). It is noticeable from the results of present investigation is that inhibition of SOD and catalase activity may increase the SNRs induced oxidative stress.

The TAC of test SNRs was determined by using a stable free radical, DPPH, as TAC is based on the decrease in absorbance of the free radical in the presence of antioxidants. The results have shown that decrease in TAC of both sizes of SNRs significantly following 1 day and 1 week post exposure periods in rats, indicating the oxidative stress induction by SNRs. The findings were revealed significantly decreased TAC of SNRs at 5 mg/kg dose following 1 month post exposure period. The oxidative stress induction was followed a dose-dependent fashion.

Reddy et al. (2011) assessed the oxidative stress and total antioxidant status following intra-tracheal instillation of multi-wall carbon nanotubes in rats at a dose of 0.2, 1 and 5 mg/kg b.w. Following instillation, the blood samples were collected at 1 day, 1 week, 1 month and 3 months post instillation of nanotubes and different parameters were estimated to assess the oxidative stress. Instillation of nanotubes in rats produced a significant dose dependent decrease of total antioxidant status, GSH, SOD, catalase activity and increased MDA levels than control group. Kiranmai & Reddy (2013) evaluated antioxidant status following intra-tracheal instillation of MgO NPs at a dose of 1 and 5 mg/kg of b.w. in rats and the blood samples were collected at 1 day, 1 week and 1 month post instillation periods. Intra-tracheal instillation of MgO NPs produced a significant dose-dependent decrease in blood TAC, SOD and catalase levels.

Similar to the above studies, our investigation has shown the elevated levels of MDA and depletion of GSH, SOD, catalase and TAC activity are strongly associated with ROS production and lipid peroxidation, demonstrating the induction of oxidative stress in rats following instillation of SNRs. The reduction in the antioxidant capacity in SNRs instilled rats shows the reduction in antioxidant defense mechanisms. The results propose possible occupational health risk in chronic exposures of SNRs.

The intra-tracheal instillation of 10 nm SNRs in rats has shown greater elevated levels of lipid peroxidation and depletion of GSH, SOD, catalase and TAC activity, indicating the greater induction of oxidative stress when compared with the 25 nm SNRs, representing the size-dependent induction of oxidative stress of SNRs.

Some of the previous studies also conducted experiments on size-dependent toxicity of SNPs and suggesting the size based toxicity. One of such type of investigation conducted by Soderstjerna et al. (2014) on 20 and 80 nm silver and gold

NPs using an *in vitro* tissue culture model of the mouse retina. TEM analysis revealed cellular and nuclear uptake of gold and silver NPs in all neuronal layers of the retina and significantly superior numbers of apoptotic cells as well as an increased number of oxidative stressed cells were found by 20 nm NPs. Andrea et al. (2012) evaluated the effects of 20 and 40 nm SNPs using a mixed primary cell model consisting of neurons, astrocytes and a minor proportion of oligodendrocytes. Both SNPs have shown size-dependent cytotoxicity, generation of ROS and acute calcium response, indicating oxidative stress. Rona et al. (2014) evaluated the toxic effects of 10, 20, 40, 60 and 100 nm SNPs by treating with the human LoVo cell line, an intestinal epithelium model. The cellular uptake by confocal laser scanning microscopy and various cytotoxicity parameters were displayed size-dose-dependent toxicity.

Conclusions

The intra-tracheal instillation of 10 and 25 nm SNRs in rats results in elevated levels of lipid peroxidation and depleted levels of GSH, SOD, catalase and TAC, indicating oxidative stress induction by the test SNRs. Finally, the SNRs induced dose-size-dependent oxidative stress following intra-tracheal instillation in rats after 1 day and 1 week post exposure periods.

Acknowledgments

The first author is grateful to University Grants Commission-Basic scientific research (UGC-BSR), New Delhi, India for providing fellowship under Research Fellowship in Science for Meritorious Students (RFSMS).

Disclosure statement

The authors report no conflicts of interest.

ORCID

Harikiran Lingabathula  <http://orcid.org/0000-0001-9990-4656>

References

- Abudayyak M, Oztas E, Arici M, Gul O. (2016). *In vitro* toxicological assessment of magnesium oxide nanoparticle exposure in several mammalian cell types. *Int J Toxicol* 35:429–37.
- Alexandra J, Dieter GW, Ludwig J, Ralf K. (2012). Oxidative stress-induced cytotoxic and genotoxic effects of nano-sized titanium dioxide particles in human HaCaT keratinocytes. *Toxicology* 296:27–36.
- Alicia A, Ana IH, Diego M, Paloma M. (2014). Cytotoxicity and ROS production of manufactured silver nanoparticles of different sizes in hepatoma and leukemia cells. *J Appl Toxicol* 34:413–23.
- Andrea H, Stephanie R, Alexandre M, et al. (2012). Effects of silver nanoparticles on primary mixed neural cell cultures: uptake, oxidative stress and acute calcium responses. *Toxicol Sci* 126:457–68.
- Animesh KO, Stefan F, Sumeet K, et al. (2013). Synthesis of well-dispersed silver nanorods of different aspect ratios and their antimicrobial properties against gram positive and negative bacterial strains. *J Nanobiotechnol* 11:42.

- Anreddy RNR, Yellu NR, Devarakonda RK, Vurimindi H. (2010). Multi wall carbon nanotubes induce oxidative stress and cytotoxicity in human embryonic kidney (HEK 293) cells. *Toxicology* 272:11–16.
- Chen X, Schluesener HJ. (2008). Nanosilver: a nanoparticle in medical application. *Toxicol Lett* 176:1–12.
- Coradeghini R, Gioria S, Garcia CP, et al. (2013). Size-dependent toxicity and cell interaction mechanisms of gold nanoparticles on mouse fibroblasts. *Toxicol Lett* 217:205–16.
- Dubas ST, Pimpan V. (2008). Humic acid assisted synthesis of silver nanoparticles and its application to herbicide detection. *Mater Lett* 62:2661–63.
- Favi PM, Valencia MM, Elliott PR, et al. (2015). Shape and surface chemistry effects on the cytotoxicity and cellular uptake of metallic nanorods and nanospheres. *J Biomed Mater Res A* 103:3940–55.
- Harikiran L, Bhikku A, Narsimha RY. (2015). *In vitro* cytotoxicity of gold and silver nanorods using different human cell lines. *Latin Am J Pharm* 34:1277–82.
- Harikiran L, Narsimhareddy Y. (2016). Cytotoxicity, oxidative stress, and inflammation in human Hep G2 liver epithelial cells following exposure to gold nanorods. *Toxicol Mech Methods* 26:340–47.
- Igor P, Isabelle P, Brigitte B, et al. (2011). Cytotoxicity and oxidative stress induced by different metallic nanoparticles on human kidney cells. *Part Fibre Toxicol* 8:10.
- Jennifer M, Jacek Z, Anna L, Maciej W. (2016). Prolonged Effects of Silver Nanoparticles on p53/p21 Pathway-Mediated Proliferation, DNA damage response, and methylation parameters in HT22 hippocampal neuronal cells. *Mol Neurobiol*. doi: 10.1007/s12035-016-9688-6.
- Kiranmai G, Reddy AR. (2013). Antioxidant status in MgO nanoparticle-exposed rats. *Toxicol Ind Health* 29:897–903.
- Kiranmai G, Mahendar P, Rama NRA. (2013). Assessment of pulmonary toxicity of MgO nanoparticles in rats. *Environ Toxicol* 30:308–14.
- Lankveld DP, Oomen AG, Krystek P, et al. (2010). The kinetics of the tissue distribution of silver nanoparticles of different sizes. *Biomaterials* 31:8350–61.
- Lepock JR, Frey HE, Hallewell RA. (1990). Contribution of conformational stability and reversibility of unfolding to the increased thermostability of human and bovine superoxide dismutase mutated at free cysteines. *J Biol Chem* 265:21612–18.
- Li S, Zhi GY, Wen BG, et al. (2015). Silver nanorod array electrodes and their application for detection of low concentration chloropropanol in aqueous media. *Appl Mech Mater* 697:136–39.
- Maqsood A, Mohamad SA, Siddiqui MKJ. (2010). Silver nanoparticle applications and human health. *Clin Chim Acta* 411:1841–48.
- Marin S, Vlasceanu GM, Tiplea RE, et al. (2015). Applications and toxicity of silver nanoparticles: a recent review. *Curr Topics Med Chem* 15:1596–604.
- Marquis BJ, Love SA, Braun KL, Haynes CL. (2009). Analytical methods to assess nanoparticle toxicity. *Analyst* 134:425–39.
- Mytilineou C, Kramer BC, Yabut JA. (2002). Glutathione depletion and oxidative stress. *Parkinsonism Relat Disord* 8:385–87.
- Pengjuan X, Jing X, Shichang L, Zhuo Y. (2012). Nano copper induced apoptosis in podocytes via increasing oxidative stress. *J Hazard Mater* 241:279–86.
- Porntipa C, Somsong L, Sittiruk R, et al. (2013). Silver nanoparticles induce toxicity in A549 cells via ROS-dependent and ROS-independent pathways. *Toxicol in Vitro* 27:330–38.
- Reddy AR, Rao MV, Krishna DR, et al. (2011). Evaluation of oxidative stress and antioxidant status in rat serum following exposure of carbon nanotubes. *Regul Toxicol Pharmacol* 59:251–57.
- Reddy AR, Reddy YN, Krishna DR, Himabindu V. (2012). Pulmonary toxicity assessment of multiwalled carbon nanotubes in rats following intratracheal instillation. *Environ Toxicol* 27:211–19.
- Rona M, Rita R, Madeleine R, et al. (2014). Exposure to silver nanoparticles induces size- and dose-dependent oxidative stress and cytotoxicity in human colon carcinoma cells. *Toxicol in Vitro* 28:1280–9.
- Rosella C, Sabrina G, Cesar PG, et al. (2013). Size-dependent toxicity and cell interaction mechanisms of gold nanoparticles on mouse fibroblasts. *Toxicol Lett* 217:205–16.
- Rothen RB, Brown DM, Piallier-Boyles M, et al. (2010). Relating the physicochemical characteristics and dispersion of multiwalled carbon nanotubes in different suspension media to their oxidative reactivity *in vitro* and inflammation *in vivo*. *Nanotoxicology* 4:331–42.
- Saunders BR. (2012). Hybrid polymer/nanoparticle solar cells: preparation, principles and challenges. *J Colloid Interface Sci* 369:1–15.
- Soderstjerna E, Bauer P, Cedervall T, et al. (2014). Silver and gold nanoparticles exposure to *in vitro* cultured retina – Studies on nanoparticle internalization, apoptosis, oxidative stress, glial- and microglial activity. *Plos One* 9:e105359.
- Subramanian V, Manjula IN, Alan GJ, et al. (2013). Silver nanorod arrays for photocathode applications. *Appl Phys Lett* 103:161112.
- Sur I, Cam D, Kahraman M, Baysal A. (2010). Interaction of multi-functional silver nanoparticles with living cells. *Nanotechnology* 21:175104.
- Susann G, Lars E, Tore S. (2013). Silver nanoparticle-induced cytotoxicity in rat brain endothelial cell culture. *Toxicol in Vitro* 27:305–13.
- Valentine JS, Hart PJ. (2003). Misfolded CuZnSOD and amyotrophic lateral sclerosis. *Proc Natl Acad Sci USA* 100:3617–22.
- Votyakova TV, Reynolds IJ. (2004). Detection of hydrogen peroxide with Amplex Red: interference by NADH and reduced glutathione auto-oxidation. *Arch Biochem Biophys* 431:138–44.
- Wan-Seob C, Minjung C, Jinyoung J, et al. (2009). Acute toxicity and pharmacokinetics of 13 nm-sized PEG-coated gold nanoparticles. *Toxicol Appl Pharmacol* 236:16–24.
- Warheit DB, Webb TR, Reed KL, et al. (2007). Pulmonary toxicity study in rats with three forms of ultrafine- TiO₂ particles: differential responses related to surface properties. *Toxicology* 230:90–104.
- Wheeler CR, Salzman JA, Elsayed NM, et al. (1990). Automated assays for superoxide dismutase, catalase, glutathione peroxidase, and glutathione reductase activity. *Anal Biochem* 184:193–99.
- Wijnhoven SWP, Peijnenburg WJGM, Herberths CA, et al. (2009). Nano-silver – a review of available data and knowledge gaps in human and environmental risk assessment. *Nanotoxicology* 3:109–38.
- Xiaomei L, Kristin S, Laetitia B, et al. (2015). Silver nanoparticle toxicity and association with the alga *Euglena gracilis*. *Environ Sci Nano* 2:594–602.
- Yah CS, Iyuke SE, Simate GS, et al. (2011). Continuous synthesis of multi-walled carbon nanotubes from xylene using the swirled floating catalyst chemical vapor deposition technique. *J Mater Res* 26:623–32.
- Zelko IN, Mariani TJ, Folz RJ. (2002). Superoxide dismutase multigene family: a comparison of the CuZn-SOD (SOD1), Mn-SOD (SOD2), and EC-SOD (SOD3) gene structures, evolution, and expression. *Free Radic Biol Med* 33:337–49.
- Zhang J, Johnston G, Stebler B, Keller ET. (2001). Hydrogen peroxide activates NFκB and the interleukin-6 promoter through NFκB-inducing kinase. *Antioxid Redox Signal* 3:493–504.

ASSESSMENT OF EXTRAPULMONARY TOXICITY INDUCED BY CARBON NANOMATERIALS FOLLOWING INTRATRACHEAL INSTILLATION IN RATS

BHIKKU ANGOTH, HARIKIRAN LINGABATHULA, NARSIMHAREDDY YELLU*

Department of Pharmacology and Toxicology, University College of Pharmaceutical Sciences, Kakatiya University, Warangal, Telangana, India. Email: ynrkuc@gmail.com

Received: 18 January 2016, Revised and Accepted: 01 February 2017

ABSTRACT

Objective: Carbon nanomaterials (CNMs) such as carbon nanofibres (CNFs), multi-wall carbon nanotubes (MWCNTs), and carbon nanorods (CNRs) were found various industrial and commercial applications. The occupational exposure for these CNMs was also increased enormously. This study evaluated the extrapulmonary toxicity induced by these CNMs.

Methods: The extrapulmonary toxicity was assessed following intratracheal instillation of test CNMs in rats after 1 day, 1 week, 1 month, and 3 months postexposure periods using serum biochemical parameters such as alanine transaminase (ALT) and creatinine using diagnostic assay kits. Further, the histopathological analysis was performed for liver and kidneys of particle exposed rats.

Results: The results have displayed that increased levels of serum ALT and creatinine were found after 1 day, 1 week, and 1 month postexposure periods indicating liver and kidney toxicity, respectively. This toxicity was further confirmed by the changes observed in the histopathological analysis of rat liver and kidneys.

Conclusion: The CNFs, MWCNTs, and CNRs able to translocate from the lungs into other extrapulmonary organs such as liver and kidney, and also cause dose-dependent toxicity to them.

Keywords: Alanine transaminase, Carbon nanomaterials, Creatinine, Toxicity.

© 2017 The Authors. Published by Innovare Academic Sciences Pvt Ltd. This is an open access article under the CC BY license (<http://creativecommons.org/licenses/by/4.0/>) DOI: <http://dx.doi.org/10.22159/ajpcr.2017.v10i5.17152>

INTRODUCTION

Carbon nanomaterials (CNMs) are a new form of crystalline carbon currently attracting intense research efforts because of their unique properties that make them suitable, as such or after modification, for many industrial developments such as in high strength materials, electronics or biomedical applications [1]. With the widespread development of commercial CNMs manufacturing and commercial application, CNMs such as multi-wall carbon nanotubes (MWCNTs), carbon nanofibers (CNF), and carbon nanorods (CNRs) are an important category of nanoparticle for health risk assessment. There is a need to address the associated bioactivity of these newly manufactured nanomaterials [2,3].

Pulmonary retention and extrapulmonary redistribution of inhaled nanoparticles have been considered to be important contributing factors of cardiorespiratory diseases. Varying the characteristics of carbon nanoparticles, such as size, surface charge, attachment of ligands, or surfactant coatings, offers the possibility for site-specific targeting of different regions of the gastro-intestinal tract. The fast transit of material through the intestinal tract (on the order of hours), together with the continuous renewal of epithelium, led to the hypothesis that nanomaterials will not remain there for indefinite periods [4].

The ingested nanoparticles have eliminated rapidly: 98% in the feces within 48 hours and most of the remainder via urine [3]. However, other studies indicate that certain nanoparticles can translocate to blood, spleen, liver, bone marrow, lymph nodes, kidneys, lungs, brain and can also be found in the stomach and small intestine. Oral uptake of polystyrene spheres of various sizes (50 nm-3 µm) by rats resulted in a systemic distribution to liver, spleen, blood, and bone marrow [5].

Recently, some investigations were evaluated the *in vitro* toxicity of different nanoparticles in human cell lines through various biomarkers and reported the cytotoxicity and oxidative stress induction [6-8]. Initial studies focused on the respiratory effects of pulmonary exposure of various nanoparticles but were limited by the lack of knowledge concerning the extra-pulmonary toxicity [9-11]. Some nanoparticles characterized by their ability to translocate, from their site of deposition in the lungs to the blood and the brain [12,13]. In this study, we have evaluated the ability of the MWCNTs, CNFs, and CNRs to translocate into extra-pulmonary organs like liver and kidney, and also evaluated the extrapulmonary toxicity of these CNMs in rats following intratracheal instillation.

METHODS

The MWCNTs, CNFs, and CNRs were purchased from Sigma-Aldrich, USA. Quartz powder (QZ) and carbonyl iron (CI) were obtained from S.D. Fine chemicals, India. Phosphate buffer saline (PBS) and Tween 80 were procured from HiMedia Laboratories Ltd., Mumbai. Serum alanine transaminase (ALT) and serum creatinine assay kits were purchased from Span diagnostics, India.

Experimental animals

Groups of male wistar albino rats (Hyderabad, India) of 6-9 weeks old at study start (mean weights in the range of 220-275 g) were selected and housed in polypropylene cages in a room where the congenial temperature was 26±2°C and 12 hrs light and dark cycles were maintained. The animals were allowed to acclimatize to the environment for 7 days and supplied with a standard pellet diet and water *ad libitum*. All procedures using animals were reviewed and approved by the Institutional Animal Care and Use Committee of Kakatiya University.

Preparation of fine-dust suspensions

Fine particle suspensions of CNMs were prepared with a nontoxic dispersion vehicle for instillation into rat lungs [14,15]. The products are extremely difficult to disperse even in the presence of a dispersing agent. All the CNMs suspensions were prepared in PBS + 1% Tween 80 at a concentration of 10 mg/mL by briefly shearing (2 minutes in a small glass homogenizing tube) and subsequently sonicating (1-2 minutes) the samples. All the samples with different concentrations were re-sonicated on the day of dosing before the instillation.

Intratracheal instillation

The rats were anesthetized with 3-5% isoflurane in a small chamber and individual rats were secured on an inclined plastic platform and anesthetization continued via a small nose cone. The trachea was exposed by a 1 cm incision on the ventral neck skin for instillation of the dust suspension [16]. The intratracheal fast instillation/nebulization procedure for rats was modified to ensure that instilled material was delivered into the lungs of rats with a good distribution [17].

Experimental design

Groups of rats were instilled intratracheally with single dose of 1 mg/kg or 5 mg/kg of CNF, MWCNT, CNR, CI and quartz-crystalline silica particles (QZ). All the particles were prepared in a volume of 1.0% Tween 80 and phosphate-buffered saline and subjected to polytron dispersion [18]. Groups of PBS-Tween, CI, and QZ instilled rats were served as solvent control, negative control, and positive control, respectively.

Collection of blood samples and biochemical analysis

Blood samples were collected from all the group of rats by retro-orbital sinus puncture, under mild ether anesthesia and serum was obtained by immediate centrifugation of blood samples using BIOFUGE cooling centrifuge at 3000 rpm for 10 minutes at room temperature. The blood samples were collected from all the group of rats at 24 hrs, 1 week, 1 month, and 3 months postinstillation intervals and were used to estimate suitable biomarkers (enzyme levels) which represent the organ/tissue toxicity. Evaluation of ALT levels was specifically used to assess the liver toxicity and estimation of serum creatinine levels assesses the renal toxicity. The biochemical assays were performed on serum samples for the estimation of creatinine and ALT using respective diagnostic kit methods.

Histopathological studies of extrapulmonary organs

The extrapulmonary vital organs (liver and kidney) of all the control and particles exposed rats were collected at 24 hrs, 1 week, 1 month and 3 months postinstillation intervals of CNMs. These tissues were used for the histopathological examination to assess the extrapulmonary toxicity of CNMs. The isolated tissues were fixed in 10% v/v neutral buffered formalin and processed using routine histological techniques. The liver and kidney tissues were embedded in paraffin and stained using hematoxylin and eosin (H and E) dyes for histopathological evaluations.

Statistical analysis

All the experimental values were expressed as mean±standard deviation and were compared with control value at each time point. One-way analysis of variance and Dunnett test were used to compare means

Table 1: Serum ALT levels (IU/L) in rats exposed to CNFs, MWCNTs and CNRs

Group	Postinstillation period			
	1 day	1 week	1 month	3 months
PBS+1% Tween 80	29.54±2.12	29.20±0.80	27.60±2.30	26.30±1.23
CI 1 mg/kg	29.92±1.90	30.18±1.23	30.34±3.01	30.09±2.15
CI 5 mg/kg	31.21±2.36	31.84±2.12	31.55±2.18	31.37±3.12
CNFs 1 mg/kg	38.58±4.12*	44.32±4.50**	52.49±4.23***	46.76±3.56*
CNFs 5 mg/kg	45.15±4.92**	50.54±4.30**	59.97±4.56***	53.18±4.23**
MWCNTs 1 mg/kg	36.33±3.12*	41.15±3.58**	49.36±3.96**	44.72±2.36*
MWCNTs 5 mg/kg	42.64±4.12*	47.54±3.26**	55.25±4.78***	51.67±2.47**
CNRs 1 mg/kg	34.13±1.23*	38.28±3.56*	41.47±3.45**	40.61±3.78*
CNRs 5 mg/kg	39.62±2.50*	43.41±3.60**	49.18±3.56**	47.55±3.60**
QZ 1 mg/kg	33.24±3.45*	39.53±3.12*	41.83±3.48**	41.29±2.96*
QZ 5 mg/kg	38.78±4.35*	44.12±1.23**	50.74±3.96**	45.90±2.98*

Data were expressed as mean±SD (n=6); Significance was indicated by *p<0.05, **p<0.01, ***p<0.001 versus control treated rats. ALT: Alanine transaminase, BPS: Phosphate buffer saline, CI: Carbonyl iron, CNFs: Carbon nanofibers, MWCNTs: Multi wall carbon nanotubes, CNRs: Carbon nanorods, QZ: Quartz, SD: Standard deviation

Table 2: Serum creatinine levels (mg/dL) in rats exposed to CNFs, MWCNTs and CNRs

Group	Postinstillation period			
	1 day	1 week	1 month	3 months
PBS+1% Tween 80	0.79±0.11	0.79±0.10	0.75±0.23	0.72±0.20
CI 1 mg/kg	0.80±0.17	0.81±0.14	0.88±0.15	0.82±0.19
CI 5 mg/kg	0.82±1.12	0.82±0.18	0.91±0.18	0.84±0.16
CNFs 1 mg/kg	1.04±0.25*	1.08±0.32*	1.29±0.32**	1.03±0.27
CNFs 5 mg/kg	1.29±0.28**	1.41±0.39***	1.32±0.42**	1.12±0.35
MWCNTs 1 mg/kg	1.02±0.16*	1.06±0.25*	1.23±0.32*	1.02±0.29
MWCNTs 5 mg/kg	1.26±0.25**	1.36±0.40**	1.25±0.41**	1.08±0.16
CNRs 1 mg/kg	0.98±0.26	1.01±0.34*	1.12±0.34*	1.04±0.34
CNRs 5 mg/kg	1.23±0.31*	1.31±0.23**	1.23±0.36*	1.04±0.23
QZ 1 mg/kg	0.92±0.19	0.98±0.19	1.11±0.45*	1.07±0.35
QZ 5 mg/kg	1.22±0.23*	1.29±0.36**	1.21±0.39*	1.03±0.26

Data were expressed as mean±SD (n=6); Significance was indicated by *p<0.05, **p<0.01, ***p<0.001 versus control treated rats. BPS: Phosphate buffer saline, CI: Carbonyl iron, CNFs: Carbon nanofibers, MWCNTs: Multi wall carbon nanotubes, CNRs: Carbon nanorods, QZ: Quartz, SD: Standard deviation

from the control group and each of the groups exposed to particulates, and the statistical significance was judged at the 0.05 probability level. Significance was indicated by: * $p < 0.05$, ** $p < 0.01$, *** $p < 0.001$ versus control (n=6).

RESULTS

Similar to the QZ, exposures of CNFs, MWCNTs, and CNRs in rats resulted in a dose-dependent increase in ALT levels at all postexposure periods (Table 1), but the significant ($p < 0.001$) increase in ALT levels were observed with 5 mg/kg doses of all CNMs.

Intratracheal instillation of CNFs, MWCNTs, and CNRs in rats resulted in a dose-dependent increase in creatinine levels at all postexposure periods (Table 2), but the significant ($p < 0.001$) increase in creatinine levels were observed with 5 mg/kg dose at 1 week of postinstillation period of CNFs.

The liver and kidney tissues exposed to various CNMs were isolated at 1 day, 1 week, 1 month, and 3 months postexposure periods and the histopathological changes were presented in Figs. 1 and 4. The rat livers after 1 week and 1 month postinstillation periods have shown congestion of central vein, shrinkage or ballooning of

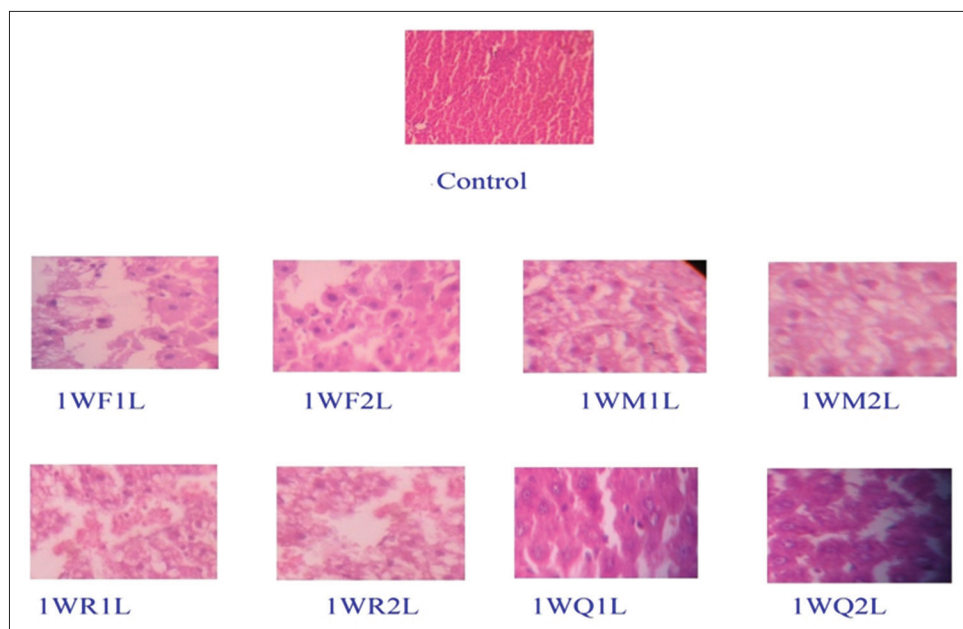


Fig. 1: Light micrograph of rat liver tissue at 1 week postinstillation exposure; control: PBS+1% Tween 80; 1WF1L: CNF (1 mg/kg); 1WF2L: CNF (5 mg/kg); 1WM1L: MWCNT (1 mg/kg); 1WM2L: MWCNT (5 mg/kg); 1WR1L: CNR (1 mg/kg); 1WR2L: CNR (5 mg/kg); 1WQ1L: Quartz (1 mg/kg); 1WQ2L: Quartz (5 mg/kg)

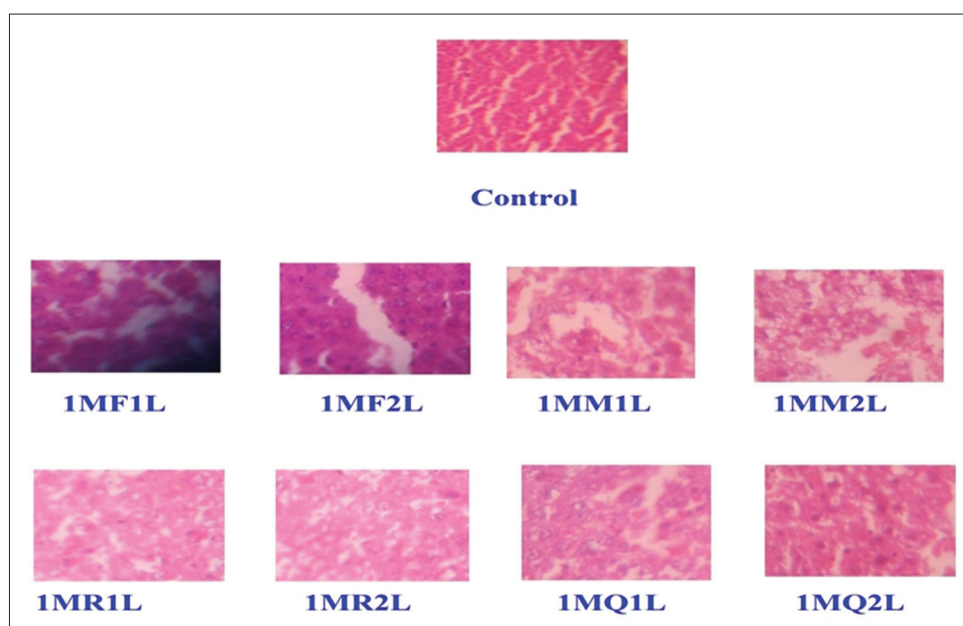


Fig. 2: Light micrograph of rat liver tissue at 1 month postinstillation exposure; control: PBS+1% Tween 80; 1MF1L: CNF (1 mg/kg); 1MF2L: CNF (5 mg/kg); 1MM1L: MWCNT (1 mg/kg); 1MM2L: MWCNT (5 mg/kg); 1MR1L: CNR (1 mg/kg); 1MR2L: CNR (5 mg/kg); 1MQ1L: Quartz (1mg/kg); 1MQ2L: Quartz (5 mg/kg)

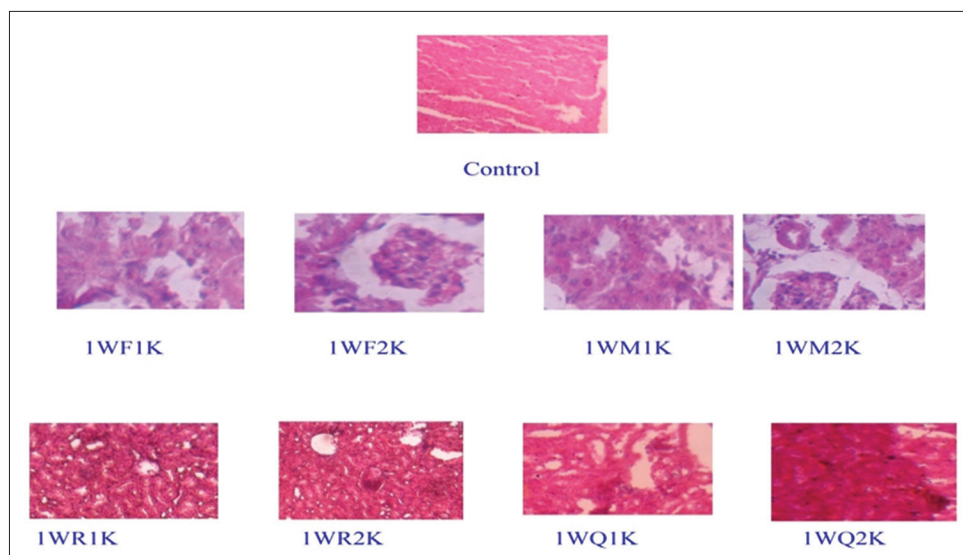


Fig. 3: Light micrograph of rat kidney tissue at 1 week postinstillation exposure; control: PBS+1% Tween 80; 1WF1K: CNF (1 mg/kg), 1WF2K: CNF (5 mg/kg) WM1K: MWCNT (1 mg/kg); 1WM2K: MWCNT (5 mg/kg); 1WR1K: CNR (1 mg/kg); 1WR2K: CNR (5 mg/kg); 1WQ1K: Quartz (1 mg/kg); 1WQ2K: Quartz (5 mg/kg)

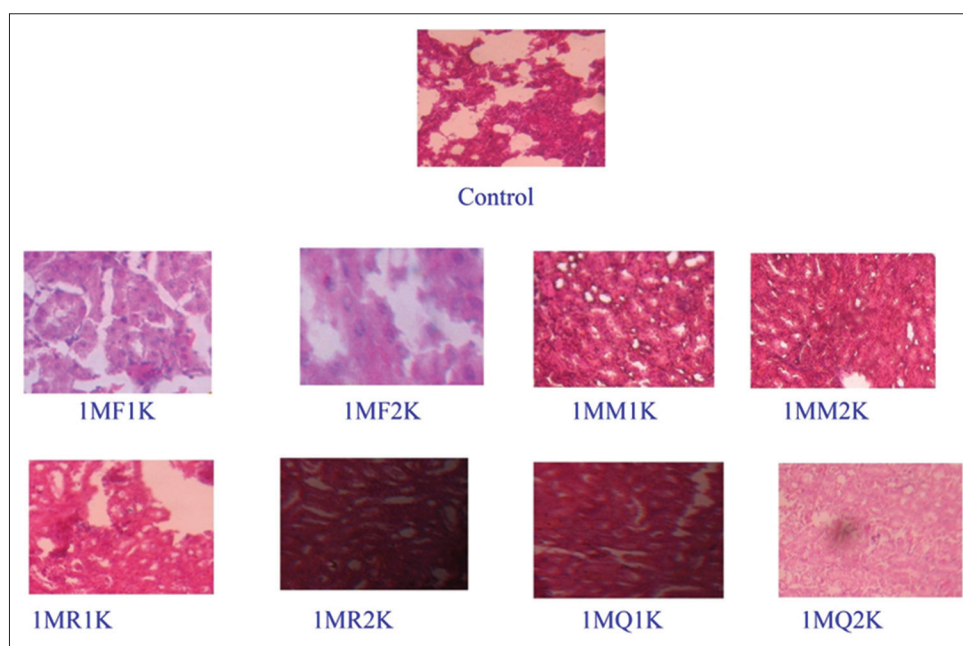


Fig. 4: Light micrograph of rat kidney tissue at 1 month postinstillation exposure; control: PBS+1% Tween 80; 1MF1K: CNF (1 mg/kg); 1MF2K: CNF (5 mg/kg); 1MM1K: MWCNT (1 mg/kg); 1MM2K: MWCNT (5 mg/kg); 1MR1K: CNR (1 mg/kg); 1MR2K: CNR (5 mg/kg); 1MQ1K: Quartz (1 mg/kg); 1MQ2K: Quartz (5 mg/kg)

hepatocytes, necrosis, and degeneration with fat globules. There were no remarkable changes in liver tissue during 1 day and 3 months postexposure periods.

The histology of rat kidneys after 1 week and 1 month postexposure was displayed tubular dilation, increased inflammatory infiltrates, thinned outer cortex, focal areas showing necrosis and degeneration. There were no remarkable changes were found in the kidneys after 1 day and 3 months postexposure periods.

DISCUSSION

This study investigated the ability of the different types of carbon nanoparticles to translocate into extrapulmonary organs such as

liver and kidney, and also evaluated the extrapulmonary toxicity in rats following intratracheal instillation of CNMs. Exposure of these CNMs at different doses does not produce any mortality in exposed rats. Exposure of QZ and these CNMs produced a dose-dependent periportal lymphocytic infiltration, congestion of sinusoids, ballooning, foamy degeneration of hepatocytes, fatty changes and finally focal inflammation and necrosis at 1 week and 1 month postinstillation periods. However, the significant tubular necrosis and interstitial nephritis take place with a dose of 5 mg/kg at 1 week of postinstillation of CNFs.

Exposures of these CNMs produced progressive liver and kidney damage which were confirmed by elevated levels of respective

biomarkers of cell injury and inflammation. Analysis of serum for tissue damage biomarkers (serum ALT and creatinine) levels revealed that these enzyme levels in CNMs exposed rats (1 and 5 mg/kg b.w) were significantly higher than control at all the mentioned postexposure periods. The results of this study also showed the greater toxicity of CNFs than MWCNTs and CNRs.

Some of the reported the pulmonary toxicities induced by different CNMs such as single wall carbon nanotubes, MWCNTs and CNFs following intratracheal instillation in rats after 1 day, 1 week, 1 month, and 3 months postexposure periods [19-21]. However, our results suggest the dose-dependent extra-pulmonary (liver and kidney) toxicities of intratracheally instilled CNFs, MWCNTs, and CNRs in rats, which was further confirmed by the histopathological examination of these organs of particle exposed rats. These extrapulmonary toxicities of CNMs might be due to the translocation into the liver and kidneys.

Once the particles have reached pulmonary interstitial sites, uptake into the blood circulation in addition to lymphatic pathways can occur, a pathway that again is dependent on particle size, favoring nanosized particles. Translocation of nanoparticles from the lung to the blood and extrapulmonary organs has been documented for various nanoparticles. For example, 60 minutes after intratracheal instillation of hamsters with nanocolloid albumin labeled with technetium-99m, detectable levels of the labeled nanoparticles were found in the blood, liver, heart, spleen, kidneys, and brain [13]. In this study also, MWCNT translocate mainly into the liver and produces liver toxicity than other extra-pulmonary sites.

Berry *et al.* was the first to describe translocation of nano sized particles across the alveolar epithelium using intratracheal instillations of 30 nm gold particles in rats [22]. Evidence in humans for the translocation of inhaled NSP into the blood circulation is ambiguous, with one study showing rapid appearance in the blood and significant accumulation of label in the liver of humans inhaling 99Tc-labelled 20 nm carbon particles [12], while another study using the same labeled particles reported no such accumulation [23].

Taken together all of the evidence from animal and human studies for alveolar translocation of various nanoparticles, it is likely that this pathway exists in humans as well; however, in addition to particle size, the extent of extrapulmonary translocation is highly dependent on particle surface chemistry, the amount of inhaled nanoparticles and potential degradation by lysosomal enzymes before transport to the lymphatic circulation. Translocation to the blood circulation could provide a mechanism for a direct particle effect on the cardiovascular system as an explanation for epidemiological findings of cardiovascular effects associated with inhaled ambient ultra fine particles [24-26]. All these above studies were supported our results for translocation and extrapulmonary toxicity induced by the test CNMs.

CONCLUSION

In summary, the intratracheal instillation of test CNMs increased the serum ALT and creatinine levels following 1 day, 1 week and 1 month postexposure periods resulting in liver and kidney toxicity, respectively. This further confirmed by histopathological analysis of liver and kidneys. The order of extrapulmonary toxicity induced by the test CNMs was CNFs > MWCNTs > CNRs. Finally, the CNFs, MWCNTs, and CNRs able to translocate from the lungs into other extrapulmonary

organs such as liver and kidney, and also cause dose-dependent toxicity to them.

REFERENCES

1. Prasanta D, Nilimanka D. Carbon nanotubes: It's role in modern health care. *Int J Pharm Pharm Sci* 2013;5(4):9-13.
2. Oberdörster E. Manufactured nanomaterials (fullerenes, C60) induce oxidative stress in the brain of juvenile largemouth bass. *Environ Health Perspect* 2004;112(10):1058-62.
3. Oberdörster G, Oberdörster E, Oberdörster J. Nanotoxicology: An emerging discipline evolving from studies of ultrafine particles. *Environ Health Perspect* 2005;113(7):823-39.
4. Hoet PH, Brüske-Hohlfeld I, Salata OV. Nanoparticles - Known and unknown health risks. *J Nanobiotechnology* 2004;2(1):12.
5. Deloncle R, Guillard O, Huguet F, Clanet F. Modification of the blood-brain barrier through chronic intoxication by aluminum glutamate. Possible role in the etiology of Alzheimer's disease. *Biol Trace Elem Res* 1995;47(1-3):227-33.
6. Lingabathula H, Yellu N. Cytotoxicity, oxidative stress, and inflammation in human Hep G2 liver epithelial cells following exposure to gold nanorods. *Toxicol Mech Methods* 2016;26(5):340-7.
7. Harikiran L, Bhikku A, Narsimha RY. *In vitro* cytotoxicity of gold and silver nanorods using different human cell lines. *Lat Am J Pharm* 2015;34(7):1277-82.
8. Bhikku A, Harikiran L, Durgaiha G, Narsimha RY. Cytotoxicity evaluation of carbon nanomaterials on human cell lines using MTT assay. *Int J Pharm Pharm Sci* 2014;6(10):379-82.
9. Gelli K, Porika M, Anreddy RN. Assessment of pulmonary toxicity of MgO nanoparticles in rats. *Environ Toxicol* 2015;30(3):308-14.
10. Warheit DB, Brock WJ, Lee KP, Webb TR, Reed KL. Comparative pulmonary toxicity inhalation and instillation studies with different TiO2 particle formulations: Impact of surface treatments on particle toxicity. *Toxicol Sci* 2005;88(2):514-24.
11. Warheit DB, Hansen JF, Yuen IS, Kelly DP, Snajdr SI, Hartsky MA. Inhalation of high concentrations of low toxicity dusts in rats results in impaired pulmonary clearance mechanisms and persistent inflammation. *Toxicol Appl Pharmacol* 1997;145(1):10-22.
12. Nemmar A, Hoet PH, Vanquickenborne B, Dinsdale D, Thomeer M, Hoylaerts MF, *et al.* Passage of inhaled particles into the blood circulation in humans. *Circulation* 2002;105(4):411-4.
13. Nemmar A, Vanbilloen H, Hoylaerts MF, Hoet PH, Verbruggen A, Nemery B. Passage of intratracheally instilled ultrafine particles from the lung into the systemic circulation in hamster. *Am J Respir Crit Care Med* 2001;164(9):1665-8.
14. Driscoll KE, Costa DL, Hatch G, Henderson R, Oberdorster G, Salem H, *et al.* Intratracheal instillation as an exposure technique for the evaluation of respiratory tract toxicity: Uses and limitations. *Toxicol Sci* 2000;55(1):24-35.
15. Leong BK, Coombs JK, Sabaitis CP, Rop DA, Aaron CS. Quantitative morphometric analysis of pulmonary deposition of aerosol particles inhaled via intratracheal nebulization, intratracheal instillation or nose-only inhalation in rats. *J Appl Toxicol* 1998;18(2):149-60.
16. Lam CW, James JT, Latch JN. Pulmonary toxicity of simulated lunar and Martian dusts in mice: II. Biomarkers of acute responses after intratracheal instillation. *Inhal Toxicol* 2002;14(9):917-28.
17. Lam CW, James JT, McCluskey R, Hunter RL. Pulmonary toxicity of single-wall carbon nanotubes in mice 7 and 90 days after intratracheal instillation. *Toxicol Sci* 2004;77(1):126-34.
18. Warheit DB, Webb TR, Reed KL, Frerichs S, Sayes CM. Pulmonary toxicity study in rats with three forms of ultrafine-TiO2 particles: Differential responses related to surface properties. *Toxicology* 2007;230(1):90-104.
19. Reddy AR, Reddy YN, Krishna DR, Himabindu V. Pulmonary toxicity assessment of multiwalled carbon nanotubes in rats following intratracheal instillation. *Environ Toxicol* 2012;27(4):211-9.
20. Warheit DB, Laurence BR, Reed KL, Roach DH, Reynolds GA, Webb TR. Comparative pulmonary toxicity assessment of single-wall

- carbon nanotubes in rats. *Toxicol Sci* 2004;77(1):117-25.
21. Hamilton RF Jr, Wu Z, Mitra S, Shaw PK, Holian A. Effect of MWCNT size, carboxylation, and purification on *in vitro* and *in vivo* toxicity, inflammation and lung pathology. *Part Fibre Toxicol* 2013;10(1):57.
 22. Berry JP, Arnoux B, Stanislas G, Galle P, Chretien J. A microanalytic study of particles transport across the alveoli: Role of blood platelets. *Biomedicine* 1977;27(9-10):354-7.
 23. Brown JS, Zeman KL, Bennett WD. Ultrafine particle deposition and clearance in the healthy and obstructed lung. *Am J Respir Crit Care Med* 2002;166(9):1240-7.
 24. Pekkanen J, Peters A, Hoek G, Tiittanen P, Brunekreef B, de Hartog J, et al. Particulate air pollution and risk of ST-segment depression during repeated submaximal exercise tests among subjects with coronary heart disease: The exposure and risk assessment for fine and ultrafine particles in ambient air (ULTRA) study. *Circulation* 2002;106(8):933-8.
 25. Mercer RR, Scabilloni JF, Hubbs AF, Battelli LA, McKinney W, Friend S, et al. Distribution and fibrotic response following inhalation exposure to multi-walled carbon nanotubes. *Part Fibre Toxicol* 2013;10:33.
 26. Mercer RR, Scabilloni JF, Hubbs AF, Wang L, Battelli LA, McKinney W, et al. Extrapulmonary transport of MWCNT following inhalation exposure. *Part Fibre Toxicol* 2013;10:38.



NANO TITANIUM INDUCES CYTOTOXICITY AND OXIDATIVE STRESS IN HUMAN LUNG CELLS

Durgaiah Gandamalla, Harikiran Lingabathula and Narsimhareddy Yellu*

Department of Pharmacology and Toxicology, University College of Pharmaceutical Sciences,
Kakatiya University, Warangal, Telangana, India-506009.

*Corresponding Author Email: ynrucpsc@gmail.com

ABSTRACT

The titanium dioxide nanoparticles (TNP) are widely using in skin care, biosensing and many other commercial applications. TNP, 82% anatase / 18% rutile, with primary average diameter of 22 ± 6 nm (TNP 20), 87 ± 16 nm (TNP100). So TNP 20 and TNP 100 cell-particle interactions with human cells and human exposure risk are gaining much importance due to their extensive pharmaceutical and nanobased applications. The potential high-risk exposure for TNP generally inhalation route was the most considered. So, the present study investigates the *in vitro* cytotoxicity and oxidative stress upon exposure to human lung epithelial cells (A549) using 3-(4, 5-dimethyl thiazol-2-yl)-2, 5-diphenyl tetrazolium bromide (MTT). The oxidative stress bioindicators like lactate dehydrogenase (LDH) leakage, glutathione (GSH), lipid peroxidation (TBARS) levels were estimated. Both the TNP 20 and TNP 100 were decreased the cell viability and caused cell membrane damage via increased LDH in A549 cells for 48 h post exposure. The TNP exposure to lung cells resulted in decreased GSH levels and increased TBARS levels were indication of oxidative stress development. The TNP 20 have shown significant toxicity against all tested oxidative stress parameters when compare to TNP 100 and quartz treated cells. Finally, the results indicating that the tested both the TNP were induced cytotoxicity and oxidative stress in A549 post exposed cells. So, the *in vitro* data could help in risk/hazard assessment of TNP in relevance to human toxicology.

KEY WORDS

TNP 20, TNP 100, MTT Assay, Cytotoxicity, Oxidative Stress

INTRODUCTION

Titanium dioxide nanoparticles (TNP) are used extensively in numerous commercial applications such as sunscreens, pigments, paints, cosmetics, plastics, paper, an anticaking or whitening agent (Wang *et al.*, 2014). As their production volume and multiple applications in various industrial sectors have been raising safety concerns in the present nanoworld (Bhatt and Tripathi, 2011). As of now very few authors have screened the TNP toxicity using human cell line. They include TNP 26 nm induce DNA damage and cell cycle arrest in human alveolar cells, A549 (Kansara *et al.*, 2015).

Rollerova *et al.*, 2015 studied some aspects of toxicity and future developments related to TNP. Harikiran *et*

al., 2015 reported that the gold NP 10, 25 nm sized were produced cytotoxicity and oxidative stress in liver, Hep G2 cells. Short-term exposure to low doses of nanosized TNP and potential modulatory effects on intestinal cells was studied by Ammendolia *et al.*, 2017. Simone *et al.*, 2016 revealed that the bulk and nano titanium induces subtle changes after their exposure to human astrocytes, D384 and skin, HaCaT cells. Role of TNP size, shape and surface area that would affect the toxicity was studied.

The emerging trends of nanotoxicology area in public health and disease from agri-food to nanotherapeutic applications (Banerjee *et al.*, 2016). Indeed, it is important to predict the possible toxicity effects of TNP in human lung cells due to their high-volume

production, wide spread use of applications and high risk of occupational exposure. So, the occupational exposure to TNP was producing unknown health complications in the humans and animals. Due to their nano size, their entry into the lungs via inhalation was much focused in several studies since the last decade (Piperigkou *et al.*, 2016). The TNP interaction with lung tissue (primary target) via inhalation route was studied for possible toxicity effects. The objective of the present study was cell-particles interaction, cytotoxicity and oxidative stress induction using MTT assay and determination of oxidative stress parameters upon post exposure to A549 cells for 48 h with various dose ranges by *in vitro*. To evaluate the potential mechanisms of cytotoxicity, different types of oxidative stress parameters including cell membrane damage (LDH leakage assay), reduced glutathione (GSH assay), lipid peroxidation product (TBARS assay) levels quantitatively determined and were compared to control and NQTZ (positive control) treated cells.

MATERIALS AND METHODS

Test Particles and Chemicals

The test poly ethylene glycol (PEG) coated TNP 20 and TNP 100 were purchased from Sigma Aldrich, USA. Quartz (QTZ) particles (>100 nm; 99.94% purity) were obtained from Berkely Springs, West Virginia, USA. The fetal bovine serum (FBS), Dulbecco's modified eagle's medium (DMEM), 1% L-glutamine, 1% penicillin-streptomycin antibiotic solution, phosphate buffer saline (PBS) and trypsin-EDTA 0.25% were obtained from Himedia, Mumbai, India. The MTT was purchased from Sigma-Aldrich, USA. All the biochemical assay kits were purchased from BioVision, USA.

Cell culture and treatment

Human lung (A549) cells were revived from National Center for Cell Sciences (NCCS), India with a job number 1615. The flasks were checked for their fungal and bacterial contamination. The passage number 18 cells were used. Lung cells were grown in DMEM supplemented with 10% fetal bovine serum, 1% L-glutamine and 1% penicillin-streptomycin antibiotic solution. Cells were seeded at 2, 50,000 cells/flask in a total volume of 10 mL. After achieving confluence, cells were trypsinized and seeded into 96 well plates at the rate of 3.0×10^4 cells/0.1 mL. The cell cultures were maintained in a 5% CO₂ incubator (WTC Binder, Germany) at 37°C. The test TNP were prepared as

suspensions in PBS as solvent with < 1% PEG as stabilizer. The different concentrations 1-300ug/mL were used for screening of possible toxicity effects in human lung cells.

CYTOTOXICITY ASSAY

The effect of test TNP on the cellular proliferation and viability was determined by using MTT assay method (Tomankova *et al.*, 2015). The yellow tetrazolium salt was reduced by dehydrogenase enzymes present in mitochondria of metabolically active cells, to generate reducing equivalents, NADH and NADPH. The lung cells were seeded into 96 well plates and add test TNP suspensions (100 µL, in quadruplicate) in media. The microtiter plate was incubated at 37°C for 48 h in 5% CO₂ incubator and 20 µL of MTT (5 mg/mL) was added to each well. The plate was again incubated for 2 h. The formazan product was dissolved in DMSO (80 µL) and followed by aluminum foil wrapping to prevent the oxidation of the dye. The plate was placed on a rotary shaker for 2 hours for proper mixing. The absorbance was recorded using ELISA reader at 470 nm. The test absorbance was compared with that of solvent control to get the cell viability (Bhikku *et al.*, 2014).

OXIDATIVE STRESS PARAMETERS ESTIMATION

The lung cell extract was prepared after cell loading into a 96 well plate at a density of 3.0×10^4 cells/well in 100 µL of culture medium. To each well, 100 µL of increasing concentrations of test TNP suspensions were added in quadruplicate. The microtiter plate was incubated in 5% CO₂ incubator at 37°C for 48 h. The supernatants were transferred into fresh 96 well plates and assayed according to the manufacturer's protocol for estimation of LDH, GSH and TBARS levels respectively.

LACTATE DEHYDROGENASE (LDH) LEAKAGE ASSAY

LDH is a soluble zinc containing enzyme present in the cytosol. It is released into surrounding culture medium upon cell injury or lysis during apoptosis and necrosis. LDH leakage into the culture medium can be used as a sign of cell membrane integrity, and therefore used as a measurement of cytotoxicity.

This assay measures cell death in response to chemicals or environmental pollutants using a coupled two step reaction. In the first step, LDH enzyme catalyzes the reduction of NAD⁺ to generate NADH and H⁺ by oxidation of lactate to pyruvate. In the second step of reaction, diaphorase uses the newly generated NADH and H⁺ to catalyze the reduction of a tetrazolium salt to colored formazan which absorbs strongly at 490-520

nm. The quantity of formazan generated is proportional to the amount of LDH leakage into the culture medium for measurement of oxidative stress (Harikiran *et al.*, 2016).

GLUTATHIONE (GSH) ASSAY

Glutathione is chemically a tripeptide (γ -glutamylcysteinyl glycine), distributed in plants, animals and human beings. This assay employs an optimized enzymatic recycling process, using glutathione reductase, for the quantification of GSH. The sulphhydryl group of GSH reacts with 5,5'-dithio-bis-2-nitrobenzoic acid (DTNB) and generates a yellow colored TNB (5-thio-2-nitrobenzoic acid). The mixed disulfide generated is reduced by glutathione reductase to recycle the GSH and produce more TNB. The quantity of TNB generation is directly proportional to the concentration of GSH in the cell sample. The absorbance of TNB was measured at 405- 414 nm and GSH levels were estimated in the cell sample (Shukla *et al.*, 2015).

LIPID PEROXIDATION ASSAY

Malondialdehyde (MDA) was formed on lipid peroxidation naturally. The MDA content was

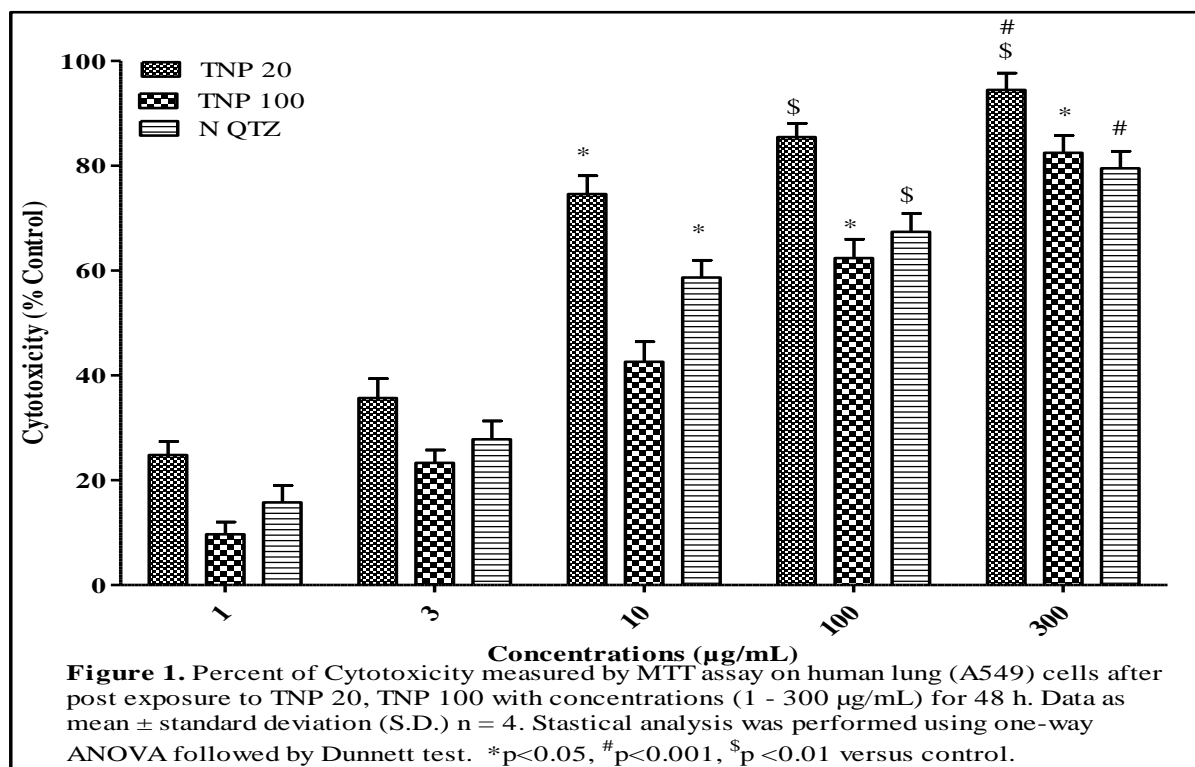
measured indirectly in terms of thiobarbituric acid reactive substances (TBARS). The determination of TBARS is a well-established method for extent of lipid peroxidation. This assay was a simple, reproducible and standardized tool for estimation of lipid peroxides in cell lysates. The TBARS were measured colorimetrically at 530-540 nm under high temperatures and acidic conditions (Chellappa *et al.*, 2015).

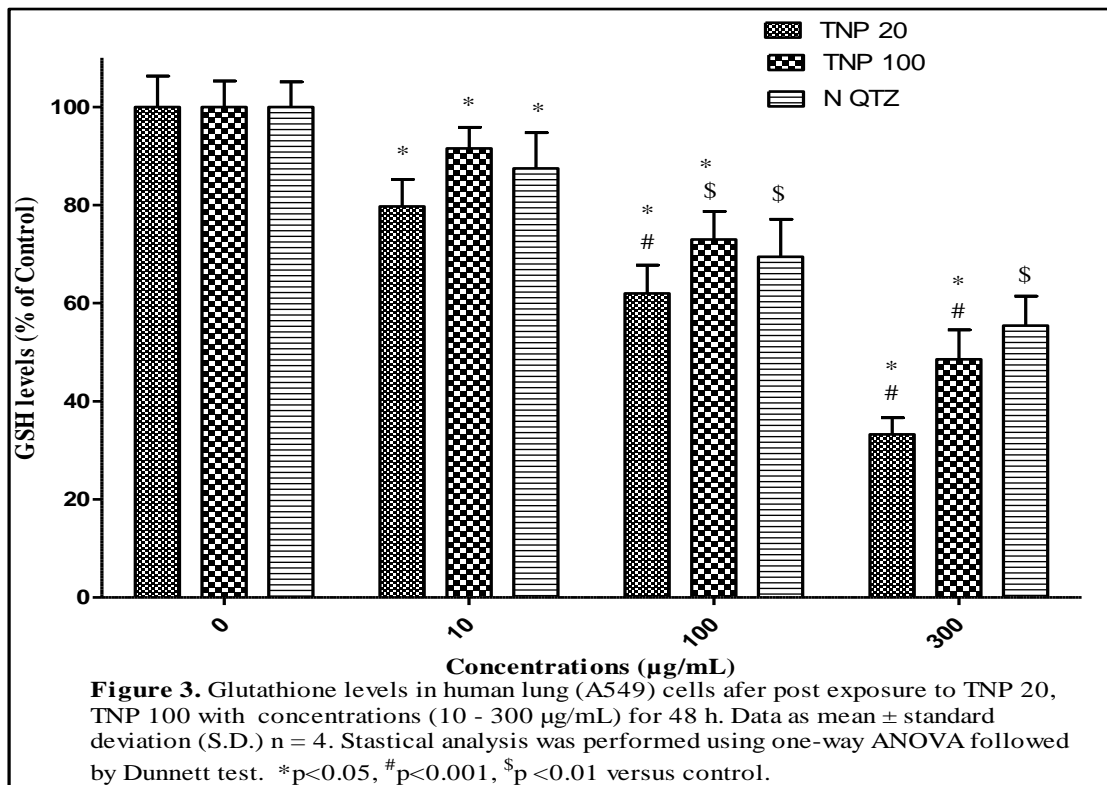
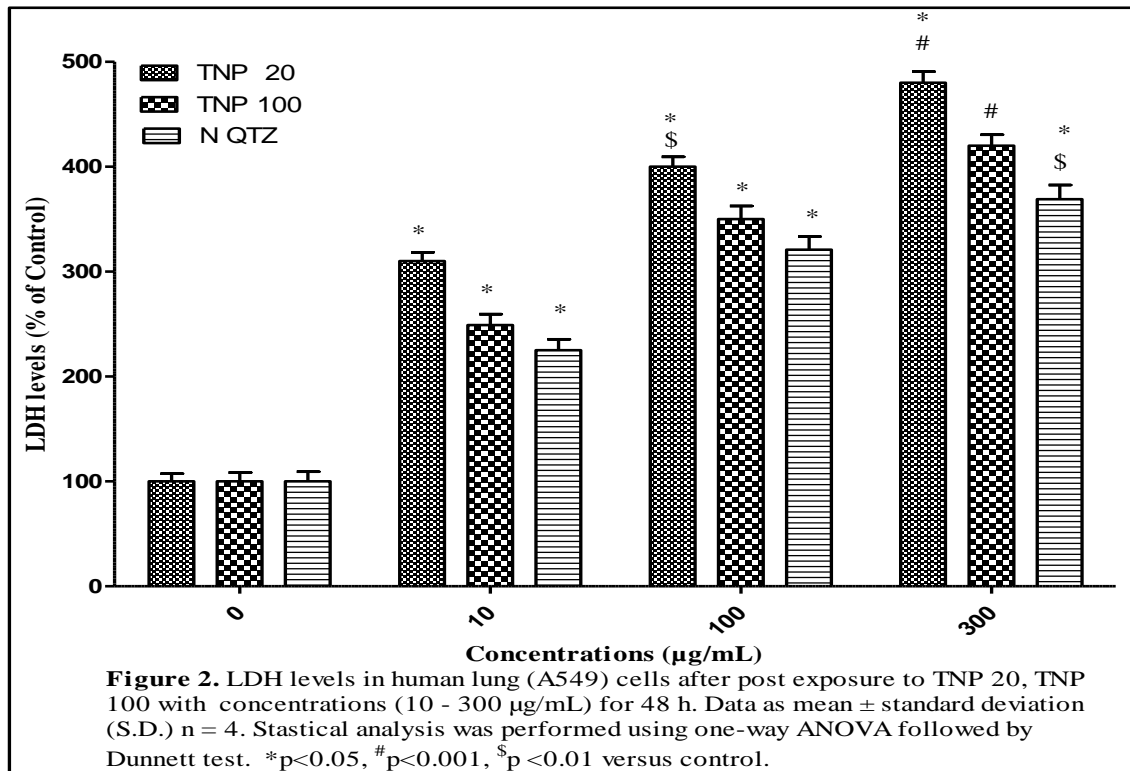
Statistical Analysis

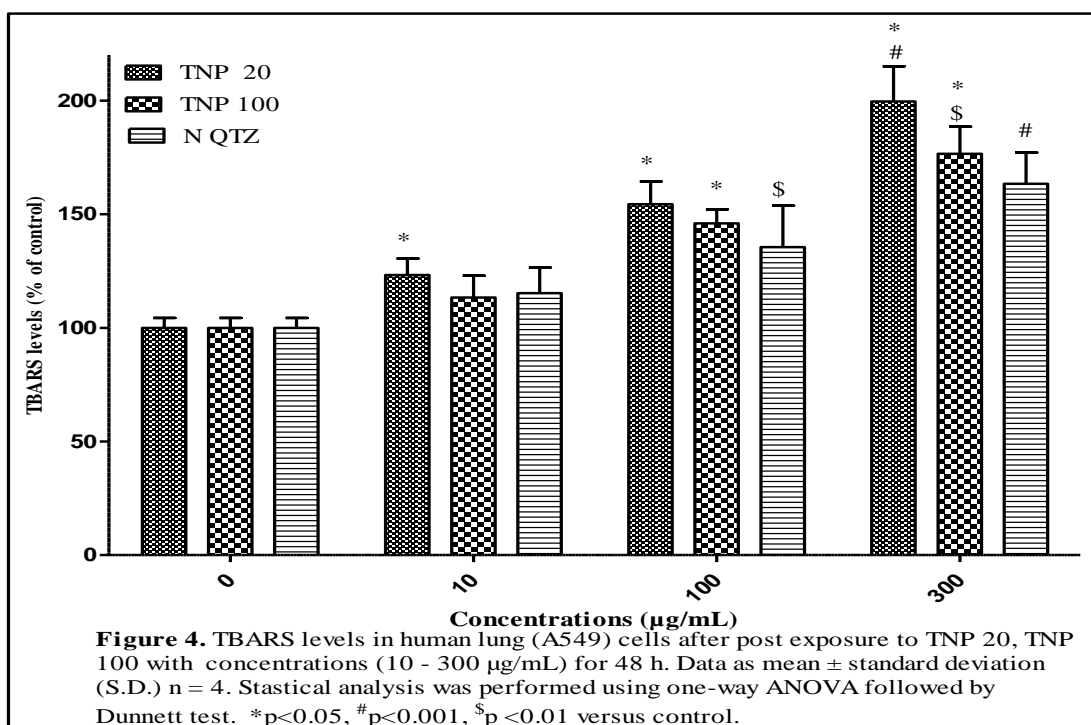
All the data were analyzed and expressed as the percentage of control. Statistical analysis was performed using one-way ANOVA followed by Dunnett test. The statistical significance was assigned at * $p < 0.05$, $^{\$}p < 0.01$, $^{\#}p < 0.001$ versus control cells. NQTZ used as a positive control.

RESULTS

The cell viability reduction was measured by using MTT assay. The lung cells were exposed to TNP 20 and TNP 100 for 48 h, results showed that TNP 20 induced significant cytotoxicity at the doses 100 and 300 $\mu\text{g/mL}$ shown in Figure 1.







The cell viability was decreased in a dose dependent manner. Both TNP were significantly ($p < 0.001$) decreased the cell viability when compared with control cells. TNP 20 showed highest cell viability reduction 94.41 % at 300 ($p < 0.001$) µg/mL than TNP 100 and NQTZ. The cell viability at lower concentrations 1 and 3 µg/mL were reduced non- significantly.

The cytotoxicity and oxidative stress was measured by cell membrane damage, determined through LDH leakage assay. Because, LDH is a cytosolic enzyme present in normal cells and cell membrane damage results it's leakage into the extracellular fluid. Lung cells exposed to TNP 20 and TNP 100 significantly increased the LDH levels shown in Figure 2. Both the TNP 20 and TNP 100 were increased the LDH leakage at doses 100 and 300 µg/mL concentrations significantly ($p < 0.001$). The effect of TNP 20 on LDH levels observed that 2, 3, 4 folds increment were found at doses 10 ($p < 0.05$), 100 ($p < 0.01$), 300 ($p < 0.001$) µg/mL significantly in A549 cells compared to control.

GSH is responsible for maintaining cellular oxidation-reduction homeostasis in cells; any changes in GSH levels leads to characteristic functional damage of cells. The reduced GSH levels of tested TNP 20 and TNP 100 were shown in Figure 3. A significant ($p < 0.001$) depletion of GSH levels were found at 100 and 300 µg/mL in A549 cells for 48 h study. 4 folds decrement of

GSH was observed for TNP 20 and 3½ folds for TNP 100 when compared to control.

The effect of TNP 20 and TNP 100 on lipid peroxidation, results were shown in figure 4 after post exposed to A549 cells for 48 h. Cells were exposed to 10, 100 and 300 µg/mL of test TNP for 48 h and the dose dependent increase of TBARS were observed. The results were indicating that there was a significant ($p < 0.001$) enhancement in TBARS levels at 100 ($p < 0.01$) and 300 ($p < 0.001$) µg/mL concentrations of both the TNP compared to control cells.

DISCUSSION

In recent decades, TNP have been increased for their worldwide applications in cosmetics, food-industries, materials for air pollution control, pharmaceuticals and personal care products. The extensive production and use of TNP has increased risk for human exposure results in unknown health complications (Rehman *et al.*, 2016). TNP enters into the human body in the form of skin care, nano-food or nanodrug delivery applications.

Due to their nano particle size, industrially released TNP can also be inhaled as air borne particles. So, safety concerns have been increasing about the possible health complications when exposed to TNP by humans and animals. Cells were exposed to different

concentrations (1-300µg/mL) among them lower doses (1 and 3 µg/mL) represent environmental exposure, while higher ones considered the possibility of a pulmonary local accumulation of TNP. This study evaluated the potential toxicity of different doses of TNP in human respiratory cells. The alveolar epithelial cells can have direct contact with the inhaled TNP (Das *et al.*, 2016).

So we have chosen A549 cell line as in vitro model to evaluate cytotoxicity and oxidative stress for 48 h exposure. The tested TNP 20 and TNP 100 induced cytotoxicity and oxidative stress in A549 cells. The MTT assay results clearly indicating that the tested TNP were reduced the cell viability significantly at higher doses 100 and 300 µg/mL after exposed to A549 cells for 48 h. The highest cell viability reduction 94.41 % was induced at the dose 300 (p<0.001) µg/mL for TNP 20. The TNP 20 and TNP 100 were reduced cell viability at lower concentrations 1 and 3 µg/mL in tested A549 cells for acute exposure (Rihane *et al.*, 2016).

The cell membrane damage induced by TNP was done by LDH leakage assay. Because LDH is a cytosolic enzyme present in normal cells can release into surrounding extracellular fluid after cell membrane damage. The results showed that increased release of LDH into culture media after TNP exposure was in a dose-dependent manner. TNP 20 and TNP 100 have showed highest release of LDH compared to control and NQTZ treated cells at 48 h exposure period.

Kongseng *et al.*, 2016 findings were similar to the results showing cytotoxicity towards A549 cells using MTT and LDH leakage assays in the present study. LDH leakage from cells into culture media is another evidence for penetration of nanoparticles into the cells and damage of cell membrane. The GSH levels were decreased drastically at the doses 100 (p<0.01) and 300 (p<0.001) µg/mL significantly. The cellular oxidative stress was determined by decreased GSH levels and increased TBARS (Ahamed *et al.*, 2016). The decreased cell viability and increased TBARS levels suggested that cell death was the primary cause of membrane damage by lipid peroxidation. The depleted GSH and increased TBARS significantly induce the oxidative stress in tested alveolar epithelial cells (A549).

CONCLUSION

So finally, we conclude that the tested TNP 20 and TNP 100 were induced cytotoxicity and oxidative stress due

to the increased LDH, TBARS and followed by decreased GSH in A549 cells for acute exposure.

ACKNOWLEDGMENTS

The first author grateful to University Grants Commission (UGC), New Delhi, India for providing funding for the present research work.

Declaration of interest

The authors report that no conflict of interest

REFERENCES

1. Wang Y., He Y., Lai Q., Fan M., Review of the progress in preparing nano TiO₂: an important environmental engineering material. *J Environ Sci* 26:2139-2177, (2014).
2. Bhatt I., Tripathi B.N., Interaction of engineered nanoparticles with various components of the environment and possible strategies for their risk assessment. *Chemosphere*, 82:308-317, (2011).
3. Kansara K., Patel P., Shah D., Shukla R.K., Singh S., Kumar A., et al., TiO₂ nanoparticles induce DNA double strand breaks and cell cycle arrest in human alveolar cells. *Environ Mol Mutagen*, 56:204-217, (2015).
4. Rollerova E., Tulinska J., Liskova A., Kuricova M., Kovriznych J., Mlynarcikova A., et al., Titanium dioxide nanoparticles: some aspects of toxicity/focus on the development. *Endocr Regul*, 49:97-112, (2015).
5. Harikiran L., Bhikku A., Narsimha R.Y., *In vitro* cytotoxicity of gold and silver nanorods using different human cell lines. *Lat Am J Pharm*, 34:1277-1282, (2015).
6. Ammendolia M.G., Iosi F., Maranghi F., Tassinari R., Cubadda F., Aureli F., et al., Short-term oral exposure to low doses of nano-sized TiO₂ and potential modulatory effects on intestinal cells. *Food Chem Toxicol*, 102:63-75, (2017).
7. Simone U., De Lonati D., Ronchi A., Coccini T., Brief exposure to nanosized and bulk titanium dioxide forms induces subtle changes in human D384 astrocytes. *Toxicol Lett*, 254:8-21, (2016).
8. Banerjee J.A., Gogoi R., Wong J., Mitragotri S., Role of nanoparticle size, shape and surface chemistry in oral drug delivery. *J Cont Rel*, 238:176-185, (2016).
9. Piperigkou Z., Karamanou K., Engin A.B., Gialeli C., Docea A.O., Vynios D.H., et al., Emerging aspects of nanotoxicology in health and disease: from agri-culture and food sector to cancer therapeutics, *Food Chem. Toxicol*, 91:42-57, (2016).
10. Tomankova K., Horakova J., Harvanova M., Malina L., Soukupova J., Hradilova S., et al., Cytotoxicity, cell uptake and microscopic analysis of titanium dioxide and silver

- nanoparticles *in vitro*. Food Chem Toxicol, 82:106-115, (2015).
11. Bhikku A., Harikiran L., Durgaiah G., Narsimha R.Y., Cytotoxicity evaluation of carbon nanomaterials on human cell lines using MTT assay. Int J Pharm Pharm Sci, 6:379-382, (2014).
 12. Harikiran L., Narsimha R.Y., Cytotoxicity, oxidative stress, and inflammation in human Hep G2 liver epithelial cells following exposure to gold nanorods. Toxicol Mech Meth 26:340-347, (2016).
 13. Shukla R.K., Kumar A., Pandey A.K., Singh S.S., Dhawan A., Titanium dioxide nanoparticles induce oxidative stress-mediated apoptosis in human keratinocyte cells. J Biomed Nanotechnol, 7:100-101, (2011).
 14. Chellappa M., Anjaneyulu U., Manivasagam G., Vijayalakshmi U., Preparation and evaluation of the cytotoxic nature of TiO₂ nanoparticles by direct contact method. Int J Nanomed, 10:31-41, (2015).
 15. Rehman F.U., Zhao C., Jiang H., Wang X., Biomedical applications of nano-titania in theranostics and photodynamic therapy. Biomater Sci 4:40-54, (2016).
 16. Das S., Sen B., Debnath N., Recent trends in nanomaterials applications in environmental monitoring and remediation. Environ Sci Pollut Res Int, 22:18333-18344, (2015).
 17. Rihane N., Nury T., Imen M., Mir L., Sakly E.I., Amara M., Lizard G., Microglial cells (BV-2) internalize titanium dioxide nanoparticles: toxicity and cellular responses. Environ Sci Pollut Res Int, 23:9690-9699, (2016).
 18. Kongseng S., Yoovathaworn K., Wongprasert K., Chunhabundit R., Sukwong P., Pissuwan D., Cytotoxic and inflammatory responses of TiO₂ nanoparticles on human peripheral blood mononuclear cells. J Appl Toxicol, 36:1364-1373, (2016).
 19. Ahamed M., Akhtar M.J., Khan M.A., Alhadlaq H.A., Alshamsan A., Cobalt iron oxide nanoparticles induce cytotoxicity and regulate the apoptotic genes through ROS in human liver cells (HepG2). Colloids Surf B Biointerfac 148: 665-673, (2016).

***Corresponding Author:**

Narsimha Reddy Y*

Email: ynrucpsc@gmail.com



Assessment of pulmonary toxicity of gold nanorods following intra-tracheal instillation in rats



Harikiran Lingabathula, Narsimhareddy Yellu*

Department of Pharmacology and Toxicology, University College of Pharmaceutical Sciences, Kakatiya University, Warangal, Telangana, 506009, India

ARTICLE INFO

Keywords:

Gold nanorods
Intra-tracheal instillation
Pulmonary toxicity
Bronchoalveolar lavaged fluid

ABSTRACT

The present investigation was aimed to evaluate the pulmonary toxicity of 10 and 25 nm gold nanorods (GNRs) following intra-tracheal instillation in rats using bronchoalveolar lavage (BAL) fluid and lung histopathological analysis. The GNRs displayed that the dose-dependent toxicity via elevated lactate dehydrogenase leakage, alkaline phosphatase, lipid peroxidation and total microprotein levels in BAL fluids after 1 day, 1 week and 1 month post exposure periods. All the parameters were returned to normal values after 3 months post exposure period may be due to recovery. The rat lung histopathology displayed that accumulation of macrophages, inflammatory response and tissue thickening for both sizes of GNRs. 10 nm GNRs increased all BAL fluid parameters significantly following 1 day, 1 week and 1 month post exposure periods whereas 25 nm GNRs have shown similar effects but less extent. These investigations proposed that the dose and size dependent pulmonary toxicity of GNRs.

1. Introduction

Nanoparticles (NPs), especially gold nanoparticles (GNPs) hold great promises for future applications. GNPs are particularly exploited in organisms because of their biocompatibility (Bhattacharya and Mukherjee, 2008). Recent investigations have centered on functionalizing the GNPs as photothermal agents for hyperthermally killing pathogens (Norman, 2008; Simon, 2008). The effectiveness of the antibacterial activity of GNPs can be enhanced by adding antibiotics (Burygin, 2009). GNPs generate holes in the cell wall, resulting in the cell contents leakage and cell death. The cell death is also possible that GNPs bind to the DNA of bacteria and inhibit the uncoiling and transcription of DNA (Rai et al., 2010). The GNPs can be used to coat a wide variety of surfaces for instance, fabrics for treatment of wounds, implants and surfaces of glass to maintain hygienic conditions in the home and hospitals (Das, 2009).

GNPs can be manufactured into a variety of shapes including gold nanospheres, nanoprisms, nanobelts, nanorods, nanocages and nanotars. The chemical, optical and electromagnetic properties of GNPs are powerfully influenced by their size and shape (Yang and Cui, 2008). Gold nanorods (GNRs) are having 20 times more optical absorption efficiencies than the GNPs of the same volume (Copland et al., 2004). The scattering coefficients of GNRs are also an order of magnitude higher when compared to those of gold nanoshells and nanospheres (Jain et al., 2006). GNRs of high aspect ratio tender higher fluorescence

intensity and this property will encourage the development of techniques using GNRs in fluorescent probe micro array assays and optical biosensor applications (Li et al., 2005). Additionally, GNRs have a strong binding affinity to thiol groups permitting them to be competently conjugated with several biomolecules (Liao and Hafner, 2005).

Because of these enhanced properties of the rod shaped GNPs, the GNRs are finding various industrial and commercial applications. GNRs are useful materials for photothermal therapy, drug delivery, sensing and biomedical imaging due to unique surface plasmon resonance ranging from visible to near infrared (NIR) region, facile synthesis and easy functionalization (Stone et al., 2011; ZhiYa et al., 2013). GNRs could be used as optical sensors for Raman-based intracellular biosensing useful for cancer diagnosis and other diagnostic biomedical applications (Oyelere et al., 2007). GNRs conjugated with photo sensitizers can kill Methicillin-resistant *Staphylococcus aureus* by NIR photothermal radiation (Kuo, 2009; Pissuwan et al., 2009).

In spite of the huge applications of GNRs, the occupational exposure for these nanorods also increased enormously. Recently, some of the studies were investigated the toxicities of GNRs using different human cells and reported in vitro cytotoxicity induced by GNRs (Harikiran and Narsimhareddy, 2016; Harikiran et al., 2015; Ying et al., 2015), but there is lack of availability of pulmonary toxicity effects of GNRs in vivo. The present study was aimed to assess the potential pulmonary toxicity of rod shaped, poly ethyleneglycol (PEG) coated, 10 and 25 nm GNRs following intra-tracheal instillation in rats.

* Corresponding author.

E-mail addresses: ynrucpsc@gmail.com, ynrkuc@gmail.com (N. Yellu).

2. Materials and methods

2.1. Chemicals

Quartz particles (QTZ; 58–68 μm) of 99.95% purity were obtained from Berkely Springs, Morgan County, WV. The phosphate buffer saline and PEG were acquired from Himedia, Mumbai, India. All the biochemical assay kits were obtained from Raybiotech, New Delhi, India. The rest of the chemicals were purchased from Himedia, Mumbai, India.

2.2. Particle types

The 10 nm GNRs (GNR 10) and 25 nm GNRs (GNR 25) were procured from Sigma-Aldrich, St. Louis, MO. The GNRs were prepared as suspensions in phosphate buffer saline (PBS) with 1% PEG as stabilizer and were first ultrasonicated at 25 °C to achieve optimal dispersion. The average particle size and shape of the GNRs suspensions were determined using transmission electron microscopy (TEM; TECNAI 20, Philips, USA). At least 250 particles were used to determine the average size of nanorods.

2.3. Animals

The six weeks old male wistar rats were procured from National Institute of Nutrition, Hyderabad, India. The rats were kept one week for acclimatization before starting the experiments. The rats were housed in polypropylene cages in a room; water and feed were available ad libitum with controlled temperature (25 ± 2 °C), humidity ($55 \pm 5\%$) and a 12 h light/dark cycle during the acclimatization and experimental periods. The animals, weighed approximately 200–220 g were picked and randomly divided into different groups.

2.4. Experimental design

The test GNRs were prepared as suspensions by using a nontoxic dispersion vehicle (Warheit et al., 2005). The test GNRs and QTZ suspensions were prepared in PBS with 1% PEG by briefly shearing and subsequently sonicating (Soltec, Italy) the GNRs samples. The rats were divided into different groups ($n = 6$) and instilled with a single dose of 1 mg/kg and 5 mg/kg b.w. GNRs, QTZ and control (PBS + 1% PEG) by intra-tracheal instillation method, as this method of exposure was a reliable qualitative screen for estimating the pulmonary toxicity of inhaled particles (Yasuo et al., 2016). The different groups were Group 1: Control, Group 2: 1 mg/kg GNR 10, Group 3: 5 mg/kg GNR 10, Group 4: 1 mg/kg GNR 25, Group 5: 5 mg/kg GNR 25, Group 6: 1 mg/kg QTZ and Group 7: 5 mg/kg QTZ. The experiment was approved by the Institutional Animal Ethics Committee, UCPSC, Kakatiya University (File No. IAEC/05/UCPSC/KU/2016).

2.5. Intra-tracheal instillation

The rats were anesthetized with isoflurane in a small chamber and individual rats were secured on an inclined plastic platform and anesthetization continued via a small nose cone. A small hole was made in the trachea close to the larynx. A 24 gauge plastic catheter was inserted through the hole to the distal end of the trachea and the blunted needle was then inserted inside the plastic catheter. A 1 mL syringe already filled with 200 μL of air and 50 μL of PBS was then connected to the free end of silicone tubing to rapidly propel the test sample from the tubing and needle into the rat lungs. The incision was then sutured, swabbed with povidone iodine and anesthetized with a drop of lidocaine. The rats recovered and were active within 10–15 min after removal of the inhalation anesthetic. The incision was healed within 3–4 days and the rats were observed daily until their scheduled termination (Lam et al., 2004).

2.6. Collection of bronchoalveolar lavage fluid

The BAL fluid (15–20 mL) was collected from all the above control and test nanorod exposed rats at 1 day, 1 week, 1 month and 3 months post instillation periods (Reddy et al., 2012). The lungs of control, QTZ and test nanorod exposed rats were lavaged with a warmed PBS solution as per the procedure already depicted previously (Warheit et al., 2007). Briefly, the lungs were removed from the thoracic cavity and lavaged with a PBS solution that had been heated to 37 °C. A 10 mL syringe was used to fill the lungs with 8 mL of PBS per wash. The rat lungs were gently manipulated after incorporation of the PBS and during the withdrawal of BAL fluid. The first recovered 12 mL of lavaged fluids was used for BAL fluid analysis.

2.7. Biochemical analysis

All biochemical assays were performed on BAL fluids of 1 day, 1 week, 1 month and 3 months post instillation periods in rats for the estimation of lactate dehydrogenase (LDH), alkaline phosphatase (ALP), extent of lipid peroxidation and total microprotein (MTP) using respective diagnostic kit methods as per the manufacturer's protocol.

2.8. Lactate dehydrogenase leakage assay

LDH leakage into the BAL fluid can be used as a sign of cell membrane integrity and therefore used as a measurement of cytotoxicity (Ran et al., 2009). This assay measures cell death in response to environmental pollutants or chemical compounds using a coupled two step reaction. In the first step, LDH catalyzes the reduction of NAD^+ to produce NADH and H^+ by oxidation of lactate to pyruvate. In the second step, diaphorase uses the newly produced NADH and H^+ to catalyze the reduction of a tetrazolium salt to colored formazan which absorbs strongly at 490 nm. The quantity of formazan generated is proportional to the amount of LDH leaked into BAL fluid as a result of cytotoxicity.

2.9. Alkaline phosphatase assay

ALP activity measured to determine the Type II alveolar epithelial cell secretory activity and increased ALP levels in BAL fluids is considered to be an indicator of Type II cell toxicity (Ran et al., 2009). At pH 10.3, ALP catalyzes the hydrolysis of colourless *p*-nitrophenylphosphate (pNPP) to yellow coloured *p*-nitrophenol and phosphate. Change in absorbance due to yellow colour formation is measured kinetically at 405 nm and is proportional to ALP activity in the sample.

2.10. Lipid peroxidation assay

Malondialdehyde (MDA) is a naturally occurring by product of lipid peroxidation. The MDA content was estimated in the form of thiobarbituric acid reactive substances (TBARS) and it is a well-established method for screening and monitoring of lipid peroxidation (Yagi, 1998). The MDA-TBA adducts produced by the reaction of MDA and TBA under high temperature (90–100 °C) and acidic conditions is measured colorimetrically at 530–540 nm.

2.11. Total microprotein assay

Raises in BAL fluid protein concentrations generally were consistent with increased permeability of vascular proteins into alveolar regions, indicating a collapse in the integrity of the alveolar capillary barrier (Warheit et al., 2007). This protein determination assay is a microplate based colorimetric method for rapid total protein quantification. It is based on the well-known Bradford method (Bradford, 1976) and it takes advantage of the colour change of dye in acidic medium when it

binds to proteins. When the dye binds, there is an immediate shift of the absorption maximum from 465 to 595 nm with a simultaneous change in colour from brown to blue.

2.12. Histopathology of rat lungs

Additional groups of rats were instilled with the test nanorod types at 5 mg/kg b.w. dose as well as PBS + 1% PEG. These studies were dedicated for lung tissue analysis and histopathological evaluations of lungs (Warheit et al., 2007). The lungs of GNRs exposed rats were collected from all the groups at 1 day, 1 week, 1 month and 3 months post instillation periods. For the histopathology study, the control and particle exposed (5 mg/kg b.w.) lungs were fixed in 10% v/v neutral buffered formalin and processed using routine histological techniques. The lung tissues were embedded with paraffin, and stained by using hematoxylin and eosin (H & E) dyes for histopathological evaluations and observed under 40 \times .

2.13. Statistical analysis

The data were expressed as mean \pm SD (n = 6). Statistical analysis was performed for all the assays using one way ANOVA followed by Bonferroni posttests by using GraphPad Prism 6.0. The statistical significances were indicated by ^sp < 0.05, [#]p < 0.01, ^{*}p < 0.001 versus control and ^ap < 0.05, ^bp < 0.01, ^cp < 0.001 versus QTZ.

3. Results

The 10 and 25 nm GNRs were well dispersed in PBS with 1% PEG solution and subsequent sonication of the suspension prevents the agglomeration of nanorods. The size and shape of the both GNRs were presented in Table 1. The TEM pictures of two GNRs were showed in Fig. 1.

The BAL fluid LDH levels were significantly increased at 1 day, 1 week and 1 month post exposure versus control treated rats (Table 2). Both 10 and 25 nm GNRs at 5 mg/kg b.w. dose showed the significant (p < 0.001) increase of BAL fluid LDH levels following 1 day and 1 week versus control. The 10 nm GNRs showed significant (p < 0.001) increase in LDH levels following 1 day, 1 week and 1 month post exposure periods versus QTZ treated rats. The 10 and 25 nm GNRs enhanced the BAL fluid ALP levels in rats at all-time points tested for both doses compared to control (Table 3). The ALP levels were significantly (p < 0.001) increased for both sizes of GNRs at 5 mg/kg b.w. dose in rats. The 10 nm GNRs at higher dose displayed significant enhanced BAL fluid ALP levels following 1 day, 1 week and 1 month post exposure periods compared to QTZ treated rats.

Lipid peroxidation in test nanorods exposed rat lung BAL fluids was quantified by means of MDA estimation in the form of TBARS assay (Table 4). Both GNRs induced significant (p < 0.001) elevated levels of MDA at 1 day and 1 week post exposure periods at two doses tested versus control. The 10 nm GNRs at 5 mg/kg dose have shown significant (p < 0.05) increased levels of lipid peroxidation after 1 day and 1 week post exposure periods versus QTZ. The 10 and 25 nm GNRs at 1 and 5 mg/kg b.w. doses displayed significant (p < 0.001) elevated BAL fluid MTP levels at 1 day and 1 week (p < 0.001) post exposure periods whereas at higher dose 10 nm (p < 0.001) and 25 nm (p < 0.01) GNRs displayed significant increase in MTP levels at 3

Table 1
Characteristics of test gold nanorods.

Property	Diameter	Length	Shape
GNR 10	10 \pm 1 nm	31 \pm 3 nm	Rod
GNR 25	25 \pm 2.5 nm	50 \pm 5 nm	Rod

Data were expressed as mean \pm SD.

months post exposure period versus control (Table 5). The 10 nm GNRs at both doses have shown significant elevated levels of BAL fluid MTP levels following 1 day (p < 0.05) post exposure period versus QTZ.

The GNRs, QTZ and control exposed rat lungs were isolated from all time points tested and observed for histopathological changes were shown in Figs. 2–4. Both sizes of GNRs exposed rat lungs after 1 day post instillation showed occasional macrophage aggregation, alveolar wall thickening, inflammatory response and congested or dilated alveoli. All the histopathological changes were worsened at 1 week post instillation and showed less changes at 1 month after exposure and, were alleviated after 3 months post exposure periods, displaying the lung toxicity of test nanorods similar to the QTZ treated rat lungs.

4. Discussion

The GNRs are finding enormous applications in different areas like biological, medical, imaging, textiles, industrial and consumer applications. With the increased utilization of these GNRs, the occupational exposure is also increased. The pulmonary toxicity related to the GNRs was very little known. The present study was investigated to assess the pulmonary toxicity of two sizes (10 and 25 nm) of GNRs following intra-tracheal instillation in rats using BAL fluid and lung histopathological analysis versus control (PBS + 1% PEG) and a positive control, QTZ.

The lung cell membrane damage induced by the test nanorods was evaluated by LDH leakage assay, as LDH is a cytosolic enzyme and it can be released after damage of cell membrane can lead to cytotoxicity. ALP activity is a measure of Type II alveolar epithelial cell secretory activity and increased ALP levels in rat lung BAL fluids is considered to be an indicator of Type II cell toxicity. The pulmonary toxicity induced by cerium oxide nanoparticles were evaluated by single dose (0.5 or 1 mg/kg) intra-tracheal instillation in Sprague-Dawley rats. The BAL fluid LDH levels were elevated at 1 day post exposure and sustained 1 week post exposure but subsided to normal levels after 84 days post exposure (Katherine et al., 2016).

BAL fluid analysis for LDH was displayed that the leakage was increased with the intra-tracheal instillation of both sizes of GNRs and QTZ at 1 day, 1 week and 1 month post instillation periods for both 1 and 5 mg/kg b.w. doses. In contrast, there were little or no increased levels of LDH leakage was observed at 3 months post instillation period. Especially, the higher dose exposed rat BAL fluid LDH leakage was elevated enormously comparing to lower dose treated rats, indicating dose-dependent lung toxicity of both GNRs. BAL fluid ALP activity was revealed that the levels were elevated with the exposure of 10 and 25 nm GNRs and QTZ at 1 day and 1 week post instillation periods for both 1 and 5 mg/kg b.w. doses versus control treated rats. The 10 nm test nanorods were displayed increased ALP activity at 1 month post exposure period also. There were little or no increased levels of ALP levels were found at 3 months post exposure period. The 5 mg/kg b.w. dose instilled rat BAL fluid ALP activity was increased enormously comparing to 1 mg/kg b.w. dose treated rats, indicating dose-dependent type-II cellular toxicity of both GNRs.

Jae et al. (2011) was investigated the toxicity of GNPs following sub-chronic inhalation in rats for 3 months using whole-body inhalation chamber. Results have displayed that cytotoxicity using BAL fluid analysis of LDH, MTP and albumin, and also lung histopathology has shown minimum alveoli, increased macrophages and an inflammatory infiltrate. The pulmonary toxicity of ZnO NPs were evaluated after intra-tracheal instillation in rats revealed that the increased LDH and ALP levels were found after 1 day, 1 week and 1 month post instillation periods (Shilpa and Rama, 2012). The above studies were supported our investigated results.

Increased lipid peroxidation, induction of oxidative stress and generation of ROS have shown to be some of the crucial mechanisms in the toxicity of different types of NPs after their exposures (Alexandra et al., 2012; Khanna et al., 2015). BAL fluid total protein concentrations

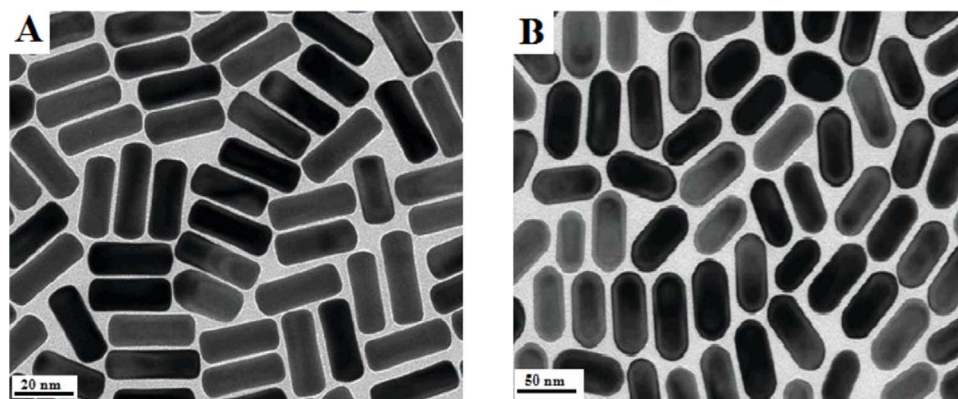


Fig. 1. Transmission electron micrographs of (A) 10 nm GNRs and (B) 25 nm GNRs.

Table 2

BAL fluid lactate dehydrogenase (LDH) levels (IU/L) following intra-tracheal instillation of GNRs in rats.

Nanorod Treatment	Post instillation period			
	1 day	1 Week	1 Month	3 Months
Control	8.35 ± 0.78	8.04 ± 0.95	7.81 ± 0.86	7.73 ± 0.69
GNR 10 (1 mg/kg)	25.69 ± 2.38 [§]	21.18 ± 2.28 [§]	11.27 ± 1.46	9.36 ± 0.84
GNR 10 (5 mg/kg)	57.32 ± 6.36 ^{§,c}	48.46 ± 4.67 ^{§,c}	28.34 ± 2.17 ^{§,c}	15.37 ± 1.28 [#]
GNR 25 (1 mg/kg)	21.76 ± 2.85 [§]	15.59 ± 2.09 [#]	10.85 ± 1.39	8.93 ± 1.11
GNR 25 (5 mg/kg)	34.58 ± 4.73 [§]	26.48 ± 3.14 [§]	14.47 ± 1.96 [§]	10.85 ± 1.09
QTZ (1 mg/kg)	23.19 ± 2.46 [§]	19.17 ± 2.12 [§]	9.81 ± 0.89	8.71 ± 1.14
QTZ (5 mg/kg)	42.96 ± 3.83 [§]	31.45 ± 2.27 [§]	18.73 ± 1.94 [§]	12.76 ± 1.16 [§]

Data were mean ± SD (n = 6).

[§] p < 0.05.

[#] p < 0.01.

^{*} p < 0.001 versus control.

^c p < 0.001 versus QTZ.

Table 3

BAL fluid alkaline phosphatase (ALP) levels (IU/L) following intra-tracheal instillation of GNRs in rats.

Nanorod Treatment	Post instillation period			
	1 day	1 Week	1 Month	3 Months
Control	6.15 ± 0.48	6.02 ± 0.46	5.95 ± 0.59	5.92 ± 0.64
GNR 10 (1 mg/kg)	19.21 ± 1.38 [§]	17.43 ± 2.15 [§]	12.34 ± 0.95 [§]	8.15 ± 0.75
GNR 10 (5 mg/kg)	26.18 ± 1.16 [§]	23.37 ± 2.05 ^{§,a}	18.49 ± 1.47 ^{§,a}	11.28 ± 0.92 [#]
GNR 25 (1 mg/kg)	16.25 ± 1.58 [§]	14.54 ± 1.94 [§]	9.12 ± 1.25	7.29 ± 0.63
GNR 25 (5 mg/kg)	22.59 ± 2.65 [§]	18.45 ± 2.13 [§]	12.24 ± 1.32 [§]	8.94 ± 0.88
QTZ (1 mg/kg)	16.98 ± 1.94 [§]	15.14 ± 1.19 [§]	9.35 ± 1.02	7.05 ± 0.58
QTZ (5 mg/kg)	24.49 ± 2.13 [§]	19.38 ± 1.69 [§]	14.97 ± 1.28 [§]	9.19 ± 0.76

Data were mean ± SD (n = 6).

[#] p < 0.01.

^{*} p < 0.001 versus control.

^a p < 0.05 versus QTZ.

generally were consistent with enhanced permeability of vascular proteins into alveolar regions, indicating a breakdown in the integrity of the alveolar-capillary barrier. Warheit et al. (2007) evaluated pulmonary toxicity of newly developed TiO₂ NPs and compare them to TiO₂ samples in two different size ranges in rats. Groups of rats were intra-tracheally instilled with 1 and 5 mg/kg b.w. doses of two TiO₂ particles (100 nm and 20 nm), QTZ particles and PBS (vehicle control). The lungs of control and particle-instilled rats were evaluated for BAL fluid inflammatory markers, cell proliferation and histopathology at post exposure time periods of 1 day, 1 week, 1 month and 3 months. The ranking of rat lung inflammation/cell proliferation/cytotoxicity and histopathological responses was QTZ > 20 nm TiO₂ > 100 nm TiO₂. The results displayed that exposures to TiO₂ NP types can produce pulmonary effects, based upon their composition and crystal structure (Warheit et al., 2007).

BAL fluid analysis for MDA levels were displayed that increased levels with the intra-tracheal instillation of both sizes of GNRs and QTZ at 1 day and 1 week post instillation periods for both 1 and 5 mg/kg b.w. doses versus control, indication of lipid peroxidation. There were little or no increased level of lipid peroxidation was observed at 1 and 3 months post instillation periods. BAL fluid MTP levels were revealed that elevated levels with the instillation of 10 and 25 nm GNRs and QTZ at 1 day, 1 week and 1 month post instillation periods for both 1 and 5 mg/kg b.w. doses versus control treated rats. There were little or no increased levels of MTP were found at 3 months post exposure period. The 10 nm test nanorods at 5 mg/kg b.w. dose instilled rat BAL fluid MDA and MTP levels were increased enormously comparing to 1 mg/kg b.w. dose treated rats and also significant increased levels were found comparing to QTZ treated rats.

These BAL fluid analysis results have shown that the 10 and 25 nm

Table 4
BAL fluid malondialdehyde (MDA) levels (nM) following intra-tracheal instillation of GNRs in rats.

Nanorod Treatment	Post instillation period			
	1 day	1 Week	1 Month	3 Months
Control	2.87 ± 0.18	2.80 ± 0.21	2.70 ± 0.23	2.63 ± 0.16
GNR 10 (1 mg/kg)	5.92 ± 0.47 ^s	5.74 ± 0.48 ^s	2.98 ± 0.19	2.77 ± 0.19
GNR 10 (5 mg/kg)	7.34 ± 0.62 ^{s,a}	7.17 ± 0.63 ^{s,a}	3.52 ± 0.23 ^s	3.19 ± 0.22
GNR 25 (1 mg/kg)	5.32 ± 0.48 ^s	5.24 ± 0.51 [#]	2.85 ± 0.21	2.74 ± 0.18
GNR 25 (5 mg/kg)	6.89 ± 0.56 ^s	6.68 ± 0.62 ^s	3.36 ± 0.28	3.01 ± 0.25
QTZ (1 mg/kg)	5.41 ± 0.46 ^s	5.19 ± 0.43 ^s	2.89 ± 0.21	2.70 ± 0.18
QTZ (5 mg/kg)	6.52 ± 0.56 ^s	6.35 ± 0.59 ^s	3.42 ± 0.22	3.14 ± 0.27

Data were mean ± SD (n = 6).

^s *p* < 0.05.

[#] *p* < 0.01.

^{*} *p* < 0.001 versus control.

^a *p* < 0.05 versus QTZ.

Table 5
BAL fluid total microprotein (MTP) levels (µg/mL) following intra-tracheal instillation of GNRs in rats.

Nanorod Treatment	Post instillation period			
	1 day	1 Week	1 Month	3 Months
Control	611.37 ± 21.58	602.38 ± 18.37	586.85 ± 19.41	566.19 ± 20.27
GNR 10 (1 mg/kg)	1109.22 ± 36.28 ^{s,a}	936.46 ± 25.45 ^s	763.32 ± 26.48 [#]	593.28 ± 24.48
GNR 10 (5 mg/kg)	1174.28 ± 34.37 ^{s,a}	1022.34 ± 32.56 ^s	811.47 ± 32.41 [#]	625.87 ± 21.37
GNR 25 (1 mg/kg)	1067.29 ± 35.65 ^s	904.75 ± 27.36 ^s	715.28 ± 28.38	574.19 ± 22.39
GNR 25 (5 mg/kg)	1111.23 ± 35.19 ^s	983.61 ± 32.47 ^s	772.18 ± 23.59 [#]	598.26 ± 19.24
QTZ (1 mg/kg)	1040.36 ± 37.91 ^s	917.26 ± 25.37 ^s	723.39 ± 27.38 ^s	571.39 ± 18.29
QTZ (5 mg/kg)	1107.58 ± 34.58 ^s	966.37 ± 33.84 ^s	781.20 ± 33.39 [#]	592.24 ± 19.47

Data were mean ± SD (n = 6).

^s *p* < 0.05.

[#] *p* < 0.01.

^{*} *p* < 0.001 versus control.

^a *p* < 0.05 versus QTZ.

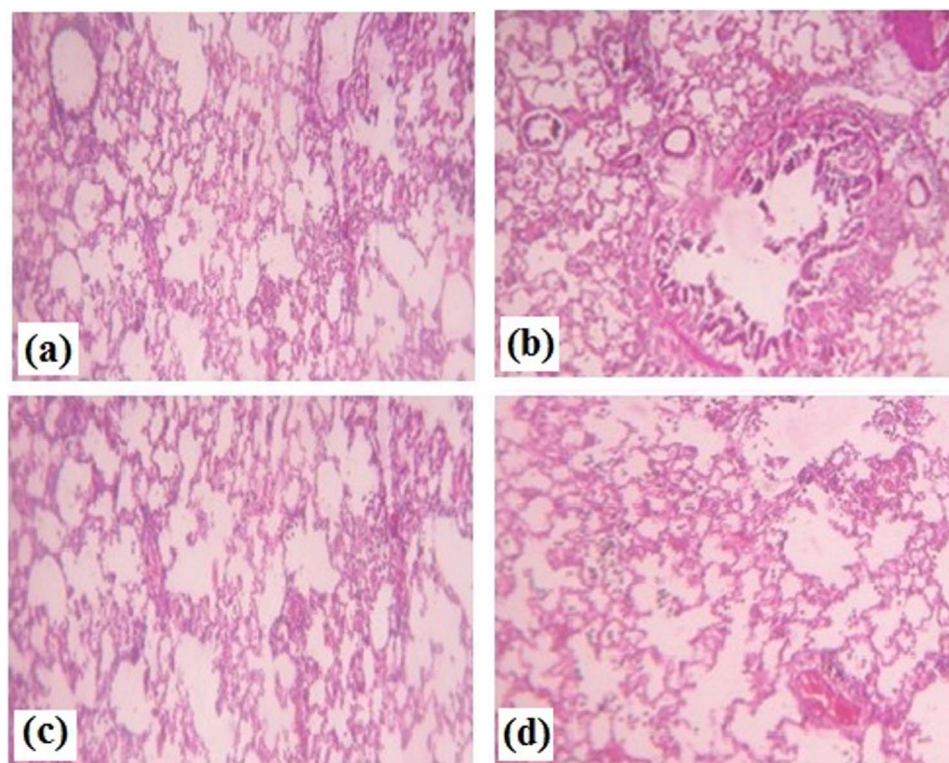


Fig. 2. Photomicrographs of rat lung tissue following intra-tracheal instillation of 1 day post exposure of (a) Control, (b) GNR 10, (c) GNR 25 and (d) QTZ.

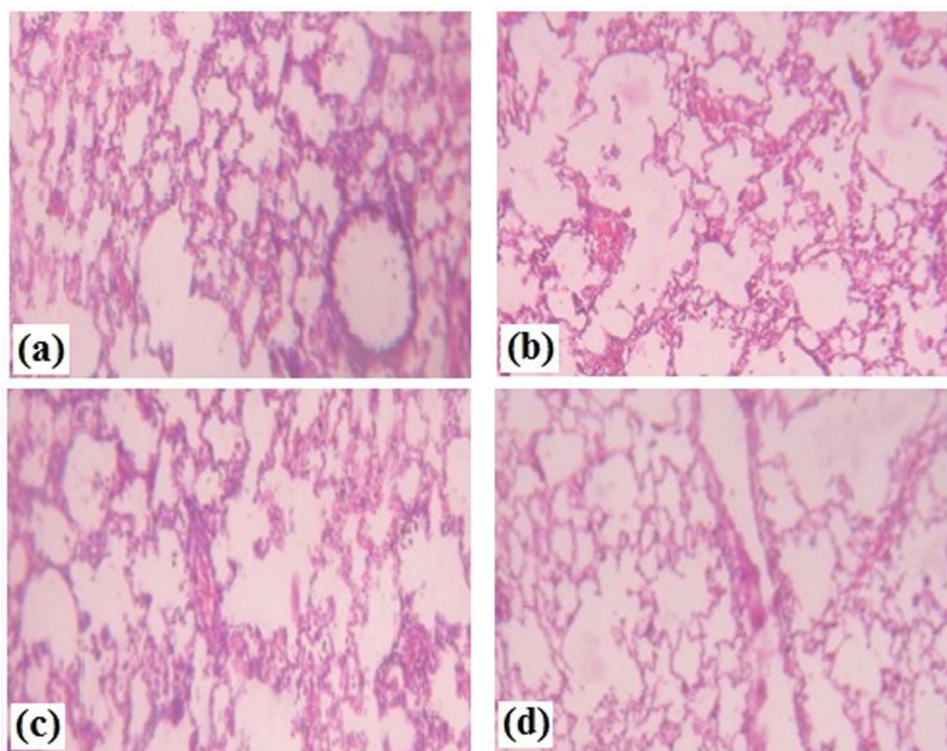


Fig. 3. Photomicrographs of rat lung tissue following intra-tracheal instillation of 1 week post exposure of (a) Control, (b) GNR 10, (c) GNR 25 and (d) QTZ.

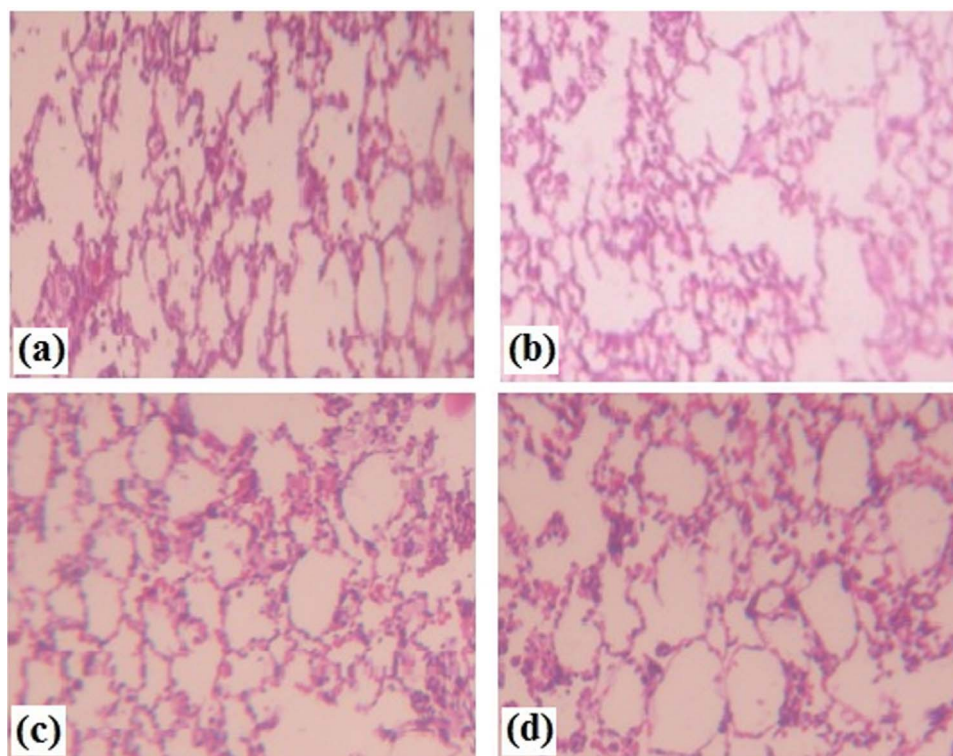


Fig. 4. Photomicrographs of rat lung tissue following intra-tracheal instillation of 1 month post exposure of (a) Control, (b) GNR 10, (c) GNR 25 and (d) QTZ.

gold nanorods induced pulmonary toxicity following intra-tracheal instillation in rats. The recent study conducted by Reddy et al. (2012) has shown the pulmonary toxicity induced by multi-wall carbon nanotubes after single dose intra-tracheal instillation in rats following 1 day, 7 days, 30 days and 90 days post instillation periods. The results displayed that increased levels of LDH, ALP, lipid peroxidation and

MTP in a dose-dependent manner and also histopathology of rat lungs have shown macrophage accumulation, alveolar damage and fibrosis. These results have supported our findings relating to pulmonary toxicity of GNRs following intra-tracheal instillation in rats.

GNRs have shown different histopathological changes in rat lungs after 1 day, 1 week and 1 month post exposure periods and the changes

were recovered or reduced after 3 months post exposure period. The GNRs exposure at 5 mg/kg b.w. dose displayed congested or dilated alveoli, aggregation of macrophages, slight inflammatory infiltrate and tissue thickening leading to fibrosis, indicating the pulmonary toxicity. Similar to our experiments, zinc oxide, magnesium oxide and titanium dioxide NPs exposure to rats following intra-trachea instillation have shown marked changes in lung histopathology like accumulation of foamy alveolar macrophages, aggregation of interstitial lymphocytes, thickening of lung tissue, infiltration of inflammatory cells and dilated or congested vessels (Gelli et al., 2013; Shilpa and Rama, 2012; Warheit et al., 2007).

BAL fluid analysis displayed that the 10 nm GNRs increased the LDH leakage, ALP levels, lipid peroxidation and MTP levels significantly following 1 day, 1 week and 1 month post exposure periods. In contrast, 25 nm GNRs have shown similar effects but less extent when compare with 10 nm GNRs, suggesting greater lung toxicity of 10 nm GNRs. These investigations suggested that the greater pulmonary toxicity of smaller sized GNRs than the bigger sized GNRs. Recently, some studies have been investigated the toxicity of different sizes of GNPs and proposed that the capability of increased cytotoxicity, oxidative stress and inflammation with smaller sized GNPs compared to bigger sized GNPs (George et al., 2012; Harikiran and narsimhareedy, 2016; Vijaykumar and Ganesan, 2013).

5. Conclusions

In summary, the 10 and 25 nm GNRs following intra-tracheal instillation in rats displayed that the dose-dependent toxicity via elevated LDH leakage, ALP, MDA and MTP levels in BAL fluids after 1 day, 1 week and 1 month post exposure periods. All the parameters were returned to control values after 3 months post exposure period may be due to recovery. The rat lung histopathology investigations also displayed that accumulation of macrophages, inflammatory response and tissue thickening for both sizes of GNRs. These investigations suggests that the dose-size-dependent pulmonary toxicity of GNRs.

Conflicts of interest

The authors declare that there are no conflicts of interest.

Acknowledgements

The first author is thankful to University Grants Commission- Basic Scientific Research (UGC-BSR), India for providing fellowship under Research Fellowship in Sciences for Meritorious Students (RFSMS).

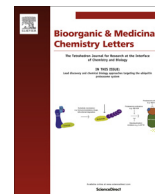
References

- Alexandra, J., Dieter, G.W., Ludwig, J., Ralf, K., 2012. Oxidative stress-induced cytotoxic and genotoxic effects of nano-sized titanium dioxide particles in human HaCaT keratinocytes. *Toxicology* 296, 27–36.
- Bhattacharya, R., Mukherjee, P., 2008. Biological properties of “naked” metal nanoparticles. *Adv. Drug Deliv. Rev.* 60, 1289–1306.
- Bradford, M.M., 1976. A rapid and sensitive method for the quantitation of microgram quantities of protein utilizing the principle of protein-dye binding. *Anal. Biochem.* 72, 248–254.
- Burygin, G.L., 2009. On the enhanced antibacterial activity of antibiotics mixed with gold nanoparticles. *Nanoscale Res. Lett.* 4, 794–801.
- Copland, J.A., Eghtedari, M., Popov, V.L., Kotov, N., Mamedova, N., Motamedi, M., Oraevsky, A.A., 2004. Bioconjugated gold nanoparticles as a molecular based contrast agent: implications for imaging of deep tumors using optoacoustic tomography. *Mol. Imaging Biol.* 6, 341–349.
- Das, S.K., 2009. Gold nanoparticles: microbial synthesis and application in water hygiene management. *Langmuir* 25, 8192–8199.
- Gelli, K., Porika, M., Anreddy, R.N., 2013. Assessment of pulmonary toxicity of MgO nanoparticles in rats. *Environ. Toxicol.* 30, 308–314.
- George, D.B., Amy, A., Marlene, B., Komandoor, E.A., Jean, C.S., Susan, M.B., 2012. Cytotoxicity and inflammation in human alveolar epithelial cells following exposure to occupational levels of gold and silver nanoparticles. *J. Nanopart. Res.* 14, 1212–1221.
- Harikiran, L., Narsimhareddy, Y., 2016. Cytotoxicity, oxidative stress, and inflammation in human Hep G2 liver epithelial cells following exposure to gold nanorods. *Toxicol. Mech. Methods* 26, 340–347.
- Harikiran, L., Bhikku, A., Narsimha, R.Y., 2015. *In vitro* cytotoxicity of gold and silver nanorods using different human cell lines. *Lat. Am. J. Pharm.* 34, 1277–1282.
- Jae, H.S., Jun, H.J., Jung, D.P., Moon, Y.S., Kyung, S.S., Hyeon, R.R., Jin, U.Y., Ki, S.J., Jayoung, J., Beom, S.H., Yong, H.C., Hee, K.C., Ji, H.L., Dong, W.K., Bruce, J.K., Je, Y., 2011. Subchronic inhalation toxicity of gold nanoparticles. *Part. Fibre Toxicol.* 8, 16.
- Jain, P.K., Lee, K.S., E.L-Sayed, I.H., E.L-Sayed, M.A., 2006. Calculated absorption and scattering properties of gold nanoparticles of different size, shape, and composition: applications in biological imaging and biomedicine. *J. Phys. Chem. B* 110, 7238–7248.
- Katherine, M.D., Anna, M.M., Melissa, A.B., Mark, B., Aleksandr, B.S., Edward, M.S., Stephen, S.L., 2016. Evaluation of the effect of valence state on cerium oxide nanoparticle toxicity following intratracheal instillation in rats. *Nanotoxicology* 10, 992–1000.
- Khanna, P., Ong, C., Bay, B.H., Baeg, G.H., 2015. Nanotoxicity: an interplay of oxidative stress, inflammation and cell death. *Nanomaterials* 5, 1163–1180.
- Kuo, W.S., 2009. Antimicrobial gold nanorods with dual-modality photodynamic inactivation and hyperthermia. *Chem. Commun.* 32, 4853–4855.
- Lam, C., James, T.J., McClusky, R., Hunter, L.R., 2004. Pulmonary toxicity of single-wall carbon nanotubes in mice 7 and 90 days after intratracheal instillation. *Toxicol. Sci.* 77, 126–134.
- Li, C.Z., Male, K.B., Hrapovic, S., Luong, J.H.T., 2005. Fluorescence properties of gold nanorods and their application for DNA biosensing. *Chem. Commun.* 31, 3924–3926.
- Liao, H., Hafner, J.H., 2005. Gold nanorod bioconjugates. *Chem. Mater.* 17, 4636–4641.
- Norman, R.S., 2008. Targeted photothermal lysis of the pathogenic bacteria, *Pseudomonas aeruginosa*, with gold nanorods. *Nano Lett.* 8, 302–306.
- Oyelere, A.K., Chen, P.C., Huang, X., El-Sayed, I.H., El-Sayed, M.A., 2007. Peptide-conjugated gold nanorods for nuclear targeting. *Bioconjugate Chem.* 18, 1490–1497.
- Pissuwan, D., Cortie, C.H., Valenzuela, S.M., Cortie, M.B., 2009. Functionalised gold nanoparticles for controlling pathogenic bacteria. *Trends Biotechnol.* 28, 207–213.
- Rai, A., Prabhune, A., Perry, C.C., 2010. Antibiotic mediated synthesis of gold nanoparticles with potent antimicrobial activity and their application in antimicrobial coatings. *J. Mater. Chem.* 20, 6789–6798.
- Ran, L., Lihong, Y., Yuepu, P., Geyu, L., Juan, Z., Yaoyao, S., Zhiping, X., Bing, Y., 2009. Pulmonary toxicity induced by three forms of titanium dioxide nanoparticles via intra-tracheal instillation in rats. *Prog. Nat. Sci.* 19, 573–579.
- Reddy, A.R., Reddy, Y.N., Krishna, D.R., Himabindu, V., 2012. Pulmonary toxicity assessment of multiwalled carbon nanotubes in rats following intratracheal instillation. *Environ. Toxicol.* 27, 211–219.
- Shilpa, G., Rama, N.R.A., 2012. Toxicological studies of zinc oxide nanomaterials in rats. *Toxicol. Environ. Chem.* 94, 1768–1779.
- Simon, D.A., 2008. Impact of gold nanoparticles combined to X-ray irradiation on bacteria. *Gold Bull.* 41, 187–193.
- Stone, J., Jackson, S., Wright, D., 2011. Biological applications of gold nanorods. *Wiley Interdiscip. Rev. Nanomed. Nanobiotechnol.* 3, 100–109.
- Vijaykumar, S., Ganesan, S., 2013. Size-dependent *in vitro* cytotoxicity assay of gold nanoparticles. *Toxicol. Environ. Chem.* 95, 277–287.
- Warheit, D.B., Brock, W.J., Lee, K.P., Webb, T.R., Reed, K.L., 2005. Comparative pulmonary toxicity inhalation and instillation and studies with different TiO₂ particle formulations: impact of surface treatments on particle toxicity. *Toxicol. Sci.* 88, 514–524.
- Warheit, D.B., Webb, T.R., Reed, K.L., Frerichs, S., Sayes, C.M., 2007. Pulmonary toxicity study in rats with three forms of ultrafine-TiO₂ particles: differential responses related to surface properties. *Toxicology* 230, 90–104.
- Yagi, K., 1998. Simple assay for the level of total lipid peroxides in serum or plasma. *Methods Mol. Biol.* 108, 101–106.
- Yang, D.P., Cui, D.X., 2008. Advances and prospects of gold nanorods. *Chem. Asian J.* 3, 2010–2022.
- Yasuo, M., Hiroto, I., Yukiko, Y., Kei, F., Kazuhiro, Y., Kazuhiro, Y., 2016. Usefulness of intratracheal instillation studies for estimating nanoparticle-induced pulmonary toxicity. *Int. J. Mol. Sci.* 17, 165.
- Ying, T., Yafeng, S., Libin, H., Gaojian, L., Changhai, L., Xiaoyan, F., Fangxing, L., Yuxia, Z., Lihui, W., Yongji, Y., 2015. *In vitro* cytotoxicity of gold nanorods in A549 cells. *Environ. Toxicol. Pharmacol.* 39, 871–878.
- ZhiYa, M., HongXing, X., YuPing, L., Bo, L., Wei, C., YuanDi, Z., 2013. Applications of gold nanorods in biomedical imaging and related fields. *Chin. Sci. Bull.* 58, 2530–2536.



Contents lists available at ScienceDirect

Bioorganic & Medicinal Chemistry Letters

journal homepage: www.elsevier.com/locate/bmcl

Design, synthesis and biological evaluation of 8-substituted-6-hydrazoneindolo[2,1-*b*]quinazolin-12(6*H*)-one scaffolds as potential cytotoxic agents: IDO-1 targeting molecular docking studies



Ramu Guda^a, Rajashekar Korra^a, Siripireddy Balaji^b, Rambabu Palabindela^a, Rakesh Eerla^c, Harikiran Lingabathula^d, Narsimha Reddy Yellu^d, Girijesh Kumar^{e,*}, Mamatha Kasula^{a,*}

^a Department of Chemistry, Kakatiya University, Warangal 506009, India

^b Department of Chemistry Vellore Institute of Technology, Tamilnadu 500046, India

^c Department of Microbiology, Kakatiya University, Warangal 506009, India

^d University College of Pharmaceutical Sciences, Kakatiya University, Warangal, Telangana 506009, India

^e Department of Chemistry and Centre for Advanced Studies in Chemistry, Panjab University, Chandigarh 160014, India

ARTICLE INFO

Article history:

Received 21 May 2017

Revised 20 August 2017

Accepted 25 August 2017

Available online 1 September 2017

Keywords:

Tryptanthrin

Cytotoxicity

Anti-oxidant activity

MTT assay

DPPH

Molecular docking

IDO1

ABSTRACT

Herein, we have reported the synthesis of 18 novel 8-substituted tryptanthrin analogues based on our earlier work. All these tryptanthrin analogues were well characterized by ¹H & ¹³C NMR, FT-IR, Mass Spectrometry and Elemental Analysis. All these 8-substituted analogues were screened for their anti-oxidant activity by DPPH radical scavenging assay. Out of all the tested compounds, **T¹¹**, **T¹²**, **T¹⁷** and **T¹⁸** showed potent anti-oxidant activity. The anti-cancer activity have been performed by using MTT assay protocol and their results depicts that compounds having the 4-pyridyl or 4-carboxyphenyl substituents at the 8th position of the tryptanthrin framework are found to be the most promising cytotoxic agent against A549, MCF-7 and HeLa human cancer cell lines compared to others as well as with the standard drug cisplatin. Moreover, the comparative molecular docking studies against the three protein receptors IDO1, EGFR and HER2 strongly suggested that IDO1 is the best target protein, which exhibits lowest binding energies of −11.73 and −11.61 kcal mol^{−1} for **T¹¹** and **T¹²** scaffolds, respectively towards the *in vitro* anti-cancer activity.

© 2017 Elsevier Ltd. All rights reserved.

Presently, cancer is one of the most challenging diseases found worldwide and also the most stimulating factor for the human morbidity and mortality. Therefore, the design and development of an anticancer drug is still one of the most challenging task for the people working in the domain of medicinal chemistry. As we know that the drug currently available in the market have several side effects on the normal cells and thus causing several abnormalities in the body despite of their enormous utilizations. The cost and availability are the another major concern of the present anti-cancer drugs.^{1,2} Hence, developing the new therapeutic drugs having the advance proficiency and efficacy on the cancer cells is one of the foremost goal for the researchers.³ In addition, to understand the molecular biology and pharmacology of cancer at a molecular level the target based drug-design and discovery is another emerging and challenging filed for the researchers.^{4–6} In

this regards, the highly developed technology in molecular biology advantages to identify many cancer targets in human body.⁷ So, considerable attention and effort have been needed for the discovery and development of new and potential anti-cancer drugs.

In this regards, indoloquinazolines received considerable curiosity in the field of therapeutic and diagnostic medicines. The natural product tryptanthrin (Indolo[2,1-*b*]quinazoline-6,12-dione) is obtained from the Chinese medicinal plants *Polygonum tinctorium* and *Isatis tinctoria* (Chinese wood) and shows significant biological activities due to the presence of indoloquinazolines moiety (Fig. 1).⁸ Furthermore, as tryptanthrin framework is derived from the isatin, which is well known inhibitors for anti-bacterial, anti-viral and anti-fungal agents and thereby also capable to influence their therapeutic effect of the concerned drugs.^{9–15} These important classes of heterocycles have attracted remarkable attention¹⁶ and possession of the researchers to investigate their synthesis, pharmacological and biological screening such as anti-leishmanial¹⁷ anti-microbial^{18,19} anti-tuberculosis²⁰ anti-inflammatory^{21–23}, anti-oxidant agents²⁴ and their cytotoxicity

* Corresponding authors.

E-mail addresses: girijeshchem@gmail.com (G. Kumar), mamathakasula2016@gmail.com (M. Kasula).

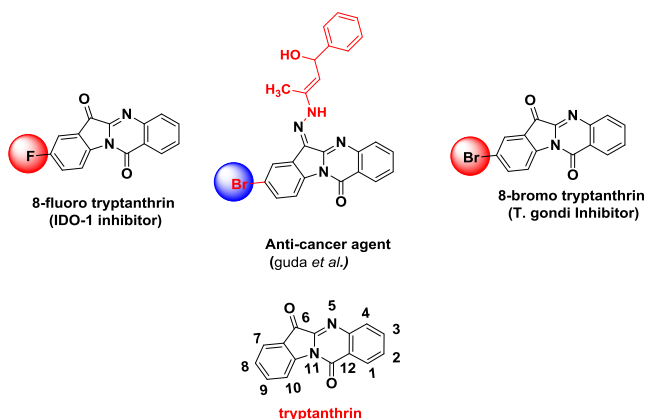
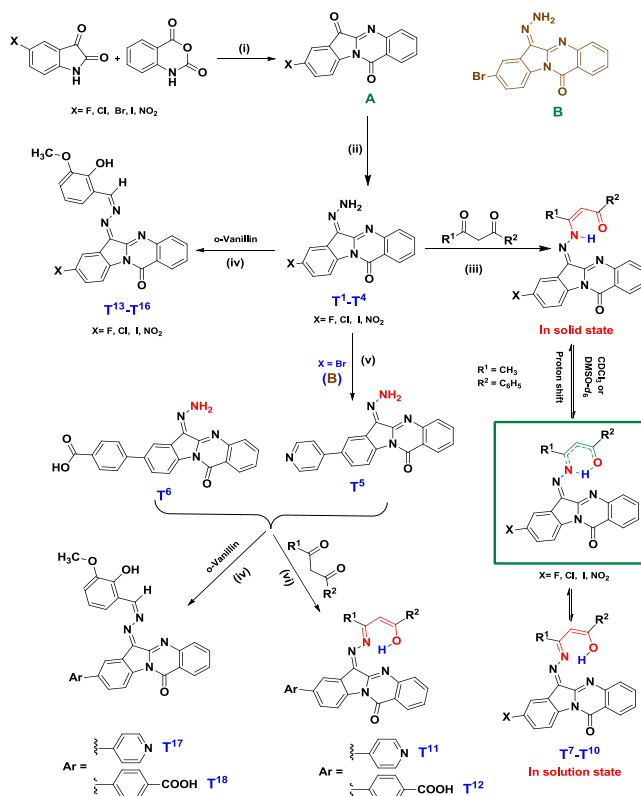


Fig. 1. Some biologically potent 8-substituted-6-hydranoindolo[2,1-*b*]quinazolin-12-(6*H*)-one derivatives.

against many cancer cell lines in mammalian cells.²⁵ This compound can control the activity of COX-2^{26,27} and inhibits the expression of nitric oxide synthase and prostaglandin E(2) in cells.^{28–30} Even though tryptanthrin has wide range of applications it has some small drawback such as poor aqueous solubility as well. Inspiring with the aforementioned fascinating importance of the tryptanthrin scaffolds, we are interested to develop some new tryptanthrin based anti-cancer agents and IDO1 inhibitor.

In literature 8-fluoro substituted tryptanthrin derivatives were successfully demonstrated as potential anti-cancer agent and IDO1-inhibitor,³¹ wherein, 8-bromo substituted hydrazono tryptanthrins were found to be an excellent cytotoxic agents as well as a good inhibitors for IDO-1 enzyme. The *in vitro* anti-cancer activity and molecular docking studies were also well exploited in our previous report.³² Herein, we have disclosed the design and synthesis of a series of 18 novel 8-substituted (F, Cl, I, NO₂, 4-pyridyl or 4-carboxyphenyl) tryptanthrin analogues **T**¹–**T**¹⁸ (Scheme 1 and Fig. 2) and investigated their anti-cancer evaluation by MTT assay using human cancer cell lines MCF-7, A549, HeLa and anti-oxidant activity screening by using DPPH radical scavenging method. The molecular docking studies were also performed using the three target proteins IDO1, EGFR and HER2. The tryptanthrin analogues **T**¹–**T**⁴ were prepared by adapting the literature protocol and using the respective substituted (F, Cl, Br, I and NO₂) indoline-2,3-dione and 2*H*-benzo[*d*][1,3]oxazine-2,4(1*H*)-dione followed by the facile condensation using the hydrazine hydrate in presence of acid.³³ Compounds **T**¹–**T**⁴ afforded **T**⁷–**T**¹⁰ and **T**¹³–**T**¹⁶ after the reaction with benzoyl acetone and *o*-vanillin, respectively in presence of acetic acid and following the literature protocol.^{34,35} Moreover, Suzuki coupling reaction of respective boronic acid and bromo substituted tryptanthrin analogue (see Scheme 1) gave **T**⁵ and **T**⁶. However, **T**¹¹ and **T**¹² were prepared by refluxing **T**⁵ and **T**⁶ with benzoyl acetone. In similar manner, **T**⁵ and **T**⁶ also afforded **T**¹⁷ and **T**¹⁸ after the reaction with *o*-vanillin. The synthetic route adapted for the preparation of all the aforementioned 8-substituted-6-hydranoindolo[2,1-*b*]quinazolin-12-(6*H*)-one and its derivatives were illustrated in Scheme 1. Whereas, details of the synthesis and characterization of these tryptanthrin analogues **T**¹–**T**¹⁸ were depicted in Supporting Information (Figs. S1–S14).

The ¹H NMR spectra of the compounds **T**¹–**T**⁶ showed two signals in the range of δ 11.02–11.35 ppm and δ 10.20–10.55 ppm, which is assigned as NH₂ protons. However, compounds **T**⁷–**T**¹² exhibits a signal in the region of δ 13.65–16.25 ppm, which corresponds to the enolic proton (–OH). The singlet appeared in the region of δ 5.45–6.35 ppm attributed to the alkene (=CH–) proton. For compounds **T**¹³–**T**¹⁸ singlet related to the =CH proton appeared in the region δ 8.57–8.45 ppm. The ¹³C NMR spectra showed the



Scheme 1. (i) Et₃N, 2–4 h, toluene, reflux. (ii) NH₂-NH₂·H₂O, 12 h, THF, reflux. (iii) Acetic acid, benzoyl acetone, reflux. (iv) *o*-vanillin, CH₃OH, reflux 12 h. (v) Na₂CO₃ (20 mL, PdCl₂(PPh₃)₂, DMF, 9 h, 110 °C, 4-pyridineboronic acid or 4-carboxyphenyl boronic acid. (vi) Acetic acid, benzoyl acetone, reflux.

signals in the region of δ 198.2–187.8 and δ 167.8–155.7 ppm related to the enolic carbon and carbonyl group of quinazoline ring and thus strengthens the aforementioned statement. The FT-IR spectrum of **T**¹² also displays peaks in the region of 3332–3375 cm⁻¹ and at 1738 cm⁻¹, which are assigned for the ν (OH) and ν (C=O), respectively. The LCMS spectrum of the compounds **T**¹¹ and **T**¹² shows peaks at *m/z* 485 and 425, which is related to the [M+H]⁺ peak of the **T**¹¹ and **T**¹², respectively.

Cytotoxic activity

All these 8-substituted-6-hydranoindolo[2,1-*b*]quinazolin-12-(6*H*)-one derivatives **T**¹–**T**¹⁸ were evaluated for their *in vitro* anti-cancer activity against the human breast cancer MCF-7, Lung cancer A549 and HeLa cervical cancer cell lines according to procedure described in literature and taking cisplatin as the reference drug.^{36,37} The structure of most potent tryptanthrin derivative is shown in Fig. 3. The relationship between surviving fraction and drug concentration was plotted to obtain the survival curves of MCF-7, A549 and HeLa (Fig. 4). The response parameter calculated was the IC₅₀ value, which corresponds to the concentration required for 50% inhibition of cell viability. Among all the 8-substituted-6-hydranoindolo[2,1-*b*]quinazolin-12-(6*H*)-one derivatives used in this studies compounds **T**⁸, **T**⁹, **T**¹¹ and **T**¹² shows better potent behavior than others. In particular **T**¹¹ and **T**¹² are showing most potent cytotoxicity against three tumor cell lines with their IC₅₀ values of 11.60 ± 1.821 μM, 9.42 ± 1.239 μM against MCF-7, 6.01 ± 1.116 μM, 7.19 ± 0.991 μM against A549 and 12.20 ± 0.239 μM, 9.42 ± 1.594 μM against HeLa, respectively, compared to the standard drug cisplatin. Compounds **T**⁸ and **T**⁹ shown moderate IC₅₀ values of 19.71 ± 0.937 μM, 19.89 ± 1.44 μM for

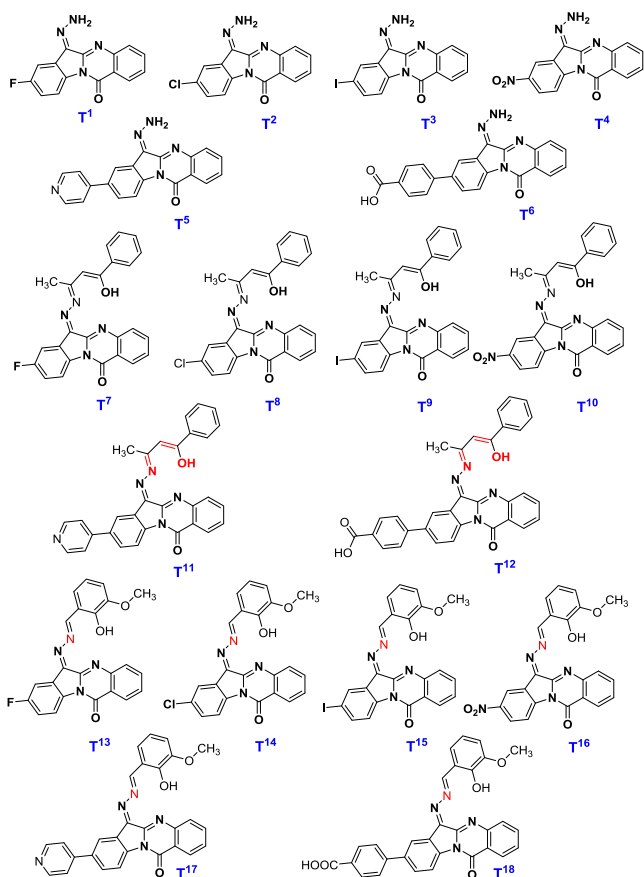


Fig. 2. Chemical structures of all the 8-substituted-6-hydrazoneindolo[2,1-*b*]quinazolin-12-(6*H*)-one derivatives.

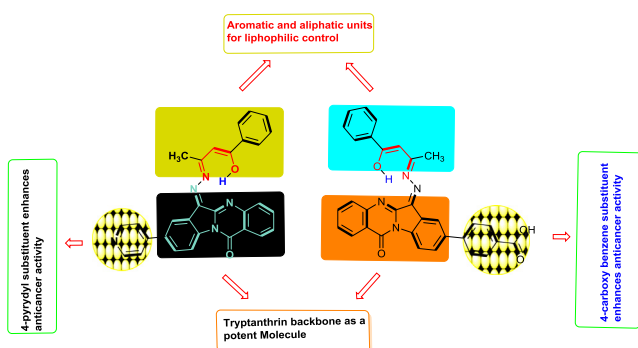


Fig. 3. Structures of most potent 8-substituted-6-hydrazoneindolo[2,1-*b*]quinazolin-12-(6*H*)-one analogues **T¹¹** and **T¹²**.

MCF-7, $18.07 \pm 0.375 \mu\text{M}$, $20.36 \pm 1.832 \mu\text{M}$ for A549 and $23.64 \pm 1.629 \mu\text{M}$, $18.82 \pm 1.168 \mu\text{M}$ for HeLa, respectively. These results indicate that compounds **T⁸**–**T¹²** show good cytotoxic activity towards the three cell lines MCF-7, A549 and HeLa. Under identical conditions the remaining compounds exhibit poor anticancer activity with the IC_{50} values ranging from $20.368 \pm 0.190 \mu\text{M}$ to $67.68 \pm 0.862 \mu\text{M}$ for the three cell lines. We have also screened cytotoxic activity of **T⁸**–**T¹²** against HEK-293 (Human Embryonic Kidney-293) using MTT-micro cultured tetrazolium assay and noticed IC_{50} values of $76.09 \pm 0.901 \mu\text{M}$, $64.12 \pm 1.482 \mu\text{M}$, $71.04 \pm 1.034 \mu\text{M}$ and $82.54 \pm 0.694 \mu\text{M}$ for **T¹¹**, **T¹²**, **T⁸** and **T⁹**, respectively and the detail results are presented in

Table 1. Notably and importantly, the results summarized in Table 1 advocated that there are no adverse effects noticed on the normal cell lines.

A closer look of the structure-activity relationship demonstrates that usually the potency of heterocyclic compounds towards biological activity mostly depends on the position and type of substituents present on the core scaffold. Substituents present at C2 and C8 position of indole and quinazolinone rings in tryptanthrin changes the cytotoxic activity against different cell lines.^{31,32} However, substituents which can influence the core moiety either by donating electrons or by withdrawing the electron density of indole ring of the tryptanthrin also effects the cytotoxicity proficiency against the different human cancer cell lines. In this work we have noticed enhanced cytotoxic activity in case of 4-pyridyl and 4-carboxyphenyl substituted (at 8th position) tryptanthrin derivatives against three human cancer cell lines MCF-7, A549 and HeLa compared with non-substituted tryptanthrin derivatives and less cytotoxicity against HEK293 (normal human cancer cell line).

In vitro anti-oxidant assay

In order to investigate the potential application of **T¹**–**T¹⁸** towards the *in vitro* anti-oxidant activity, DPPH radical scavenging assay was performed. In this experiment, 10^{-6} molar methanolic solution of the concerned compounds was used followed by the serial dilution. In small test tubes 1 mL (in each tube) mixture of scaffold (100 μL) and DPPH radical (10^{-4} M, 900 μL) were taken and incubated at 37 °C under dark conditions for 30 min (French et al. 1994). The absorbance of the DPPH solution and mixture was recorded using the UV–visible spectrophotometer. The DPPH solution exhibits λ_{max} of 517 nm (typical range of DPPH radical, Blois et al. 1958; Lu and Foo, 2000; Zhu et al. 2002). Notably, the absorbance decreases in presence of the concerned compounds with the colour change from blue to yellow. In principle, DPPH has an odd electron and thus can accept an electron or hydrogen free radical and or also able to liberate this free radical, which can be scavenged by synthesized compounds. The shifting of absorbance value towards the lower wavelength side indicates the increasing radical scavenging activity of the test compounds (Gulçin et al. 2004). The percentage of inhibition values were compared by using absorbance values of standard ascorbic acid under identical conditions. The anti-oxidant activity was considered in IC_{50} in μM (the effective concentration at which 50% of the radicals were scavenged) and shown in Table 2.^{38,39} Moreover, all the samples were tested in triplicate to maintain the accuracy and to find out the standard deviation.⁴⁰ From Table 2, it is clear that these synthesized compounds showed remarkable anti-oxidant activity compared to the standard drug. Importantly, compounds **T¹¹**, **T¹²**, **T¹⁷** and **T¹⁸** were found to be the most potent anti-oxidants with the least IC_{50} values of 6.23 μM (for **T¹¹**), 5.02 μM (for **T¹²**), 4.98 μM (for **T¹⁷**) and 5.31 μM (for **T¹⁸**), respectively, among all the synthesized compounds.

We argued that, this better *in vitro* anti-oxidant activity of compounds **T¹¹**, **T¹²**, **T¹⁷** and **T¹⁸** might be due to the presence of electron-rich functionality such as 4-pyridyl or 4-carboxyphenyl in the tryptanthrin scaffolds. The proton exchange capability between carbonyl and –NH group of compounds **T¹¹** and **T¹²** may possibly be another aspect for enhanced radical scavenging activity. Moreover, **T⁵**, **T⁸**, **T⁹**, and **T¹⁵** displaying moderate anti-oxidant activity compared with standard ascorbic acid having the IC_{50} values of 11.23 μM (for **T⁵**), 12.45 μM (**T⁸**), 11.60 μM (for **T⁹**) and 10.90 μM (for **T¹⁵**), respectively. The remaining compounds exhibit reasonable to poor anti-oxidant activity with IC_{50} value ranging from 16.45 μM to 29.71 μM . Notably, **T¹⁰** and **T¹⁶** shows

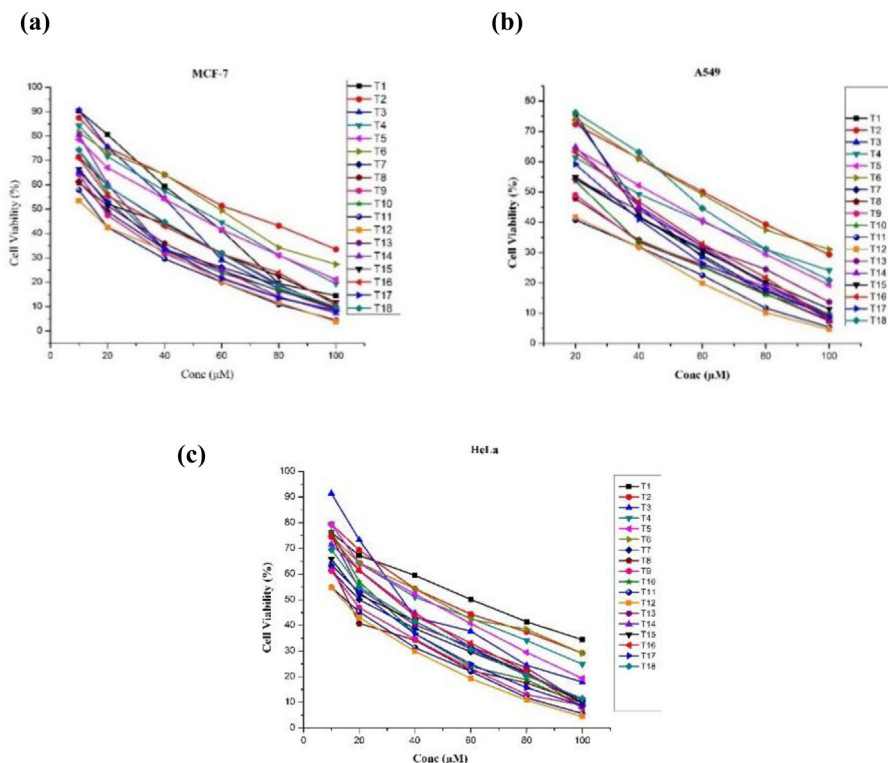


Fig. 4. (a–c) Survival curves of MCF-7, A549 and HeLa cell lines.

Table 1
Cytotoxic activities of newly synthesized 8-substituted-6-hydrazoneindolo[2,1-*b*]quinazolin-12-(6*H*)-one derivatives **T¹–T¹⁸** on human cancer cell lines MCF-7, A549 and HeLa [*in vitro* (IC₅₀ µM)].^a

S. No.	Compound	MCF-7	A549	HeLa	HEK293
1	T¹	54.55 ± 0.871	44.59 ± 0.974	67.68 ± 0.862	ND
2	T²	67.51 ± 1.453	62.12 ± 1.190	55.67 ± 1.122	ND
3	T³	44.94 ± 0.841	43.44 ± 1.454	51.05 ± 1.091	ND
4	T⁴	53.56 ± 0.745	45.55 ± 0.896	50.29 ± 0.540	ND
5	T⁵	50.38 ± 0.977	47.76 ± 0.511	44.12 ± 0.801	ND
6	T⁶	61.10 ± 1.004	62.16 ± 0.540	54.26 ± 1.538	ND
7	T⁷	20.368 ± 0.190	32.00 ± 1.230	24.46 ± 0.836	ND
8	T⁸	19.71 ± 0.937	18.07 ± 0.375	23.64 ± 1.629	71.04 ± 1.034
9	T⁹	19.89 ± 1.44	20.36 ± 1.832	18.82 ± 1.168	82.54 ± 0.694
10	T¹⁰	31.52 ± 1.234	28.39 ± 0.708	33.10 ± 0.300	ND
11	T¹¹	11.60 ± 1.821	6.01 ± 1.116	12.20 ± 0.239	76.09 ± 0.901
12	T¹²	9.42 ± 1.239	7.19 ± 0.991	9.42 ± 1.594	64.12 ± 1.482
13	T¹³	35.51 ± 1.11	31.20 ± 1.075	34.28 ± 0.886	ND
14	T¹⁴	35.38 ± 0.982	40.84 ± 1.234	36.56 ± 1.547	ND
15	T¹⁵	30.38 ± 1.021	32.29 ± 1.964	29.22 ± 1.237	ND
16	T¹⁶	34.25 ± 0.237	40.06 ± 0.873	38.03 ± 0.966	ND
17	T¹⁷	24.77 ± 1.568	32.87 ± 1.342	24.77 ± 1.452	ND
18	T¹⁸	37.07 ± 1.471	39.25 ± 1.803	32.29 ± 1.053	ND
19	Cisplatin	4.28 ± 0.355	5.14 ± 0.421	3.88 ± 0.354	ND

^a Values are expressed as mean ± SEM. Cytotoxicity as IC₅₀ for each cell line, is the concentration of compound which is reduced by 50% the optical density of treated cell with respect to untreated cell using the MTT assay.

poorest anti-oxidant activity among all the synthesized compounds with IC₅₀ values of 29.71 µM and 28.68 µM, respectively (Table 2) attributed to the presence of electron withdrawing -NO₂ group at 8-position of the tryptanthrin framework.

Molecular docking studies

Docking investigation was performed to compounds **T¹–T¹⁸** with pharmacological target proteins, indoleamine 2,3-dioxyge-

nase (IDO1), epidermal growth factor receptor (EGFR) and human epidermal growth factor receptor 2 (HER2) to compare their potential as drug candidates. IDO1, which is an attractive target in design of anti-cancer drugs as it catalyzes essential amino acid *l*-tryptophan to *N*-formylkynurenine.⁴¹ In principle, IDO1 is the primary and rate-limiting enzyme of tryptophan catabolism and responsible for the depletion of tryptophan leading to halted growth of microbes as well as *T*-cells.⁴² The EGFR is well known receptor for the members of epidermal growth factor family of extracellular

Table 2Anti-oxidant activity of 8-substituted-6-hydrazoneindolo[2,1-b]quinazolin-12-(6H)-one derivatives (**T**¹–**T**¹⁸) by DPPH assay.

S. No	Compounds	IC ₅₀ (μm)
1	T ¹	16.45
2	T ²	19.87
3	T ³	24.87
4	T ⁴	27.32
5	T ⁵	11.23
6	T ⁶	21.96
7	T ⁷	20.14
8	T ⁸	12.45
9	T ⁹	11.60
10	T ¹⁰	29.71
11	T ¹¹	6.23
12	T ¹²	5.02
13	T ¹³	21.07
14	T ¹⁴	22.21
15	T ¹⁵	10.90
16	T ¹⁶	28.68
17	T ¹⁷	4.98
18	T ¹⁸	5.31
Standard	Ascorbic acid	3.48

protein.⁴³ It induces receptor dimerization and tyrosine autophosphorylation and leads to cell proliferation, differentiation, motility and cell survival^{44–46} Over expression of EGFR is up regulated in colon cancers and most neoplasms. Whereas, mutations comprising EGFR lead to its constant activation and produces uncontrolled cell division.^{47,48} Moreover, HER2 is a member of human epidermal growth factor receptor (HER/EGFR/ERBB) family. The overexpression of oncogene play a vital role in the development and propagation of certain types of cancers such as breast, lung, stomach, ovarian, adenocarcinoma and uterine cancer (uterine serous epidermal carcinoma).^{49,50} For the reason that we have chosen IDO1, EGFR and HER2 proteins as the target receptors for the docking studies and their comparative binding energy are compiled in Table 3 (readers are advised to refer the Supporting Information for the details of docking protocol). Whereas, hydrogen bonding profile for the compounds **T**¹–**T**¹⁸ are shown in Table 4 along with residues. The comparative molecular docking demonstrations of the organic scaffolds **T**¹–**T**¹⁸ with the target receptors IDO1, EGFR and HER2 (as shown in Table 3) clearly indicates that the affinity of these drug candidates with receptor IDO1 is better than that of receptors EGFR and HER2 and that's why we have chooses

Table 3Comparative binding energies of 8-substituted-6-hydrazoneindolo[2,1-b]quinazolin-12-(6H)-one compounds **T**¹–**T**¹⁸ against IDO1, EGFR and HER2.

S. No.	Compound	Binding Energy (kcal mol ⁻¹) IDO1 (PDB id: 2dU0)	Binding Energy (kcal mol ⁻¹) EGFR (PDB id: 4hjo)	Binding Energy (kcal mol ⁻¹) HER2 (PDB id: 3ppo)
1	T ¹	-8.22	-7.24	-7.80
2	T ²	-8.88	-7.69	-7.80
3	T ³	-9.47	-8.09	-7.68
4	T ⁴	-9.04	-7.86	-7.92
5	T ⁵	-9.92	-8.94	-9.07
6	T ⁶	-8.10	-9.08	-9.29
7	T ⁷	-10.79	-8.91	-10.79
8	T ⁸	-11.20	-10.43	-10.63
9	T ⁹	-11.71	-10.76	-9.59
10	T ¹⁰	-10.91	-11.00	-10.47
11	T ¹¹	-11.73	-10.06	-10.20
12	T ¹²	-11.61	-10.49	-9.84
13	T ¹³	-10.52	-9.53	-9.84
14	T ¹⁴	-9.83	-9.05	-10.92
15	T ¹⁵	-10.31	-9.83	-10.88
16	T ¹⁶	-10.00	-9.59	-11.29
17	T ¹⁷	-10.80	-8.89	-10.84
18	T ¹⁸	-9.96	-9.41	-10.12

Table 4Binding energies, number of hydrogen bonds and residues involved in hydrogen bonding of compounds 8-substituted-6-hydrazoneindolo[2,1-b]quinazolin-12-(6H)-one **T**¹–**T**¹⁸ against IDO1.

S. No.	Compound	Binding Energy (kcal mol ⁻¹)	Number of hydrogen bonds	Residues
1	T ¹	-8.22	2	Ser167
2	T ²	-8.88	2	Ser267, Glu171
3	T ³	-9.47	2	Ser267, Glu171
4	T ⁴	-9.04	2	Ser167
5	T ⁵	-9.92	2	Glu171
6	T ⁶	-8.10	2	Arg343
7	T ⁷	-10.79	1	His346
8	T ⁸	-11.20	2	His346, Ala264
9	T ⁹	-11.71	1	His346
10	T ¹⁰	-10.91	2	His346, Ser263
11	T ¹¹	-11.73	1	His346
12	T ¹²	-11.61	1	His346
13	T ¹³	-10.52	3	Ser267, Ser167, His346
14	T ¹⁴	-9.83	2	His346
15	T ¹⁵	-10.31	2	His346
16	T ¹⁶	-10.00	2	Ser267, His346
17	T ¹⁷	-10.80	1	Ala234
18	T ¹⁸	-9.96	1	Arg343

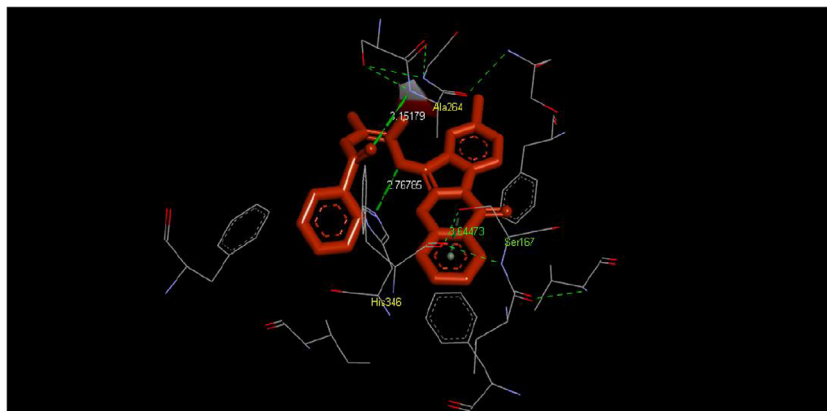


Fig. 5. Shows the binding poses and interactions of 8-substituted-6-hydrazonoindolo[2,1-*b*]quinazolin-12-(6*H*)-one analogue **T⁸** to the binding sites of target protein **IDO1** (PDB ID: 2d0U).

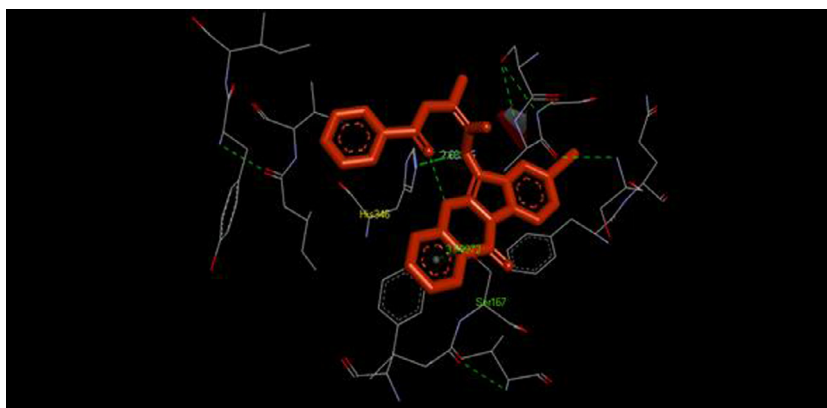


Fig. 6. Shows the binding poses and interactions of 8-substituted-6-hydrazonoindolo[2,1-*b*]quinazolin-12-(6*H*)-one analogue **T⁹** to the binding sites of target protein **IDO1** (PDB ID: 2d0U).

IDO1 as the target receptor for the details discussion. Out of these series of drug candidates exploited for the doc score, scaffolds **T¹²**, **T¹¹**, **T⁹** and **T⁸** are found to be the best inhibitors and their probable reasons are discussed below.

From [Table 3](#) it is clear that **T⁸** is a potential candidate for the anticancer drug with the binding energy of $-11.20 \text{ kcal mol}^{-1}$. Notably, **T⁸** exhibits strong hydrogen bonding interactions between amino acid His346 and *N*-atom of hydrazine tryptanthrin as well as between Ala264 and carbonyl group of benzoyl acetone with bond length of 2.7678 Å and 3.1517 Å, respectively ([Fig. 5](#)). All the other interactions are hydrophobic in nature and found between the amino acid of target receptor IDO1 and phenyl ring of tryptanthrin core with the bond distance of 3.6445 Å, which is off course larger than the drug – receptor hydrogen bonding interaction.

In a similar fashion drug **T⁹** (binding energy, $-11.71 \text{ kcal mol}^{-1}$, [Tables 3 and 4](#)) also exhibit hydrogen bonding interaction with receptor IDO1 ([Fig. 6](#)). Which takes place between His346 and nitrogen atom of hydrazono group of the tryptanthrin core with bond distance of 2.6800 Å. Whereas, the hydrophobic interaction observed between the phenyl ring of quinazoline fused tryptanthrin core and Ser167 with bond distance 3.9972 Å. Furthermore, **T¹¹** also shows drug – receptor hydrogen bonding interaction (binding energy, $-11.73 \text{ kcal mol}^{-1}$, [Tables 3 and 4](#)) analogous to **T⁹** ($-11.71 \text{ kcal mol}^{-1}$). In this case hydrogen bonding interaction took place in between His346 and nitrogen atom of hydrazono group appended to tryptanthrin moiety with bond distance of 2.7190 Å ([Fig. 7](#)). Drug **T¹¹** also features hydrophobic interactions between Ala264 and carbonyl group of benzoyl acetone attached with

tryptanthrins core in addition to interactions between Ser167 and phenyl ring of quinazoline induced tryptanthrin framework having the distance of 3.2152 Å and 3.6072 Å, respectively. The structure of complex derived from the interaction of **T¹²** and receptor IDO1 also displays hydrogen bonding interaction (binding energy, $-11.61 \text{ kcal mol}^{-1}$, [Tables 3 and 4](#)) between His346 and nitrogen atom of hydrazono tryptanthrin core with bond distance of 3.0734 Å ([Fig. 8](#)). This drug-receptor complex also features hydrophobic interaction between Ala264 and carbonyl group of benzoylacetone group of tryptanthrin core with bond distance of 3.1209 Å. Notably, all these cases the synthesized organic scaffolds (**T¹²**, **T¹¹**, **T⁹** and **T⁸**) are interacted with the target protein (receptor IDO1) through the hydrogen bonding between His346, Ala264 and/or Ser167 and different substituted functionality of the tryptanthrin core. Whereas, the affinity between the target receptor and drug candidates are enhanced via the hydrophobic interactions.⁵¹ Notably, compounds other than **T¹²**, **T¹¹**, **T⁹** and **T⁸** display moderate dock score and binding affinity against all the three protein receptors IDO1, EGFR and HER2 (see [Table 3](#) for details).

In summary, 18 novel, 8-substituted-6-hydrazonoindolo[2,1-*b*]quinazolin-12-(6*H*)-ones **T¹**–**T¹⁸** were synthesized by well-established synthetic protocol followed by the Suzuki coupling reaction and screened for their anti-oxidant, anti-cancer and molecular docking studies. The compounds **T¹²**, **T¹¹**, **T¹⁷** and **T¹⁸** were found to be the most potent anti-oxidant agents by DPPH radical scavenging assay. Whereas, **T¹²**, **T¹¹**, **T⁸** and **T⁹** are showing a promising anti-cancer activity against the MCF-7, A549, HeLa human cancer cell lines using the MTT assay protocol and using cisplatin as a

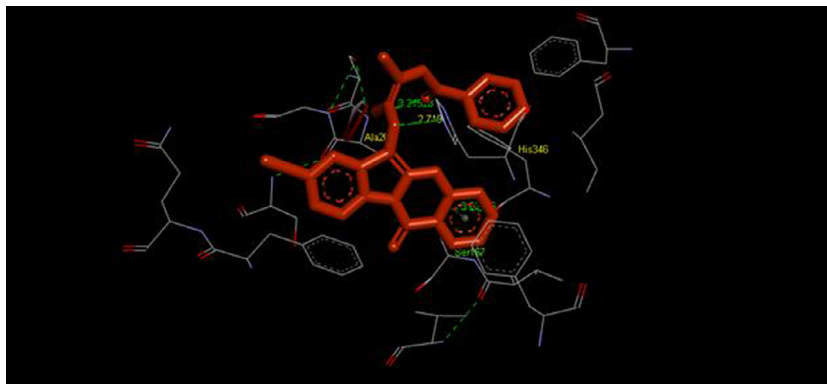


Fig. 7. Shows the binding poses and interactions of 8-substituted-6-hydrazoneindolo[2,1-b]quinazolin-12-(6H)-one analogue **T¹¹** to the binding sites of target protein **IDO1** (PDB ID: 2d0U).

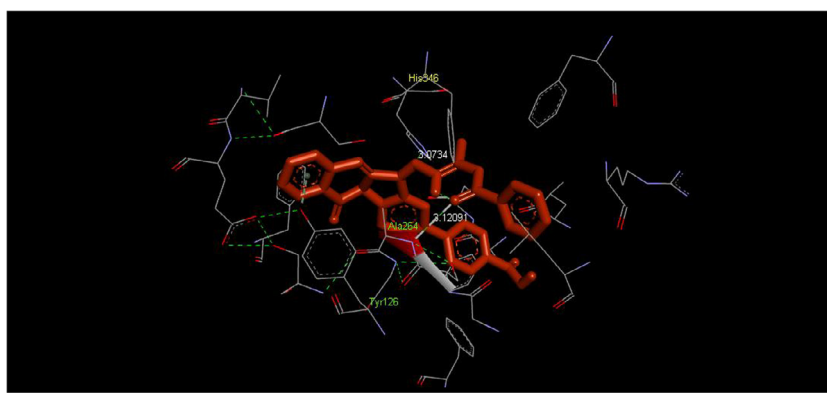


Fig. 8. Shows the binding poses and interactions of 8-substituted-6-hydrazoneindolo[2,1-b]quinazolin-12-(6H)-one analogue **T¹²** to the binding sites of target protein **IDO1** (PDB ID: 2d0U).

reference drug. We reasoned that the presence of 4-pyridyl or 4-carboxyphenyl substituents at 8th position of tryptanthrin framework might be a cause for their potent anti-cancer and anti-oxidant activity. The comparative molecular docking studies have been also performed against the three protein receptors IDO1, EGFR and HER2 and found IDO1 is the best one with binding energies of $-11.73 \text{ kcal mol}^{-1}$, $-11.61 \text{ kcal mol}^{-1}$, $-11.20 \text{ kcal mol}^{-1}$ and $-11.20 \text{ kcal mol}^{-1}$ for compounds **T¹²**, **T¹¹**, **T⁸**, and **T⁹**, respectively. Importantly, molecules having the lowest binding energies are also displaying the highest cytotoxicity against the tested MCF-7, A549, HeLa human cancer cell lines. In a similar fashion, compounds with the better binding energies also showing excellent anti-oxidant. Moreover, this results will provide advantage to the medicinal chemist in the design and development of new tryptanthrin based anti-cancer drugs in near future.

Acknowledgements

We gratefully acknowledge Prof. Samar K. Das and UGC-Networking Resource Center of the School of Chemistry, University of Hyderabad for the analytical data collection. The financial assistance from the University Grant Commission (UGC), New Delhi is also acknowledged.

A. Supplementary data

Supplementary data associated with this article can be found, in the online version, at <http://dx.doi.org/10.1016/j.bmcl.2017.08.064>.

References

- Varmus H. The new era in cancer research. *Front Cancer Res.* 2006;312:1162–1165.
- Higginson IJ, Costantini M. Dying with cancer, living well with advanced cancer. *Eur J Cancer.* 2008;44:1414–1425.
- Siegel R, Naishadham D, Jemal A. Cancer statistics. *CA Cancer J Clin.* 2013;63:11–30.
- Arun Y, Bhaskar G, Balachandran C, Ignacimuthu S, Perumal PT. Facile one-pot synthesis of novel dispirooxindole-pyrrolidine derivatives and their antimicrobial and anticancer activity against A549 human lung adenocarcinoma cancer cell line. *Bioorg Med Chem Lett.* 2013;23:1839–1845.
- Parthasarathy K, Praveen C, Balachandran C, Senthil Kumar P, Ignacimuthu S, Perumal PT. Cu(OTf)₂ catalyzed three component reaction: Efficient synthesis of spiro[indoline-3,4'-pyrano[3,2-b]pyran derivatives and their anticancer potency towards A549 human lung cancer cell lines. *Bioorg Med Chem Lett.* 2013;23:2708–2713.
- Girgis AS. Regioselective synthesis of dispiro[1H-indene-2,3'-pyrrolidine-2',3''-[3H]indole]-1,2''(1''H)-diones of potential anti-tumor properties. *Eur J Med Chem.* 2009;44:91–100.
- Esch EW, Bahinski A, Huh D. Organs-on-chips at the frontiers of drug discovery. *Nat Rev Drug Discovery.* 2015;14:248–260.
- Hashimoto T, Aga H, Chaen H, Fukuda S, Kurimoto M. Isolation and identification of anti-Helicobacter pylori compounds from polygonum tinctorium Lour. *Nat Med Tokyo.* 1999;53:27–31.
- Wang J, Tan H, Li Y, Ma Y, Li Z, Guddat LW. Chemical synthesis, in vitro acetohydroxyacid synthase (AHAS) inhibition, herbicidal activity, and computational studies of isatin derivatives. *J Agric Food Chem.* 2011;59:9892–9900.
- Zhang X-M, Guo H, Li Z-S, et al. Synthesis and evaluation of isatin-β-thiosemicarbazones as novel agents against antibiotic-resistant Gram-positive bacterial species. *Eur J Med Chem.* 2015;101:419–430.
- Surendra NP, Sivakumar S, Mayank J, Seshiah KS. Biological activities of isatin and its derivatives. *Acta Pharm.* 2005;55:27–46.
- Tan HZ, Wang WM, Shang JL, Song HB, Li ZM, Wang JG. Syntheses, crystal structures and bioactivities of two isatin derivatives. *Chin J Struct Chem.* 2011;30:502–507.
- Haga T, Nagano H, Enomoto M, Morita K, Sato M. Preparation of isatin derivatives as herbicides. Jpn. Patent 63313770: 1988

14. Schreiber K, Stephan U, Wegner G. Agent for controlling the growth of clover, especially red clover. Ger. Patent DD121011:1976.
15. Hamsch E. Isatins as selective herbicides. Ger. Patent DE1013469:1957.
16. Bird CW. The structure of methylisatoid. *Tetrahedron*. 1963;19:901–904.
17. Bhattacharjee AK, Skanchy DJ, Jennings B, Hudson TH, Brendle JJ, Werbovitz KA. Analysis of stereo electronic properties, mechanism of action and pharmacophore of synthetic indolo[2,1-b]quinazoline-6,12-dione derivatives in relation to antileishmanial activity using quantum chemical, cyclic voltammetry and 3-D-QSAR CATALYST procedures. *Bioorg Med Chem*. 2002;10:1979–1989.
18. Honda G, Tabata M, Tsuda M. The antimicrobial specificity of tryptanthrin. *Planta Med*. 1979;37:172–174.
19. Bandekar PP, Roopnarine KA, Parekh VJ, Mitchell TR, Novak MJ, Sinden RR. Antimicrobial activity of tryptanthrins in *Escherichia coli*. *J Med Chem*. 2010;53:3558–3565.
20. Mitscher LA, Baker W. Tuberculosis: A search for novel therapy starting with natural products. *Med Res Rev*. 1998;18:363–374.
21. Takei Y, Kunikata T, Aga M, et al. Tryptanthrin inhibits interferon-gamma production by Peyer's patch lymphocytes derived from mice that had been orally administered staphylococcal enterotoxin. *Biol Pharm Bull*. 2003;26:365–367.
22. Recio MC, Cerda-Nicolas M, Potterat O, Humburger M, Rios JL. Anti-inflammatory and antiallergic activity in vivo of lipophilic Isatis tinctoria extracts and tryptanthrin. *Planta Med*. 2006;72:539–546.
23. Johnson RK, Hertzberg RP. Cholinergic side effects previously reported with elliptinium acetate. *Annu Rep Med Chem*. 1990;25:129–138.
24. Kotaiah Y, Nagaraju K, Harikrishna N, Venkata Rao C, Yamini L, Vijjulatha M. Synthesis, docking and evaluation of antioxidant and antimicrobial activities of novel 1,2,4-triazolo[3,4-b][1,3,4]thiadiazol-6-yl)selenopheno[2,3-d]pyrimidines. *Eur J Med Chem*. 2014;75:195–202.
25. Sharma VM, Prasanna P, Seshu KV, et al. Novel indolo[2,1-b]quinazoline analogues as cytostatic agents: synthesis, biological evaluation and structure-activity relationship. *Bioorg Med Chem Lett*. 2002;12:2303–2307.
26. Danz H, Stoyanova S, Wippich P, Brattstrom A, Hamburger M. Identification and isolation of the cyclooxygenase-2 inhibitory principle in *Isatis tinctoria*. *Plant Med*. 2001;67:411–416.
27. Danz H, Stoyanova S, Thomet OA, Simon HU, Dannhardt G, Hamberger Ulbrich H. Inhibitory activity of tryptanthrin on prostaglandin and leukotriene synthesis. *Planta Med*. 2002;68:875–880.
28. Motoki T, Takami Y, Yagi Y, Tai A, Yamamoto I, Gohda E. Inhibition of hepatocyte growth factor induction in human dermal fibroblasts by tryptanthrin. *Biol Pharm Bull*. 2005;28:260–266.
29. Yu ST, Chen TM, Tseng SY, Chen YH. Tryptanthrin inhibits MDR1 and reverses doxorubicin resistance in breast cancer cells. *Biochem Biophys Res Commun*. 2007;358:79–84.
30. Ishihara T, Kohno K, Ushio S, Iwaki K, Ikeda M, Kurimoto M. Tryptanthrin inhibits nitric oxide and prostaglandin E2 synthesis by murine macrophages. *Eur J Pharmacol*. 2000;407:197–204.
31. Yang S, Li X, Hu F, et al. Discovery of tryptanthrin derivatives as potent inhibitors of indoleamine 2,3-dioxygenase with therapeutic activity in Lewis Lung Cancer (LLC) tumor-bearing mice. *J Med Chem*. 2013;56:8321–8331.
32. Guda R, Narsimha S, Babu R, et al. Novel substituted hydrazono indolo[2,1-b]quinazoline-6,12-dione analogues as cytostatic agents: Synthesis, crystal structure, biological evaluation and molecular docking studies. *Bioorg Med Chem Lett*. 2016;26:5517–5523.
33. Krivogorsky B, Amber Nelson C, Kelsi Douglas A, Grund P. Tryptanthrin derivatives as *Toxoplasma gondii* inhibitors—structure–activity–relationship of the 6-position. *Bioorg Med Chem Lett*. 2013;23:1032–1035.
34. Tucker AM, Grundt P. The chemistry of tryptanthrin and its derivatives. *ARKIVOC*. 2012;1:546–569.
35. Agarwal PK, Sharma SK, Sawant D, Kundu B. Application of the Pictet–Spengler reaction to aryl amine-based substrates having pyrimidine as a π -nucleophile: synthesis of pyrimidoquinolines with structural analogy to benzonaphthridines present in alkaloids. *Tetrahedron*. 2009;65:1153–1161.
36. Shekan P, Storeng R, Scudiero D, et al. New colorimetric cytotoxicity assay for anticancer-drug screening. *Natl Cancer Inst*. 1990;82:1107.
37. Monks A, Scudiero D, Shekan P, et al. Feasibility of a high-flux anticancer drug screen using a diverse panel of cultured human tumor cell lines. *J Natl Cancer Inst*. 1991;83:757–766.
38. Burits M, Bucar F. Antioxidant activity of *Nigella sativa* essential oil. *Phytother Res*. 2000;14:323–328.
39. Cuendet M, Hostettmann K, Potterat O. Iridoid glucosides with free radical scavenging properties from *Fagraea blumei*. *Helv Chim Acta*. 1997;80:1144–1152.
40. Gul MZ, Ahmad F, Kondapi AK, Qureshi IA, Ghazi IA. Antioxidant and antiproliferative activities of *Abrus precatorius* leaf extracts—an in vitro study. *BMC Complem Altern Med*. 2013;13:53.
41. "Entrez Gene: INDO indoleamine-pyrrole 2,3 dioxygenase".
42. Wang J, Yu L, Jiang C, Chen M, Ou C, Wang J. Bone marrow mononuclear cells exert long-term neuroprotection in a rat model of ischemic stroke by promoting arteriogenesis and angiogenesis. *J Brain Behav Immun*. 2013;34:56–66.
43. Herbst RS. Review of epidermal growth factor receptor biology. *Int J Rad Oncol Biol Phys*. 2004;59:21–26.
44. Sebastian J, Richards RG, Walker MP, et al. Activation and function of the epidermal growth factor receptor and erbB-2 during mammary gland morphogenesis. *Cell Growth Differ*. 1998;9:777–785.
45. McBryan J, Howlin J, Napoletano S, Martin F. Amphiregulin: role in mammary gland development and breast cancer. *J Mam Gland Biol Neopl*. 2008;13:159–169.
46. Sternlicht MD, Sunnar borg SW. The ADAM17-amphiregulin-EGFR axis in mammary development and cancer. *J Mam Gland Biol Neopl*. 2008;13:181–194.
47. Kumar V, Abbas A, Aster J. *Robbins Basic Pathology*. Philadelphia: Elsevier/Saunders; 2013. 179.
48. Lynch TJ, Bell DW, Sordella R, et al. Activating mutations in the epidermal growth factor receptor underlying responsiveness of non-small-cell lung cancer to gefitinib. *N Engl J Med*. 2004;350:2129–2139.
49. Santin AD, Bellone S, Roman JJ, McKenney JK, Pecorelli S. Trastuzumab treatment in patients with advanced or recurrent endometrial carcinoma overexpressing HER2/neu. *Int J Gynaecol Obstet*. 2008;102:128–131.
50. Buza N, Roque DM, Santin AD. HER2/neu in endometrial cancer: a promising therapeutic target with diagnostic challenges. *Arch Pathol Lab Med*. 2014;138:343–350.
51. Davis AM, Teague SJ. Hydrogen bonding, hydrophobic interactions, and failure of the rigid receptor hypothesis. *Angew Chem Int Ed*. 1999;38:736–749.

**Complimentary and personal copy for
Harikiran Lingabathula, Narsimhareddy Yellu**

www.thieme.com

**Extra Pulmonary Toxicity
Assessment of Gold and
Silver Nanorods
Following Intra Tracheal
Instillation in Rats**

**DOI 10.1055/s-0043-113255
Drug Res 2017; 67: 606–612**

This electronic reprint is provided for non-commercial and personal use only: this reprint may be forwarded to individual colleagues or may be used on the author's homepage. This reprint is not provided for distribution in repositories, including social and scientific networks and platforms.

Publishing House and Copyright:

© 2017 by
Georg Thieme Verlag KG
Rüdigerstraße 14
70469 Stuttgart
ISSN 2194-9379

Any further use
only by permission
of the Publishing House



Extra Pulmonary Toxicity Assessment of Gold and Silver Nanorods Following Intra Tracheal Instillation in Rats

Authors

Harikiran Lingabathula, Narsimhareddy Yellu

Affiliation

Department of Pharmacology and Toxicology, University College of Pharmaceutical Sciences, Kakatiya University, Warangal, Telangana, India

Key words

alanine transaminase, creatinine, gold nanorods, silver nanorods, toxicity

received 09.03.2017

accepted 05.06.2017

Bibliography

DOI <https://doi.org/10.1055/s-0043-113255>

Published online: 28.6.2017

Drug Res 2017; 67: 606–612

© Georg Thieme Verlag KG Stuttgart · New York

ISSN 2194-9379

Correspondence

Prof. Y. Narsimha Reddy

Department of Pharmacology and Toxicology

University College of Pharmaceutical Sciences

Kakatiya University, Warangal

506009, Telangana State

India

Tel.: +91/995/9289 089

ynrucpsc@gmail.com

ABSTRACT

The gold nanorods (GNRs) and silver nanorods (SNRs) are utilized in various types of industrial and commercial applications. But, there is limited availability of extra pulmonary toxicity data regarding these nanorods. The present investigation evaluated the extra pulmonary toxicity induced by 10 and 25 nm GNRs and SNRs in rats following intra tracheal instillation. The serum biochemical analysis results have shown elevated levels of serum alanine transaminase (ALT) and serum creatinine following 1 day and 1 week post instillation. GNRs have shown greatly increased serum ALT levels at 1 day, 1 week and 1 month post exposure periods compared to SNRs and quartz (QTZ) treated rats. In case of serum creatinine levels, both GNRs and SNRs have shown similar elevated levels. Histopathology studies of rat liver tissues following exposure of GNRs and SNRs displayed that congestion of central vein, shrinkage and ballooning of hepatocytes and lymphocytic infiltration leading to degeneration after 1 week and 1 month post instillation periods. The histopathology of rat kidney tissue was showed tubular dilation, degeneration and necrosis with 10 nm SNRs and 10 nm GNRs after 1 month post instillation period. The 10 nm GNRs and SNRs have shown great changes in serum biochemical analysis and histopathological studies compared to 25 nm test nanorods. These observations suggest the size and dose dependent translocation and extra pulmonary toxicity of both GNRs and SNRs.

Introduction

Nanoparticle is a particle with any outer dimension should be in the size range from 1 nm to 100 nm or having surface structure or inner structure in the nanoscale range. The nanoparticles such as metal oxide, carbon, gold, silver nanoparticles, fullerenes and quantum dots are available for various applications. The gold nanoparticles (GNPs) and silver nanoparticles (SNPs) are having great potentials in future industrial applications due to their high reactivity, high surface to volume ratio, large plasmon field area, unique physical, chemical, mechanical and optical properties [1, 2].

GNPs and SNPs are utilized in medical devices, surgical instruments, biosensors, textiles, refrigerators, cosmetics, deodorants and packaging materials for food [3–5]. Moreover, the rod shaped gold and silver nanoparticles are finding various industrial and commercial applications. Gold nanorods (GNRs) were used in the can-

cer cell imaging, photothermal therapy, gene therapy, biosensing and biomedical applications [6–9]. GNRs conjugated with photo sensitizers can kill MRSA by near infrared photothermal radiation and photodynamic antimicrobial chemotherapy [10, 11]. Silver nanorods (SNRs) are finding applications in different areas such as textile, painting and food industries, cosmetics, sunscreens, biosensing, medical devices and imaging applications [12, 13]. SNR array electrodes show great potential in the determination of trace chloropropanol [14].

Because of these huge applications of gold and silver nanorods, the occupational exposure for these materials also increased enormously. Recently, some of the studies were conducted on gold and silver nanoparticles in vitro and in vivo and reported the pulmonary toxicities induced by these nanoparticles in different human cell lines and animals [15–17]. However, the size, shape and surface coating of the nanoparticles can also affect the level of toxicity [18–

20]. Although some of the studies were investigated the toxicities of GNRs and SNRs using different human cell cultures [21–23], but there is lack of availability of extra pulmonary toxicity data related to GNRs and SNRs. The present study goal was aimed to assess the potential extra pulmonary toxicity of rod shaped, poly ethyleneglycol (PEG) coated, 10 and 25 nm gold and silver nanorods following intra tracheal instillation in rats, and compare the results with control and quartz (known toxicant; QTZ).

Materials and Methods

Chemicals

The 10 nm GNRs, 25 nm GNRs, 10 nm SNRs and 25 nm SNRs were purchased from Sigma-Aldrich, USA. QTZ particles (58–68 μm ; 99.95 % purity) were procured from Berkely Springs, USA. Phosphate buffer saline (PBS) and PEG were acquired from Himedia, India. All the biochemical assay kits were procured from Ray Biotech, India.

Animals and treatment

6 weeks old male wistar rats were procured from National Institute of Nutrition, Hyderabad, India. The rats were kept in animal house for one week in a quarantine area. Throughout the quarantine and experimental periods, the animals were housed in polypropylene cages in a room, water and feed were available ad libitum with controlled temperature ($25 \pm 2^\circ\text{C}$), humidity ($55 \pm 5\%$) and a 12-h light/dark cycle. The rats, weighed approximately 220 g were selected and randomly divided into 11 groups (6 rats in each group). The different groups of rats were exposed with a single dose of 1 mg/kg and 5 mg/kg b.w. of 10 nm GNRs (GNR 10), 25 nm GNRs (GNR 25), 10 nm SNRs (SNR 10), 25 nm SNRs (SNR 25), QTZ and control (PBS + 1 % PEG) by intra tracheal instillation method as described by Warheit et al. [24]. The experiment was approved by the Institutional Animal Ethics Committee, Kakatiya University.

Collection of blood

The blood was collected from the control, GNRs, SNRs and QTZ exposed rats by means of retro orbital plexus at 1 day, 1 week, 1 month and 3 months post instillation periods. The serum was obtained by immediate centrifugation of blood samples at 3000 rpm for 10 min at room temperature. The serum was used for the estimation of the extra pulmonary toxicity parameters.

Serum biochemical analysis

Alanine transaminase (ALT) also known as serum glutamic pyruvic transaminase, is a cytoplasmic pyridoxal phosphate dependent enzyme involved in liver gluconeogenesis. ALT is widely distributed in many tissues but is found in great quantity in the liver and to a much smaller extent in the kidneys, heart and brain [25]. ALT levels are generally low, but may increase during different disease states or in the event of tissue injury. As such, ALT levels are routinely used as indicators of liver injury [26]. Creatine, occurring either from arginine and glycine synthesis in the kidney, pancreas and liver or directly from dietary intake, is transported in blood to the brain and muscle tissue where it is phosphorylated to phosphocreatine. This phosphocreatine and free creatine in muscle is converted non-en-

zymatically to creatinine which enters into the blood and is excreted by the kidneys. Because the kidneys are responsible for clearing creatinine, determination of serum creatinine levels is a useful indicator of renal function [27]. These serum ALT and serum creatinine assays were performed by using respective diagnostic kits as per the manufacturer's protocol.

Histopathology studies

For the histopathology study of liver and kidney tissues, the control and particle exposed (5 mg/kg b.w. [28]) liver and kidneys were isolated at 1 day, 1 week, 1 month and 3 months post instillation periods. The isolated tissues were fixed in 10 % (v/v) neutral buffered formalin and processed using routine histological techniques. The test tissues were embedded with paraffin and stained by using hematoxylin and eosin (H&E) dyes for histopathological evaluations and observed under 40 X.

Statistical analysis

Data were expressed as mean \pm SD (Standard deviation). Statistical analysis was performed for all the biochemical assays using ANOVA followed by Bonferroni posttests and the statistical significances were indicated by ^s $p < 0.05$, [#] $p < 0.01$, * $p < 0.001$ vs. time-matched control and ^a $p < 0.05$, ^b $p < 0.01$, ^c $p < 0.001$ vs. time-matched QTZ treated rats.

Results

Serum biochemical analysis

Serum ALT levels were significantly ($p < 0.001$) increased at 1 day and 1 week after instillation vs. control treated rats (\blacktriangleright **Table 1**) with 10 and 25 nm test nanorods at both doses. The 10 nm GNRs ($p < 0.001$), 25 nm GNRs ($p < 0.05$) and 10 nm SNRs ($p < 0.01$) at 5 mg/kg b.w. dose showed the significant increase of ALT levels in rat following 1 month post instillation period. Both sizes of GNRs, 10 nm SNRs at both doses and 25 nm SNRs at 5 mg/kg b.w. doses have shown significantly elevated levels of ALT, which were almost greater or equal to QTZ, an indication of liver toxicity.

The serum creatinine levels were significantly ($p < 0.05$) elevated with both doses of 10 and 25 nm gold and silver nanorods at 1 day and 1 week post instillation periods in rats (\blacktriangleright **Table 2**). The 10 nm GNRs and SNRs have shown higher levels of serum creatinine than the 25 nm GNRs, 25 nm SNRs and QTZ. The both gold and silver nanorods were showed significant increased levels of serum creatinine levels following 1 day and 1 week post instillation periods at higher dose (5 mg/kg).

Histopathology

The GNRs, SNRs, QTZ and control instilled rat livers and kidneys were isolated from all post instillation periods and observed for histopathological changes were shown in \blacktriangleright **Fig. 1–3**. GNRs and SNRs instilled rat livers after 1 week and 1 month post instillation periods have shown congestion of central vein, shrinkage of hepatocytes, ballooning of hepatic cells and lymphocytic infiltration leading to degeneration. There were no significant changes found in liver during 1 day and 3 months post instillation periods. The histopathology of rat kidneys after 1 month post instillation was

► **Table 1** Serum ALT levels (IU/L) following intra tracheal instillation of GNRs and SNRs in rats.

Nanoparticle Treatment	Post instillation period			
	1 Day	1 Week	1 Month	3 Months
Control	24.59 ± 1.94	23.48 ± 1.37	22.07 ± 1.52	21.89 ± 1.26
GNR 10 (1 mg/kg)	39.29 ± 2.48 * b	34.27 ± 2.54 * a	25.38 ± 1.96	23.17 ± 1.25
GNR 10 (5 mg/kg)	47.54 ± 3.21 * c	42.31 ± 3.25 * b	30.43 ± 2.16 * b	26.43 ± 1.58
GNR 25 (1 mg/kg)	35.43 ± 2.79 *	32.23 ± 2.53 *	24.53 ± 1.84	22.03 ± 1.21
GNR 25 (5 mg/kg)	41.38 ± 3.53 *	38.47 ± 2.69 *	27.12 ± 1.79 ^s	23.36 ± 1.34
SNR 10 (1 mg/kg)	36.41 ± 2.68 *	32.89 ± 2.97 *	23.86 ± 1.35	23.48 ± 1.47
SNR 10 (5 mg/kg)	43.17 ± 3.62 *	39.85 ± 2.86 *	28.48 ± 1.74 [#]	25.12 ± 1.85
SNR 25 (1 mg/kg)	32.31 ± 2.14 *	29.48 ± 2.19 [#]	22.79 ± 1.32	21.96 ± 1.12
SNR 25 (5 mg/kg)	37.57 ± 2.53 *	34.12 ± 2.67 *	24.72 ± 1.85	22.81 ± 1.23
QTZ (1 mg/kg)	33.36 ± 2.41 *	29.31 ± 2.25 [#]	22.78 ± 1.23	22.04 ± 0.96
QTZ (5 mg/kg)	39.45 ± 2.76 *	35.58 ± 2.98 *	24.84 ± 1.11	22.93 ± 1.37

Data were mean ± SD (n = 6); ^sp < 0.05, [#]p < 0.01, * p < 0.001 vs. control; ^ap < 0.05, ^bp < 0.01, ^cp < 0.001 vs. QTZ

► **Table 2** Serum creatinine levels (mg/dL) following intra tracheal instillation of GNRs and SNRs in rats.

Nanoparticle Treatment	Post instillation period			
	1 Day	1 Week	1 Month	3 Months
Control	0.89 ± 0.11	0.86 ± 0.13	0.82 ± 0.21	0.81 ± 0.13
GNR 10 (1 mg/kg)	1.59 ± 0.23 *	1.24 ± 0.15	0.92 ± 0.11	0.93 ± 0.15
GNR 10 (5 mg/kg)	1.83 ± 0.16 *	1.59 ± 0.18 *	1.12 ± 0.23	1.02 ± 0.23
GNR 25 (1 mg/kg)	1.32 ± 0.18 ^s	1.13 ± 0.11	0.89 ± 0.19	0.87 ± 0.19
GNR 25 (5 mg/kg)	1.68 ± 0.36 *	1.42 ± 0.15 [#]	1.01 ± 0.17	0.91 ± 0.17
SNR 10 (1 mg/kg)	1.61 ± 0.31 *	1.29 ± 0.13 ^s	0.93 ± 0.19	0.96 ± 0.21
SNR 10 (5 mg/kg)	1.85 ± 0.41 *	1.64 ± 0.21 *	1.18 ± 0.23	1.05 ± 0.25
SNR 25 (1 mg/kg)	1.33 ± 0.17 ^s	1.08 ± 0.09	0.85 ± 0.17	0.84 ± 0.21
SNR 25 (5 mg/kg)	1.69 ± 0.25 *	1.41 ± 0.17 [#]	1.03 ± 0.13	0.89 ± 0.17
QTZ (1 mg/kg)	1.37 ± 0.13 ^s	1.12 ± 0.13	0.86 ± 0.19	0.86 ± 0.15
QTZ (5 mg/kg)	1.75 ± 0.22 *	1.45 ± 0.21 [#]	1.02 ± 0.25	0.94 ± 0.23

Data were mean ± SD (n = 6); ^sp < 0.05, [#]p < 0.01, * p < 0.001 vs. control treated rats

showed tubular dilation, degeneration and necrosis with 10 nm SNRs, 10 nm GNRs and QTZ. There were no significant changes were found in the histopathology of kidneys following exposure of gold and silver nanorods at 1 day, 1 week and 3 months post instillation periods in rats.

Discussion

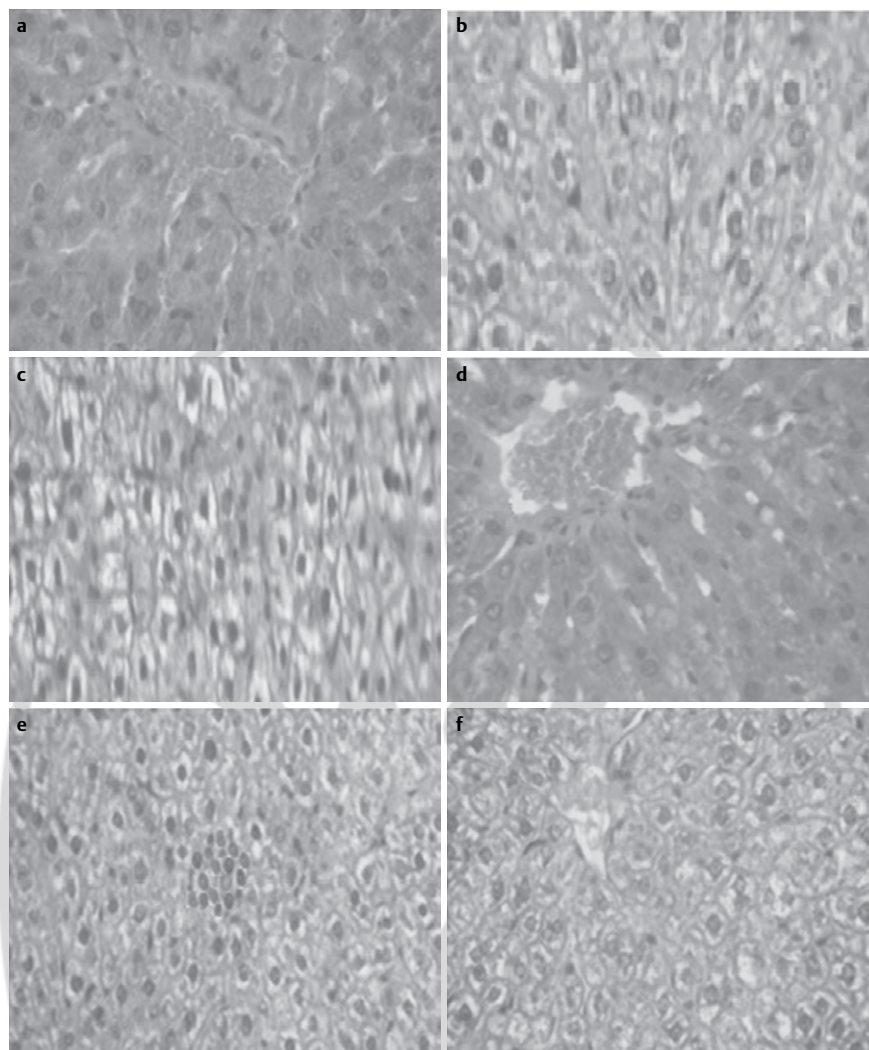
The present study was aimed to evaluate the extra-pulmonary toxicity of 10 and 25 nm gold and silver nanorods at 1 and 5 mg/kg b.w. doses following single dose intra tracheal instillation in rats by assessing the serum ALT, serum creatinine levels and histopathology studies (5 mg/kg b.w.) of rat liver and kidneys at 1 day, 1 week, 1 month and 3 months post instillation periods.

Mo et al. [29] investigated the toxicity of 22 nm ferric oxide nanoparticles (FNPs) upon intra tracheal instillation into the male rats at a dose of 4 mg/rat. Extra pulmonary distribution of FNPs in organs and its metabolism in blood, lung, urine and feces were estimated for 50 days of post exposure. Phagocytosis and clearance of agglomerated FNPs by monocytes/macrophages were observed by inductively coupled plasma mass spectrometry and histopathology studies. The results have shown intra tracheally instilled FNPs could pass

through the alveolar capillary barrier into systemic circulation. The FNPs in the lung were distributed to different organs including liver, kidney, spleen and testicle. They suggest that the effect of FNPs exposure, even at low concentration, should be evaluated because of the probable lung and systemic cumulative toxicity of the FNPs.

Our results displayed that the exposure of gold and silver nanorods revealed elevated levels of serum ALT and serum creatinine following 1 day and 1 week post exposure periods, indicating liver and kidney toxicity respectively. In contrast, there were little or no increased levels of serum biomarkers were observed at 1 month and 3 months post instillation periods. Both sizes of GNRs and SNRs at 5 mg/kg b.w. dose resulted in higher increase of serum ALT and serum creatinine when compared to 1 mg/kg b.w. dose treated rats, representing the dose dependent extra pulmonary toxicity of test nanorods. The 10 nm GNRs were displayed increased serum ALT levels at 1 day, 1 week and 1 month post exposure period and these levels were far higher than the SNRs and QTZ treated rats. In case of serum creatinine levels, both GNRs and SNRs have shown similar elevated levels. The both liver and kidney toxicities were comparable to QTZ induced extra pulmonary toxicities.

Recently, 14 nm GNRs were repeatedly administered intravenously at 3 dose levels (0.9, 9 and 90 µg) to male rats weekly for a



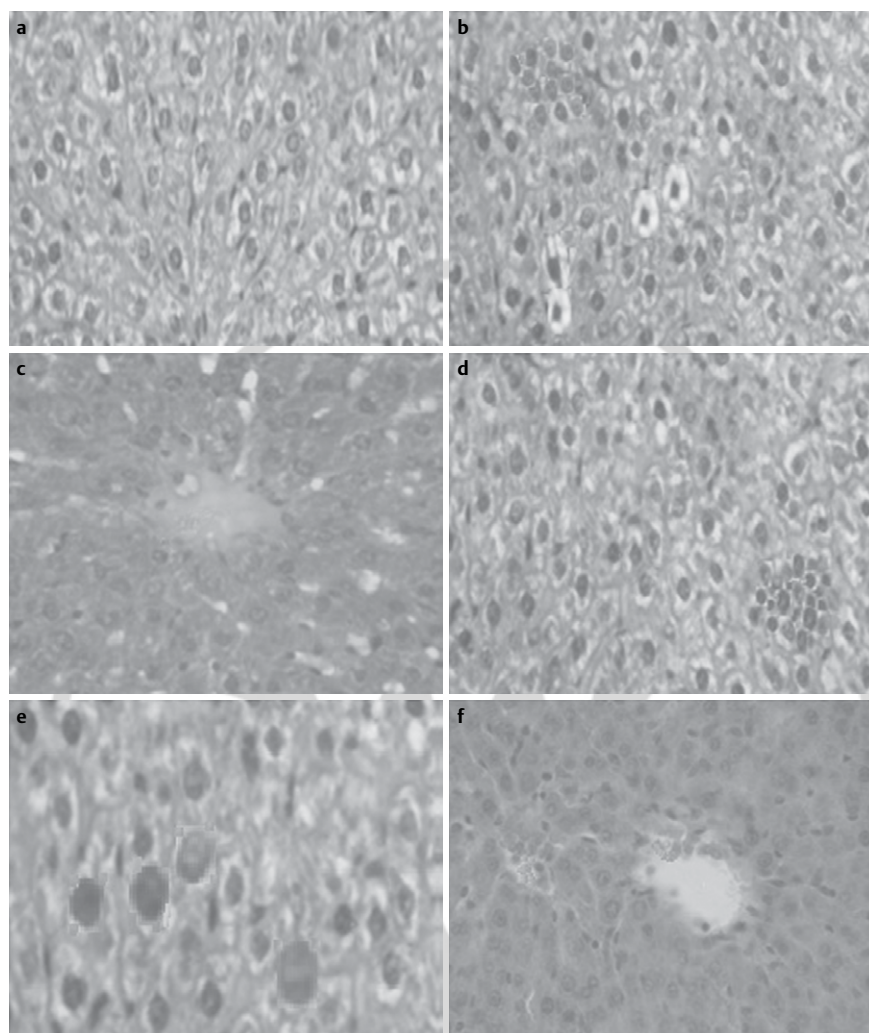
► **Fig. 1** Photomicrographs of rat liver tissue following intra tracheal instillation of 1 week post exposure of **a** Control, **b** GNR 10, **c** GNR 25, **d** SNR 10, **e** SNR 25 and **f** QTZ.

period of 7 weeks, followed by a 14 day washout period. After sacrificing, the amount of gold was quantified in the liver, lungs, spleen and kidney using neutron activation analysis. The blood samples were collected from both the test and control groups, markers of kidney and liver damage for acute and subchronic toxicity and histopathology studies were assessed. The liver had the highest amount of gold (μg) per gram of tissue after 56 days followed by the spleen, lungs and kidney. The histopathological evaluation showed little hepatotoxicity and nephrotoxicity [30].

Saeed et al. [31] investigated the liver toxicity in mice following oral administration of SNPs for 14 days. The results showed that the increased levels of liver enzymes such as ALT and aspartate aminotransferase. The liver toxicity was further confirmed by the histopathological changes in SNPs exposed mice. Magdy et al. [32] demonstrated the toxic effects of intraperitoneal administration of 8.7 nm SNPs at 1, 2 and 4 mg/kg b.w. doses daily for 28 days in female rats. Results displayed various liver histopathological le-

sions, elevated malondialdehyde and glutathione levels that were dose dependent. The tissue residues of SNPs were found in liver tissue and related to treated dose. The SNPs also induced variable chromosomal aberrations in a dose dependent manner. Our investigation results were supported by the above studies relating to liver and kidney toxicities of GNRs and SNRs in rats.

Histopathology studies of rat liver following instillation of GNRs and SNRs at 5 mg/kg b.w. dose displayed that congestion of central vein, shrinkage and ballooning of hepatocytes and lymphocytic infiltration leading to degeneration after 1 week and 1 month post instillation periods. No significant changes were found in liver after 1 day and 3 months post instillation periods. The histopathology of rat kidney following instillation of test nanorods at 5 mg/kg b.w. dose was showed tubular dilation, degeneration and necrosis with 10 nm SNRs and 10 nm GNRs after 1 month post instillation period. No significant changes were found in the histopathology of rat kid-



► **Fig. 2** Photomicrographs of rat liver tissue following intra-tracheal instillation of 1 month post exposure of **a** Control, **b** GNR 10, **c** GNR 25, **d** SNR 10, **e** SNR 25 and **(f)** QTZ.

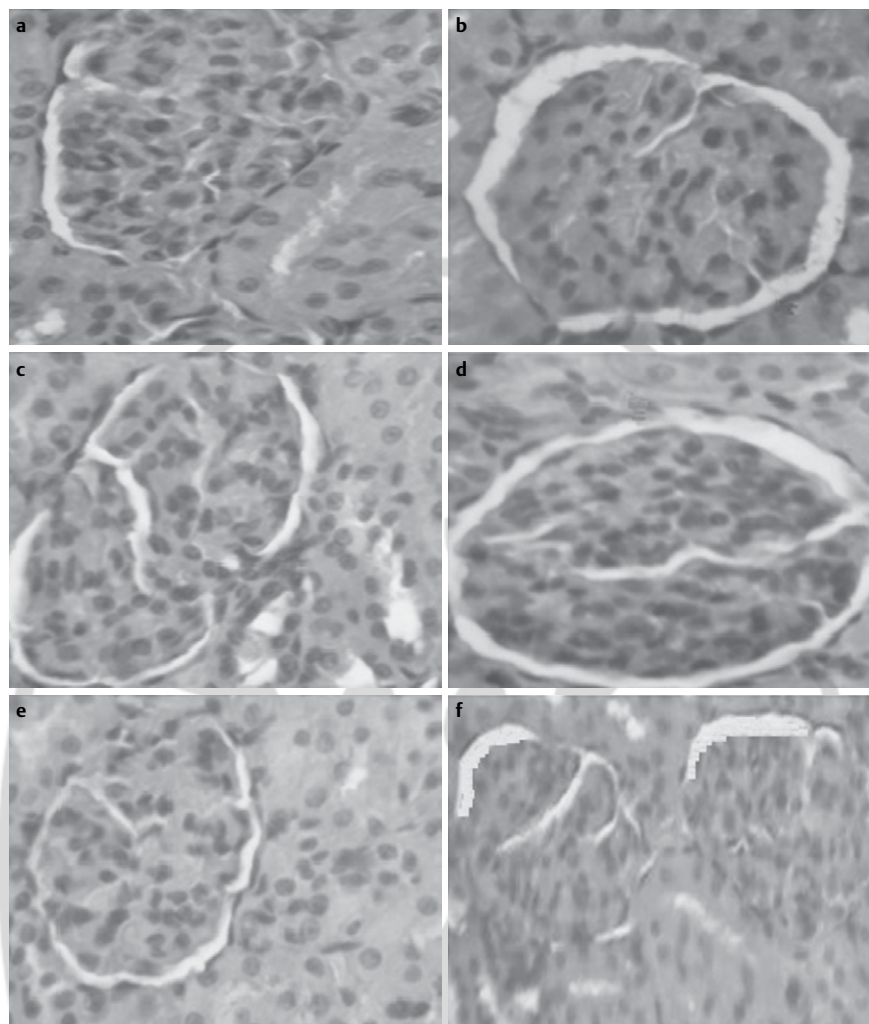
neys following exposure of test nanorods at 1 day, 1 week and 3 months post instillation periods.

One of the latest investigations evaluated the toxic effects of 23.1 nm SNPs upon oral administration for 28 days in rats. The results of histopathological findings displayed damage in lung, liver and kidney of SNPs exposed rats [33]. Mi et al. [34] examined the toxicity of GNPs in human intestinal cells as well as in rats following repeated oral administration for 14 days. Biokinetic study displayed that GNPs slowly diffused into the blood stream and slightly accumulated in kidney following oral administration in rats. The study showed that GNPs cause little toxicity in rats based on histopathological and serum biochemical analysis.

The 10 nm GNRs and SNRs have shown remarkable changes in both serum biochemical analysis and histopathological studies. The 10 nm test nanorods were showed greater increased levels of serum ALT and serum creatinine compared to 25 nm test nanorods. The 10 nm gold and silver nanorods were also showed significant

histopathological changes over 25 nm test nanorods. These observations suggest the size dependent translocation and extra pulmonary toxicity of both GNRs and SNRs. Also, the 10 nm GNRs were displayed significant higher levels of serum ALT levels compared to 10 nm SNRs and QTZ, indicating greater liver toxicity of GNRs. However, both GNRs and SNRs have shown similar levels of serum creatinine, indicating similar toxicity of GNRs and SNRs towards kidney.

Anda et al. [35] investigated the size dependent cytotoxicity of SNPs (10, 40 and 75 nm) following exposure of BEAS-2B cells by cell viability by lactate dehydrogenase assay, genotoxicity by alkaline comet assay. The results showed cytotoxicity only for the 10 nm particles. In contrast, all SNPs tested caused a raise in overall DNA damage after 1 day assessed by the comet assay. Finally, the investigation showed that small SNPs were cytotoxic for human lung cells. Mohamed and Bashir [36] conducted an investigation to assess the particle size effect of GNPs (10, 20 and



► **Fig. 3** Photomicrographs of rat kidney tissue following intra-tracheal instillation of 1 month post exposure of **a** Control, **b** GNR 10, **c** GNR 25, **d** SNR 10, **e** SNR 25 and **f** QTZ.

50 nm) on the hepatic tissue in rats for 3 or 7 days. The GNPs exposure were results in liver histopathological changes such as cloudy swelling, hydropic degeneration, fatty degeneration, portal and lobular infiltrate and congestive dilated central veins. These alterations were size dependent with smaller ones induced the most effects. Some of the previous investigations on gold and silver nanoparticles have shown size dependent toxicity using in vitro and in vivo models [37–39] were supported our size dependent toxicities of GNRs and SNRs.

Conclusion

Finally, the 10 nm and 25 nm GNRs and SNRs have shown significantly elevated levels of serum biochemical enzymes such as ALT and creatinine, representing liver and kidney toxicity respectively. The intra tracheal instillation of test nanorods in rats further sug-

gesting the extra pulmonary toxicity of GNRs and SNRs by histopathological changes occurred in rat liver and kidneys. The investigation was proposing the dose and size dependent translocation and extra-pulmonary toxicity of GNRs and SNRs in rats.

Acknowledgements

The first author is very grateful to UGC-BSR (University Grants Commission-Basic Scientific Research) section, New Delhi, India for providing RFSMS (Research Fellowship in Sciences for Meritorious Students) fellowship for conducting the research.

Conflict of interest

The authors declare that there are no conflicts of interest.

References

- [1] Coradeghini R, Gioria S, Garcia CP et al. Size-dependent toxicity and cell interaction mechanisms of gold nanoparticles on mouse fibroblasts. *Toxicol Lett* 2013; 217: 205–216
- [2] Marin S, Vlasceanu GM, Tiplea RE et al. Applications and toxicity of silver nanoparticles: A recent review. *Curr Top Med Chem* 2015; 15: 1596–1604
- [3] Chen X, Schluesener HJ. Nanosilver: A nanoparticle in medical application. *Toxicol Lett* 2008; 176: 01–12
- [4] Kim JS, Kuk E, Yu KN et al. Antimicrobial effects of silver nanoparticles. *Nanomedicine* 2007; 3: 95–101
- [5] Wijnhoven SWP, Peijnenburg WJGM, Herberts CA et al. Nano-silver – a review of available data and knowledge gaps in human and environmental risk assessment. *Nanotoxicology* 2009; 3: 109–138
- [6] Huang X, El-Sayed IH, Qian W et al. Cancer cells assemble and align gold nanorods conjugated to antibodies to produce highly enhanced, sharp, and polarized surface Raman spectra: A potential cancer diagnosis marker. *Nano Lett* 2007; 7: 1591–1597
- [7] Huang X, El-Sayed IH, Qian W et al. Cancer cell imaging and photothermal therapy in the near-infrared region by using gold nanorods. *J Am Chem Soc* 2006; 128: 2115–2120
- [8] Huff TB, Hansen MN, Zhao Y et al. Controlling the cellular uptake of gold nanorods. *Langmuir* 2007; 23: 1596–1599
- [9] Yu C, Irudayaraj J. Multiplex biosensor using gold nanorods. *Anal Chem* 2007; 79: 572–579
- [10] Kuo WS, Chang CN, Chang YT et al. Antimicrobial gold nanorods with dual-modality photodynamic inactivation and hyperthermia. *Chem Comm* 2009; 32: 4853–4855
- [11] Pissuwan D, Cortie CH, Valenzuela SM et al. Functionalised gold nanoparticles for controlling pathogenic bacteria. *Trends Biotechnol* 2009; 28: 207–213
- [12] Dubas ST, Pimpan V. Humic acid assisted synthesis of silver nanoparticles and its application to herbicide detection. *Mater Lett* 2008; 62: 2661–2663
- [13] Maqsood A, Mohamad SA, Siddiqui MKJ. Silver nanoparticle applications and human health. *Clin Chim Acta* 2010; 411: 1841–1848
- [14] Li S, Zhi GY, Wen BG et al. Silver nanorod array electrodes and their application for detection of low concentration chloropropanol in aqueous media. *App Mech Mater* 2015; 697: 136–139
- [15] Bin G, Lei S, Ke-Wu H et al. GNRs@SiO₂-FA in combination with radiotherapy induces the apoptosis of Hep G2 cells by modulating the expression of apoptosis-related proteins. *Int J Mol Med* 2015; 36: 1282–1290
- [16] Jennifer M, Jacek Z, Anna L et al. Prolonged effects of silver nanoparticles on p53/p21 pathway-mediated proliferation, DNA damage response, and methylation parameters in HT22 hippocampal neuronal cells. *Mol Neurobiol* 2016, doi:10.1007/s12035-016-9688-6
- [17] Xiaomei L, Kristin S, Laetitia B et al. Silver nanoparticle toxicity and association with the alga *Euglena gracilis*. *Environ Sci Nano* 2015; 2: 594–602
- [18] Lankveld DP, Oomen AG, Krystek P et al. The kinetics of the tissue distribution of silver nanoparticles of different sizes. *Biomaterials* 2010; 31: 8350–8361
- [19] Rothen RB, Brown DM, Piallier-Boyles M et al. Relating the physico-chemical characteristics and dispersion of multiwalled carbon nanotubes in different suspension media to their oxidative reactivity in vitro and inflammation in vivo. *Nanotoxicology* 2010; 4: 331–342
- [20] Sur I, Cam D, Kahraman M et al. Interaction of multifunctional silver nanoparticles with living cells. *Nanotechnology* 2010; 21: 175104
- [21] Harikiran L, Bhikku A, Narsimha RY. In vitro cytotoxicity of gold and silver nanorods using different human cell lines. *Lat Am J Pharm* 2015; 34: 1277–1282
- [22] Harikiran L, Narsimhareddy Y. Cytotoxicity, oxidative stress, and inflammation in human Hep G2 liver epithelial cells following exposure to gold nanorods. *Toxicol Mech Meth* 2016; 26: 340–347
- [23] Ying T, Yafeng S, Libin H et al. In vitro cytotoxicity of gold nanorods in A549 cells. *Environ Toxicol Pharmacol* 2015; 39: 871–878
- [24] Warheit DB, Brock WJ, Lee KP et al. Comparative pulmonary toxicity inhalation and instillation and studies with different TiO₂ particle formulations: Impact of surface treatments on particle toxicity. *Toxicol Sci* 2005; 88: 514–524
- [25] Yang RZ, Park S, Reagan WJ et al. Alanine aminotransferase isoenzymes: Molecular cloning and quantitative analysis of tissue expression in rats and serum elevation in liver toxicity. *Hepatology* 2009; 49: 598–607
- [26] Pratt DS, Kaplan MM. Evaluation of abnormal liver-enzyme results in asymptomatic patients. *N Engl J Med* 2000; 342: 1266–1271
- [27] Bowers LD, Wong ET. Kinetic serum creatinine assays II. A critical evaluation and review. *Clin Chem* 1980; 26: 555–561
- [28] Warheit DB, Webb TR, Reed KL et al. Pulmonary toxicity study in rats with three forms of ultrafine- TiO₂ particles: Differential responses related to surface properties. *Toxicology* 2007; 230: 90–104
- [29] Mo TZ, Wei YF, Yun W et al. Particokinetics and extrapulmonary translocation of intratracheally instilled ferric oxide nanoparticles in rats and the potential health risk assessment. *Toxicol Sci* 2009; 107: 342–351
- [30] Clinton R, Jan RZ, Hylton B et al. Bioaccumulation and subchronic toxicity of 14 nm gold nanoparticles in rats. *Molecules* 2016; 21: 763
- [31] Saeed HM, Roya JS, Simin A. Toxic effects of silver nanoparticles on liver and some hematological parameters in male and female mice (*Mus musculus*). *Biol Trace Elem Res* 2015; 165: 153–158
- [32] Magdy MEM, Taher ASE, Halima SA et al. Evaluation of hepatotoxic and genotoxic potential of silver nanoparticles in albino rats. *Exp Toxicol Pathol* 2014; 67: 21–29
- [33] Yara MA, Asrar MH, El BAI et al. Evaluation of acute and subchronic toxicity of silver nanoparticles in normal and irradiated animals. *Br J Pharmacol Toxicol* 2015; 6: 22–38
- [34] Mi RJ, Song HB, Mi RG et al. Toxicity and biokinetics of colloidal gold nanoparticles. *Nanomaterials* 2015; 5: 835–850
- [35] Anda RG, Sara S, Inger OW et al. Size-dependent cytotoxicity of silver nanoparticles in human lung cells: The role of cellular uptake, agglomeration and Ag release. *Part Fibre Toxicol* 2014; 11: 11
- [36] Mohamed AKA, Bashir MJ. Histological alterations in the liver of rats induced by different gold nanoparticle sizes, doses and exposure duration. *J Nanobiotechnol* 2012; 10: 5
- [37] Muthu IS, Kalimuthu K, Selvaraj B et al. Size-based cytotoxicity of silver nanoparticles in bovine retinal endothelial cells. *Nanosci Meth* 2012; 1: 56–77
- [38] Susann G, Lars E, Tore S. Silver nanoparticle-induced cytotoxicity in rat brain endothelial cell culture. *Toxicol In Vitro* 2013; 27: 305–313
- [39] Vijaykumar S, Ganesan S. Size-dependent in vitro cytotoxicity assay of gold nanoparticles. *Toxicol Environ Chem* 2013; 95: 277–287

ISSN 0975-2331 (Print)
0975-4385 (Online)
DOI: 10.5958/0975-4385.2017.00036.X

Vol. 09| Issue-04|
October - December 2017

Available online at
www.anvpublication.org

Research Journal of
Pharmacognosy and Phytochemistry
Home page www.rjpponline.org



RESEARCH ARTICLE

Evaluation of Anti Cancer Activity of *Kydia calycina* Roxb. Leaf Extract on Different Cancer Cell Lines

Baburao Bhukya, Harikiran Lingabathula, Narsimhareddy Yellu*

Department of Pharmacology, University College of Pharmaceutical Sciences, Kakatiya University, Warangal, Telangana, India-506009

*Corresponding Author E-mail: ynrucpsc@gmail.com

ABSTRACT:

To study the anticancer effects of *Kydia calycina* using various human cancer cell cultures, *in vitro* by MTT assay, ROS generation and caspase-3 activities. Human cervical carcinoma (HeLa) cells, human breast cancer (MCF-7) cells and human neuroblastoma (IMR-32) cells were maintained in a 5% CO₂ incubator at 37°C. Different concentrations of leaf extract of *Kydia calycina* in serum free culture medium were freshly prepared and used for cytotoxic activity by MTT assay, ROS generation and apoptotic effect by caspase-3 activity. The plant extract has revealed that greater percentage inhibition in all types of cancer cells in a dose dependent manner by MTT assay. The IC₅₀ values of *K. calycina* extract were found to be 41.17, 46.90 and 39.49 µg/mL against HeLa, MCF-7 and IMR-32 respectively. The apoptotic activity of *Kydia calycina* methanolic leaf extract was evaluated through ROS generation and caspase-3 activity. The results showed that the extract has significantly increased the ROS production and caspase-3 levels in all the cell cultures in a dose dependent manner. Further studies are warranted to elucidate the anticancer activity of *K. calycina*.

KEYWORDS: *Kydia calycina*; cell viability; ROS; caspase-3; cytotoxicity.

INTRODUCTION:

Plants and their products for treatment of diseases have been used extensively by humans for many years^{1,2}. Medicinal plants have gained huge interests from researchers around the world because of their positive biological activity. Chemoprevention, a relatively new and promising strategy to prevent cancer, is defined as the use of natural dietary compounds and/or synthetic substances to block, inhibit, reverse, or retard the process of carcinogenesis. Various cancer chemopreventive agents can encourage apoptosis in premalignant and malignant cells *in vivo* and/or *in vitro*, which is conceivably another anticancer mechanism^{3,4}.

Many of publications showed the effect of many herbal plants in treatment of wide range of illnesses. Also several naturally produced herbal formulations are currently available for cancer patients. As most of chemotherapeutic agents were cytotoxic to normal cells and developed drug resistance^{5,6}. Therefore scientific consideration and test of traditionally used herbs for the treatment of different malignancies could be also considered as a very valuable source for new chemotherapeutic drugs^{6,7}.

Kydia calycina is distributed in Himalayas from the Indus eastwards to Myanmar and in peninsular India from Maharashtra and Madhya Pradesh, principally in mixed, moist, deciduous forests. The leaves are applied to relieve body pains, lumbago and arthritis, a poultice of the leaves is used to treat skin diseases⁸. *K. calycina* leaf

Received on 11.07.2017 Modified on 19.08.2017
Accepted on 20.09.2017 ©A&V Publications All right reserved
Res. J. Pharmacognosy and Phytochem. 2017; 9(4): 197-202.
DOI: 10.5958/0975-4385.2017.00036.X

and stem bark paste applied for ulcers and skin diseases⁹. The *K. calycina* seed oil was reported to contain cyclopropenoid fatty acid apart from normal fatty acids¹⁰ and Hibiscoquinone B, Hibiscone C, 8-formyl-2,7-dihydroxy-5-isopropyl-1-methoxy-3-methyl naphthalene were isolated from stem heartwood of *Kydia calycina*¹¹. The *Kydia calycina* methanolic leaf extract was reported to having Analgesic, Anti-inflammatory and Hepatoprotective activity^{12,13}. So, the present study evaluated the cytotoxic effects of methanolic extracts of *K. calycina* using various human cancer cell cultures, *in vitro*.

MATERIALS AND METHODS:

Plant material:

The leaves of *Kydia calycina* were collected from Thirupathi hills, Andhra Pradesh, India. It was authenticated by Prof. V. Raju, Department of Botany, Kakatiya University, Warangal, India.

Preparation of extracts:

Kydia calycina leaf is were made free from the adherent foreign material and air-dried. Then they were coarsely powdered and macerated with methanol in a round bottom flask for 7 days separately. The content of the flask were stirred intermittently to ensure the efficiency of the extraction. After a week, they were filtered and concentrated under reduced pressure to yield corresponding extracts, and the extracts were kept in a desiccator to remove moisture and stored properly until used.

Cell culture and treatment:

Human cervical carcinoma (HeLa) cells, human breast cancer (MCF-7) cells and human neuroblastoma (IMR-32) cells were procured from NCCS, Pune. The cells were used between passages 10 and 15. All these cells were grown in suitable culture media supplemented with 10% FBS, 1% L-glutamine and 1% penicillin-streptomycin antibiotic solution. Cells were seeded at 250,000 cells/flask in a total volume of 10 mL.

When confluent, all the cells were trypsinized as described above, and seeded in 96 well plates at the rate of 1.0×10^4 cells/0.1 mL. All the cell cultures were maintained in a 5% CO₂ incubator at 37°C. Different concentrations of extract of *Kydia calycina* such as in serum free culture medium were freshly prepared and used for cytotoxic activity.

MTT assay method:

Measurement of cell viability and proliferation forms the basis for numerous *in vitro* assays of a cell population's response to external factors. The reduction of tetrazolium salts is widely believed as a reliable way to study cell proliferation. The effect of test fractions on the cellular

proliferation and viability was determined by using MTT assay method¹⁴. The yellow tetrazolium salt was reduced by dehydrogenase enzymes present in metabolically active cells, to produce reducing equivalents such as NADH and NADPH. The formazan product has low aqueous solubility and was present as purple crystals. The resulting formazan was dissolved by using dimethyl sulfoxide (DMSO) permitted the convenient quantification of product development. The intensity of the product color was measured at 562 nm and was directly proportional to the number of living cells in the culture¹⁵.

The adherent cells were trypsinized according to protocol and were re-suspended in fresh medium after centrifugation. Cell suspension was mixed thoroughly by pipetting several times to get a uniform single cell suspension. 10-15 passages were conducted before performing the experiment to evaluate the cytotoxicity. Different dilutions of fractions were made in media with final PBS+1% PEG (solvent control) concentration in the well to be less than 1%. 100 µL (0.1 mL) of cell suspension was transferred aseptically to each well of a 96 well plate and to it 100 µL of solvent/fraction (in triplicate) in media was added. The plate was then incubated at 37°C for 48 h in 5% CO₂ incubator. After 48 h of incubation, 20 µL of MTT was added to each well and the micro titer plate was again incubated for 2 h. 80 µL of lysis buffer was added to each well, the plate was wrapped in aluminum foil to prevent the oxidation of the dye. The plate was placed on a rotary shaker for 2 h to solubilize the purple formazan crystals. The absorbances were recorded on the ELISA reader at 562 nm wavelength. The absorbance of the test was compared with that of solvent control to get the percent cytotoxicity^{16,17}.

Measurement of ROS generation:

Generation of ROS was assessed by using a cell-permeable fluorescent signal H2DCF-DA as an indicator for ROS^{18,19}. As described previously, H2DCF-DA is oxidized to a highly green fluorescent 2070-dichlorofluorescein (DCF) by the generation of ROS. Cancer cell lines were pretreated with various concentrations of test extract for 24 h. After 24 h incubation period, the cells were washed with cold phosphate buffer solution (PBS) and incubated with 100 µmol/L H2DCF-DA for another 30 min at 37°C.

DCF fluorescence intensity was measured using the fluorescence plate reader (Varioskan Flash Multimode Reader, Waltham, MA) at excitation/emission of 488/525 nm. The determinations were carried out thrice in triplicate, ensuring each time that the number of cells per treatment group were the same to ensure reproducibility. The values were expressed as % relative fluorescence compared to the control.

Caspase-3 assay:

Caspases are members of the aspartate specific cysteinyl protease family. Caspase-3 exists in cells as an inactive 32 kDa proenzyme, called pro-caspase-3. Pro-caspase-3 is cleaved into active 17 and 12 kDa subunits by upstream proteases such as caspase-6, caspase-8 and granzyme B during apoptosis. The over expression of caspase-3 can result in initiation of apoptosis. Likewise, the inhibition of caspase-3 can prevent cells from entering into the apoptotic pathway. The activation of caspase-3 is used as a biomarker in evaluation of apoptosis and in understanding mechanisms of apoptosis induction²⁰.

The assay is based on colorimetric finding of the chromophore *p*-nitroaniline (*p*NA) after cleavage from the DEVD-*p*NA, a labeled substrate. The *p*NA light emission can be quantified using a microtiter plate reader at 405 nm. Assessment of the absorbances of *p*NA from an apoptotic sample with an uninduced control allows determination of the fold raise in caspase-3 activity²¹.

Statistical analysis:

Data were expressed as Mean±SEM. Significance was calculated using one way ANOVA followed by Dunnet's multiple comparison tests compared to control.

RESULTS AND DISCUSSION:

Natural products or their derivatives have been exhibited to have significant anticancer potentials due to their ability to inhibit tumor growth, angiogenesis and

metastasis without many side effects²². Recent publications showed the effect of many herbal plants in treatment of wide range of illnesses. Also several naturally produced herbal formulations are currently available for cancer patients. Most of the chemotherapeutic agents were cytotoxic to normal cells and build up drug resistance. Therefore scientific consideration and test of traditionally used herbs for the treatment of various malignancies could be also considered as a very important source for new chemotherapeutic drugs²³.

The *in vitro* cytotoxicity of methanolic extract of *Kydia calycina* were evaluated against three different cancer cell cultures, such as human cervical carcinoma (HeLa), human breast cancer (MCF-7) and human neuroblastoma (IMR-32) cells by using MTT assay, which is based on the reduction of MTT at different concentrations (10, 20, 40, 80 and 160 µg/ml). After 48 h of treatment, *K* calycina methanolic extract exhibited higher inhibitory effect against all tumor cells, with varying efficiencies and selectivities while others caused marginal cell inhibition (Figure 1). The IC₅₀ (concentration of the fraction causing 50% cell death) values of test fractions were given in Table 1. Among the methanolic extract have revealed that greater percentage inhibition in all types of cancer cells in a dose dependent manner. The IC₅₀ values of *Kydia calycina* extract were found to be 41.17, 46.90 and 39.49 µg/mL against HeLa, MCF-7 and IMR-32 respectively.

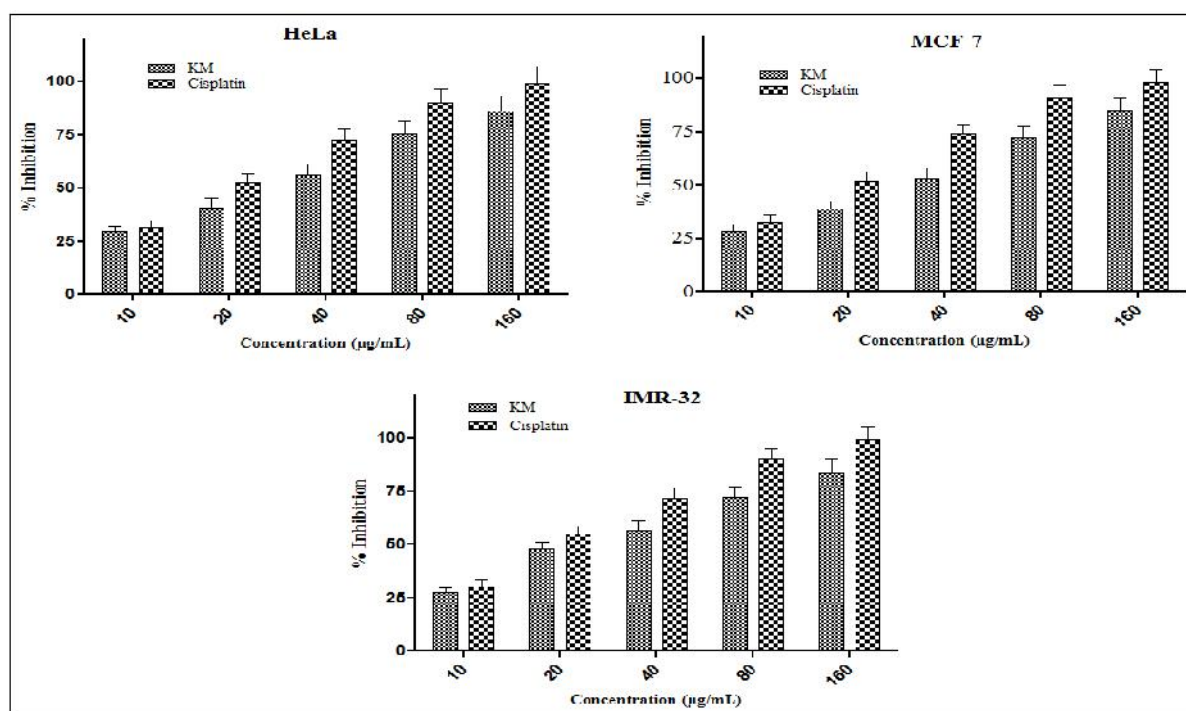


Figure 1. Effect of methanolic extract on cytotoxicity of HeLa, MCF-7 and IMR-32 cancer cell lines; Data were Mean±SEM

Table 1. The IC₅₀ values of different *Kydia calycina* extracts using various cell lines

Extract	IC ₅₀ Values (µg/mL)		
	HeLa	MCF-7	IMR-32
KM	41.17±1.84**	46.90±2.46*	39.41±3.03**
STD	13.49±1.09***	12.04±1.10***	13.69±0.96***

KM-*Kydia calycina* Methanolic extract; STD- Cisplatin; Data were Mean±SEM; *p<0.05, **p<0.01 and ***p<0.001 compared to control.

Since the cytotoxicity of methanolic were greater, we further evaluated to reveal the mechanism for its cytotoxicity. For this purpose, we evaluated the apoptotic activity through ROS generation and caspase-3 activities of test extract all three cancer cell lines. The results showed that the both fractions have significantly increased the ROS production in all the cell cultures (Figure 2). Excess accumulation of ROS leads to cellular damage and inflammation of the tissues²⁴. ROS plays a major role in cellular senescence paving way to cell

death; therefore there is an urgent need for potential therapeutics that may prevent oxidative stress induced neurodegeneration. It is highly possible that the pro-oxidant effect is responsible for the apoptotic activity of these extracts and ROS are key signaling molecules to modulate cell death²⁵. Accumulating evidence indicates that cancer cells produce high levels of ROS that lead to a state of increased basal oxidative stress. The increased production of ROS in cancer cells was observed in *in vitro* studies²⁶. Ahamad et al. demonstrated that naringenin leads to cell death in cancer cells via inducing ROS generation²⁷. We therefore investigated the effectiveness of test extracts in generation of ROS. We found that exposure of all three cancer cells with these extract dramatically enhanced generation of intracellular ROS at different levels in a dose dependent manner in all cell lines.

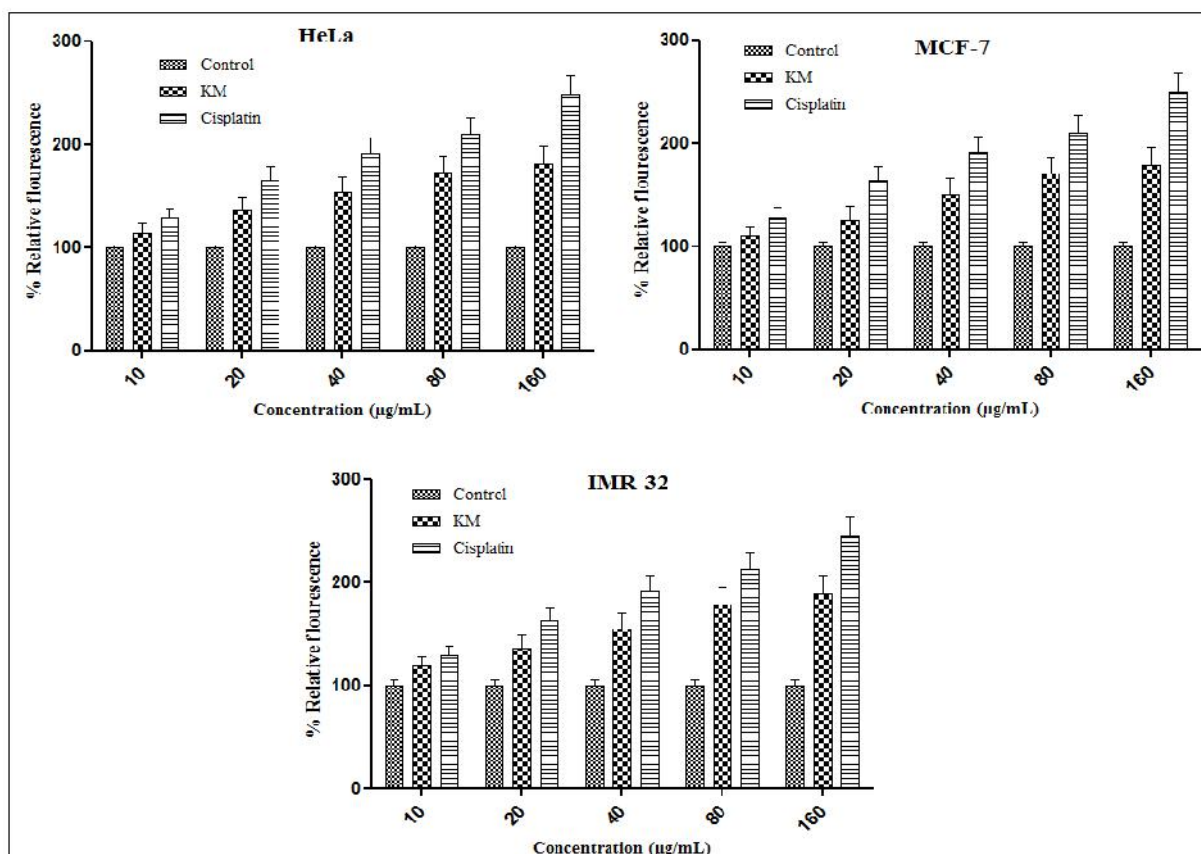


Figure 2. ROS generation effect of methanolic extract on HeLa, MCF-7 and IMR-32 cancer cell lines; Data were Mean±SEM

Intracellular caspase 3 activation is a key stage in the apoptotic pathway. Hence, we tested the effect of treatment with our plant fractions on intracellular caspase 3 enzymatic activity. Different human cancer cells were treated with the plant fractions and caspase 3 enzymatic activity within the cells was measured (Figure 3). Since caspase 3 activity rises while cells die and cell

numbers drop, it was essential to normalize caspase 3 activity to the number of cells, to obtain more accurate results. The results here are expressed as the percent increase in caspase 3 activity in treated cells compared to cells added with DMSO. Caspase-3 levels were significantly increased with *K. calycina* extract in HeLa (p<0.05), MCF-7 (p<0.05) and IMR-32 (p<0.01) cancer

cells. Realizing the potential of plant derived compounds to develop as drugs against cancer, information on novel anti-cancer compounds from Himalayan region were retrieved from literature. The chemical structures of fifteen such anti-cancer compounds were modeled and

optimized and their binding patterns were explored against nine selected molecular targets implicated in cell proliferation and apoptosis, which provided insights into their molecular mechanism of inhibition²⁸.

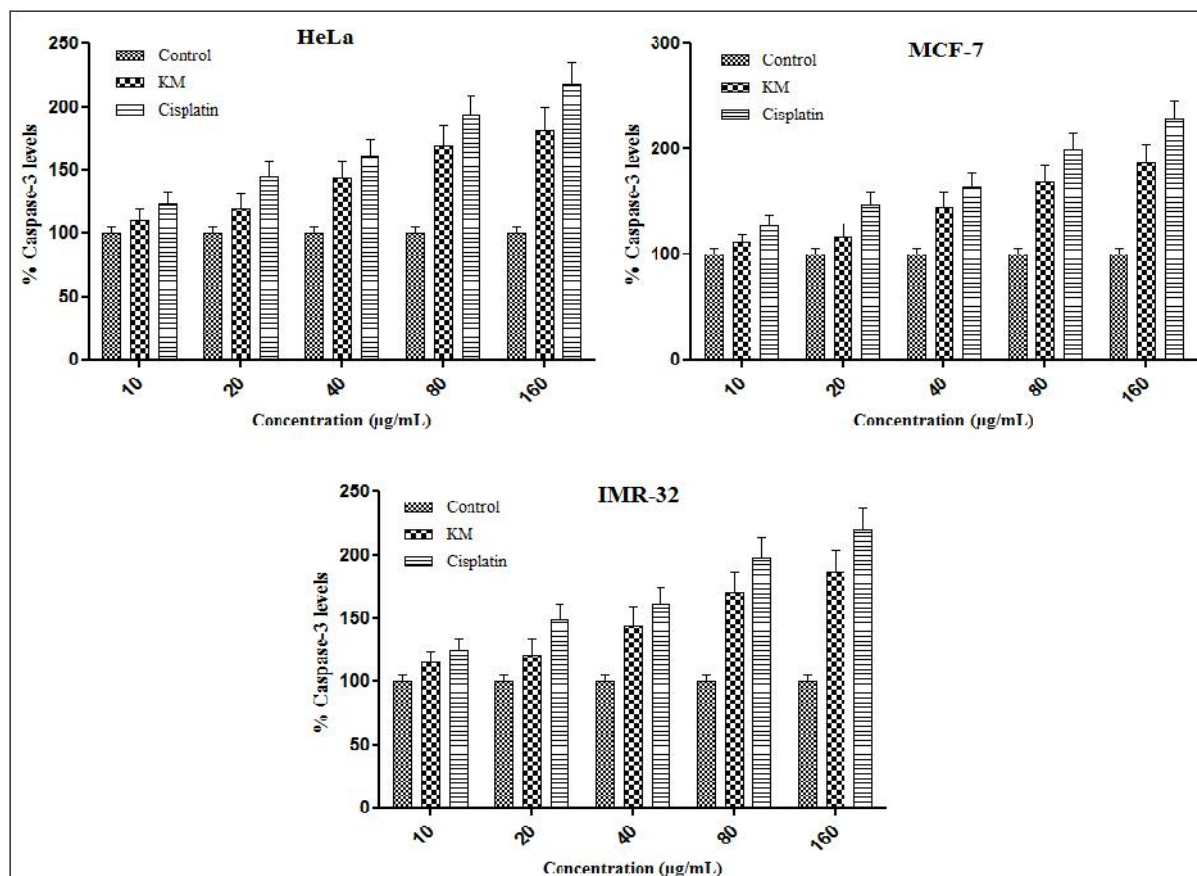


Figure 3. Caspase-3 levels of methanolic extract on HeLa, MCF-7 and IMR-32 cancer cell lines; Data were Mean±SEM

CONCLUSIONS:

In summary, among the four *K. calycina* leaf extract the showed increased percentage inhibition of MCF-7, HeLa and IMR-32 cells by MTT assay. Moreover, the apoptotic activity revealed that the plant extracts have displayed significant increased generation of ROS and caspase-3 activities in all cancer cell lines in a dose dependent fashion. Further studies are warranted to elucidate the molecular mechanisms of isolated compounds of *Kydia calycina*.

ACKNOWLEDGEMENTS:

The first author is thankful to University Grants Commission (UGC), New Delhi, INDIA for providing Post Doctoral Fellowship.

CONFLICT OF INTEREST:

The authors declare no conflict of interest.

REFERENCES:

- Suppakul P, Miltz J, Sonneveld K and Bigger SW. Antimicrobial properties of basil and its possible application in food packaging. *Journal of Agricultural and Food Chemistry* 2003; 51: 3197-3207.
- Arzu BY, Fatma PK and Arzu UT. *In vitro* antibacterial and antitumor activities of some medicinal plant extracts, growing in Turkey. *Asian Pacific Journal of Tropical Medicine* 2012; 6: 616-624.
- Hail JN, Cortes M, Drake EN and Spallholz JE. Cancer chemoprevention: a radical perspective. *Free Radical Biology and Medicine* 2008; 45: 97-110.
- Kiruthika B, Palghat and Raghunathan P. Anticancer activity of *Zea mays* leaf extracts on oxidative stress-induced Hep2 cells. *Journal of Acupuncture and Meridian Studies* 2013; 6(3): 149-158.
- Singh S, Singh PP, Roberts LR and Sanchez W. Chemopreventive strategies in hepatocellular carcinoma. *Nature Reviews Gastroenterology and Hepatology* 2014; 11(1): 45-54.
- Yu SZ. Primary prevention of hepatocellular carcinoma. *Journal of Gastroenterology and Hepatology* 1995; 10(6): 674-82.
- Maram S, Khilo K, Mahmoud MZ, Mahmoud GE, Walied A, Walaa A. Anticancer activity of *Aloe vera* and *Calligonum comosum* extracts separately on hepatocellular carcinoma cells. *Asian Pacific Journal of Tropical Biomedicine* 2015; 5(5): 375-381.

8. Parrotta JA. Healing plants of peninsular India. CABI publishing, New Delhi. 2001.
9. Ramarao N and Henry AN. The ethnobotany of eastern ghats in Andhra Pradesh, India. BSI publication, Botanical survey of India. 1996.
10. Daulatabad CD, Ankalagi KK and Desai VA. Cyclopropenoid and fatty acid composition of *Kydia calycina* seed oil. European Journal of Lipid science and Technology 2006; 91(6): 237-238.
11. Joshi KC, Sing P and Taneja S. A sesquiterpenoid naphthol from *Kydia calycina*. Planta Medica 1983; 49(10): 127.
12. Baburao B, Rama NRA, Carey MW and Krishna MG. Analgesic and anti-inflammatory activities of leaf extract of *Kydia calycina* Roxb. Bangladesh Journal of Pharmacology 2009; 4: 101-104.
13. Parameshwar H, Babu RB, Ravi KB, Narsimha RY and Krishna MG. Hepatoprotective effect of methanolic extract of the leaves of *Kydia calycina* on carbon tetrachloride induced hepatotoxicity in albino rats. African Journal of Pharmacy and Pharmacology 2011; 5(16): 1920-1924.
14. Jun SL, Won-Kyo J, Myung HJ, Taek RY and Hyung KK. Sanguinarine induces apoptosis of HT-29 human colon cancer cells via the regulation of Bax/Bcl-2 ratio and caspase-9-dependent pathway. International Journal of Toxicology 2012; 31: 70-77.
15. Carmichael J, De-Graff WG, Gazdar AF, Minna JD and Mitchell JB. Evaluation of a tetrazolium-based semiautomated colorimetric assay: Assessment of chemosensitivity testing. Cancer Research 1987; 47: 936-942.
16. Allely MC, Seudero DA and Monks A. Feasibility of drug screening with panels of human tumor cell lines using micro culture tetrazolium assay. Cancer Research 1998; 8: 589-601.
17. Harikiran L, Bhikku A and Narsimha RY. *In vitro* cytotoxicity of gold and silver nanorods using different human cell lines. Latin American Journal of Pharmacy 2015; 34: 1277-1282.
18. Min KJ, Jung KJ and Kwon TK. Carnosic acid induces apoptosis through reactive oxygen species-mediated endoplasmic reticulum stress induction in human renal carcinoma Caki cells. Journal of Cancer Prevention 2014; 19(3): 170-178.
19. Wu T, Qiang L, Chen FH, Zhao Q, Yang Z and Zou MJ. LFG-500, a newly synthesized flavonoid, induced a reactive oxygen species-mitochondria-mediated apoptosis in hepatocarcinoma cells. Biomedicine and Preventive Nutrition 2011; 1(2): 132-138.
20. Harikiran L and Narsimhareddy Y. Cytotoxicity, oxidative stress, and inflammation in human Hep G2 liver epithelial cells following exposure to gold nanorods. Toxicology Mechanisms and Methods 2016; 26: 340-347.
21. Casciola RL, Nicholson DW, Chong T, Rowan KR, Thornberry NA and Miler DK. Apopain/CPP32 cleaves proteins that are essential for cellular repair: a fundamental principle of apoptotic death. Journal of Experimental Medicine 1996; 183: 1957-1964.
22. Abdurrahim K, Ismail K, Murat D, Fatemeh B and Baki T. Cytotoxic, genotoxic and apoptotic effects of naringenin-oxime relative to naringenin on normal and cancer cell lines. Asian Pacific Journal of Tropical Biomedicine 2016; 6(10): 872-880.
23. Maram S, Kh K, Mahmoud MZ, Mahmoud GE, Waled A and Walaa A. Anticancer activity of *Aloe vera* and *Calligonum comosum* extracts separately on hepatocellular carcinoma cells. Asian Pacific Journal of Tropical Biomedicine 2015; 5(5): 375-381.
24. Murphy MP, Holmgren A, Larsson NG, Halliwell B and Chang CJ. Unraveling the biological roles of reactive oxygen species. Cell Metabolism 2011; 13: 361-366.
25. Wu CC and Bratton SB. Regulation of the intrinsic apoptosis pathway by reactive oxygen species. Antioxidants and Redox Signaling 2013; 19(6): 546-558.
26. Halliwell B. Oxidative stress and cancer: have we moved forward? Biochemistry Journal 2007; 401: 1-11.
27. Ahamad MS, Siddiqui S, Jafri A, Ahmad S, Afzal M and Arshad M. Induction of apoptosis and antiproliferative activity of naringenin in human epidermoid carcinoma cell through ROS generation and cell cycle arrest. PLOS One 2014; 9(10): e110003.
28. Arun BG, Atanu B, Mohammad AA. Exploring the physicochemical profile and the binding patterns of selected novel anticancer Himalayan plant derived active compounds with macromolecular targets. Informatics in Medicine Unlocked 2016; 5: 1-14.

Cytotoxic effects of *Kydia calycina* leaf fractions on different human cancer cell cultures

Baburao Bhukya, Harikiran Lingabathula, Narsimha Reddy Yellu*

Department of Pharmacology, University College of Pharmaceutical Sciences, Kakatiya University, Warangal, Telangana, India

Abstract

Objective: The objective of the study was to study the cytotoxic effects of effects of different fractions of *Kydia calycina* using various human cancer cell cultures, *in vitro* by MTT assay, reactive oxygen species (ROS) generation and caspase-3 activities. **Materials and Methods:** Human cervical carcinoma (HeLa) cells, human breast cancer (MCF-7) cells and human neuroblastoma (IMR-32) cells were maintained in a 5% CO₂ incubator at 37°C. Different concentrations of fractions of *K. calycina* such as toluene fraction (KT), ethyl acetate fraction (KE), butanone fraction (KB), and aqueous fraction (KAq) in serum-free culture medium were freshly prepared and used for cytotoxic activity by MTT assay, ROS generation and apoptotic effect by caspase-3 activity. **Results:** Among the four fractions, the KE and KB fractions have revealed that greater percentage inhibition in all types of cancer cells in a dose-dependent manner by MTT assay. The IC₅₀ values of KE fraction were found to be 38.35, 40.47, and 36.83 µg/mL against HeLa, MCF-7, and IMR-32, respectively. The apoptotic activity was evaluated through ROS generation and caspase-3 activities of KE and KB. The results showed that both fractions have significantly increased the ROS production and caspase-3 levels in all the cell cultures in a dose-dependent manner. **Conclusions:** The present investigation has shown that the KE and KB fractions of *K. calycina* displayed significant cytotoxic activity against all three cancer cells by decreased cell viability, increased generation of ROS and caspase-3 activities.

Key words: Caspase-3, cell viability, *Kydia calycina*, reactive oxygen species and Reactive species

INTRODUCTION

Recently, medicinal plants occupy an important position for being the major sources of drug discovery, irrespective of its categorized groups (herb, shrub, or tree). Plants have been essential in treating different forms of diseases including cancer. According to the World Health Organization, 80% of the people living in the rural areas depend on medicinal plants as primary healthcare system. These practices are solely depends on the knowledge of the use of traditional medicinal plants.^[1,2] Cancer chemoprevention is defined as the use of materials of natural source, biological agents, chemical or synthetic compounds to reverse, prevent, or suppress carcinogenic progression of invasive cancer.^[3] Natural products are formulated to generate different types of effective drugs to augment anticancer activities. Proper understanding of the complex synergistic interaction of various constituents of

anticancer herbs, would help in formulating the design to hit the cancerous cells without damaging the normal cells of the body.^[1,2]

Cancer is a disease characterized by the uncontrolled proliferation of the cells. As a cell progresses from normal to cancerous, the biological imperative to survive and perpetuate forces fundamental alterations in cells behavior. The definite cause of the disease in different sections is still to be investigated clearly.^[4] Cancer is thus, a class of diseases,

Address for correspondence:

Prof. Narsimha Reddy Yellu, Department of Pharmacology, University College of Pharmaceutical Sciences, Kakatiya University, Warangal, Telangana, India. Phone: +91-9849577976, E-mail: ynrkuc@gmail.com.

Received: 15-06-2017

Revised: 25-11-2017

Accepted: 07-12-2017

classified by the type of cell that is primarily affected. To combat cancer United States National Cancer Institute has undergone 2070 anticancer clinical trials, in which 150 more drug combinations have been successfully recorded against cancer. The search for the cancer drug discovery from Natural sources started with the investigations done by Hartwell and his coworkers in the late 1960's with the application of a phytochemical, podophyllotoxin, and its derivatives from the plant *Podophyllum peltatum*. Further discoveries lead to isolate anticancer compounds from plants such as *Camptotheca acuminata*, *Catharanthus roseus*, and also *Taxus brevifolia*. Vinblastine, Vincristine, Camptothecin, and Taxol are the well-known potential anticancer agents derived from these plants which are found to be effective against various types of cancer.^[5]

Advances in the clinical researchers for agents which treat various cancers have been increased over the years and as result numbers of agents have been initiated. The organic compounds present in various plants could exaggerate to reduce the toxicity caused due to chemotherapy. Task of modulating the adverse effect is possible only through requisite perspective regarding the specificity of these molecules with combination therapy.^[6]

The cytotoxic and antitumor drugs are generally non-selective and kill normal proliferating cells. Identification of active cancer specific agents remains a needful area in drug screening and drug discovery mechanisms. Much more emphasis has been put on discovering new agents that target tumor cells more efficiently and selectively with negligible toxic effects on normal cells.^[7,8] Although the molecular mechanisms of its antiproliferative and apoptotic effects have not been cleared, increasing evidence has supported that the increase of reactive oxygen species (ROS) generation contributes to the treatment of cancer cells.^[9,10]

Kydia calycina is distributed in Himalayas from the Indus eastwards to Myanmar and in peninsular India from Maharashtra and Madhya Pradesh, principally in mixed, moist, deciduous forests. The leaves were alternate, 7.5–15 cm long and wide, usually 3–7 lobed, apex angled or rounded, base cordate, palmate 7-nerved, hoary-tomentose beneath, and petioles 2.5–5 cm. The leaves are applied to relieve body pains, lumbago and arthritis, a poultice of the leaves is used to treat skin diseases.^[11] *K. calycina* leaf and stem bark paste applied for ulcers and skin diseases.^[12] The *K. calycina* seed oil was reported to contain cyclopropenoid fatty acid apart from normal fatty acids,^[13] and Hibiscoquinone C, Hibiscoquinone B, 8-formyl-2,7-dihydroxy-5-isopropyl-1-methoxy-3-methyl naphthalene were isolated from stem heartwood of *K. calycina*.^[14] The *K. calycina* methanolic leaf extract was reported to having analgesic, anti-inflammatory and hepatoprotective activity.^[15,16] Hence, the present study evaluated the cytotoxic effects of different leaf fractions of *K. calycina* using various human cancer cell cultures, *in vitro*.

MATERIALS AND METHODS

Plant Material

The leaves of *K. calycina* were collected from Tirupati hills, Andhra Pradesh, India. It was authenticated by Prof. V. Raju, Department of Botany, Kakatiya University, Warangal, India.

Preparation of Extracts

Leaves of *K. calycina* were made free from the adherent foreign material and air-dried. Then they were coarsely powdered and macerated with methanol in a round bottom flask for 7 days separately. The content of the flask was stirred intermittently to ensure the efficiency of the extraction. After a week, they were filtered and concentrated under reduced pressure to yield corresponding extracts, and the extracts were kept in a desiccator to remove moisture and stored properly until used.

The methanolic extracts of *K. calycina* were dispersed in sufficient amount of distilled water separately and fractionated with toluene, ethyl acetate and butan-2-one in succession. The obtained fractions and the aqueous residues were concentrated under reduced pressure to yield corresponding extracts.

Cell Culture and Treatment

Human cervical carcinoma (HeLa) cells, human breast cancer (MCF-7) cells and human neuroblastoma (IMR-32) cells were procured from NCCS, Pune. The cells were used between passages 10 and 15. All these cells were grown in suitable culture media supplemented with 10% FBS, 1% L-glutamine, and 1% penicillin-streptomycin antibiotic solution. Cells were seeded at 250,000 cells/flask in a total volume of 10 mL. When confluent, all the cells were trypsinized as described above and seeded in 96 well plates at the rate of 1.0×10^4 cells/0.1 mL. All the cell cultures were maintained in a 5% CO₂ incubator at 37°C. Different concentrations of fractions of *K. calycina* such as toluene fraction (KT), ethyl acetate fraction (KE), butanone fraction (KB), and aqueous residue (KAq) in serum-free culture medium were freshly prepared and used for the cytotoxic activity.

MTT Assay Method

Measurement of cell viability and proliferation forms the basis for numerous *in vitro* assays of a cell population's response to external factors. The reduction of tetrazolium salts is widely believed as a reliable way to study cell proliferation. The effect of test fractions on the cellular proliferation and viability was determined using MTT assay method.^[17] The yellow tetrazolium salt was reduced by dehydrogenase enzymes present in metabolically active cells, to produce

reducing equivalents such as NADH and NADPH. The formazan product has low aqueous solubility and was present as purple crystals. The resulting formazan was dissolved by using dimethyl sulfoxide (DMSO) permitted the convenient quantification of product development. The intensity of the product color was measured at 562 nm and was directly proportional to the number of living cells in the culture.^[18]

The adherent cells were trypsinized according to protocol and were re-suspended in fresh medium after centrifugation. Cell suspension was mixed thoroughly by pipetting several times to get a uniform single cell suspension. 10–15 passages were conducted before performing the experiment to evaluate the cytotoxicity. Different dilutions of fractions were made in media with final phosphate buffer solution (PBS)+1% PEG (solvent control) concentration in the well to be <1%. 100 μ L (0.1 mL) of cell suspension was transferred aseptically to each well of a 96 well plate and it 100 μ L of solvent/fraction (in triplicate) in media was added. The plate was then incubated at 37°C for 48 h in 5% CO₂ incubator. After 48 h of incubation, 20 μ L of MTT was added to each well, and the microtiter plate was again incubated for 2 h. 80 μ L of lysis buffer was added to each well; the plate was wrapped in aluminum foil to prevent the oxidation of the dye. The plate was placed on a rotary shaker for 2 h to solubilize the purple formazan crystals. The absorbances were recorded on the ELISA reader at 562 nm wavelength. The absorbance of the test was compared with that of solvent control to get the percent cytotoxicity.^[19,20]

Measurement of ROS Generation

Generation of ROS was assessed using a cell-permeable fluorescent signal H₂DCF-DA as an indicator for ROS.^[21,22] As described previously, H₂DCF-DA is oxidized to a highly green fluorescent 2070-dichlorofluorescein (DCF) by the generation of ROS. Cancer cell lines were pretreated with various concentrations of KE and KB fractions for 24 h. After 24 h incubation period, the cells were washed with cold PBS and incubated with 100 mmol/L H₂DCF-DA for another 30 min at 37°C. DCF fluorescence intensity was measured using the fluorescence plate reader (Varioskan Flash Multimode Reader, Waltham, MA) at excitation/emission of 488/525 nm. The determinations were carried out thrice in triplicate, ensuring each time that the number of cells per treatment group was the same to ensure reproducibility. The values were expressed as % relative fluorescence compared to the control.

Caspase-3 Assay

Caspases are members of the aspartate-specific cysteinyl protease family. Caspase-3 exists in cells as an inactive 32 kDa proenzyme, called procaspase-3. Procaspase-3 is cleaved into active 17 and 12 kDa subunits by upstream proteases such as caspase-6, caspase-8, and granzyme B

during apoptosis. The overexpression of caspase-3 can result in the initiation of apoptosis. Likewise, the inhibition of caspase-3 can prevent cells from entering into the apoptotic pathway. The activation of caspase-3 is used as a biomarker in the evaluation of apoptosis and in understanding mechanisms of apoptosis induction.^[23]

The assay is based on a colorimetric finding of the chromophore *p*-nitroaniline (*p*NA) after cleavage from the DEVD-*p*NA, a labeled substrate. The *p*NA light emission can be quantified using a microtiter plate reader at 405 nm. Assessment of the absorbances of *p*NA from an apoptotic sample with an uninduced control allows determination of the fold raise in caspase-3 activity.^[24]

Statistical Analysis

Data were expressed as mean \pm SEM. Significance was calculated using one-way ANOVA followed by Dunnett's multiple comparison tests compared to control.

RESULTS AND DISCUSSION

Natural products or their derivatives have been exhibited to have significant anticancer potentials due to their ability to inhibit tumor growth, angiogenesis and metastasis without many side effects.^[25] Recent publications showed the effect of many herbal plants in the treatment of wide range of illnesses. Furthermore, several naturally produced herbal formulations are currently available for cancer patients. Most of the chemotherapeutic agents were cytotoxic to normal cells and build up drug resistance. Therefore, scientific consideration and test of traditionally used herbs for the treatment of various malignancies could be also considered as a very important source for new chemotherapeutic drugs.^[26]

The *in vitro* cytotoxicity of four different fractions of *K. calycina* such as toluene fraction (KT), ethyl acetate fraction (KE), butanone fraction (KB), and aqueous residue (KAq) were evaluated against three different cancer cell cultures, such as human cervical carcinoma (HeLa), human breast cancer (MCF-7), and human neuroblastoma (IMR-32) cells using MTT assay, which is based on the reduction of MTT at different concentrations (10, 30, 100, 300, and 500 μ g/ml). After 48 h of treatment, KE and KB fractions exhibited higher inhibitory effect against all tumor cells, with varying efficiencies and selectivities while others caused marginal cell inhibition [Figure 1]. The IC₅₀ (concentration of the fraction causing 50% cell death) values of test fractions were given in Table 1. Among the four fractions, the KE and KB fractions have revealed that greater percentage inhibition in all types of cancer cells in a dose-dependent manner. Moreover, the KE fraction has shown superior cytotoxicity than KB fraction. The IC₅₀ values of KE fraction were found

to be 38.35, 40.47, and 36.83 µg/mL against HeLa, MCF-7, and IMR-32, respectively.

Since the cytotoxicity of KE and KB was greater, we further evaluated to reveal the mechanism for its cytotoxicity. For this purpose, we evaluated the apoptotic activity through ROS generation and caspase-3 activities of KE and KB against all three cancer cell lines. The results showed that both fractions have significantly increased the ROS production in all the cell cultures [Figure 2]. ROS production was significantly elevated with KE fraction ($P < 0.01$) in all cancer cells. Whereas, KB fraction showed increased ROS generation ($P < 0.05$) in all cancer cells. Excess accumulation of ROS leads to cellular damage and inflammation of the tissues.^[27] ROS plays a major role in cellular senescence paving way to cell death; therefore, there is an urgent need for potential therapeutics that may

prevent oxidative stress-induced neurodegeneration. It is highly possible that the pro-oxidant effect is responsible for the apoptotic activity of these extracts and ROS are key signaling molecules to modulate cell death.^[28] Accumulating evidence indicates that cancer cells produce high levels of ROS that lead to a state of increased basal oxidative stress. The increased production of ROS in cancer cells was observed in *in vitro* studies.^[29] Ahamad *et al.* demonstrated that naringenin leads to cell death in cancer cells through inducing ROS generation.^[30] We, therefore, investigated the effectiveness of KE and KB fractions in generation of ROS. We found that exposure of all three cancer cells with these fractions dramatically enhanced generation of intracellular ROS at different levels in a dose-dependent manner in all cell lines.

Intracellular caspase-3 activation is a key stage in the apoptotic pathway. Hence, we tested the effect of treatment with our plant fractions on intracellular caspase-3 enzymatic activity. Different human cancer cells were treated with the plant fractions and caspase-3 enzymatic activity within the cells was measured [Figure 3]. Since caspase-3 activity rises while cells die and cell numbers drop, it was essential to normalize caspase-3 activity to the number of cells, to obtain more accurate results. The results here are expressed as the percent increase in caspase-3 activity in treated cells compared to cells added with DMSO. Caspase-3 levels were significantly increased with KE fraction in HeLa ($P < 0.05$), MCF-7 ($P < 0.05$), and IMR-32 ($P < 0.01$) cancer cells. Whereas, KB fraction showed increased caspase-3 levels in HeLa ($P < 0.05$) and

Table 1: The IC₅₀ values of different *Kydia calycina* fractions using various cell lines

Extract	IC ₅₀ values (µg/mL)		
	HeLa	MCF-7	IMR-32
KT	108.47±2.72*	114.14±3.16*	76.44±2.16**
KE	38.35±1.34***	40.47±2.13***	36.83±1.78***
KB	69.23±2.89***	80.82±2.45***	93.4±2.67**
KAq	98.92±3.14*	97.82±3.45*	109.32±3.78*

KT: *Kydia calycina* toluene fraction, KE: *Kydia calycina* ethyl acetate fraction, KB: *Kydia calycina* butanone fraction, KAq: *Kydia calycina* aqueous residue, data were mean±SEM, * $P < 0.05$, ** $P < 0.01$, *** $P < 0.001$ compared to control

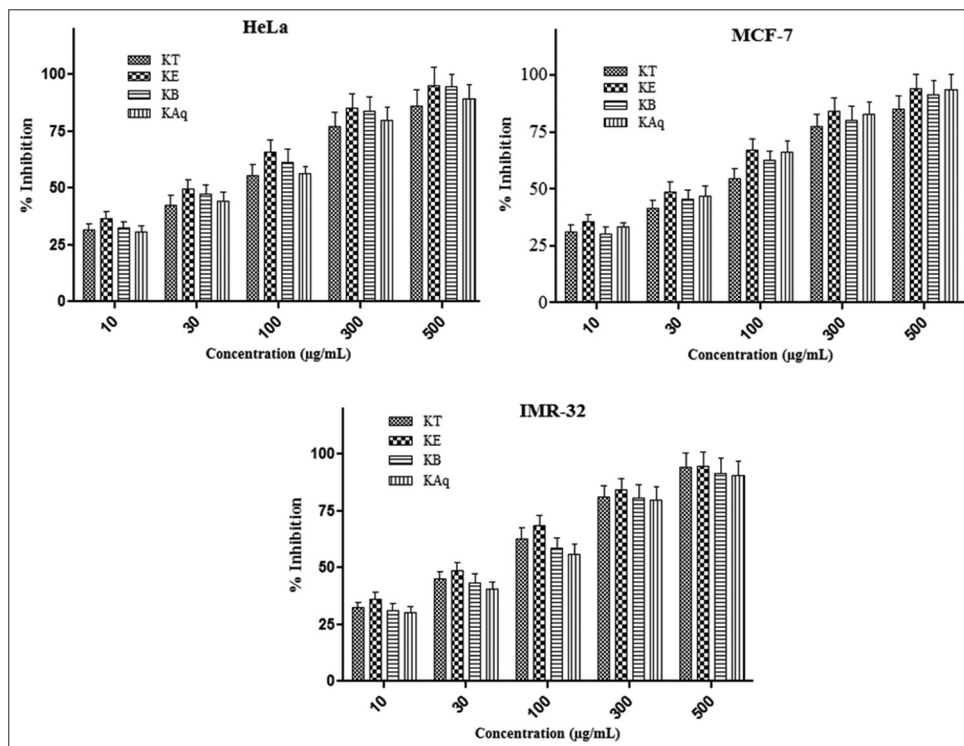


Figure 1: Effect of different fractions on cytotoxicity of HeLa, MCF-7, and IMR-32 cancer cell lines; data were mean±SEM

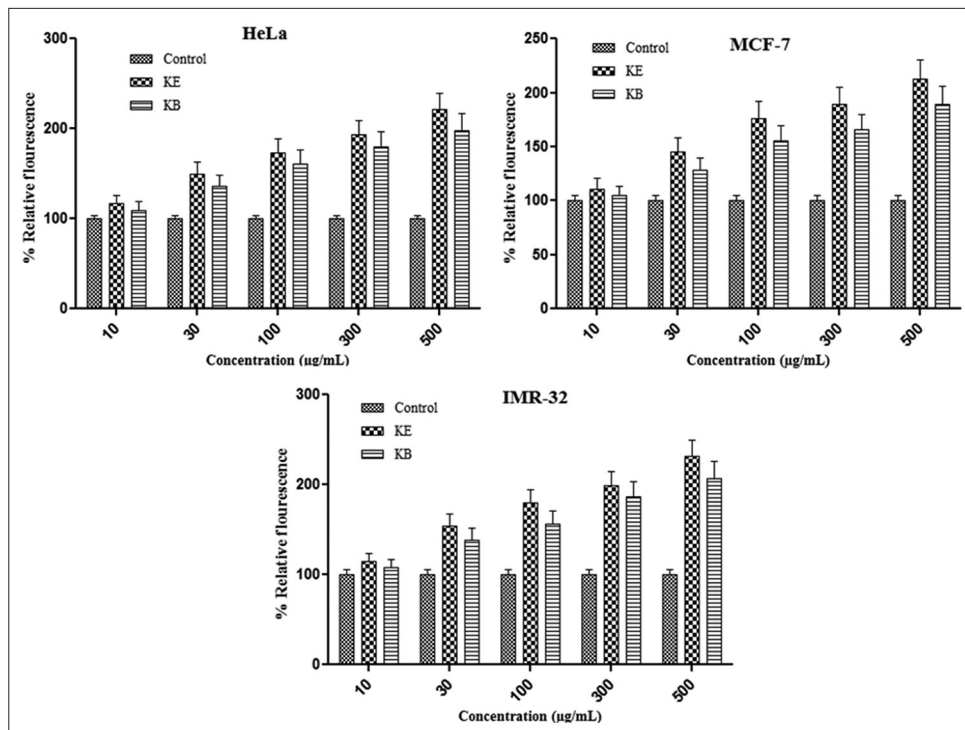


Figure 2: Reactive oxygen species generation effect of different fractions on HeLa, MCF-7, and IMR-32 cancer cell lines, data were mean±SEM

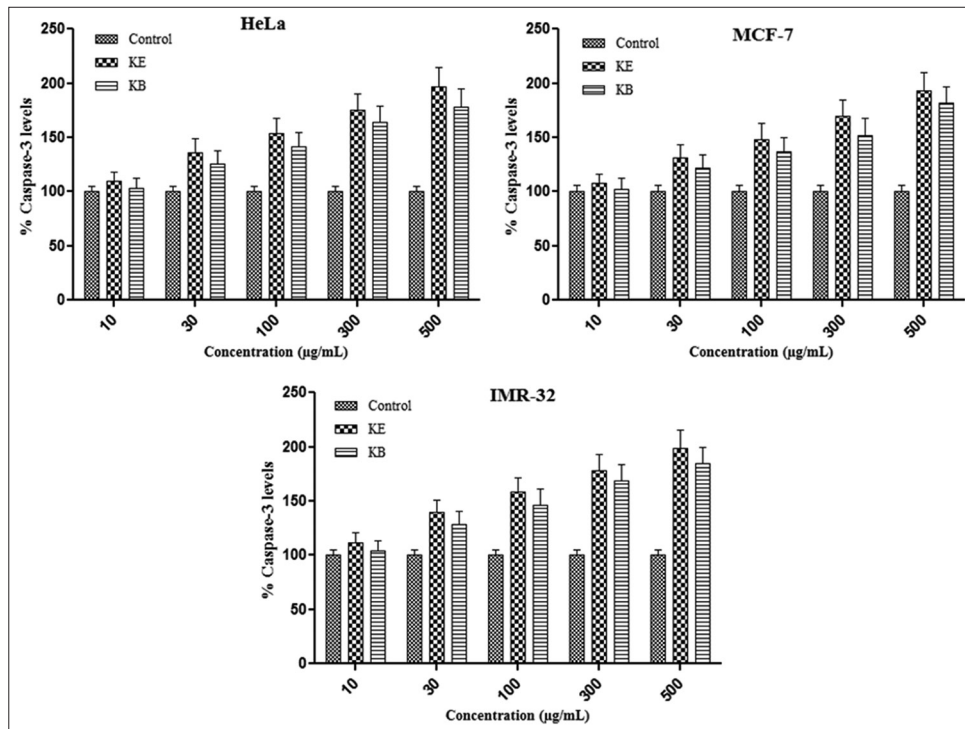


Figure 3: Caspase-3 levels of different fractions on HeLa, MCF-7, and IMR-32 cancer cell lines, data were mean±SEM

IMR-32 ($P < 0.05$) cancer cells. Sherine *et al.* evaluated the mechanism of cell death induced by *Petunia punctata* by caspase-3 colorimetric assay, before and after treatment with the extract. The results showed that the treatment of Panc-1 cells with *P. punctata* strongly induces increased

caspase-3 activity. Furthermore, caspase-3 activity in *P. punctata*-treated cells was reduced in the presence of a caspase-3 specific apoptosis inhibitor. This suggests the involvement of caspase-3 in triggering apoptosis in *P. punctata*-treated Panc-1 cells.^[31]

CONCLUSIONS

In summary, among the four *K. calycina* fractions, the KE and KB fractions were showed increased percentage inhibition of HeLa, MCF-7, and IMR-32 cells by MTT assay. Moreover, the apoptotic activity revealed that both KE and KB fractions have displayed significant increased generation of ROS and caspase-3 activities in all cancer cell lines in a dose-dependent fashion. Further studies are warranted to elucidate the molecular mechanisms of isolated compounds of *K. calycina*.

ACKNOWLEDGMENTS

The first author is grateful to University Grants Commission (UGC), New Delhi, India, for providing Postdoctoral Fellowship.

Source of Support: Nil. Conflict of Interest: None declared.

REFERENCES

- Larkin T. Herbs are often more toxic than magical. *FDA Consum* 1983;17:4-11.
- Saxe TG. Toxicity of medicinal herbal preparations. *Am Fam Physician* 1987;35:135-42.
- Fridlender M, Kapulnik Y, Koltai H. Plant derived substances with anti-cancer activity: From folklore to practice. *Front Plant Sci* 2015;6:799.
- Ashworth A, Christopher LJ, Reis-Filho S. Genetic Interactions in cancer progression and treatment. *Cell* 2011;145:30-8.
- Cragg GM, Newman DJ. Plants as a source of anti-cancer agents. *J Ethnopharmacol* 2005;100:72-9.
- Bos AM, De Vos FY, de Vries EG, Beijnen JH, Rosing H, Mourits MJ. A phase I study of intraperitoneal topotecan in combination with intravenous carboplatin and paclitaxel in advanced ovarian cancer. *Eur J Cancer* 2005;41:539-48.
- Benedekovic G, Kovacevic I, Popsavin M, Francuz JM, Koji V, Bogdanovic G, *et al.* Divergent total synthesis of crass lactones B and C and evaluation of their ant proliferative activity. *Tetrahedron* 2015;71:4581-9.
- Lavrard H, Salvetti B, Mathieu V, Rodriguez F, Kiss R, Delfourne E, *et al.* Synthesis and *in vitro* antiproliferative activity of amido and amino analogues of the marine alkaloid isogranulatimide. *Chem Med Chem* 2015;10:607-9.
- Park JH, Jin CY, Lee BK, Kim GY, Choi YH, Jeong YK, *et al.* Naringenin induces apoptosis through down regulation of akt and caspase-3 activation in human leukemia THP-1 cells. *Food Chem Toxicol* 2008;46:3684-90.
- Gach K, Długosz A, Janecka A. The role of oxidative stress in anticancer activity of sesquiterpene lactones. *Naunyn Schmiedebergs Arch Pharmacol* 2015;388:477-86.
- Parrotta JA. *Healing Plants of Peninsular India*. New Delhi: CABI Publishing; 2001.
- Ramarao N, Henry AN. *The Ethnobotany of Easternghats in Andhra Pradesh, India*. BSI, Calcutta: Botanical Survey of India. BSI Publication; 1996.
- Daulatabad CD, Ankalagi KK, Desai VA. Cyclopropenoid and fatty acid composition of *Kydia calycina* seed oil. *Eur J Lipid Sci Tech* 2006;91:237-8.
- Joshi KC, Sing P, Taneja S. A sesquiterpenoid naphthol from *Kydia calycina*. *Plant Med* 1983;49:127.
- Baburao B, Rama NR, Carey MW, Krishna MG. Analgesic and anti-inflammatory activities of leaf extract of *Kydia calycina* Roxb. *Bangladesh J Pharmacol* 2009;4:101-4.
- Parameshwar H, Babu RB, Ravi KB, Narsimha RY, Krishna MG. Hepatoprotective effect of methanolic extract of the leaves of *Kydia calycina* on carbon tetrachloride induced hepatotoxicity in albino rats. *Afr J Pharm Pharmacol* 2011;5:1920-4.
- Lee JS, Jung WK, Jeong MH, Yoon TR, Kim HK. Sanguinarine induces apoptosis of HT-29 human colon cancer cells via the regulation of bax/Bcl-2 ratio and caspase-9-dependent pathway. *Int J Toxicol* 2012;31:70-7.
- Carmichael J, DeGraff WG, Gazdar AF, Minna JD, Mitchell JB. Evaluation of a tetrazolium-based semiautomated colorimetric assay: Assessment of chemosensitivity testing. *Cancer Res* 1987;47:936-42.
- Allely MC, Seudero DA, Monks A. Feasibility of drug screening with panels of human tumor cell lines using micro culture tetrazolium assay. *Cancer Res* 1998;8:589-601.
- Harikiran L, Bhikku A, Narsimha RY. *In vitro* cytotoxicity of gold and silver nanorods using different human cell lines. *Lat Am J Pharm* 2015;34:1277-82.
- Min KJ, Jung KJ, Kwon TK. Carnosic acid induces apoptosis through reactive oxygen species-mediated endoplasmic reticulum stress induction in human renal carcinoma caki cells. *J Cancer Prev* 2014;19:170-8.
- Wu T, Qiang L, Chen FH, Zhao Q, Yang Z, Zou MJ, *et al.* LFG-500, a newly synthesized flavonoid, induced a reactive oxygen species-mitochondria-mediated apoptosis in hepatocarcinoma cells. *Biomed Prev Nutr* 2011;1:132-8.
- Lingabathula H, Yellu N. Cytotoxicity, oxidative stress, and inflammation in human hep G2 liver epithelial cells following exposure to gold nanorods. *Toxicol Mech Methods* 2016;26:340-7.
- Casciola RL, Nicholson DW, Chong T, Rowan KR, Thornberry NA, Miler DK, *et al.* Apopain/CPP32 cleaves proteins that are essential for cellular repair: A fundamental principle of apoptotic death. *J Exp Med* 1996;183:1957-64.
- Abdurrahim K, Ismail K, Murat D, Fatemeh B, Baki T. Cytotoxic, genotoxic and apoptotic effects of

- naringenin-oxime relative to naringenin on normal and cancer cell lines. *Asian Pac J Trop Biomed* 2016;6:872-80.
26. Maram S, Kh K, Mahmoud MZ, Mahmoud GE, Walied A, Walaa A. Anticancer activity of *Aloe vera* and *Calligonum comosum* extracts separately on hepatocellular carcinoma cells. *Asian Pac J Trop Biomed* 2015;5:375-81.
 27. Murphy MP, Holmgren A, Larsson NG, Halliwell B, Chang CJ, Kalyanaraman B, *et al.* Unraveling the biological roles of reactive oxygen species. *Cell Metab* 2011;13:361-6.
 28. Wu CC, Bratton SB. Regulation of the intrinsic apoptosis pathway by reactive oxygen species. *Antioxid Redox Signal* 2013;19:546-58.
 29. Halliwell B. Oxidative stress and cancer: Have we moved forward? *Biochem J* 2007;401:1-1.
 30. Ahamad MS, Siddiqui S, Jafri A, Ahmad S, Afzal M, Arshad M, *et al.* Induction of apoptosis and antiproliferative activity of naringenin in human epidermoid carcinoma cell through ROS generation and cell cycle arrest. *PLoS One* 2014;9:e110003.
 31. George S, Bhalerao SV, Lidstone EA, Ahmad IS, Abbasi A, Cunningham BT, *et al.* Cytotoxicity screening of Bangladeshi medicinal plant extracts on pancreatic cancer cells. *BMC Complement Altern Med* 2010;10:52.

Source of Support: University Grants Commission (UGC), New Delhi, India for providing Post Doctoral Fellowship.
Conflict of Interest: The authors declare that there are no potential conflicts of interest.



Assessment of oxidative stress induced by gold nanorods following intra-tracheal instillation in rats

Harikiran Lingabathula & Narsimhareddy Yellu

To cite this article: Harikiran Lingabathula & Narsimhareddy Yellu (2018) Assessment of oxidative stress induced by gold nanorods following intra-tracheal instillation in rats, Drug and Chemical Toxicology, 41:2, 141-146, DOI: [10.1080/01480545.2017.1321012](https://doi.org/10.1080/01480545.2017.1321012)

To link to this article: <https://doi.org/10.1080/01480545.2017.1321012>



Published online: 15 May 2017.



Submit your article to this journal [↗](#)



Article views: 12



View related articles [↗](#)



View Crossmark data [↗](#)

RESEARCH ARTICLE



Assessment of oxidative stress induced by gold nanorods following intra-tracheal instillation in rats

Harikiran Lingabathula  and Narsimhareddy Yellu 

Department of Pharmacology and Toxicology, University College of Pharmaceutical Sciences, Kakatiya University, Warangal, India

ABSTRACT

Gold nanorods (GNRs) are used for their wide variety of applications in various industries. There is a little availability of data related to toxicity and ecological implications of these GNRs. The study evaluated the oxidative stress induction following intra-tracheal instillation of 1 and 5 mg/kg b.w. doses of 10 and 25 nm GNRs by estimating various oxidative stress markers including lipid peroxidation (malondialdehyde; MDA), glutathione (GSH), superoxide dismutase (SOD), catalase and total antioxidant capacity (TAC) after 1 day, 1 week, 1 month, and 3 months post exposure periods. The results have shown increased MDA levels and decreased GSH levels following 1 day and 1 week post exposure periods, indicating induction of oxidative stress. Also, the SOD, catalase and TAC levels were significantly decreased following exposure of both 10 and 25 nm GNRs after 1 day and 1 week after exposures, indicating the inhibition of antioxidant defense mechanisms. Moreover, the 10 nm GNRs at 5 mg/kg dose displayed greater changes in all the estimated parameters, representing dose and size based induction of oxidative stress by GNRs. In contrast, a little change was observed during 1 month and 3 months post exposure periods, may be due to recovery. Finally, the GNRs induced dose-size-dependent oxidative stress induction by various oxidative stress markers following intra-tracheal instillation in rats.

ARTICLE HISTORY

Received 21 November 2016
Revised 29 March 2017
Accepted 8 April 2017

KEYWORDS

Gold nanorods; oxidative stress; superoxide dismutase; catalase; toxicity

Introduction

Gold nanorods (GNRs) have 20 times or more optical absorption efficiencies than the gold based nanoparticles (NPs) of the same volume (Copland *et al.* 2004). The scattering coefficients per micron of GNRs are also an order of magnitude higher when compared to those of gold nanospheres and nanoshells (Jain *et al.* 2006). In addition, GNRs have a strong binding affinity to thiol groups permitting them to be competently conjugated with numerous biomolecules after stabilizing with polyethylene glycol (Liao and Hafner 2005). Functionalization of the GNRs with antibodies or other biomolecules (Huff *et al.* 2007) allows their specific attachment to any target cell. GNRs of high aspect ratio offer a higher fluorescence intensity and this property will encourage the development of techniques using GNRs in fluorescent probe micro array assays and optical biosensor applications for DNA analysis (Li *et al.* 2005).

GNRs could be used as optical sensors for Raman-based intracellular biosensing useful for cancer diagnosis and other diagnostic biomedical applications (Oyelere *et al.* 2007). There have also been developments in respect of using GNRs in refractometric biomolecular sensors (Chen *et al.* 2007, Yu and Irudayaraj 2007). GNRs conjugated with photo sensitizers can kill MRSA by NIR photothermal radiation and photodynamic antimicrobial chemotherapy (Kuo 2009, Pissuwan *et al.* 2009). The study clearly showed that GNRs conjugated with a hydrophilic photo sensitizer such as toluidine blue O act as dual

function agents in hyperthermia and photodynamic inactivation against methicillin-resistant *Staphylococcus aureus* (Gil 2007, Perni 2009).

NPs induced oxidative stress triggers cell signaling pathways resulting in increased expression of pro-inflammatory and fibrotic cytokines. Some NPs have been shown to activate inflammatory cells such as macrophages and neutrophils which can result in the increased production of reactive oxygen species (ROS). The mechanism for ROS generation is different for each NP type and to date the exact underlying cellular mechanism for ROS generation is incompletely understood and remains to be elucidated. The oxidative stress induction and generation of ROS may play a major role in the toxicity of many types of NPs (He *et al.* 2011).

GNRs are utilized enormously for their potential applications in different industries, as the occupational exposures for these GNRs are also increased. The principal exposures for NPs are through inhalation, ingestion and dermal contact (Oberdorster *et al.* 2005). In particular, the inhaled NPs are likely to reach the alveoli and have shown significant toxicity effects in deep regions of lung (Mohamed *et al.* 2011). Till date, there is a little availability of the toxicity data of rod shaped gold NPs towards humans. Some of the recent studies evaluated the *in vitro* toxicity of GNRs using different human cell lines and the results displayed that the cytotoxicity through oxidative stress induction (Tianxun *et al.* 2014, Harikiran *et al.* 2015, Ying *et al.* 2015). The present study was

aimed to assess the general mechanisms involved in the toxicity of rod shaped, PEG coated, 10 nm and 25 nm GNRs following intra-tracheal instillation in rats, *in vivo* by using estimation of enzymatic and non-enzymatic oxidative stress parameters.

Materials and methods

Chemicals

The 10 nm GNRs (GNR 10) and 25 nm GNRs (GNR 25) were purchased from Sigma-Aldrich (St. Louis, MO) with Lot numbers MKBH3815V and MKBH3819V, respectively. Quartz (QTZ) particles (58–68 μm) were procured from Berkeley Springs, WV. α,α -Diphenyl- β -picryl hydrazyl (DPPH), 1,1,3,3-tetraethoxy propane (TEP) and *o*-dianisidine were purchased from Sigma-Aldrich (St. Louis, MO). All the rest of chemicals were acquired from Himedia (Mumbai, India).

Animals

Male Wistar rats of six weeks old were kept one week in a quarantine area. Throughout the quarantine and experimental periods, the rats were housed in polypropylene cages in a room; water and feed were available freely with controlled temperature ($25 \pm 2^\circ\text{C}$), humidity ($55 \pm 5\%$) and a 12 h light/dark cycle. The rats weighed approximately 220 g were selected and used for the present study.

Experimental design

The 10 and 25 nm GNRs and QTZ suspensions were prepared in PBS with 1% PEG by briefly shearing and subsequently sonicating (1–2 min) the samples. All the test nanorod samples were re-sonicated on the day of dosing before the instillation (Reddy *et al.* 2011). The rats were divided into different groups ($n=6$) and instilled with a single dose of control (PBS +1% PEG), 1 mg/kg 10 nm GNRs, 5 mg/kg 10 nm GNRs, 1 mg/kg 25 nm GNRs, 5 mg/kg 25 nm GNRs, 1 mg/kg QTZ, and 5 mg/kg QTZ by intra-tracheal instillation method as described previously (Kiranmai and Reddy 2013), because this technique of exposure was a reliable qualitative screen for assessing the toxicity of inhaled NPs (Yasuo *et al.* 2016). Briefly, the rats were anesthetized with isoflurane and anesthetization was continued via a small nose cone. A small hole was made in the trachea and a 24 gauge plastic catheter was inserted through the hole to the distal end of the trachea through a blunted needle. A syringe already filled with 200 μL of air and 50 μL of PBS was connected to the free end of silicone tubing to rapidly propel the GNRs sample from the tubing and needle into the lungs of rats. The incision was sutured, swabbed with povidone iodine and anesthetized with lidocaine. The rats recovered and were active within 10–15 min. Here, QTZ exposure was used as positive control to compare the results of the test nanorods (Reddy *et al.* 2012). The study was approved by Institutional Animal Ethics Committee, UCPSc, Kakatiya University (Approval no.: IAEC/04/UCPSc/KU/2016).

Collection of blood and biochemical analysis

The blood was collected from the control, GNRs and QTZ exposed rats by means of retro orbital plexus at 1 day, 1 week, 1 month, and 3 months post instillation periods. The serum was obtained by immediate centrifugation of blood samples at 3000 rpm for 10 min at room temperature. All samples were stored at -20°C until analysis. All biochemical assays were performed at 1 day, 1 week, 1 month, and 3 months post instillation periods in rats for the estimation of different oxidative stress markers and antioxidant capacity using following parameters.

Lipid peroxidation assay

Thiobarbituric acid reactive substance (TBARS) is a well-established assay for screening and monitoring lipid peroxidation. Malondialdehyde (MDA) forms a 1:2 adduct with thiobarbituric acid (TBA). The MDA–TBA adduct formed from the reaction of MDA in samples with TBA can be measured colorimetrically (Reddy *et al.* 2012). To precipitate the proteins, 0.5 mL of 30% trichloroacetic acid was added to 0.5 mL of serum and vortexed for 30 s. The clear supernatant was taken after centrifuging at 3000 rpm for 10 min. To the supernatant, 500 μL of 1% TBA solution and 500 μL of water were added and this solution was heated for 1 h at 98°C . The solutions were cooled to room temperature and kept in ice for 5 min. The pink color was read at 532 nm using spectrophotometer against TEP as standard.

Glutathione assay

GSH is a key intracellular tripeptide thiol composed of glutamic acid, cysteine and glycine. Glutathione reductase reduces oxidized glutathione to reduced glutathione in the presence of NADPH. Subsequently, the 5,5'-dithiobis-2-nitro benzoic acid (DTNB) reacts with the thiol group of GSH to produce a colored compound (Beulter *et al.* 1963, Mytilineou *et al.* 2002). To 0.5 mL of citrated blood, 0.5 mL of 5% trichloroacetic acid solution was added to precipitate the proteins and centrifuged at 3000 rpm for 10 min. To 0.1 mL of supernatant, 0.5 mL of DTNB reagent and 1 mL of sodium phosphate buffer were added. Absorbance of the yellow color developed was measured at 412 nm. The GSH content was determined from standard graph by using pure glutathione.

Superoxide dismutase (SOD) assay

This assay can be used to determine whether a compound is a general, free radical or a scavenger specific for the superoxide anion. In this assay, free radicals are generated by photo-oxidation of *o*-dianisidine sensitized by riboflavin. A general free radical scavenging compound results in decrease in the oxidized dianisidine measurable by UV/visible spectrophotometer. In contrast, any compound which specifically scavenges $\text{O}_2^{\bullet-}$ increases the amount of oxidized dianisidine and hence will have an augmentary effect (Zelko *et al.* 2002, Valentine and Hart 2003).

Three milliliters of packed blood cells were lysed by the addition of equal volume of cold deionized water. Hemoglobin was then precipitated by the addition of chloroform:ethanol (1.5:1). This was diluted with 500 μ L of water and centrifuged for 15 minutes at 3000 rpm. The supernatant containing SOD was taken for the measurement of its activity. 0.88 mL of riboflavin solution was added to 60 μ L of o-dianisidine solution and to this 100 μ L of clear separated SOD sample was added and optical density was measured at 460 nm. The cuvette containing reaction mixture was transferred to the illuminating box, illuminated for 4 min and optical density was re-measured against blank containing ethanol in place of enzyme. The change in the optical density was determined. The SOD content was determined using pure bovine SOD.

Catalase assay

The rate of disintegration of hydrogen peroxide into water and oxygen is proportional to the concentration of catalase. The absorbance of hydrogen peroxide solution can be easily measured at 240 nm, on decomposition of hydrogen peroxide by catalase, the absorbance decreases with time. The enzyme activity could be arrived at from this decrease (Votyakova and Reynolds 2004).

2.5 mL of phosphate buffer was added to 0.1 mL of serum and incubated at 25 °C for 30 min. After transferring into a cuvette, the absorbance was measured at 240 nm, 650 μ L of hydrogen peroxide solution was added to initiate the reaction. The change in absorbance was measured for 3 min. The average change in absorbance per minute for each assay was calculated and the results were expressed in terms of IU/mL of serum. The catalase content was determined using pure catalase. One international unit of catalase is the enzyme that decomposes one μ M of hydrogen peroxide per minute at 25 °C.

Total antioxidant capacity assay

For the estimation of total antioxidant capacity (TAC), we used a stable free radical DPPH, at the concentration of 0.2 mM in methanol (Aurelia *et al.* 2009). 0.1 mL of serum was deproteinated by the addition of 1 mL of methanol, vortexed for 30 s and centrifuged at 3000 rpm for 30 min to separate the proteins. 1.5 mL of methanol and 0.5 mL of DPPH solution were added to the clear supernatant, mixed thoroughly and absorbance was read at 517 nm against blank, prepared in an identical way but without the addition of serum. Ascorbic acid was used as a reference standard and the TAC was expressed in terms of nM of ascorbic acid.

Statistical analysis

The data were expressed as mean \pm SD ($n = 6$). Statistical analysis was performed for all the assays using one way ANOVA followed by Dunnett's test. The statistical significance was indicated by $\$p < 0.05$, $\#p < 0.01$, $*p < 0.001$ versus time-matched control treated rats.

Table 1. Malondialdehyde levels (nM) following intra-tracheal instillation of GNRs in rats.

Treatment	Post instillation period			
	1 Day	1 Week	1 Month	3 Months
Control	6.87 \pm 0.74	6.81 \pm 0.77	6.05 \pm 0.85	5.94 \pm 0.68
GNR 10 (1 mg/kg)	9.39 \pm 0.89#	9.14 \pm 0.94#	7.09 \pm 0.97	6.24 \pm 0.85
GNR 10 (5 mg/kg)	10.48 \pm 1.25*	11.95 \pm 0.98*	7.94 \pm 0.68\$	6.51 \pm 0.72
GNR 25 (1 mg/kg)	7.95 \pm 0.93	8.11 \pm 0.59	6.47 \pm 0.85	6.05 \pm 0.69
GNR 25 (5 mg/kg)	8.86 \pm 1.14\$	9.32 \pm 1.12#	6.85 \pm 0.94	6.12 \pm 0.85
QTZ (1 mg/kg)	8.47 \pm 0.76	8.23 \pm 0.78	6.72 \pm 0.68	6.04 \pm 0.63
QTZ (5 mg/kg)	9.54 \pm 1.12#	10.62 \pm 1.13*	7.17 \pm 0.79	6.17 \pm 0.59

Data were expressed as mean \pm SD ($n = 6$).

$\$p < 0.05$, $\#p < 0.01$, $*p < 0.001$ versus control treated rats.

Table 2. Glutathione levels (μ M) following intra-tracheal instillation of GNRs in rats.

Treatment	Post instillation period			
	1 Day	1 Week	1 Month	3 Months
Control	342.24 \pm 28.85	353.85 \pm 30.47	361.36 \pm 33.47	373.26 \pm 32.75
GNR 10 (1 mg/kg)	144.58 \pm 12.97*	227.93 \pm 24.56*	291.87 \pm 27.86\$	342.74 \pm 28.67
GNR 10 (5 mg/kg)	78.47 \pm 7.25*	93.14 \pm 8.14*	208.54 \pm 19.74*	317.29 \pm 26.53
GNR 25 (1 mg/kg)	162.95 \pm 17.36*	241.32 \pm 21.45*	314.84 \pm 29.46	356.98 \pm 31.72
GNR 25 (5 mg/kg)	114.96 \pm 12.38*	159.69 \pm 14.67*	235.12 \pm 19.27#	326.36 \pm 22.32
QTZ (1 mg/kg)	141.25 \pm 15.62*	213.94 \pm 22.59*	298.58 \pm 16.38	356.53 \pm 30.69
QTZ (5 mg/kg)	97.63 \pm 9.41*	148.26 \pm 15.57*	243.84 \pm 21.23*	324.31 \pm 21.79

Data were expressed as mean \pm SD ($n = 6$).

$\$p < 0.05$, $\#p < 0.01$, $*p < 0.001$ versus control treated rats.

Results

Lipid peroxidation

The MDA levels were increased following intra-tracheal instillation of GNRs and QTZ treated rats at 1 day and 1 week post exposure periods (Table 1), indicating lipid peroxidation. The 10 nm GNRs have shown significant elevated lipid peroxidation following 1 day and 1 week post exposure periods at 1 mg/kg ($p < 0.01$) and 5 mg/kg ($p < 0.001$) b.w. doses. The 25 nm GNRs at 5 mg/kg b.w. dose significantly increased the MDA levels following 1 day ($p < 0.05$) and 1 week ($p < 0.01$) post exposure periods compared to control. Also, the 10 nm GNRs increased the MDA levels compared to QTZ exposed rats.

Estimation of glutathione

Similar to QTZ, the GSH levels were decreased following intra-tracheal instillation of GNRs treated rats at 1 day, 1 week, and 1 month post exposure periods (Table 2). The 10 nm GNRs have shown significant depleted GSH levels following 1 day ($p < 0.001$), 1 week ($p < 0.001$), and 1 month ($p < 0.05$) post exposure periods at 1 mg/kg and 5 mg/kg b.w. doses versus control treated rats, whereas the 25 nm GNRs at 5 mg/kg b.w. dose only significantly decreased the GSH content following 1 day ($p < 0.001$), 1 week ($p < 0.001$), and 1 month ($p < 0.01$) post exposure periods.

Estimation of superoxide dismutase

The SOD levels in rat blood following exposure of GNRs, QTZ and control estimated at 1 day, 1 week, 1 month, and 3 months post exposure periods are presented in Table 3.

Table 3. Superoxide dismutase levels (IU/mL) following intra-tracheal instillation of GNRs in rats.

Treatment	Post instillation period			
	1 Day	1 Week	1 Month	3 Months
Control	41.47 ± 4.54	41.13 ± 4.73	42.53 ± 4.58	43.24 ± 4.69
GNR 10 (1 mg/kg)	26.31 ± 3.96*	25.89 ± 2.97*	39.85 ± 4.25	41.13 ± 4.56
GNR 10 (5 mg/kg)	18.47 ± 2.56*	16.36 ± 2.13*	35.54 ± 3.96\$	38.64 ± 3.89
GNR 25 (1 mg/kg)	31.46 ± 3.85#	29.34 ± 3.35#	40.42 ± 4.37	42.18 ± 4.79
GNR 25 (5 mg/kg)	26.68 ± 2.97*	24.42 ± 2.96*	38.35 ± 4.14	40.86 ± 4.34
QTZ (1 mg/kg)	28.25 ± 3.14*	27.87 ± 2.96*	39.96 ± 4.69	42.46 ± 5.34
QTZ (5 mg/kg)	24.54 ± 2.87*	22.85 ± 2.79*	38.57 ± 3.69	41.36 ± 4.79

Data were expressed as mean ± SD ($n = 6$).

\$ $p < 0.05$, # $p < 0.01$, * $p < 0.001$ versus control treated rats.

Table 4. Catalase levels (IU/mL) following intra-tracheal instillation of GNRs in rats.

Treatment	Post instillation period			
	1 Day	1 Week	1 Month	3 Months
Control	45.27 ± 5.38	44.23 ± 5.86	45.86 ± 4.68	46.64 ± 5.63
GNR 10 (1 mg/kg)	28.85 ± 3.14*	27.36 ± 3.17*	40.62 ± 4.21	43.56 ± 4.65
GNR 10 (5 mg/kg)	19.95 ± 2.34*	18.27 ± 2.34*	31.38 ± 3.52*	39.87 ± 3.57
GNR 25 (1 mg/kg)	30.64 ± 3.61*	29.85 ± 3.16*	41.57 ± 4.41	44.15 ± 4.87
GNR 25 (5 mg/kg)	24.46 ± 2.87*	22.98 ± 2.54*	36.52 ± 3.85\$	42.34 ± 4.47
QTZ (1 mg/kg)	29.74 ± 3.12*	28.47 ± 2.68*	40.81 ± 4.57	44.21 ± 4.63
QTZ (5 mg/kg)	23.85 ± 2.75*	22.53 ± 2.35*	36.97 ± 3.43\$	41.86 ± 4.15

Data were expressed as mean ± SD ($n = 6$).

\$ $p < 0.05$, * $p < 0.001$ versus control treated rats.

Similar to QTZ, the 10 nm GNRs have displayed significantly decreased levels of SOD following 1 day and 1 week post exposure periods ($p < 0.001$) at both doses whereas at 5 mg/kg dose has shown significantly decreased SOD levels following 1 month post exposure ($p < 0.05$). 25 nm GNRs have shown decreased levels of SOD following 1 day and 1 week post exposure periods at 1 mg/kg dose ($p < 0.01$) and 5 mg/kg dose ($p < 0.001$).

Estimation of catalase

The 10 nm GNRs have shown significant depleted levels of catalase following 1 day and 1 week post exposure periods ($p < 0.001$) at both doses whereas at 5 mg/kg dose significantly decreased catalase levels were found following 1 month post exposure ($p < 0.001$). 25 nm GNRs have shown decreased levels of catalase following 1 day and 1 week post exposure periods at both doses ($p < 0.01$) and at 5 mg/kg dose significantly ($p < 0.05$) decreased levels were found following 1 month post exposure (Table 4). Similar decreased levels of catalase were found with QTZ exposure, indicating toxicity of GNRs.

Estimation of total antioxidant capacity

The TAC levels in rat serum upon intra-tracheal instillation of GNRs, QTZ and control estimated are presented in Table 5. The 10 nm GNRs have displayed significantly decreased levels of TAC following 1 day and 1 week post exposure periods ($p < 0.001$) at both doses whereas at 5 mg/kg dose has shown significantly decreased TAC levels following 1 month post exposure ($p < 0.001$). 25 nm GNRs have shown decreased levels of TAC following 1 day ($p < 0.001$), 1 week ($p < 0.001$), and

Table 5. Total antioxidant capacity (nM) following intra-tracheal instillation of GNRs in rats.

Treatment	Post instillation period			
	1 Day	1 Week	1 Month	3 Months
Control	14.54 ± 1.12	14.91 ± 1.38	15.85 ± 1.37	16.37 ± 1.85
GNR 10 (1 mg/kg)	9.52 ± 0.87*	10.87 ± 1.24*	13.14 ± 1.51\$	15.56 ± 1.68
GNR 10 (5 mg/kg)	7.34 ± 0.68*	8.58 ± 0.94*	10.42 ± 1.12*	13.78 ± 1.36
GNR 25 (1 mg/kg)	10.12 ± 0.98*	11.46 ± 1.32#	13.97 ± 1.32	15.89 ± 1.69
GNR 25 (5 mg/kg)	8.79 ± 0.81*	9.36 ± 0.84*	11.68 ± 0.96#	14.21 ± 1.59
QTZ (1 mg/kg)	10.61 ± 1.16*	11.85 ± 1.12\$	14.21 ± 1.25	15.46 ± 1.52
QTZ (5 mg/kg)	8.89 ± 0.93*	9.43 ± 0.93*	11.87 ± 1.12#	14.85 ± 1.37

Data were expressed as mean ± SD ($n = 6$).

\$ $p < 0.05$, # $p < 0.01$, * $p < 0.001$ versus control treated rats.

1 month ($p < 0.05$) post exposure periods at 5 mg/kg dose. 25 nm GNRs also decreased the TAC significantly ($p < 0.001$) at 1 mg/kg dose following 1 day post instillation period.

Discussion

The GNRs are extensively used in various industrial, commercial, and imaging applications. But the related health risks associated with these GNRs are sparsely known. Some studies evaluated the toxicity of these GNRs using human cell cultures *in vitro* (Harikiran *et al.* 2015, Ying *et al.* 2015). Some of the previous studies proposed that the toxicity of different NPs were primarily due to induction of oxidative stress and production of ROS (Igor *et al.* 2011, Alicia *et al.* 2014, Abudayyak *et al.* 2016). So, the present study was to assess the oxidative stress and TAC of 10 nm and 25 nm GNRs, QTZ and control (PBS +1% PEG) at 1 and 5 mg/kg b.w. doses following intra-tracheal instillation in rats using estimation of various oxidative stress parameters after 1 day, 1 week, 1 month, and 3 months post exposure periods.

The results have shown that the intra-tracheal instillation of 10 and 25 nm GNRs revealed increased levels of serum MDA levels (lipid peroxidation) and decreased blood GSH levels following 1 day and 1 week post exposure periods at 5 mg/kg b.w. dose, whereas slight or no change was detected at 1 month and 3 months post exposure periods, may be due to recovery. Induction of oxidative stress can be expressed in terms of GSH estimation and is an important antioxidant that is oxidized during oxidative stress (Marquis *et al.* 2009). ROS production and subsequent oxidative stress induction was manifested by increased levels of MDA and reduction in GSH content. Both GNRs and QTZ might have resulted in ROS generation and oxidative stress induction via elevated MDA levels and depleted GSH content following instillation after 1 day and 1 week post exposure periods.

Recently, Jiali *et al.* (2015) evaluated the intracellular ROS generation and oxidative stress by GNRs exposure in HCT 116 cells with different concentrations. The results have shown that dose-dependent ROS activation and oxidative stress induction in cells lead to autophagy. On the other hand, the free radical scavenger *n*-acetylcysteine markedly avoided GNRs induced ROS generation and oxidative stress induction. These facts demonstrated that the autophagy induced by the GNRs is mediated through the generation of intracellular ROS and oxidative stress induction. The enzymatic oxidative stress markers in rat blood following intra-tracheal instillation of 10

and 25 nm GNRs at 1 mg/kg and 5 mg/kg b.w. doses have shown significantly depleted levels of SOD and catalase after 1 day and 1 week post exposure periods. In contrast, there was no significant depletion in these both SOD and catalase after 1 month and 3 months post exposure periods, may be due to recovery. Similar to QTZ, the SOD and catalase levels following exposure of GNRs displayed a dose-dependent decrease. Antioxidant defense enzymes such as SOD and catalase can prevent the oxidative damage from ROS. SOD catalyzes the dismutation of the superoxide anion into hydrogen peroxide and molecular oxygen. Catalase is one of the major antioxidant enzymes that destroy hydrogen peroxide by dismutation (Reddy *et al.* 2011). Our results suggest that the inhibition of these antioxidant defense enzymes may increase the oxidative stress induction by GNRs.

The TAC of 10 and 25 nm GNRs were determined by using a stable free radical, DPPH. The findings displayed the decrease in TAC of 10 and 25 nm GNRs, QTZ significantly after 1 day and 1 week post exposure periods in rats, indicating the induction of oxidative stress by GNRs. The results also displayed significantly reduced TAC of test nanorods at 5 mg/kg dose after 1 month post exposure. The reduced TAC in GNRs instilled rats suggests the reduction in antioxidant defense mechanisms. The recent investigations assessed the oxidative stress induction and antioxidant status following intra-tracheal instillation of MgO NPs and multi wall carbon nanotubes at a dose of 0.2, 1, and 5 mg/kg of b.w. in rats and the blood samples were withdrawn at 1, 7, 30, and 90 days of post instillation periods. The exposure of both NPs produced a significant dose-dependent decrease in blood GSH, TAC, SOD, and catalase levels, and increased lipid peroxidation (Reddy *et al.* 2011, Kiranmai and Reddy 2013). The present study also results in increased levels of MDA and decreased levels of GSH, SOD, catalase, and TAC activity is strongly related to lipid peroxidation and induction of oxidative stress in rats following exposure of GNRs. These findings suggest the possible occupational health risk upon chronic exposures of GNRs.

The 10 nm GNRs at lower dose (1 mg/kg) also showed significantly elevated MDA levels and depleted GSH levels. In contrast, 25 nm GNRs did not show significant change, corresponding to the size-dependent toxicity. The exposure of 10 nm GNRs in rats has also shown greater depleted levels of SOD, catalase and TAC activity, indicating the greater induction of oxidative stress and antioxidant capacity when compared to the 25 nm GNRs, proposing the size-dependent induction of oxidative stress. The recent study evaluated the *in vitro* toxicity following exposure of different sizes of GNRs in human Hep G2 cell lines. The results revealed the size-dependent toxicity of GNRs due to oxidative stress induction, cell membrane damage and release of inflammatory mediator (Harikiran and Narsimhareddy 2016). Soderstjerna *et al.* (2014) investigated 20 and 80 nm gold NPs toxicity using an *in vitro* tissue culture model of the mouse retina. Transmission electron microscopy revealed that the 20 nm gold NPs have shown cellular and nuclear uptake in all neuronal layers of the retina and increased number of oxidative stressed cells. These findings suggest the size based oxidative stress induction of GNRs.

Conclusions

In summary, the two sizes (10 and 25 nm) of GNRs have shown increased lipid peroxidation and decreased GSH, SOD, catalase, and antioxidant capacity leading to induction of oxidative stress. Moreover, the GNRs induced dose- and size-based oxidative stress induction by various oxidative stress markers following intra-tracheal instillation in rats.



Acknowledgements

The first author is very grateful to University Grants Commission (UGC), India for providing fellowship under Basic Scientific Research-Research Fellowship in Science for Meritorious Students (BSR-RFSMS).

Disclosure statement

The authors declare that there are no potential conflicts of interest.

ORCID

Harikiran Lingabathula  <http://orcid.org/0000-0001-9990-4656>
Narsimhareddy Yellu  <http://orcid.org/0000-0002-2969-7855>

References

- Abudayyak, M., *et al.*, 2016. *In vitro* toxicological assessment of magnesium oxide nanoparticle exposure in several mammalian cell types. *International journal of toxicology*, 35, 429–437.
- Alicia, A., *et al.*, 2014. Cytotoxicity and ROS production of manufactured silver nanoparticles of different sizes in hepatoma and leukemia cells. *Journal of applied toxicology*, 34, 413–423.
- Aurelia, M.P., Mihaela, C.C., and Andrei, F.D., 2009. Total antioxidant capacity of some commercial fruit juices: electrochemical and spectrophotometrical approaches. *Molecules*, 14, 480–493.
- Beulter, D.V., Durm, O., and Kelly, B.M., 1963. Improved method for the determination of blood glutathione. *Journal of laboratory and clinical medicine*, 61, 882–888.
- Chen, C.D., *et al.*, 2007. Sensing capability of the localized surface plasmon resonance of gold nanorods. *Biosensors & bioelectronics*, 22, 926–932.
- Copland, J.A., *et al.*, 2004. Bioconjugated gold nanoparticles as a molecular based contrast agent: implications for imaging of deep tumors using optoacoustic tomography. *Molecular imaging and biology*, 6, 341–349.
- Gil, T.J., 2007. Lethal photosensitisation of *Staphylococcus aureus* using a toluidine blue O–tiopronin–gold nanoparticle conjugate. *Journal of materials chemistry*, 17, 3739–3746.
- Harikiran, L. and Narsimhareddy, Y., 2016. Cytotoxicity, oxidative stress, and inflammation in human Hep G2 liver epithelial cells following exposure to gold nanorods. *Toxicology mechanisms and methods*, 26, 340–347.
- Harikiran, L., Bhikku, A., and Narsimha, R.Y., 2015. *In vitro* cytotoxicity of gold and silver nanorods using different human cell lines. *Latin American journal of pharmacy*, 34, 1277–1282.
- He, X., Young, S., and Schwegler-Berry, D., 2011. Multiwalled carbon nanotubes induce a fibrogenic response by stimulating reactive oxygen species production, activating NF- κ B signaling, and promoting fibroblast-to-myofibroblast transformation. *Chemical research in toxicology*, 12, 2237–2248.
- Huff, T.B., *et al.*, 2007. Controlling the cellular uptake of gold nanorods. *Langmuir*, 23, 1596–1599.
- Igor, P., *et al.*, 2011. Cytotoxicity and oxidative stress induced by different metallic nanoparticles on human kidney cells. *Particle and fibre toxicology*, 8, 10.

- Jain, P.K., *et al.*, 2006. Calculated absorption and scattering properties of gold nanoparticles of different size, shape, and composition: applications in biological imaging and biomedicine. *Journal of physical chemistry B*, 110, 7238–7248.
- Jiali, W., *et al.*, 2015. Surface chemistry but not aspect ratio mediates the biological toxicity of gold nanorods *in vitro* and *in vivo*. *Scientific reports*, 5, 11398.
- Kiranmai, G. and Reddy, A.R., 2013. Antioxidant status in MgO nanoparticle-exposed rats. *Toxicology & industrial health*, 29, 897–903.
- Kuo, W.S., 2009. Antimicrobial gold nanorods with dual-modality photodynamic inactivation and hyperthermia. *Chemical communications*, 32, 4853–4855.
- Li, C.Z., *et al.*, 2005. Fluorescence properties of gold nanorods and their application for DNA biosensing. *Chemical communications*, 31, 3924–3926.
- Liao, H. and Hafner, J.H., 2005. Gold nanorod bioconjugates. *Chemistry of materials*, 17, 4636–4641.
- Marquis, B.J., *et al.*, 2009. Analytical methods to assess nanoparticle toxicity. *Analyst*, 134, 425–439.
- Mohamed, B.M., *et al.*, 2011. Activation of stress-related signalling pathway in human cells upon SiO₂ nanoparticles exposure as an early indicator of cytotoxicity. *Journal of nanobiotechnology*, 9, 29.
- Mytilineou, C., Kramer, B.C., and Yabut, J.A., 2002. Glutathione depletion and oxidative stress. *Parkinsonism & related disorders*, 8, 385–387.
- Oberdorster, G., Oberdorster, E., and Oberdorster, J., 2005. Nanotoxicology: an emerging discipline evolving from studies of ultra-fine particles. *Environmental health perspectives*, 113, 823–839.
- Oyelere, A.K., *et al.*, 2007. Peptide-conjugated gold nanorods for nuclear targeting. *Bioconjugate chemistry*, 18, 1490–1497.
- Perni, S., 2009. The antimicrobial properties of light-activated polymers containing methylene blue and gold nanoparticles. *Biomaterials*, 30, 89–93.
- Pissuwan, D., *et al.*, 2009. Functionalised gold nanoparticles for controlling pathogenic bacteria. *Trends in biotechnology*, 28, 207–213.
- Reddy, A.R., *et al.*, 2011. Evaluation of oxidative stress and anti-oxidant status in rat serum following exposure of carbon nanotubes. *Regulatory toxicology and pharmacology*, 59, 251–257.
- Reddy, A.R., *et al.*, 2012. Pulmonary toxicity assessment of multiwalled carbon nanotubes in rats following intratracheal instillation. *Environmental toxicology*, 27, 211–219.
- Soderstjerna, E., *et al.*, 2014. Silver and gold nanoparticles exposure to *in vitro* cultured retina – studies on nanoparticle internalization, apoptosis, oxidative stress, glial- and microglial activity. *PLoS One*, 9, e105359.
- Tianxun, G., *et al.*, 2014. *In vitro* toxicity and bioimaging studies of gold nanorods formulations coated with biofunctional thiol-PEG molecules and pluronic block copolymers. *Beilstein journal of nanotechnology*, 5, 546–553.
- Valentine, J.S. and Hart, P.J., 2003. Misfolded CuZnSOD and amyotrophic lateral sclerosis. *Proceedings of the national academy of sciences of the United States of America*, 100, 3617–3622.
- Votyakova, T.V. and Reynolds, I.J., 2004. Detection of hydrogen peroxide with Amplex Red: interference by NADH and reduced glutathione auto-oxidation. *Archives of biochemistry and biophysics*, 431, 138–144.
- Yasuo, M., *et al.*, 2016. Usefulness of intra-tracheal instillation studies for estimating nanoparticle-induced pulmonary toxicity. *International journal of molecular sciences*, 17, 165.
- Ying, T., *et al.*, 2015. *In vitro* cytotoxicity of gold nanorods in A549 cells. *Environmental toxicology and pharmacology*, 39, 871–878.
- Yu, C. and Irudayaraj, J., 2007. Multiplex biosensor using gold nanorods. *Analytical chemistry*, 79, 572–579.
- Zelko, I.N., Mariani, T.J., and Folz, R.J., 2002. Superoxide dismutase multi-gene family: a comparison of the CuZn-SOD (SOD1), Mn-SOD (SOD2), and EC-SOD (SOD3) gene structures, evolution, and expression. *Free radical biology and medicine*, 33, 337–349.



Nano titanium exposure induces dose- and size-dependent cytotoxicity on human epithelial lung and colon cells

Durgaiah Gandamalla, Harikiran Lingabathula & Narsimhareddy Yellu

To cite this article: Durgaiah Gandamalla, Harikiran Lingabathula & Narsimhareddy Yellu (2019) Nano titanium exposure induces dose- and size-dependent cytotoxicity on human epithelial lung and colon cells, *Drug and Chemical Toxicology*, 42:1, 24-34, DOI: [10.1080/01480545.2018.1452930](https://doi.org/10.1080/01480545.2018.1452930)

To link to this article: <https://doi.org/10.1080/01480545.2018.1452930>



Published online: 03 Apr 2018.



Submit your article to this journal [↗](#)



Article views: 43





View Crossmark data [↗](#)

RESEARCH ARTICLE



Nano titanium exposure induces dose- and size-dependent cytotoxicity on human epithelial lung and colon cells

Durgaiah Gandamalla , Harikiran Lingabathula  and Narsimhareddy Yellu 

Department of Pharmacology and Toxicology, University College of Pharmaceutical Sciences, Kakatiya University, Warangal, India

ABSTRACT

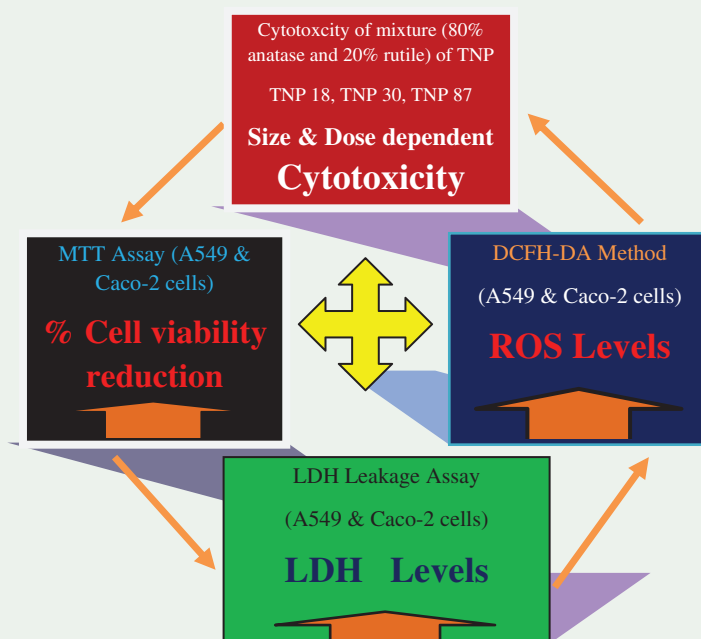
The productions as well as use of Titanium dioxide nanoparticles (TNPs) were rapidly increasing in the present nano-world. The TNP becomes an inevitable part our daily life in the form of cosmeceutical, bio-medical, and nano-pharmaceutical applications. The TNPs are either inhaled or ingested into the human body through common routes of exposure like the lungs and the oral-gastrointestinal tract (GIT). Human lung and colon were exposed to test particles, TNP 18 nm (TNP 18), TNP 30 nm (TNP 30), and TNP 87 nm (TNP 87) with a dose range 0.1–100 µg/ml. The effect of exposure was determined using MTT, LDH, and DCFH-DA methods. The TNP 18, TNP 30, and TNP 87 significantly ($p < 0.001$) reduced cell viability in a dose- and a size-dependent manner in 60 and 100 µg/ml. The lowest IC₅₀ values 21.80 and 24.83 µg/ml were observed in A549 and Caco-2 for the smallest size, TNP 18. Further, for TNP 30, IC₅₀ values were 23.30 and 28.59 µg/ml compared to Nano QTZ 43.82 and 45.86 µg/ml. The EC₂₅ values of LDH leakage were 5.83 and 9.50 µg/ml for TNP 18 in lung and colon cells. Besides, ROS levels increased significantly at doses 60 ($p < 0.01$) and 100 ($p < 0.001$) µg/ml in two cells. The smaller size particle, TNP 18 has produced a significant ($p < 0.05$) toxic effect at the lowest dose i.e., 10 µg/ml. Therefore, we conclude that TNP 18, TNP 30, and TNP 87 induced a dose- and size-dependent cytotoxicity via decreased cell viability, increased LDH and ROS levels by *in vitro* methods.

ARTICLE HISTORY

Received 27 August 2017
Revised 10 March 2018
Accepted 11 March 2018

KEYWORDS

Nano titanium; TEM characterization; cytotoxicity; IC₅₀; ROS release



Introduction

Built nanoparticles (NP) are monetarily created materials with not less than one measurement under 100 nm (De Berardis *et al.* 2010). NPs are ordered in view of their physicochemical properties and basically carbon, metal oxides based sort.

The metal oxide NPs that are important for industrial and bio-medical applications are TiO₂, SiO₂, ZnO, CeO₂, Al₂O₃, Fe₃O₄, and Ag (Mirzaei *et al.* 2016). Metal oxide NPs are broadly utilized for an assortment of utilizations including catalysis, sensors, natural remediation, squander water, medicines,

propelled tranquilize conveyance frameworks, restorative diagnostics, propelled laser innovation, nanostructure impurities, frameworks on chip, synthetic sensors and wear-safe coatings (Ivask *et al.* 2015, Alvarez *et al.* 2016, Odzak *et al.* 2017, Rahman *et al.* 2017). Physicochemical properties of nanoparticles, such as crystallinity, size, shape, charge, and surface zone can affect the toxicity profile on target cell cultures (Tomankova *et al.* 2015, Uboldi *et al.* 2016).

Titanium dioxide nanoparticles (TNPs) are among the largest exposure nanomaterials (NM) utilized for makeup, covering/cleaning operators, plastics, paints, sunscreens, pharmaceuticals, cleansers, inserts, and sustenance (Piccinno *et al.* 2012, Lu *et al.* 2015, Simeonidis *et al.* 2015, Yang *et al.* 2015). TNPs are among the major contaminated particles that were released into the environment over the past decade (Naidu *et al.* 2016). The potential impact of TNPs on human health and the environment has raised safety concerns owing to their wide application range. Further, the *in vitro* tests and experimental protocols could help in better understanding of the plausible toxicity of TNPs on human health (Kroll *et al.* 2011).

TNPs possess different physicochemical properties like size, shape, and surface chemistry which might affect its bio- and nano-activity. Because of small size, TNPs easily enters into the human and animal body and environment as a whole. This study mainly focuses on the inhalation and oral routes for TNP entry. Inhaled particles will interact with human lung cells (Morimoto *et al.* 2016) and are then translocated to the liver, kidney, and brain apart from the lungs and gastrointestinal tract (GIT) (Yang *et al.* 2017). The *in vitro* study results will be of significant help in assessing the extent of risk for TNP associated industry workers and different end product users (Aschberger *et al.* 2011).

Ursini *et al.* (2014) reported a dose-dependent decrease in the viability of alveolar and bronchial epithelial cells (A549 and BEAS-2B) after 24 h exposure to 1, 5, 10, 20, and 40 $\mu\text{g/ml}$ of TNP (16–43 nm) using a WST-1 Assay. The cytotoxic dose was found to be 40 $\mu\text{g/ml}$ of TNP mixture (79% anatase and 21% rutile) in both cell lines. George *et al.* (2015) studied exposure of Calu-3 bronchial epithelial cells to 16–100 nm SiO_2 and reported size dependent translocation and toxicity. Toxic effect of rutile TNP (50 nm) nano-composite on Hep G2 cell line was studied (Bessa *et al.* 2017).

Armand *et al.* (2016) studied cell viability reduction, reactive oxygen species (ROS) measurement, and genotoxic impact of TNP (24 \pm 6 nm) on alveolar epithelial cells after exposing them to 1–50 $\mu\text{g/ml}$ TNP mixture (86% anatase and 14% rutile) for acute, subacute toxicity. The authors explained how ROS is playing a key role in oxidative stress-mediated cytotoxicity using *in vitro* studies (Manke *et al.* 2013, Guadagnini *et al.* 2015, Abdal *et al.* 2017).

The above studies clearly inferred that cell and size specific toxicity is gaining much importance in the field of nanotoxicology. Further, the human risk exposure routes such as inhalation and ingestion (oral) have been studied to interpret dose- and size-dependent toxicity in human cell lines (Xia *et al.* 2013, Shang *et al.* 2014, Lopes *et al.* 2016).

Accordingly, the size- and dose-dependent toxicity of different sized TNP 18, TNP 30, and TNP 87 were particularly

interesting due to high demand of global production, biomedical application, and occupational risk exposure. Thus, this study aims to evaluate the potential toxicity of TNP with different doses using 3-(4,5-dimethyl thiazol-2-yl)-2,5-diphenyl tetrazolium bromide (MTT), lactate dehydrogenase (LDH), and intracellular ROS levels by DCFH-DA methods.

Materials and methods

Chemicals

The TNP 18, TNP 30, and TNP 87 were purchased from Sigma Aldrich, Mumbai, India. TNP is a mixture of anatase and rutile (80% anatase and 20% rutile) nano-powder (99.50% purity). Nano Quartz (Nano QTZ) particles (<100 nm; 99.94% purity) were purchased from Berkely Springs, WV. The Dulbecco's modified eagles medium (DMEM), Iscove's Modified Dulbecco's Medium (IMDM), 1% L-glutamine, 1% penicillin-streptomycin antibiotic solution, Trypsin-EDTA, and phosphate buffer saline (PBS) were purchased from Himedia, Mumbai, India. The LDH assay kit was purchased from Sigma Chemicals Co. Ltd. (St. Louis, MO). *In vitro* ROS assay kit was purchased from Cell Biolabs, San Diego, CA.

Characterization of TNP

The TNP 18, TNP 30, and TNP 87 nano-powder were dispersed in de-ionized water (DI)/MilliQ (Direct-Q[®] 3 UV Water Purification System, Mumbai, India) at a concentration of 400 $\mu\text{g/ml}$ and sonicated for 10 min with 10% amplitude (40W, Ultrasonic Probe Sonicator, Mumbai, India). The TNP suspension (100 μg metal/ml) stock was prepared in the DI. Primary size, shape, and agglomeration status of NP were determined using TEM (EM 208, FEI Company, Mumbai, India). For the TEM study, 6 ml of TNP suspensions was applied directly on TEM copper grids, coated with a layer of amorphous carbon.

The zeta potential was measured by zetasizer instrumentation (Nano ZS90, Malvern Instruments, Malvern, UK) and the specific surface area was measured through Brunauer, Emmett, and Teller (BET). Size distributions of the three TNPs were studied. The hydrodynamic size of TNP was studied using Dynamic Light Scattering (DLS). The TNP suspension (100 $\mu\text{g/ml}$) stock was resonicated for 3 min before adding them to a 96 well plate (De Berardis *et al.* 2010; Ammendolia *et al.* 2017).

Human lung (A549) and Caco-2 cells were purchased from National Center for Cell Sciences (NCCS), Pune, India. They have been received with different job numbers. Cell culture flasks were checked for sterility and were kept free from microorganisms. The cells were sub-cultured with passage number 16. Further, the A549 cells were grown in DMEM and Caco-2 cells were in IMDM with 10% FBS, 1% antibiotic-antimycotic solution, 1% glutamax and 1 mM sodium pyruvate.

TNP (10 mg/ml) stock was prepared and sonicated for 15 min before the experiment. The working stocks were prepared in a complete cell culture medium. Cells were seeded with a cell density of 370 000 cells/flask in a total volume of 5–8 ml and were allowed them to grow in a CO_2 incubator.

Cells were loaded with a cell density of 3.0×10^4 cells/0.1 ml after trypsinization. The density of TNP was 1 g/ml at 25 °C. Different concentrations of TNP and positive control (Nano QTZ) suspensions were prepared in serum-free culture medium and were used for cytotoxicity screening.

Cytotoxicity (MTT) assay

The impact of test TNP on the cellular proliferation and viability were determined by using MTT assay (Mosmann 1983). MTT assay was performed to determine the dose-response curve of different sized TNP 18, TNP 30, and TNP 87. TNP of different concentrations, i.e., 1–300 µg/ml was used to explore cytotoxicity. Briefly, A549 and Caco-2 cells were grown in culture media (DMEM/IDMM) until 80% confluency was achieved under good cell culture practices (GCCP). Further, 3×10^4 cells/well seeded into a 96 well plate (Tarsons, Mumbai, India) and which was kept overnight for incubation. TNP test suspensions of 100 µl volumes were added in triplicate each well using multi-channel pipette under aseptic conditions (laminar air flow unit).

The plate was then incubated at 37 °C for 48 h in a CO₂ incubator (WTC Binder, Tuttlingen, Germany) and 20 µl MTT (5 mg/ml) solution was added to each well (Harikiran *et al.* 2015). The plate was again incubated for 2 h, 80 µl DMSO was added to each well. Then the plate was wrapped in aluminum foil to prevent the oxidation of the dye and was placed on a rotary shaker (Remi Equipments, Mumbai, India) for 2 h. The absorbance was measured at 540 nm using multi-well plate ELISA reader (BioTek™ Instruments, Winooski, VT). The percent of cytotoxicity was calculated by comparing the test absorbance with that of control (Ammendolia *et al.* 2017).

Lactate dehydrogenase (LDH) leakage assay

The cellular membrane integrity assay was a non-radioactive and high-throughput method to detect the leakage of a cytoplasmic enzyme, lactate dehydrogenase (LDH) from the damaged cells. Historically, cytotoxic cell death was evaluated by determining damage to the plasma membrane (Korzeniewski and Callewaert 1983). The cytotoxicity assay can measure intracellular LDH leakage through the impaired plasma membrane. LDH is a soluble cytoplasmic enzyme can be released into extra-cellular space when the plasma membrane is damaged. The leakage of LDH into cell culture media was quantified using a tetrazolium salt (Challa and Chan 2010).

LDH produces reduced nicotinamide adenine dinucleotide (NADH) when it catalyzes the oxidation of lactate to pyruvate. The tetrazolium salt is converted to a colored formazan product using newly synthesized NADH in the presence of an electron acceptor. The amount of formazan was quantified colorimetrically and different concentrations of (0.1–300 µg/ml) TNP were used to expose the two cell lines for 48 h. The amount of LDH release was the sign of necrotic cell damage which was measured by multiwellplate reader (BioTek™ Elx800™ Instruments, Winooski, VT) at absorbance 490 nm (Chen *et al.* 2016).

Intracellular ROS generation assessment by DCFH-DA

The intracellular production of ROS was evaluated with the fluorescence marker DCFH-DA (2,7-dichlorodihydrofluorescein diacetate). DCFH-DA is a fluorimetric probe, which passively enters the cell and forms a highly fluorescent compound dichlorofluorescein (DCF) by reacting with ROS (Wan *et al.* 1993). Briefly 5×10^5 cells were seeded into 12 well plates and pre-incubated for 48 h. After incubation, different concentrations of TNP (0.1–300 µg/ml) were exposed to cells for a period of 4 h. The cells were then rinsed with PBS and subsequently stained with 1 ml of 5 µM DCFH-DA allowed to incubate for 45 min in the dark at 37 °C and 5% CO₂.

Excess DCFH-DA was removed and replaced with 200 µl PBS. Fluorescence was measured using a multiwellplate reader (BioTek™ FLx800™ Instruments, Winooski, VT) with excitation and emission at wavelength 450 and 535 nm, respectively. Cells incubated without TNP were used as a negative control and Nano QTZ as a positive control. Data were expressed as relative fluorescence intensity units. Results were obtained from three independent experiments performed in triplicate (Abdal *et al.* 2017).

Statistical analysis

MTT, LDH, and DCFH-DA assays data were expressed as the mean ± SD of at least three independent experiments, unless stated otherwise. IC₃₀, IC₅₀, EC₂₅, and EC₅₀ values were calculated by using REGTOX program: macro Excel™. Statistical analysis was performed using the GraphPad Prism 6.0 software (GraphPad Software, La Jolla, CA). The TNP treated vs. the untreated controls were analyzed using one-way ANOVA followed by Bonferroni *post-hoc* test. Significance was assigned as **p* < 0.05, \$*p* < 0.01, #*p* < 0.001. Nano QTZ was used as a positive control.

Results

Characterization of TNP

The TNP 18, TNP 30, and TNP 87 mixture of anatase and rutile (80% anatase and 20% rutile) were characterized for physicochemical properties, such as size, zeta potential, surface area, and hydrodynamic size which is summarized in Table 1. Figure 1 shows representative TEM images of three different sized TNP which confirmed the size and shape as described by Sigma-Aldrich. The average particle diameters of three different sizes TNP were 15: 84 ± 3.59 nm (A), 24.59 ± 5.60 nm (B), and 81.80 ± 4.27 (C). Particle size distributions were measured by TEM analysis for each particle has shown in Figure 2. TNP formed different sizes of agglomerates with varying sizes. All the particles were spherical in shape as shown in Figure 1 (De Berardis *et al.* 2010; Ivask *et al.* 2015).

Cytotoxicity by MTT assay

The cytotoxic results of TNP 18, TNP 30, and TNP 87 exposed to A549 cells were investigated by MTT assay are shown in

Table 1. Physicochemical characteristics of studied titanium dioxide nanoparticles (TNP).

Particle type	Average TEM diameter of TNP (nm) ^a	Zeta potential (mV) ^b in DI	Specific surface area (m ² /g) ^c	Shape ^a	Hydrodynamic size (nm) ^d in DI
TNP 18	15.84 ± 6.59	-43.29	48.73	Spherical	124 ± 12
TNP 30	24.59 ± 8.60	-14.25	23.39	Spherical	172 ± 2.9
TNP 85	81.80 ± 5.27	-8.60	11.60	Spherical	486 ± 37

DI: deionized water.

^aAverage diameter and shape of TNP by transmission electron microscopy.

^bZeta potential by Zetasizer.

^cSpecific surface area by Brunauer, Emmett and Teller (BET).

^dHydrodynamic size by dynamic light scattering (DLS).

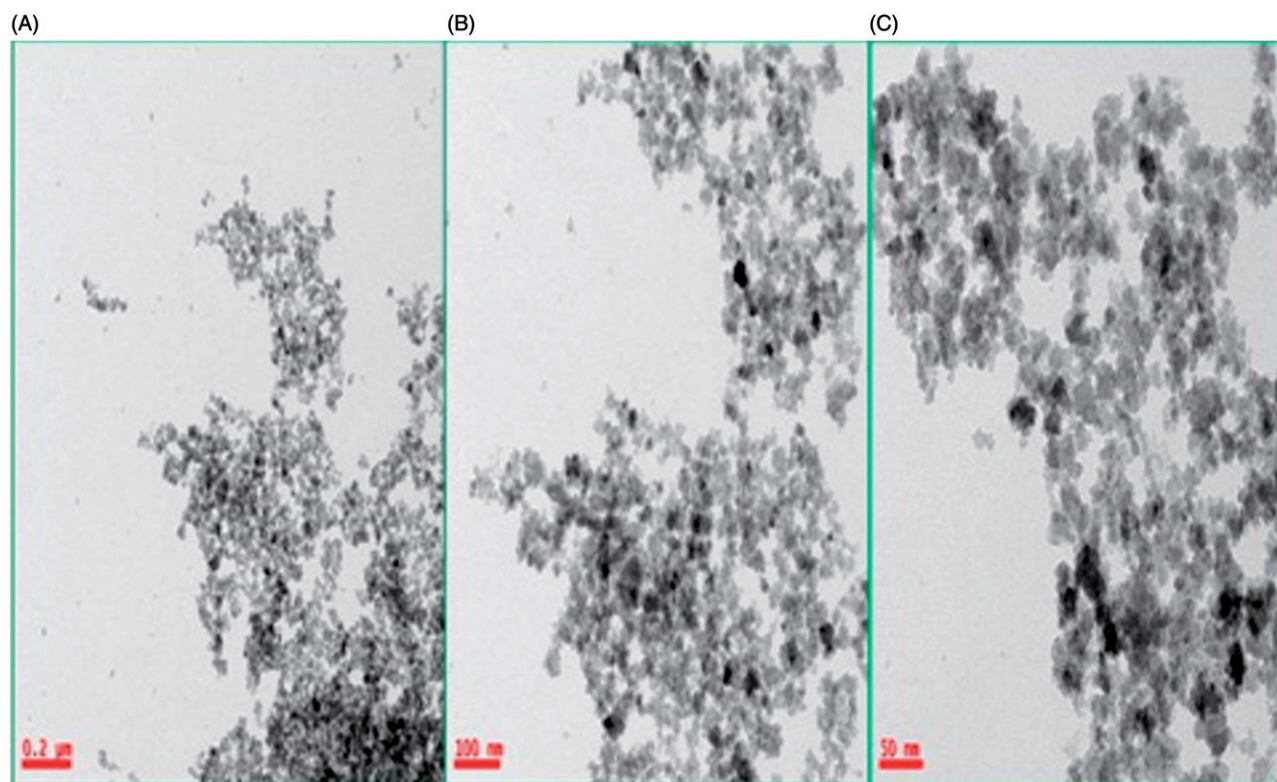


Figure 1. TEM characterization of titanium dioxide nanoparticles. Imaged at 80 k × magnifications. (A) TNP 18 nm, (B) TNP 30 nm, and (C) TNP 87 nm.

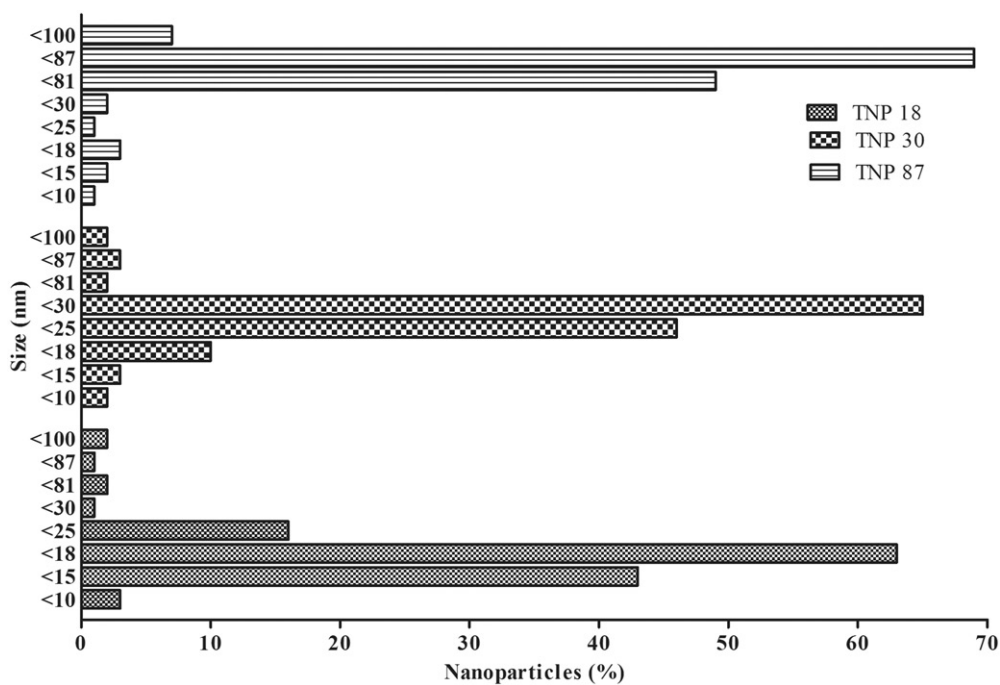


Figure 2. Particles size distributions by TEM analysis.

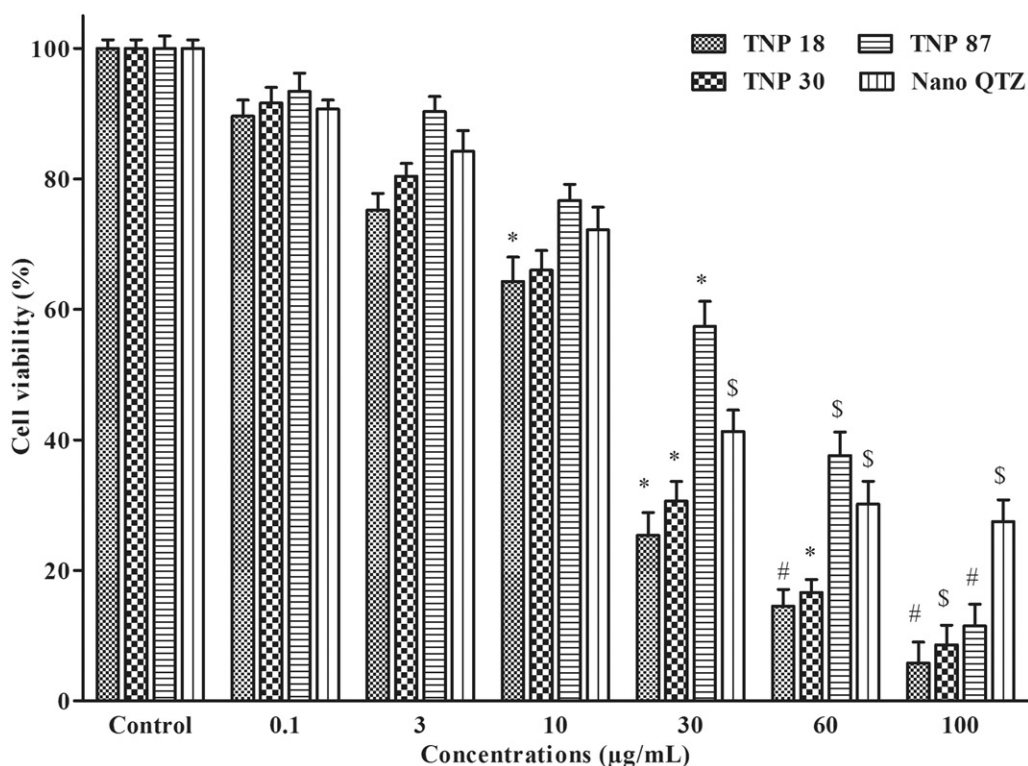


Figure 3. Cytotoxicity assessment by MTT assay on human lung (A549) cells exposure to 18, 30, and 87 nm TNPs concentrations (0.1–100 µg/ml) for 48 h. Data as mean ± standard deviation (SD) $n = 3$. Statistical analysis was performed using one-way ANOVA followed by Bonferroni *post-hoc* test. * $p < 0.05$, # $p < 0.001$, \$ $p < 0.01$ vs. control.

Figure 3. In the MTT assay, cells (A549 and Caco-2) were exposed to increasing concentrations of (0.1–100 µg/ml) for 48 h post exposure. The non-significant cell reduction was found at lower concentrations (0.1 and 3 µg/ml) in A549 and Caco-2 cells. The results indicate reduced cell viability with the doses 30, 60, and 100 µg/ml for both the smaller sized TNP 18 and TNP 30.

TNP 18 significantly reduced cell viability as much as 39.64, 74.60, 85.29, and 94.49% at the doses 10 ($p < 0.05$), 30 ($p < 0.05$), 60 ($p < 0.01$), and 100 ($p < 0.01$) µg/ml significantly, compared to control (untreated cells) after 48 h post exposure in A549 cells. For TNP 30, the reduced the cell viability was found to be 35.3, 69.39, 83.40, and 91.40% with the increasing doses 30 ($p < 0.05$), 60 ($p < 0.05$), and 100 ($p < 0.01$) µg/ml, respectively. However, TNP 87, reduced cell viability as much as 42.60, 62.39, and 88.49% at doses 30 ($p < 0.05$), 60 ($p < 0.01$), and 100 ($p < 0.001$), respectively. The IC_{50} (the concentration at which 50% cells were inhibited) values were calculated for three TNPs. The IC_{25} and IC_{50} values of the tested TNP after being exposed to A549 and Caco-2 cells are shown in Table 2. The IC_{50} values were 21.80, 23.30, and 34.90 µg/ml for TNP 18, TNP 30, and TNP 87, respectively, compared to Nano QTZ, 43.82 µg/ml.

Cytotoxicity of all the tested TNP histograms after 48 h post exposure in Caco-2 cells are presented in Figure 4. The concentration-dependent cell viability reduction was reported to be 73.60, 84.89, and 94.00% which were statistically significant for increasing concentrations 30 ($p < 0.05$), 60 ($p < 0.001$), and 100 ($p < 0.001$) µg/ml after TNP 18 post exposure. The TNP 30 also reduced the cell viability such as

Table 2. The IC_{25} and IC_{50} values of TNP on a549 and Caco-2 cell lines by MTT assay method.

S. No	Particle Type	A549 ^a		Caco-2 ^b	
		IC_{30} (µg/ml)	IC_{50} (µg/ml)	IC_{30} (µg/ml)	IC_{50} (µg/ml)
1	TNP 18	06.83 ± 1.39	21.80 ± 2.18	09.85 ± 2.90	24.83 ± 2.16
2	TNP 30	07.59 ± 2.17	23.30 ± 2.10	80.96 ± 2.37	28.59 ± 2.60
3	TNP 87	09.81 ± 3.20	34.90 ± 3.83	10.61 ± 2.84	36.70 ± 3.16
4	Nano QTZ	12.40 ± 2.39	43.82 ± 3.18	13.93 ± 2.41	45.86 ± 3.09

Values are expressed as mean ± SD.

^aA549: the human epithelial lung cancer cells.

^bCaco-2: the human epithelial colon cancer cells.

58.83, 79.39, and 92.5% with statistically significant against the test doses 30 ($p < 0.01$), 60 ($p < 0.001$), and 100 ($p < 0.01$) µg/ml compared to control. Therefore, the TNP 18, TNP 30, and TNP 87 produced a dose- and size-dependent cytotoxicity in A549 and Caco-2 cells. The IC_{50} values were 24.40, 28.59, and 36.70 µg/ml for TNP 18, TNP 30, and TNP 87 compared to Nano QTZ, 45.86 µg/ml in Caco-2 cells which is shown in Table 2.

Lactate dehydrogenase (LDH) leakage assay

The three different sized TNP 18, TNP 30, and TNP 87 induced significant membranolytic effect at the higher doses, i.e., 10, 60, and 100 µg/ml after 48 h of exposure in two cell lines, as shown in Figures 5 and 6. TNP 18 exposure to A549 cells resulted in 1^{1/2}, 2^{1/2}, 3^{1/2}, and 4^{1/2} fold increments for the doses 10 ($p < 0.05$), 30 ($p < 0.05$), 60 ($p < 0.001$), and 100 ($p < 0.001$) µg/ml, respectively, compared to control. TNP 30 and TNP 87 were produced 2^{1/2}, 3^{1/2}, 4 and 1^{1/2}, 3^{1/4}, 4 fold

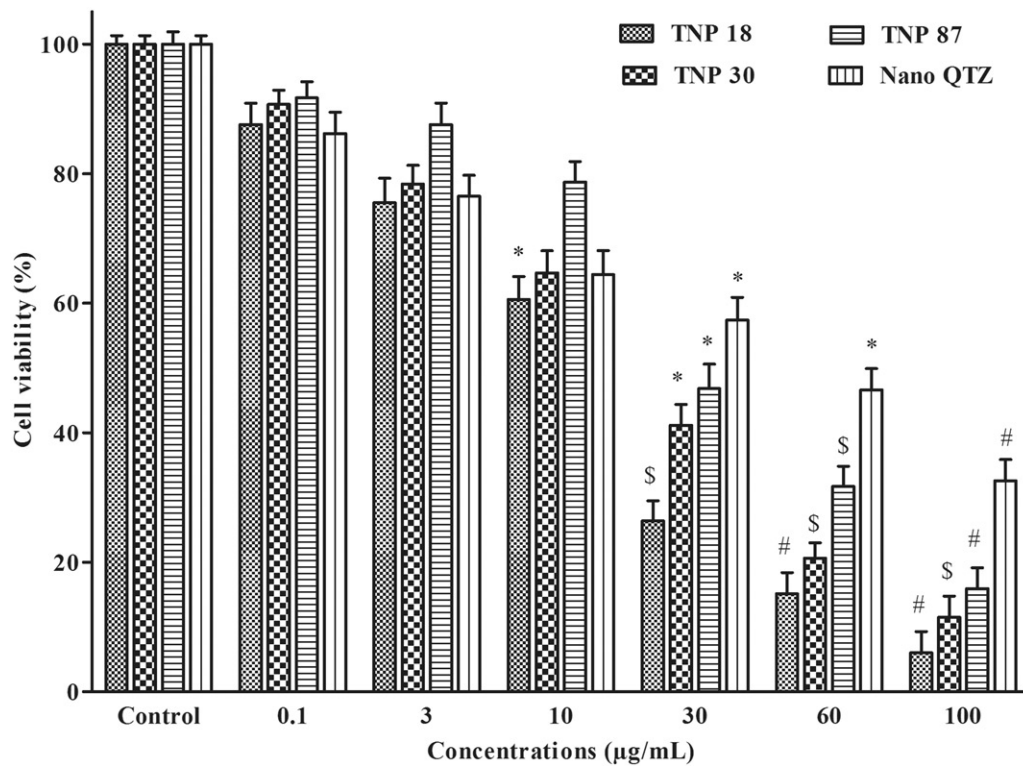


Figure 4. Cytotoxicity assessment by MTT assay on human epithelial colon (Caco-2) cells exposure to 18, 30, and 87 nm TNP concentrations (0.1–100 µg/ml) for 48 h. Data as mean \pm standard deviation (SD) $n=3$. Statistical analysis was performed using one-way ANOVA followed by Bonferroni *post-hoc* test. * $p < 0.05$, # $p < 0.001$, \$ $p < 0.01$ vs. control.

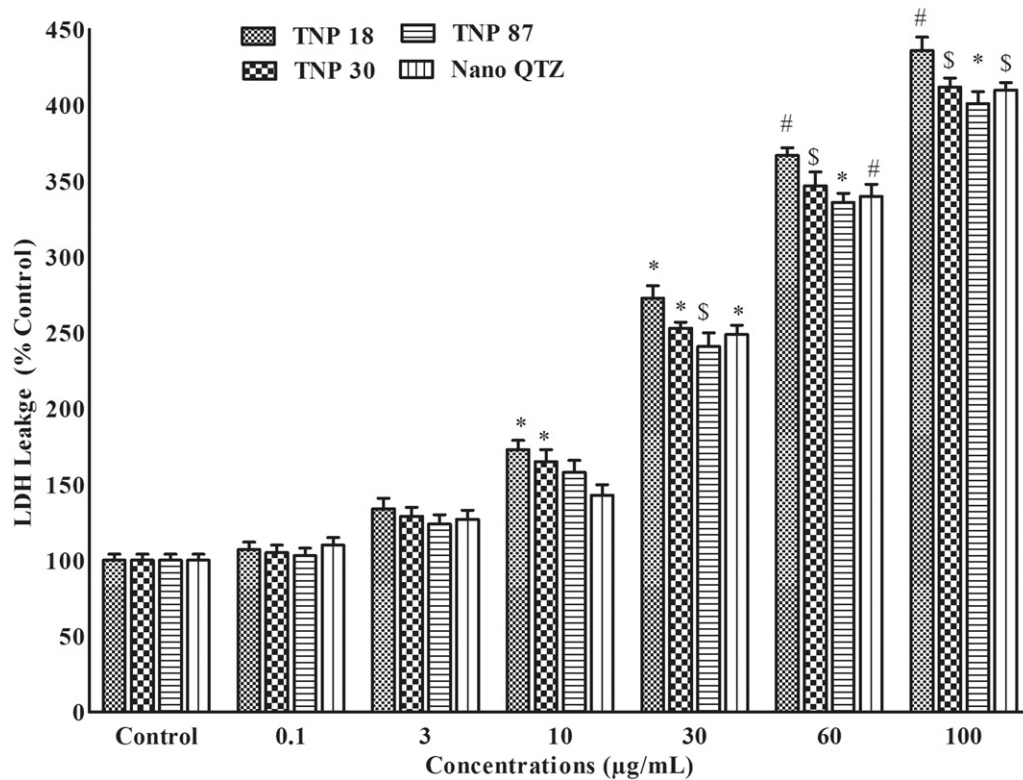


Figure 5. Cytotoxicity assessment by LDH method. LDH release from human lung (A549) cells exposure to 18, 30, and 87 nm TNP concentrations (0.1–100 µg/ml) for 48 h. Data as mean \pm standard deviation (SD) $n=3$. Statistical analysis was performed using one-way ANOVA followed by Bonferroni *post-hoc* test. * $p < 0.05$, # $p < 0.001$, \$ $p < 0.01$ vs. control.

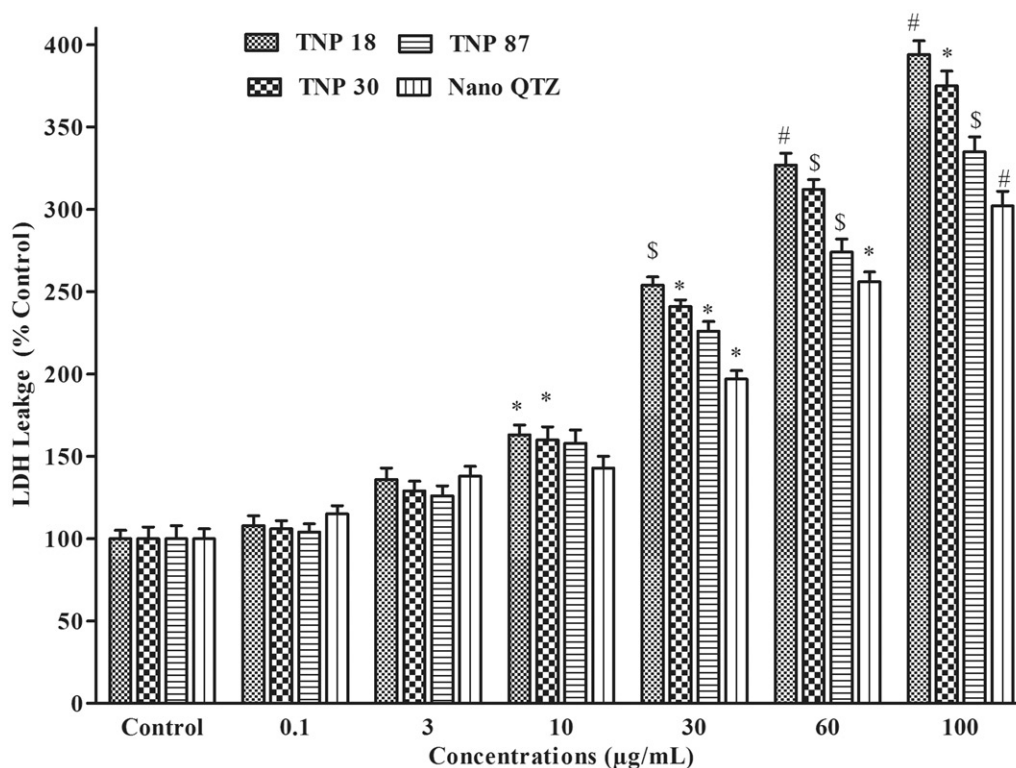


Figure 6. Cytotoxicity assessment by LDH method. LDH release from human colon (Caco-2) cells exposure to 18, 30, and 87 nm TNP concentrations (0.1–100 µg/ml) for 48 h. Data as mean ± standard deviation (SD) $n=3$. Statistical analysis was performed using one-way ANOVA followed by Bonferroni *post-hoc* test. * $p < 0.05$, # $p < 0.001$, \$ $p < 0.01$ vs. control.

Table 3. The EC_{25} and EC_{50} values of the TNP on A549 and Caco-2 cell lines LDH assay method for 48 h post exposure study.

S. No	Particle type	A549 ^a		Caco-2 ^b	
		EC_{25} (µg/ml)	EC_{50} (µg/ml)	EC_{25} (µg/ml)	EC_{50} (µg/ml)
1	TNP 18	05.83 ± 1.83	13.27 ± 3.19	09.50 ± 2.18	17.83 ± 3.59
2	TNP 30	06.89 ± 2.51	16.90 ± 3.70	12.73 ± 2.82	30.59 ± 3.50
3	TNP 87	09.40 ± 3.09	25.41 ± 3.05	14.97 ± 2.70	39.70 ± 3.67
4	Nano QTZ	13.18 ± 2.73	38.82 ± 3.26	16.93 ± 3.81	40.86 ± 3.17

Values are expressed as mean ± SD.

^aA549: the human epithelial lung cancer cells.

^bCaco-2: the human epithelial colon cancer cells.

increments in post exposed A549 cells for 30, 60, and 100 µg/ml, which is shown in Figure 5. The EC_{25} and EC_{50} (the concentration at which 50% of the effect was obtained) were calculated for three TNPs and results are shown in Table 3. The EC_{50} values were 13.27, 16.90, and 25.41 µg/ml for TNP 18, TNP 30, and TNP 87, respectively, compared to Nano QTZ, 38.82 µg/ml in A549 cells.

Post exposure of Caco-2 cells to TNP 18 resulted in 1, 1^{1/2}, 3, and 4 fold increment of LDH levels with 10 ($p < 0.05$), 30 ($p < 0.01$), 60 ($p < 0.001$), and 100 ($p < 0.001$) µg/ml doses, which is shown in Figure 6. The LDH leakage was increased by 1/2, 3/4, 2, 3^{1/2} and 1, 1^{1/2}, 3^{1/4} fold increments were found for the both TNP 30 and TNP 87 for 10, 30, 60, and 100 µg/ml after 48 h post exposure of Caco-2 cells. Thus, the membranolitic/cell damage assay results clearly indicated that the TNP 18, TNP 30, and TNP 87 produced a dose and size dependent cytotoxic effect in A549 and Caco-2 cell lines. The EC_{50} values were 17.83, 30.59, and 39.70 µg/ml compared to Nano QTZ, 40.86 µg/ml for TNP 18, TNP 30, and TNP 87 in Caco-2 cells.

Intracellular reactive oxygen species (ROS) measurement

A549 and Caco-2 cells exposure to TNP 18, TNP 30, and TNP 87 induced 10–18 fold increase of ROS levels at higher doses 60 ($p < 0.01$) and 100 ($p < 0.01$) µg/ml compared to control for 48 h post exposure. As depicted in Figure 7, TNP 18 and TNP 30 produced a dose-dependent increase in ROS levels up to an extent 3^{1/2}, 7, 13^{1/2}, 18 and 1^{1/2}, 6^{1/2}, 12^{1/2}, 16 folds for the doses 10, 30, 60, and 100 µg/ml, respectively in post exposed A549 cells.

As shown in Figure 8, the Caco-2 cells produced a significant increase in ROS levels at a lower dose 10 µg/ml for TNP 18 only compared to Nano QTZ. Further, TNP 18 produced a significant increase in ROS levels at doses 30 ($p < 0.05$), 60 ($p < 0.001$), and 100 ($p < 0.001$) µg/ml. TNP 30 has shown 7^{1/2} to 15 fold increase in ROS release significantly against the doses 30 ($p < 0.05$), 60 ($p < 0.01$), and 100 ($p < 0.001$) µg/ml compared to control. Therefore, results indicated that the relative release of ROS in A549 and Caco-2 cells was observed in a dose and a size-dependent manner.

Discussion

TNP 18, TNP 30, and TNP 87 were homogeneous within the examined vials and all the particles were spherical in shape. The *in vitro* tests were performed in order to assess the toxic potential of the different sized TNPs because of its enormous production and cosmaceutical, dental, food and consumer applications. Therefore, their use in production, accumulation in environmental deposition and release into human habitat

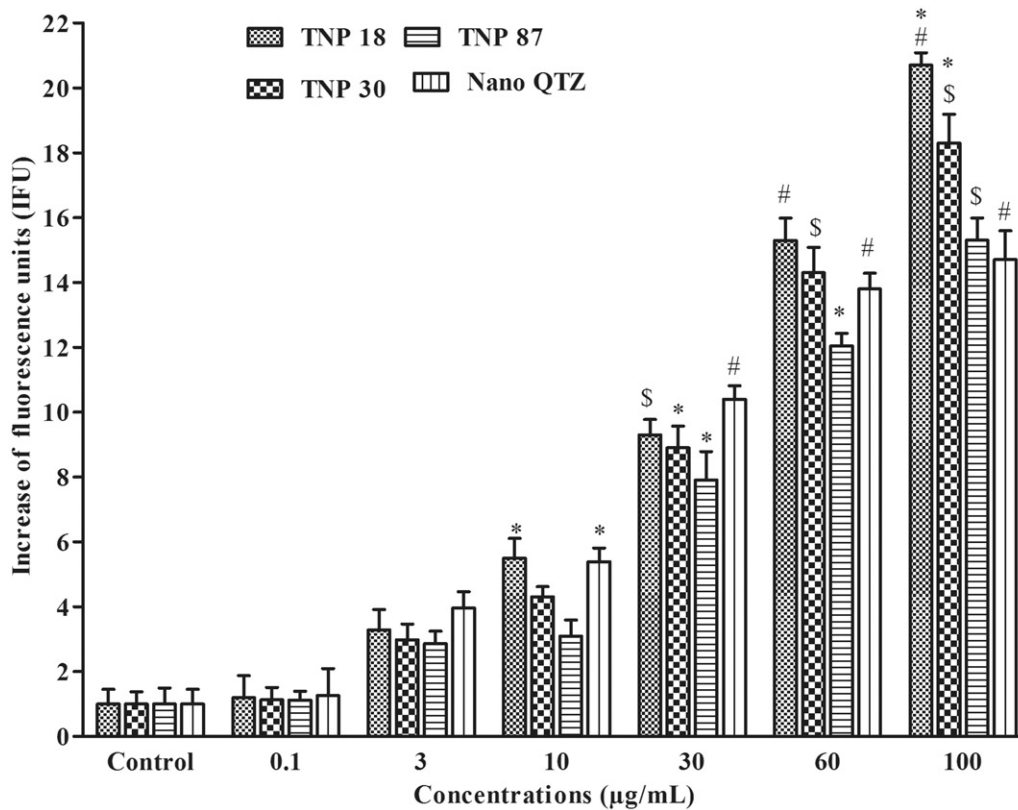


Figure 7. Relative ROS intracellular release measured by DCFH-DA assay on human lung (A549) cells exposure to 18, 30, and 87 nm TNP concentrations (0.1–100 µg/ml) for 48 h. Data as mean \pm standard deviation (SD) $n=3$. Statistical analysis was performed using one-way ANOVA followed by Bonferroni *post-hoc* test. * $p < 0.05$, # $p < 0.001$, § $p < 0.01$ vs. control.

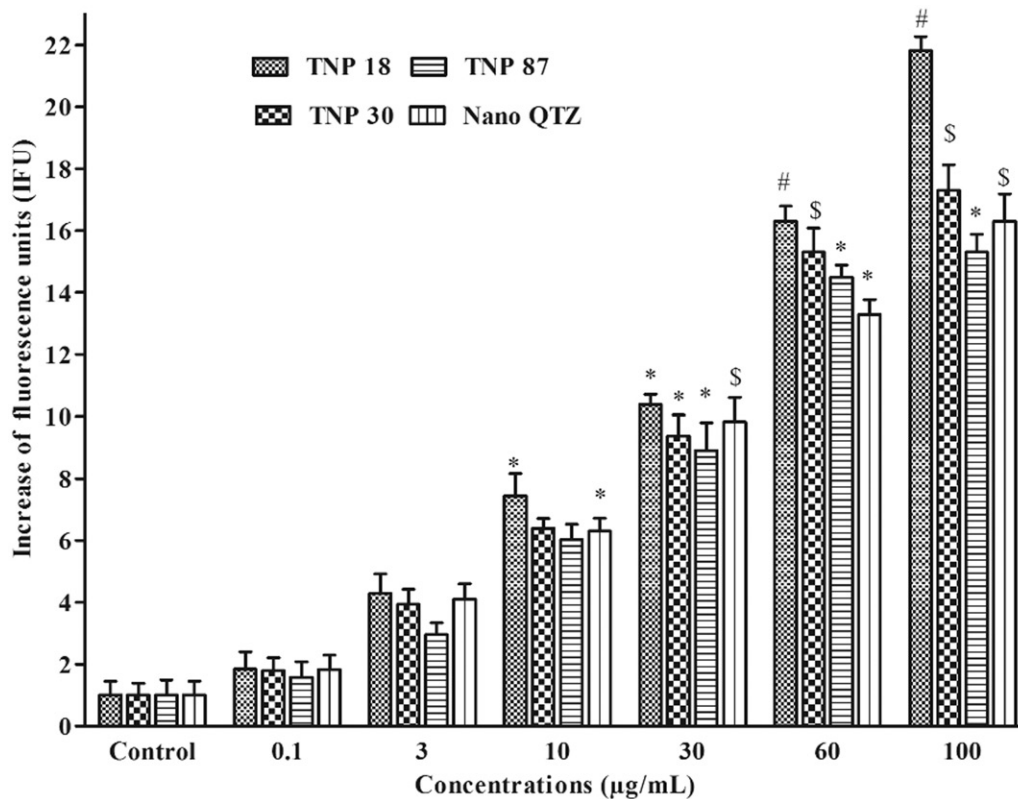


Figure 8. Relative ROS intracellular release measured by DCFH-DA assay on human colon (Caco-2) cells exposure to 18, 30, and 87 nm TNP concentrations (0.1–100 µg/ml) for 48 h. Data as mean \pm standard deviation (SD) $n=3$. Statistical analysis was performed using one-way ANOVA followed by Bonferroni *post-hoc* test. * $p < 0.05$, # $p < 0.001$, § $p < 0.01$ vs. control.

has become an inevitable yet high-risk prospect (Guadagnini *et al.* 2015).

This study evaluated the potential toxicity of varying sizes of a mixture (80% anatase and 20% rutile) of TNP 18, TNP 30, and TNP 87 on two cell cultures A549 and Caco-2 upon a single exposure under *in vitro* conditions. This study also revealed the effects of size and dose on the cell viability, membrane integrity, and intracellular ROS after 48 h post exposure using MTT assay.

TNP with size (5–100 nm) were actively up-taken by A549 cells and internalized by endocytosis, which is a fundamental biological process used by cells and extracellular matrix to internalize bio-molecules based on their physicochemical properties (Shang *et al.* 2014, Grant *et al.* 2015). A size-dependent uptake was observed for nano silver, gold, and titanium oxide particles in different cell lines (Park *et al.* 2011). The toxicity of particles could be correlated with their physicochemical properties such as smaller particles have higher toxicity due to a smaller size, hydrodynamic diameter and larger surface area (Hussain *et al.* 2009, Cai *et al.* 2011, DeLoid *et al.* 2017).

Titma *et al.* (2016) reported toxicity of Co_3O_4 , CuO, Mn_3O_4 , Sb_2O_3 , ZnO, and TiO_2 with different doses, i.e., 3.125–100 $\mu\text{g}/\text{ml}$ of varying sizes on A549 and Caco-2 cells for 0–9 d using resazurin assay *in vitro*. The toxicity assessment of testing NP was done by according to EC_{25} and EC_{50} values for acute and long-term exposure on two cell cultures.

Gamze and Mustafa (2017) studied the origins of the toxic response of a 140 nm TNP and a 50 nm AuNP using three cell lines, i.e., A549, vein (HUVEC), and skin (L929). The triglycerides and cholesterol levels were found to increase with alveolar inflammation, oxidative stress, and impaired mitochondrial dysfunction in A549 cells when post exposed for 24 h using WST-1 assay. Therefore, the study concluded that the level of toxicity is the cell line specific (A549 and HUVEC) and dose-dependent for anatase type TNP.

Manosij *et al.* (2017) reported the effect of three different crystal phases/forms (anatase, anatase and rutile, and rutile mixture of TNP (20–26 nm) with regard to internalization of the TNP, cytotoxic response, oxidative stress, and DNA damage. The cytotoxic response was observed at a concentration 25 $\mu\text{g}/\text{ml}$ for the tested particles. Yue *et al.* (2017) studied the two different sized TNP 25 nm (nanotube type) and TNP 60 nm (anatase type) and found that they induced size and concentration (0.1–100 $\mu\text{g}/\text{ml}$) dependent cytotoxicity for 24, 48, or 72 h after being exposed to A549 and 16HBE cells. They found that TNP 25 and 60 nm were produced a dose- and size-dependent cytotoxicity in two cell lines due to reduced cell viability, increased ROS levels, DNA methylations, and cell death.

Very little is known about the impact of the size and dose of the TNP mixture (80% anatase and 20% rutile) on human cell lines, especially with three different sizes TNP 18, TNP 30, and TNP 87. This study further investigated the influence of size and concentration on cellular cytotoxicity of exposed cell cultures. In this study, the toxic potential of commercial grade TNP of three different sizes and specific surface area particles was studied to understand possible cell-particle

interactions for cytotoxicity assessment by MTT, LDH, and ROS levels in A549 and Caco-2 cells.

The cell lines selected for the study reflected the potential routes of exposure, including inhalation (Brun *et al.* 2014) and gastrointestinal system (De-Angelis *et al.* 2013, Heringa *et al.* 2016). The cell viability assay results revealed that A549 cells were more sensitive than Caco-2 cells. The cell viability was reduced at higher concentrations (100 and 300 $\mu\text{g}/\text{ml}$) in both cell lines. The significant cell viability reduction was not observed in both the cell lines at lower concentrations, i.e., 0.1 and 3 $\mu\text{g}/\text{ml}$ upon exposure to three different sized TNPs. Size- and dose-dependent cytotoxicity was observed on two tested cell lines according to the dose-response curve obtained in A549 cells as depicted in Figure 3 and Caco-2 cells as shown in Figure 4 for 48 h post exposure.

Smaller sized TNP 18 has shown moderate adverse effects in both human epithelial alveolar and colon cells at lower concentrations compared to TNP 30 and TNP 87 at higher concentrations. The cell viability reduction of TNP 18, TNP 30, and TNP 87 histograms is presented in Figures 3 and 4. The transient size- and dose-dependent decrease in cell number in both the cell lines upon exposure to three different sized TNP with increasing concentrations. The IC_{50} values were 21.80, 23.30, and 34.90 $\mu\text{g}/\text{ml}$ for TNP 18, TNP 30, and TNP 87, respectively, compared to Nano QTZ of 43.82 $\mu\text{g}/\text{ml}$ in A549 cells. The results of a study correlate with that of smaller size particles which induced greater cytotoxicity at lower concentrations due to their higher surface area and other physicochemical properties (Di Virgilio *et al.* 2010, Cai *et al.* 2011, Lopes *et al.* 2016).

This study revealed that size and dose play a key role in the determination of toxicity potential of TNPs. In addition, this study agrees with an earlier study which reported that the 25 and 60 nm TNP produces a size-dependent cytotoxicity for 48 h post exposure in human alveolar epithelial cells and reported a dose-dependent cytotoxicity of 80 $\mu\text{g}/\text{ml}$ (Yue *et al.* 2017).

The membrane integrity (LDH leakage assay) levels were found to be increased at higher concentrations, i.e., 60 and 100 $\mu\text{g}/\text{ml}$ in both the cell lines. A549 cells were sensitive to TNP exposure compared to Caco-2 cells with regard to the percentage of LDH leakage depending upon the EC_{25} and EC_{50} values extra-cellularly. The TNP 18 exposure to A549 cells resulted in $1^{1/2}$, $2^{1/2}$, $3^{1/2}$, and $4^{1/2}$ fold increment for the doses 10 $\mu\text{g}/\text{ml}$ ($p < 0.05$), 30 $\mu\text{g}/\text{ml}$ ($p < 0.05$), 60 $\mu\text{g}/\text{ml}$ ($p < 0.001$), and 100 ($p < 0.001$) $\mu\text{g}/\text{ml}$ compared to control.

In addition, the increment of $1^{1/2}$ to 4 folds for 60 $\mu\text{g}/\text{ml}$ ($p < 0.01$) and 100 $\mu\text{g}/\text{ml}$ ($p < 0.001$) in Caco-2 cells for 48 h post exposure of TNP 18, shown in Figure 6. The EC_{50} was calculated for three TNP and the results were shown in Table 3. The EC_{25} values were 5.83 and 9.50 $\mu\text{g}/\text{ml}$ for A549 and Caco-2 cells, respectively, upon 48 h post exposure to TNP 18 (mixture of anatase and rutile). Therefore, the greater the LDH leakage severe will be the damage to cells post exposed to TNPs. Besides, LDH leakage could be a sign of membrane damage as a result of which cellular contents come out, followed inflammatory responses and finally resulting in cell death (Xiong *et al.* 2013).

Thus, the decrease in cell viability and increased in LDH levels indicates the TNP induced cytotoxicity in the human epithelial alveolar and colon cells at higher concentrations 60 and 100 µg/ml for 48 h post exposure. Plasma membrane integrity assay results revealed that the membranolytic effect by LDH leakage reinforces the cytotoxicity results obtained with MTT method.

Harikiran and Narsimhareddy (2016) also observed that smaller size gold nano-rods (GNR 10 nm) caused severe membrane damage when compared to larger size GNR 25 nm at doses 30 and 50 µg/ml in Hep G2 cells for 24 post exposure. The results of the study by Yan *et al.* (2017) are in agreement with the findings of the present study, which indicate that LDH levels increased significantly at 0.4 mg/ml significantly upon exposure to smaller size 37 nm TNP compared to larger size i.e., 91.5 nm TNP in adipose-derived stromal cells (ADSCs).

The cytotoxicity assessment of TNP was indicated by increased ROS levels in both the cell lines. The size- and dose-dependent increment of ROS was observed in A549 cells as shown in Figure 7. The results were clearly indicating that the relative ROS release was increased drastically with concentrations (0.1–100 µg/ml) for 48 h post exposure in human epithelial lungs and colon cells. In Figures 7 and 8, ROS levels were found to be 3 to 18^{1/2} and 5^{1/2} to 19^{1/2} folds more for both the A549 and Caco-2 cells for TNP 18.

The oxidative stress was observed as a result of increased levels of LDH and ROS in the cells exposed to different sized 30 nm TNP (Allouni *et al.* 2012, Zhongyuan *et al.* 2017). The reported findings were similar to our present study results. TNPs of different sizes produced a size- and dose-dependent ROS release both *in vitro* and *in vivo* (Meena *et al.* 2015, Chen *et al.* 2016). Akhtar *et al.* (2016) reported dose-dependent ROS levels stimulated by copper-oxide NP in A549 cells. The amount of ROS released was found to be size- and dose-dependent on exposing cell cultures to different sized NP by *in vitro*.

Conclusions

The study results clearly indicate the occurrence of size- and dose-dependent cytotoxicity in both cell lines upon exposure to higher concentrations of TNP (80% anatase and 20% rutile) for 48 h. The LDH and ROS levels, DCFH-DA assay results reinforced the cytotoxicity of three different sized mixture of TNP exposed to two different cell lines. The increased LDH and ROS levels resulted in development of oxidative stress. Therefore, the study concludes that smaller sized TNP 18 induced greater toxicity at lower concentrations than the bigger sized TNP 30 and TNP 87 owing to their varying physicochemical properties. On the basis of the findings of the two cell lines, the order of TNPs on cytotoxicity was TNP 18 > TNP 30 > TNP 87. Therefore, size- and dose-dependent cytotoxicity was induced in TNPs exposed cell cultures. Further, in order to understand the mechanism of toxicity induced by these TNPs, further *in vivo* investigations are required to be carried out.

Acknowledgments

Authors thank the NCCS, Pune, India for supply of cell lines for this study.



Disclosure statement

The authors report that there are no conflicts of interest.

Funding

The first author was grateful to the University Grants Commission (UGC), New Delhi, India, for support of funding in the form National Fellowship.

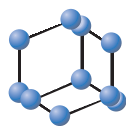
ORCID

Durgaiah Gandamalla  <http://orcid.org/0000-0003-4151-4406>
Harikiran Lingabathula  <http://orcid.org/0000-0001-9990-4656>
Narsimhareddy Yellu  <http://orcid.org/0000-0002-2969-7855>

References

- Abdal, D.A., Hossain, M.K., Lee, S.B., *et al.*, 2017. The role of reactive oxygen species (ROS) in the biological activities of metallic nanoparticles. *International Journal of Molecular Sciences*, 18, 120.
- Akhtar, M.J., *et al.*, 2016. Dose-dependent genotoxicity of copper oxide nanoparticles stimulated by reactive oxygen species in human lung epithelial cells. *Toxicology and Industrial Health*, 32, 809–821.
- Allouni, Z.E., *et al.*, 2012. Role of physicochemical characteristics in the uptake of TiO₂ nanoparticles by fibroblasts. *Toxicology in Vitro*, 26, 469–479.
- Alvarez, P.M., *et al.*, 2016. Insights into the removal of terbuthylazine from aqueous solution by several treatment methods. *Water Research*, 98 (7), 334–343.
- Ammendolia, M.G., *et al.*, 2017. Short-term oral exposure to low doses of nano-sized TiO₂ and potential modulatory effects on intestinal cells. *Food and Chemical Toxicology*, 102, 63–75.
- Armand, L., *et al.*, 2016. Long-term exposure of A549 cells to titanium dioxide nanoparticles induces DNA damage and sensitizes cells towards genotoxic agents. *Nanotoxicology*, 10 (7), 913–923.
- Aschberger, K., *et al.*, 2011. Analysis of currently available data for characterizing the risk of engineered nanomaterials to the environment and human health—lessons learned from four case studies. *Environment International*, 37, 1143–1156.
- Bessa, M.J., *et al.*, 2017. Moving into advanced nanomaterials. Toxicity of rutile TiO₂ nanoparticles immobilized in nanokaolin nanocomposites on HepG2 cell line. *Toxicology and Applied Pharmacology*, 316, 114–122.
- Brun, E., *et al.*, 2014. Titanium dioxide nanoparticle impact and translocation through *ex vivo*, *in vivo* and *in vitro* gut epithelia. *Particle and Fibre Toxicology*, 11, 13.
- Cai, K., *et al.*, 2011. Correlation of the cytotoxicity of TiO₂ nanoparticles with different particle sizes on a sub-200-nm scale. *Small*, 7, 3026–3031.
- Challa, S., and Chan, F.K., 2010. Going up in flames necrotic cell injury and inflammatory diseases. *Cellular and Molecular Life Sciences*, 67, 324–353.
- Chen, C.W., *et al.*, 2016. Evaluation of the intracellular uptake and cytotoxicity effect of TiO₂ nanostructures for various human oral and lung cells under dark conditions. *Toxicology Research*, 5, 303–311.
- De-Angelis, I., *et al.*, 2013. Comparative study of ZnO and TiO₂ nanoparticles: physicochemical characterisation and toxicological effects on human colon carcinoma cells. *Nanotoxicology*, 7, 1361–1372.
- De Berardis, B., *et al.*, 2010. Exposure to ZnO nanoparticles induces oxidative stress and cytotoxicity in human colon carcinoma cells. *Toxicology and Applied Pharmacology*, 246, 116–127.

- DeLoid, G.M., *et al.*, 2017. Preparation, characterization, and in vitro dosimetry of dispersed, engineered nanomaterials. *Nature Protocols*, 12, 355–371.
- Di Virgilio, A.L., Reigosa, M., and de Mele, M.F., 2010. Response of UMR 106 cells exposed to titanium dioxide and aluminum oxide nanoparticles. *Journal of Biomedical Materials Research Part A*, 92, 80–86.
- Gamze, K., and Mustafa, C., 2017. Investigating the origins of toxic response in TiO₂ nanoparticle-treated cells. *Nanomaterials*, 7, 83.
- George, I., *et al.*, 2015. Metallic oxide nanoparticle translocation across the human bronchial epithelial barrier. *Nanoscale*, 7, 4529–4544.
- Grant, D.N., *et al.*, 2015. In vitro electromagnetic stimulation to enhance cell proliferation in extracellular matrix constructs with and without metallic nanoparticles. *Journal of Biomedical Materials Research Part B Applied Biomaterials*, 103, 1532–1540.
- Guadagnini, R., *et al.*, 2015. Toxicity evaluation of engineered nanoparticles for medical applications using pulmonary epithelial cells. *Nanotoxicology*, 9, 25–32.
- Harikiran, L., Bhikku, A., and Narsimha, R.Y., 2015. In vitro cytotoxicity of gold and silver nanorods using different human cell lines. *Latin American Journal of Pharmacy*, 34, 1277–1282.
- Harikiran, L., and Narsimahareddy, Y., 2016. Cytotoxicity, oxidative stress, and inflammation in human Hep G2 Liver epithelial cells following exposure to gold nanorods. *Toxicology Mechanisms and Methods*, 26, 340–347.
- Heringa, M.B., *et al.*, 2016. Risk assessment of titanium dioxide nanoparticles via oral exposure, including toxicokinetic considerations. *Nanotoxicology*, 11, 1–11.
- Hussain, S., *et al.*, 2009. Oxidative stress and proinflammatory effects of carbon black and titanium dioxide nanoparticles: role of particle surface area and internalized amount. *Toxicology*, 260, 142–149.
- Ivask, A., *et al.*, 2015. Toxicity of 11 metal oxide nanoparticles to three mammalian cell types in vitro. *Current Topics in Medicinal Chemistry*, 15, 1914–1929.
- Korzeniewski, C., and Callewaert, D.M., 1983. An enzyme-release assay for natural cytotoxicity. *Journal of Immunological Methods*, 64, 313–320.
- Kroll, A., *et al.*, 2011. Cytotoxicity screening of 23 engineered nanomaterials using a test matrix of ten cell lines and three different assays. *Particle and Fibre Toxicology*, 8, 9.
- Lopes, V.R., *et al.*, 2016. Dose dependent autophagic effect of titanium dioxide nanoparticles in human HaCaT cells at non-cytotoxic levels. *Journal of Nanobiotechnology*, 14, 22.
- Lu, P.J., *et al.*, 2015. Analysis of titanium dioxide and zinc oxide nanoparticles in cosmetics. *Journal of Food and Drug Analysis*, 23, 587–594.
- Manke, A., Wang, L., and Rojanasakul, Y., 2013. Mechanisms of nanoparticle-induced oxidative stress and toxicity. *BioMed Research International*, 2013, 942916.
- Manosij, G., *et al.*, 2017. Cyto-genotoxic and DNA methylation changes induced by different crystal phases of TiO₂-np in bronchial epithelial (16-HBE) cells. *Mutation Research Fundamental and Molecular Mechanisms of Mutagenesis*, 796, 1–12.
- Meena, R., Kumar, S., and Paulraj, R., 2015. Titanium oxide (TiO₂) nanoparticles in induction of apoptosis and inflammatory response in brain. *Journal of Nanoparticle Research*, 17, 1–14.
- Mirzaei, A., Leonardi, S.G., and Neri, G., 2016. Detection of hazardous volatile organic compounds (VOCs) by metal oxide nanostructures-based gas sensors. *Ceramics International*, 42, 15119–15141.
- Morimoto, Y., *et al.*, 2016. Evaluation of pulmonary toxicity of zinc oxide nanoparticles following inhalation and intratracheal instillation. *Nanotoxicology*, 10, 607–618.
- Mosmann, T., 1983. Rapid colorimetric assay for cellular growth and survival: application to proliferation and cytotoxicity assays. *Journal of Immunological Methods*, 65, 55–63.
- Naidu, R., Espana, V.A.A., and Liu, Y.J., 2016. Emerging contaminants in the environment: risk-based analysis for better management. *Chemosphere*, 154, 350–357.
- Odzak, N., Kistler, D., and Sigg, L., 2017. Influence of daylight on the fate of silver and zinc oxide nanoparticles in natural aquatic environments. *Environmental Pollution*, 226, 1–11.
- Park, J., *et al.*, 2011. Size dependent macrophage responses and toxicological effects of Ag nanoparticles. *Chemical Communications*, 47, 4382–4384.
- Piccinno, F., *et al.*, 2012. Industrial production quantities and uses of ten engineered nanomaterials in Europe and the world. *Journal of Nanoparticle Research*, 14, 1–11.
- Rahman, M.M., *et al.*, 2017. Fabrication of selective chemical sensor with ternary ZnO/SnO₂/Yb₂O₃ nanoparticles. *Talanta*, 170, 215–223.
- Shang, L., Nienhaus, K., and Nienhaus, G.U., 2014. Engineered nanoparticles interacting with cells: size matters. *Journal of Nanobiotechnology*, 12, 1.
- Simeonidis, K., *et al.*, 2015. Optimizing magnetic nanoparticles for drinking water technology: the case of Cr(VI). *The Science of the Total Environment*, 535, 61–68.
- Titma, T., *et al.*, 2016. Toxicity of antimony, copper, cobalt, manganese, titanium and zinc oxide nanoparticles for the alveolar and intestinal epithelial barrier cells in vitro. *Cytotechnology*, 68, 2363–2377.
- Tomankova, K., *et al.*, 2015. Cytotoxicity, cell uptake and microscopic analysis of titanium dioxide and silver nanoparticles in vitro. *Food and Chemical Toxicology*, 82, 106–115.
- Uboldi, C., *et al.*, 2016. Role of the crystalline form of titanium dioxide nanoparticles: rutile, and not anatase, induces toxic effects in Balb/3T3 mouse fibroblasts. *Toxicology In Vitro*, 31, 137–145.
- Ursini, C.L., *et al.*, 2014. Evaluation of cytotoxic, genotoxic and inflammatory response in human alveolar and bronchial epithelial cells exposed to titanium dioxide nanoparticles. *Journal of Applied Toxicology*, 34, 1209–1219.
- Wan, C.P., Myung, E., and Lau, B.H., 1993. An automated micro-fluorometric assay for monitoring oxidative burst activity of phagocytes. *Journal of Immunological Methods*, 159, 131–138.
- Xia, T., *et al.*, 2013. Interlaboratory evaluation of in vitro cytotoxicity and inflammatory responses to engineered nanomaterials: the NIEHS Nano GO Consortium. *Environmental Health Perspectives*, 121, 683–690.
- Xiong, S., *et al.*, 2013. Specific surface area of titanium dioxide (TiO₂) particles influences cyto and photo-toxicity. *Toxicology*, 304, 132–140.
- Yan, X., *et al.*, 2017. Cell based cytotoxicity assays for engineered nanomaterials safety screening: exposure of adipose derived stromal cells to titanium dioxide nanoparticles. *Journal of Nanobiotechnology*, 15, 50.
- Yang, X., *et al.*, 2017. Particle-specific toxicity and bioavailability of cerium oxide (CeO₂) nanoparticles to Arabidopsis thaliana. *Journal of Hazardous Materials*, 322, 292–300.
- Yang, Z., Li, W., and Zhang, X., 2015. Toxicology of nanosized titanium dioxide: an update. *Archives of Toxicology*, 89, 2207–2217.
- Yue, M., *et al.*, 2017. Titanium dioxide nanoparticles induce size dependent cytotoxicity and genomic DNA hypomethylation in human respiratory cells. *RSC Advances*, 7, 23560–23572.
- Zhongyuan, G., *et al.*, 2017. Titanium dioxide nanoparticle ingestion alters nutrient absorption in an in vitro model of the small intestine. *NanoImpact*, 5, 70–82.



Drug Design, Synthesis and *In Vitro* Evaluation of Substituted Benzofurans as Hsp90 Inhibitors



Sundeep Kadasi^{1,2}, Thadeu E.M.M. Costa^{3,4}, Neha Arukala¹, Mallika Toshakani¹, Chaitanya Dugginetti¹, Sreekanth Thota³, Sayan D. Gupta¹, Shiva Raj², Carmen Penido^{3,4}, Maria G. Henriques^{3,4}, Nulgumnalli M. Raghavendra^{1,3,5,*}

¹Department of Pharmaceutical Chemistry, Gokaraju Rangaraju College of Pharmacy, Osmania University, Hyderabad, India; ²Department of Chemistry, Osmania University, Hyderabad, India; ³National Institute for Science and Technology on Innovation on Neglected Diseases (INCT/IDN), Center for Technological Development in Health (CDTS), Fiocruz, Rio de Janeiro, Brazil; ⁴Department of Applied Pharmacology, Farmanguinhos, Fiocruz, Rio de Janeiro, Brazil; ⁵Department of Medicinal Chemistry and Molecular Pharmacology, College of Pharmacy, Purdue University, West Lafayette, IN, USA

Abstract: Background: Heat shock protein 90 is a molecular chaperone required for the stability and function of several client proteins that promote cancer cell growth and/or survival. Discovery of Hsp90 inhibitors has emerged as an attractive target of research in cancer therapeutics. Natural products like geldanamycin and radicicol are established Hsp90 inhibitors, but face limitations with toxicity and inactivity, by *in vivo* studies respectively. However, they lay the logical starting point for the design of novel synthetic or semi-synthetic congeners as Hsp90 inhibitors.

Objective: In this article, the structure based drug design of substituted 2-aryl/heteroarylidene-6-hydroxybenzofuran-3(2H)-one analogues to optimize and mimic the pharmacophoric interactions of the valid Hsp90 inhibitor radicicolis focused.

Method: *In silico* docking study was performed by Surflex dock-Geom (SYBYL- X 1.2 drug discovery suite) and the designed ligands were chemically synthesized by conventional method using resorcinol and chlororesorcinol as starting materials. Two dimensional chemical similarity search was carried out to identify the chemical space of 'SY' series in comparison with reported Hsp90 inhibitors. The *in vitro* cell proliferation assay (*resazurin reduction method*) and proteomic investigation (DARTS) was carried out on whole cell lysate to evaluate anticancer activity.

Results: The chemical structures of all the synthesized compounds were confirmed by IR, ¹H-NMR and Mass spectral analysis. The results of chemical similarity search show that SY series fit it in the chemical space defined by existing Hsp90 inhibitors. *In vitro* cell proliferation assay, against human melanoma and breast cancer cell lines, identified 'SY3' as the promising anticancer agent amongst the series.

Conclusion: Docking studies, 2D chemical similarity search, resazurin reduction assay and qualitative proteomic analysis identify 'SY3' as a promising Hsp90 inhibitor amongst the series.

Keywords: Anticancer activity, benzofurans, DARTS, drug design, docking studies, Hsp90.

1. INTRODUCTION

Heat shock protein 90 (Hsp90), an ATP driven chaperone protein is one of the important targets in cancer therapy [1]. A multitude of Hsp90 client proteins, such as, Her-2, Bcr-abl, Akt, C-Raf, Braf^{V600E}, CDK4 and estrogen receptor are

oncogenic and are considered as the hallmarks of malignancy [2, 3]. These client proteins depend on Hsp90 machinery for their proper conformational stability, protecting themselves from degradative ubiquitin-proteasome pathway [4-6]. Although Hsp90 is expressed in normal cells, their expression is upregulated in cancer cells; this helps the Hsp90 inhibitors killing cancer cells selectively compared to normal cells [7]. All these facts have made Hsp90 to emerge promising target for the development of new antineoplastic agents for a variety of human cancers.

*Address correspondence to this author at the Center for Technological Development in Health (CDTS), Fundação Oswaldo Cruz, Av. Brasil 4036, Prédio da Expansão, 8º Andar, Sala 814, Manguinhos, 21040-361 Rio de Janeiro, RJ, Brazil; Tel/Fax: +55-21-2290-0494; E-mail: nmraghava@yahoo.in

Natural products geldanamycin, radicicol and their semi-synthetic derivatives are explored for Hsp90 inhibitory activity [8, 9]. Some of them such as DMAG and 17-AAG are being investigated in preclinical trials [10-15] and some new SAR studies on geldanamycin are gaining importance [16]. PU3, the first synthetic purine derivative designed to inhibit Hsp90, provided a space for the modifications on the synthetic chemical compound for improved anticancer properties [12]. PU3, acquires a bent shape (C) conformation similar to ADP/ATP in the N-terminal ATP binding site of Hsp90 and sequentially, a prototype congener PU24FC1, was developed which exhibited an IC₅₀ value of 2-7 μM in various cancer cell lines [17-19]. Several heterocyclic scaffolds (Fig. 1) having Hsp90 inhibitory potency were discovered successively, viz. pyrazole (CCT018159, followed by more potent 5-amide congener 'VER-49009') and isoxazole (VER-50589, exhibited 17 fold lesser K_d value in Hsp90β than VER-49009), many are in clinical trials, and there is a high scope for them to enter the market for cancer treatment [20, 21]. Recently, onalespib (resorcinol derivative), has been proved effective in imatinib sensitive (GIST882, GIST-T1) and resistant (GIST430, GIST48) cell lines and is being pursued for anticancer activity in clinical trials [22]. All these efforts and endeavors highlight the need for the exploration of novel chemical entities as Hsp90 inhibitors with better anticancer activity.

In continuation of our ongoing attempts to discover novel scaffolds as Hsp90 inhibitors [23-25], we report the structure based drug design (SBDD) of benzofuran-3(2H)-one analogues (SY1-SY10) providing their 2D chemical similarity search, chemical synthesis, analytical characterization. In addition, *in vitro* tumor assays against mammalian cancer cells and proteomics analysis against Hsp90 are reported in this paper.

2. RESULTS AND DISCUSSION

2.1. Chemistry

The synthesis of substituted 2-aryl/heteroarylidene-6-hydroxybenzofuran-3(2H)-one (SY1-SY10) (depicted in

Scheme 1) was done with classical Friedel crafts acylation of chloro acetyl chloride of resorcinol (M1)/chloro resorcinol (S1) separately, to yield corresponding chloro-acetylated derivatives (M2/S2), in the presence of a lewis acid (AlCl₃) in diethyl ether as a solvent. The intermediates (M2/S2) were cyclized individually by substitution reaction in the alkaline conditions (alc. NaOH solution), to yield benzofuranones (M3/S3). To obtain a bent 'C' shape conformation for the designed ligands in the active site of Hsp90; M3/S3 (intermediates) were subjected to Claisen-Schmidt condensation reaction by the treatment with various aromatic aldehydes to yield substituted 2-aryl/heteroarylidene-6-hydroxybenzofuran-3(2H)-one (SY1-SY10) in 52% - 72% yield. The formation of title compounds under Claisen Schmidt conditions is confirmed by appearance of sharp singlet for enone 'H' at δ 6.90-7.1 ppm, and a broad peak for phenolic 'H' around δ 10- 12 ppm. IR absorption frequency ranging from 1650-1680 cm⁻¹, for carbonyl (C=O) in a conjugated system and C-O (stretch) around 1150 cm⁻¹ for (Z)-2-aryl/heteroarylidene-5-chloro-6-hydroxybenzofuran-3(2H)-one derivatives also gave evidence of the structural information of the title compounds. Mass spectral analysis also confirmed the structures of all the compounds. All the title compounds were found to be in the Z-isomer conformation, as it is the most stable conformation possible. The Z-isomerism of the title 2-benzylidene-benzofuran-3(2H)-one was also suggested on the basis of calculation of heat of formations of both the Z and E isomers by AM1 (the Austin Model 1) method. AM1 method highlights that the Z isomer 2-benzylidene-benzofuran-3(2H)-one is more stable than the E isomer by 1.98 kcal/mole [26-28].

2.2. Molecular Docking

SYBYL-X 1.2 drug discovery suite, comprising Surflex dock-Geom program was used to perform molecular docking of substituted 2-aryl/heteroarylidene-6-hydroxybenzofuran-3(2H)-one (SY1-SY10) in the rigid binding site of Hsp90 (PDB ID: 1YET). Radicicol, owing to its significant Hsp90 inhibitor potency *in vitro* was utilized as a structural lead in the design of benzofuranone analogues (SY1-SY10). SBDD

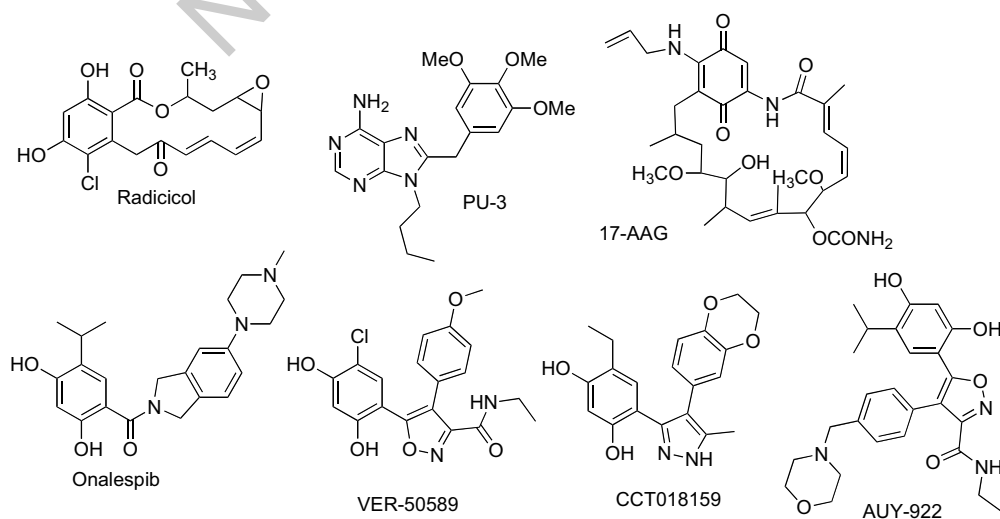


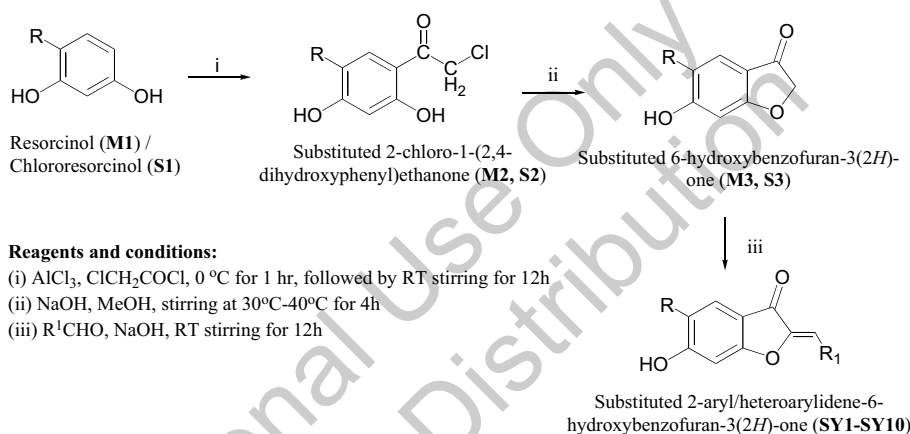
Fig. (1). Chemical structures of Hsp90 inhibitors.

of benzofuran-3(2H)-one analogues (SY1-SY10) mimicking resorcinolic moiety (of RD) was carried out with an intention that, the proposed analogues (SY1-SY10) align the resorcinol scaffold into the ATP binding site of Hsp90 for essential interactions. Substituted 2-aryl/heteroarylidene-6-hydroxybenzofuran-3(2H)-one (SY1-SY10) presumed a bent 'C' shaped conformation essential for binding in the active site of Hsp90. *In silico* docking results, identified SY1-SY3 as promising molecules based on the total score (expressed as calculated $-\log [K_d]$) and a consensus score (generated post docking minimization, which depends on multiple scoring functions) to evade bias and make docking analysis more predictive. Molecular docking results are shown in Table 1. The benzofuran-3(2H)-one analogues occupied the adenyl binding site of the Hsp90, firmly anchoring in the protein by a crucial hydrogen bonding between carbonyl at 3-position with 'OH' of Thr184 (SY1-SY3); an interaction akin to 'lactone' group of radicicol with Thr184 (see Fig. 2 A, B, C for

RD, SY2 and SY3 binding interactions). Another important intermolecular H-bonding is observed between 'O' of benzofuranone scaffold (SY1-SY3) and 'NH₂' (of amide) of Asn51 (similar to hydrogen bonding between epoxy linkage of radicicol with 'NH₂' of Asn51. The hydrophobic interactions for the compounds (SY1-SY10) and RD were observed with amino acids Leu48, Ile49, Ala55, Met98, Ile91, Val92, Leu107, Val136, Phe138, Val150 and Val186.

2.3. Assessment of Chemical Similarity

Organic chemical entities occur in several shapes, molecular dimensions and parameters, usually described and categorized by certain "descriptors" such as molecular weight, logP value, topology, etc. The assessment of chemical similarity is a quantitative approach to analyze how best the designed molecules fit the chemical space defined by existing molecules for certain pharmacological activity. To



Scheme 1. Chemical synthetic scheme for the preparation of substituted 2-aryl/heteroarylidene-6-hydroxybenzofuran-3(2H)-one (SY1-SY10).

Table 1. Surflex Dock-Geom docking results of against Hsp90 protein (PDB ID: 1YET).

Compound	Total Score ¹	C Score ²	Polar ³	G Score ⁴	PMF Score ⁵	D Score ⁶	Chem Score ⁷	Crash ⁸
SY1	3.89	4	1.28	-135	-0.72	-592	-28.93	-0.91
SY2	4.06	3	1.28	-149	22.38	-514	-32.85	-1.08
SY3	4.18	3	1.25	-151	23.51	-482	-30.57	-0.78
SY4	3.22	1	2.47	-78	-7.29	-313	-24.60	-0.27
SY5	3.57	0	2.23	-108	17.73	-188	-23.77	-0.25
SY6	3.17	0	2.45	-109	22.61	-284	-21.72	-0.90
SY7	3.20	2	1.28	-106	6.50	-381	-28.64	-0.37
SY8	4.12	1	2.93	-69	8.30	-309	-19.65	-0.36
SY9	3.48	2	1.19	-96	1.57	-638	-24.90	-0.66
SY10	3.31	2	2.43	-111	8.20	-468	-25.37	-0.97
Radicicol	3.28	3	3.62	-201	-2.38	-637	-35.43	-2.71

¹Total score: It represents the total surflex dock score expressed as (-logK_d). ²C score (The consensus score): It evaluates a protein-ligand pair based on multiple scoring functions.

³Polar: It defines the polar interaction between the ligand and the protein. ⁴G score: It is based on hydrogen bonding, ligand-protein complex, and internal (ligand-ligand) energies.

⁵PMF score: It is the free energies of interactions for protein-ligand atom pairs. ⁶D score: It is based on van der waals interaction between protein and the ligand. ⁷Chem score: It includes terms for hydrogen bonding, metal-ligand interaction, lipophilic contact and rotational entropy, along with an intercept term. ⁸Crash: It represents appropriate penetration of a ligand into the active site of the protein.

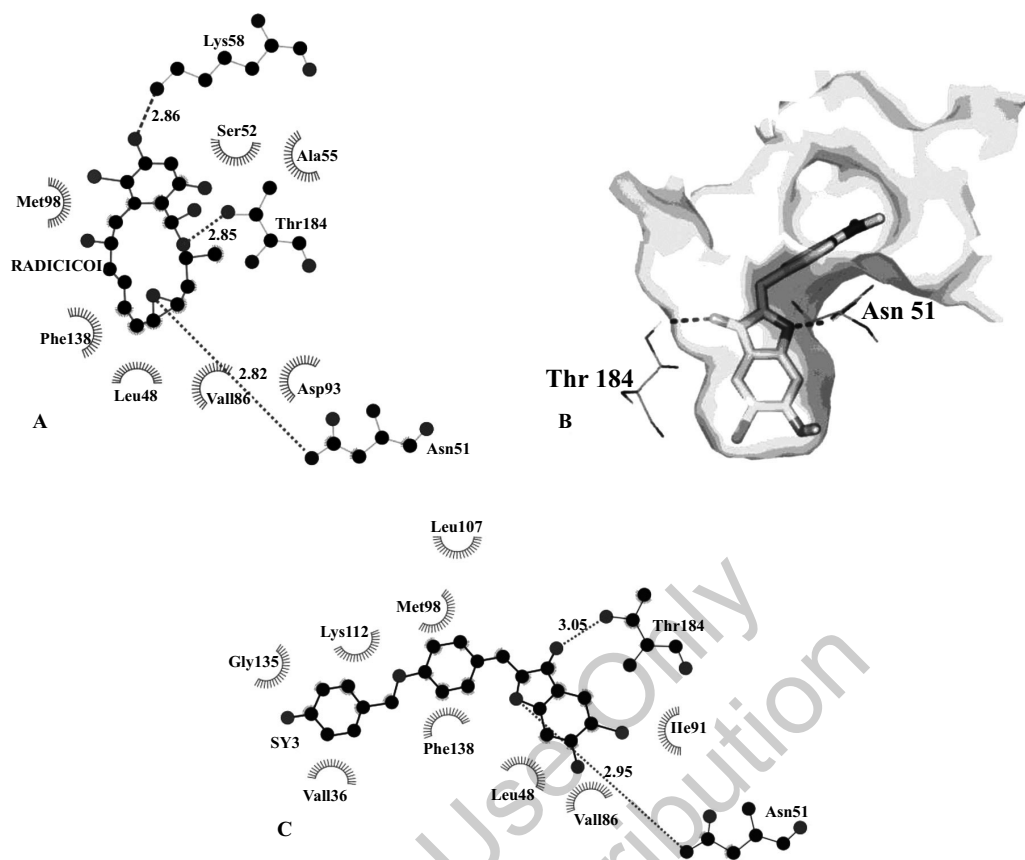


Fig. (2). A. 2D-diagrams for docking interactions generated by LIGPLOT for Radicicol (PDB ID: 1YET); B. Compound SY2 exhibiting common H-bonding interactions with amino acids Asn51 and Thr184 (PDB ID: 1YET) C. Compound SY3 (Thr184 and Asn51) in the active site of Hsp90 (PDB ID: 1YET).

assess the chemical similarity of ‘SY series’ in comparison with reported Hsp90 inhibitors, the 2D molecular descriptors for the designed molecules (SY series) were analyzed by Chemaxon’s tools and compared with the existing Hsp90 inhibitors (PY-IS and PU series). Compounds SY1-SY10, occupied the similar chemical space defined by Hsp90 inhibitors (See Fig. 3 and Table S-1 (supplementary information)), with an almost overlapping logP value, which invariably signifies good partitioning effect as that of PU, PY-IS series indicating the promising biological properties. Rotatable bond count with a median value of ‘3’ and aliphatic bond count/3, with a median value of ‘4’ in SY series, provides enough conformational flexibility for proper orientation and binding interactions in the ATP binding site of the Hsp90 protein. ‘SY’ series holding good donor count guides crucial binding interactions in the active site of Hsp90 protein. Important descriptors such as logP, rotatable bond count, aliphatic bond count, donor count, etc indicates that SY compounds occupy the similar chemical space as that of reported PU and PY-IS series as Hsp90 inhibitors.

2.4. In Vitro Cell Proliferation Assay

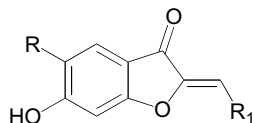
Resazurin reduction assay was done on human melanoma cells (A375 and SKMEL-28) and breast cancer cells (MDAMB-468) using 17-AAG as reference compound (results shown in Table 2). SY3 emerge as the promising com-

pound amongst the series. SY3 exhibited IC_{50} of 18.5 μM against A375 melanoma, IC_{50} of 22.3 μM against MDA-MB-468 breast cancer and IC_{50} of 37.4 μM against SK-MEL-28 melanoma cells. 17-AAG showed IC_{50} of 5.20, 2.03 and 1.33 against A375, SK-MEL-28 and MDA-MB-468 cells respectively. Anti-cancer property of SY3 could be attributed to the presence of a polar ‘F’ atom (aids in solubility) at 4’ position of the benzene ring (aids partitioning). In addition as per *in silico* screening, the important polar interaction of SY3 with Thr184 and Asn51 of Hsp90 might have contributed to the promising anti-proliferative activity. Maximum occupancy of the receptor site with the ligand was observed with SY3, which also exhibited least crash (penalty) in the binding site supporting the *in vitro* results. Other compounds were not found to have significant anti-proliferative activity.

2.5. Drug Affinity Responsive Target Stability (DARTS) Proteomics Assay

Based on the results of *in vitro* cytotoxic assays, we carried out the study on Hsp90 protein interaction to elucidate the mechanistic pathway of anticancer activity. DARTS, proteomics approach to investigate small molecule binding to targets using protease-based digestion was performed on cell lysate of the MDA MB468 cancer cells. The DARTS assay demonstrated that compound SY3 protects Hsp90 β from protease thermolysin digestion; its properties were

Table 2. Cell proliferative assay by resazurin reduction method.



Compd ¹	R	R ₁	IC ₅₀ (μM) ± SEM		
			A375 ¹	SK-MEL-28 ²	MDA-MB-468 ³
SY1	Cl	-C ₆ H ₃ -3,4-OCH ₃	94.3 ± 0.34	87.4 ± 0.42	74.7 ± 0.23
SY2	Cl	-C ₆ H ₄ -4-N(CH ₃) ₂	85.0 ± 0.19	61.0 ± 0.08	77.1 ± 0.19
SY3	Cl	-C ₆ H ₄ -4-OCH ₂ C ₆ H ₄ (p)F	18.4 ± 0.06	37.4 ± 0.06	22.3 ± 0.06
SY4	Cl	-2-C ₄ H ₃ O	76.3 ± 0.32	78.4 ± 0.26	84.7 ± 0.45
SY5	Cl	-C ₆ H ₄ -4-Cl	83.2 ± 0.35	77.5 ± 0.22	88.3 ± 0.39
SY6	Cl	-C ₆ H ₄ -4-OH	97.3 ± 0.45	81.0 ± 0.43	89.4 ± 0.32
SY7	H	-C ₆ H ₄ -4-Cl	89.9 ± 0.43	78.9 ± 0.36	88.3 ± 0.56
SY8	H	-C ₆ H ₃ -3,4-OCH ₃	87.4 ± 0.43	76.5 ± 0.33	78.3 ± 0.34
SY9	H	-C ₆ H ₂ -3,4,5-OCH ₃	78.3 ± 0.39	79.3 ± 0.29	76.4 ± 0.14
SY10	H	-C ₆ H ₃ -2,5-OCH ₃	79.4 ± 0.29	70.0 ± 0.24	78.6 ± 0.31
17-AAG	Structure is given in Fig. 1.		5.20 ± 0.18	2.03 ± 0.04	1.33 ± 0.06

¹Data represent the IC₅₀ values for a 3 day exposure to normalized to no drug controls and is the mean of triplicate experiments performed, Concentration for SY1-SY3 compounds were 3.12-100 μM, 17-AAG was tested at 0.31-5 μM; ²mamalian malignant melanoma; ³mamalian breast cancer.

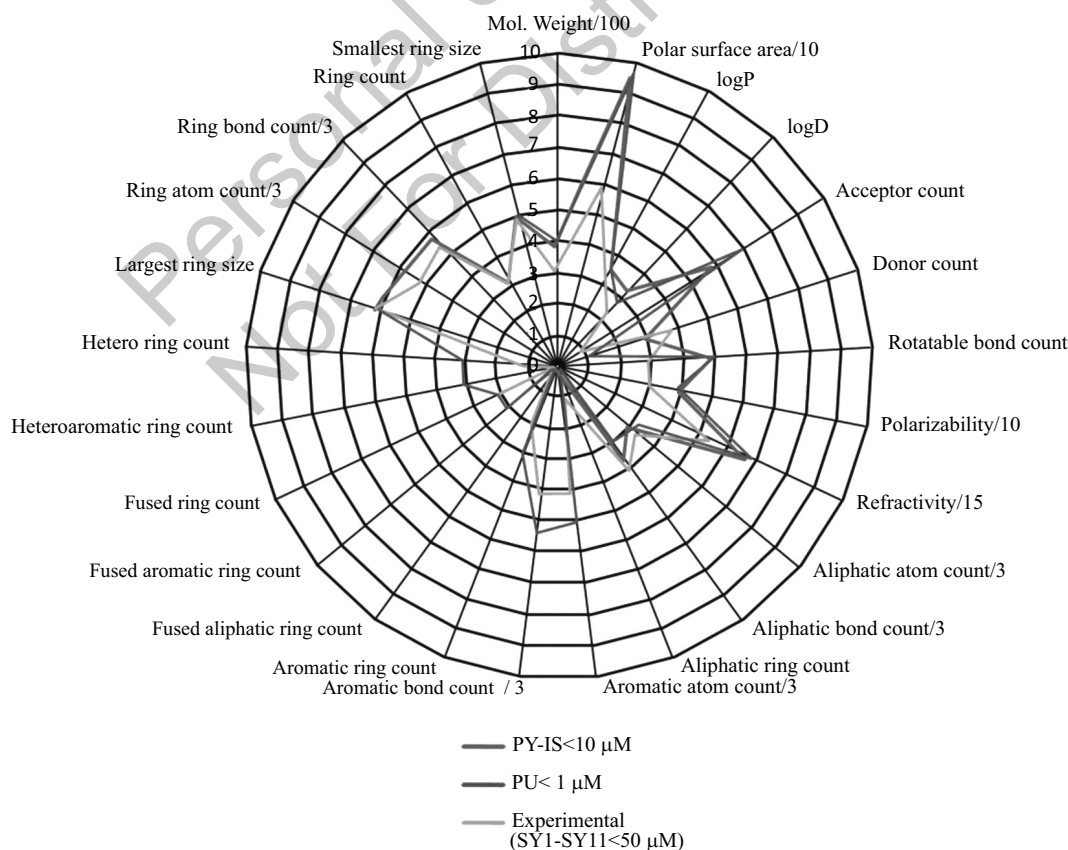


Fig. (3). Radar views of three classes of Hsp90 inhibitors: Reported purine family (PU) (IC₅₀ <1 μM); reported pyrazole-isoxazole family (PY-IS) (IC₅₀ <10 μM); designed benzofuran family (SY). Median values are represented for each molecular descriptor.

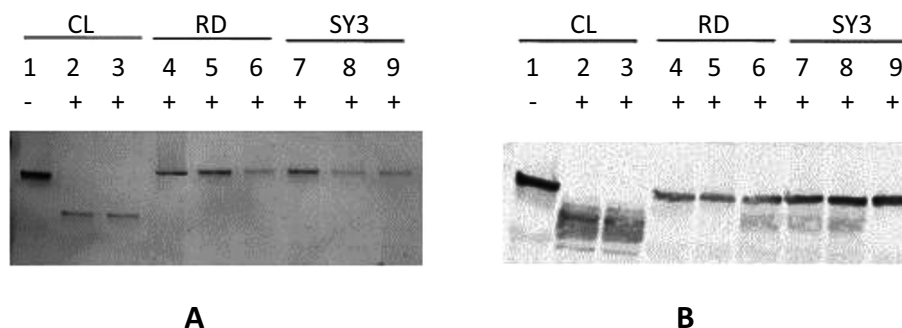


Fig. (4). Proteomic analysis of Compound **SY3** and RD mediated protection of Hsp90 in MDA-MB-468 lysate (Figure A, SDS page, detection by silver stain; Figure B, Western blot, detection by fluorescence imaging): Lane (L) 1: Cell lysate (CL); L2: CL + Thermolysin (T), 10 min; L3: CL + T, 20 min; 4: CL + RD; 5: CL + RD + T, 10 min; 6: CL + RD + T, 20 min; 7: CL + **SY3**; 8: CL + **SY3** + T, 10 min; 9: CL + **SY3** + T, 20 min. Compound **SY3** and RD in 1 mM concentration protect Hsp90 from thermolysin degradation.

comparable to Hsp90 protective action of radicicol (Fig. 4). Identification of Hsp90 protection was done by silver staining the SDS page gel and by fluorescence detection of Hsp90 antibody labeled western blot. Compound **SY3** and radicicol bind to Hsp90 and provides structural stability against proteolytic action of thermolysin. Untreated cancer cell lysates were found to have completely degraded Hsp90. Stable complex formation of Hsp90 with **SY3** and radicicol could be attributed to their crucial hydrogen bonding interactions with Thr184 and Asn51 of Hsp90.

3. EXPERIMENTAL

3.1. Chemistry

¹H-NMR spectra were recorded on Bruker Avance300 MHz NMR spectrometer (Bruker BioSpin AG, Fallanden, Switzerland); chemical shifts (δ) were reported in parts per million (ppm) with tetramethylsilane as an internal standard. Uncorrected melting points were determined on an electro thermal melting point apparatus. Mass fragmentation was recorded on an API2000 LC/MS mass spectrometer (Bruker Daltonics Inc., Billerica, MA, USA). Column chromatography was performed on silica gel (300-400 mesh). Infrared spectra were obtained from FT-IR-Affinity-1 Spectrometer (Shimadzu, Japan). Unless otherwise noted, all solvents and reagents were commercially available and used without further purification.

3.1.1. General Procedure for Synthesis Substituted 2-chloro-1-(2,4-dihydroxyphenyl) Ethanone (**M2**, **S2**)

Resorcinol (**M1**) / Chlororesorcinol (**S1**) (10 mmol) was added to a dispersion of anhydrous AlCl₃ (10 mmol) in diethyl ether (30 mL) taken in a round bottomed flask with stirring at 0°C. Subsequently, a solution of chloro acetylchloride (10 mmol) in diethyl ether (10 mL) was added drop wise to the pre-stirred mixture (caution: the addition procedure discussed so far should be done carefully, slowly and in small quantities at 0°C, as it is an exothermic reaction) and extended stirring for 4-5 h at 30°C. The reaction completion was analyzed by TLC examination. Later, the solvent ether was distilled and the residue was quenched with dilute HCl (20 mL). The resulting mixture was extracted with di-

chloromethane (2 x 50 mL) and the combined organic extracts were dried over anhydrous Na₂SO₄, filtered and concentrated under reduced pressure. The resulting solid was recrystallized from ethanol to give substituted 2-chloro-1-(2,4-dihydroxyphenyl) ethanone (**M2**, **S2**).

3.1.2. General Procedure for Synthesis of Substituted 6-hydroxybenzofuran-3(2H)-one (**M3**, **S3**)

2-Chloro-1-(2,4-dihydroxyphenyl) ethanone (**M2**) / 2-chloro-1-(5-chloro-2,4-dihydroxyphenyl) ethanone (**S2**) (3 mmol) was dissolved in ethanol (10 mL) with stirring, followed by the addition of NaOH solution (3 mmol of NaOH dissolved in 5 mL of water) and stirred at 50°C for 1-2 h. After completion of the reaction, ethanol was distilled off and the solid residue obtained was washed with copious amount of water. The crude product obtained was dried and recrystallized from ethanol yielding substituted 6-hydroxybenzofuran-3(2H)-one (**M3**, **S3**).

3.1.3. General Procedure for Synthesis of Substituted 2-aryl/heteroarylidene-6-hydroxy benzofuran-3(2H)-one (**SY1-SY10**)

3.1.3.1. Synthesis of compounds **SY8** and **SY10** are reported earlier [29].

To a solution of substituted 6-hydroxybenzofuran-3(2H)-one (**M3**, **S3**) (3 mmol) and aldehyde derivatives (3 mmol) in methanol; NaOH solution (3 mmol in water) was added, followed by stirring at 30-40°C for 3-4 h. The reaction progress was monitored by TLC examination. After completion of the reaction, the contents were quenched with ice cold water (20 mL) and the resulting precipitate was filtered, dried and subjected to purification by flash chromatography.

3.1.3.2. (Z)-2-(3,4-dimethoxybenzylidene)-5-chloro-6-hydroxybenzofuran-3(2H)-one (**SY1**)

Yield 65%, mp 187°C; IR (KBr, cm⁻¹): 3504, 2937, 2843, 1664, 1589, 1510, 1267, 1161, 1147; ¹H-NMR (300 MHz, DMSO-*d*₆) δ : 3.8 (s, 6H, O-CH₃), 6.8 (s, 1H), 6.9 (s, 1H), 7.0 (d, *J*=8.4Hz, 1H), 7.5 (d, 1H), 7.6 (s, 1H), 7.7 (s, 1H), 12.04 (s, 1H); ESI-MS, *m/z*: 333.2 [M+H]⁺.

3.1.3.3. (Z)-2-(4-(dimethylamino)benzylidene)-5-chloro-6-hydroxybenzofuran-3(2H)-one (SY2)

Yield 70%, mp 253°C; IR (KBr, cm^{-1}): 3387, 1680, 1606, 1284, 1147, 1128; $^1\text{H-NMR}$ (300 MHz, $\text{DMSO-}d_6$) δ : 3.0 (s, 6H), 6.7 (s, 1H), 6.8 (d, $J=8.7\text{Hz}$, 2H), 7.1 (s, 1H), 7.7 (s, 1H), 7.8 (d, $J=8.7\text{Hz}$, 2H), 12.2 (s, 1H); ESI-MS, m/z : 316.1 $[\text{M}+\text{H}]^+$.

3.1.3.4. (Z)-2-(4-(4-fluorobenzoyloxy)benzylidene)-5-chloro-6-hydroxybenzofuran-3(2H)-one (SY3)

Yield 72%, mp 193°C; IR (KBr, cm^{-1}): 3057, 1680, 1591, 1263, 1155; $^1\text{H-NMR}$ (300 MHz, $\text{DMSO-}d_6$) δ : 5.2 (s, 2H), 6.8 (s, 1H), 6.9 (s, 1H), 7.1 (d, $J=8.6\text{Hz}$, 2H), 7.2 (t, $^3J_{\text{H-F,H-H}}=8.8\text{Hz}$, 8.7Hz, 2H), 7.5 (dd, $^3J_{\text{H-H}}=8.2\text{Hz}$, $^4J_{\text{H-F}}=5.8$, 2H), 7.7 (s, 1H), 7.9 (d, $J=8.6\text{Hz}$, 2H), 12.1 (s, 1H); ESI-MS, m/z : 397.4 $[\text{M}+\text{H}]^+$.

3.1.3.5. (Z)-5-chloro-2-((furan-2-yl)methylene)-6-hydroxybenzofuran-3(2H)-one (SY4)

Yield 63%, mp 263°C; IR (KBr, cm^{-1}): 3201, 1670, 1593, 1276; $^1\text{H-NMR}$ (300 MHz, $\text{DMSO-}d_6$) δ : 6.7 (m, 1H), 6.8 (s, 1H), 6.9 (s, 1H), 7.1 (d, $J=3.2\text{Hz}$, 1H), 7.7 (s, 1H), 7.9 (s, 1H); ESI-MS, m/z : 263.3 $[\text{M}+\text{H}]^+$.

3.1.3.6. (Z)-2-(4-chlorobenzylidene)-5-chloro-6-hydroxybenzofuran-3(2H)-one (SY5)

Yield 55%, mp 303°C; IR (KBr, cm^{-1}): 3062, 3032, 1681, 1589, 1286; $^1\text{H-NMR}$ (300 MHz, $\text{DMSO-}d_6$) δ : 6.8 (s, 1H), 7.0 (s, 1H), 7.5 (d, $J=8.5\text{Hz}$, 2H), 7.7 (s, 1H), 7.9 (d, $J=8.4\text{Hz}$, 2H), 12.2 (s, 1H); ESI-MS, m/z : 307.1 $[\text{M}+\text{H}]^+$.

3.1.3.7. (Z)-2-(4-hydroxybenzylidene)-5-chloro-6-hydroxybenzofuran-3(2H)-one (SY6)

Yield 70%, mp 336°C; IR (KBr, cm^{-1}): 3309, 1654, 1560, 1271, 1166; $^1\text{H-NMR}$ (300 MHz, $\text{DMSO-}d_6$) δ : 6.7 (s, 1H), 6.8-6.9 (d, $J=8.4\text{Hz}$, 2H), 7.0 (s, 1H), 7.7 (s, 1H), 7.8 (d, $J=8.5\text{Hz}$, 2H), 10.2 (s, 1H); ESI-MS, m/z : 289.2 $[\text{M}+\text{H}]^+$.

3.1.3.8. (Z)-2-(4-chlorobenzylidene)-6-hydroxybenzofuran-3(2H)-one (SY7)

Yield 52%, mp 332°C; IR (KBr, cm^{-1}): 3502, 1678, 1597; $^1\text{H-NMR}$ (300 MHz, $\text{DMSO-}d_6$) δ : 6.6 (d, $J=8.4\text{Hz}$, 1H), 6.7 (s, 1H), 6.8 (s, 1H), 7.5 (d, $J=8.4\text{Hz}$, 2H), 7.6 (d, $J=8.4\text{Hz}$, 1H), 7.9 (d, $J=8.4\text{Hz}$, 2H); ESI-MS, m/z : 273.2 $[\text{M}+\text{H}]^+$.

3.1.3.9. (Z)-2-(3,4-dimethoxybenzylidene)-6-hydroxybenzofuran-3(2H)-one (SY8)

Yield 72%, mp 203°C; IR (KBr, cm^{-1}): 3154, 1680, 1514, 1267, 1145, 1130, 1095; $^1\text{H-NMR}$ (300 MHz, $\text{DMSO-}d_6$) δ : 3.8 (s, 6H), 6.6 (d, $J=8.4\text{Hz}$, 1H), 6.7 (s, 1H), 6.8 (s, 1H), 7.0 (d, $J=8.5\text{Hz}$, 1H), 7.5-7.6 (m, 3H), 11.1 (s, 1H); ESI-MS, m/z : 297.2 $[\text{M}+\text{H}]^+$.

3.1.3.10. (Z)-2-(3,4,5-trimethoxybenzylidene)-6-hydroxybenzofuran-3(2H)-one (SY9)

Yield 70%, mp 293°C; IR (KBr, cm^{-1}): 3161, 1660, 1591, 1458, 1271, 1132; $^1\text{H-NMR}$ (300 MHz, $\text{DMSO-}d_6$) δ : 3.7-3.8

(s, 9H); 6.6 (d, $J=8.3\text{Hz}$, 1H), 6.7 (s, 1H), 6.8 (s, 1H), 7.5 (m, 3H), 11.1 (s, 1H); ESI-MS, m/z : 329.1 $[\text{M}-\text{H}]^+$.

3.1.3.11. (Z)-2-(2,5-dimethoxybenzylidene)-6-hydroxybenzofuran-3(2H)-one (SY10)

Yield 62%, mp 303°C; IR (KBr, cm^{-1}): 3164, 1660, 1591, 1458, 1277, 1132; $^1\text{H-NMR}$ (300 MHz, $\text{DMSO-}d_6$) δ : 3.66 (s, 3H), 3.73 (s, 3H), 6.4 (s, 1H), 6.5 (d, $J=8\text{Hz}$, 1H), 6.7 (d, $J=8.2\text{Hz}$, 1H), 6.8 (d, $J=8.1\text{Hz}$, 1H), 6.9 (s, 1H), 7.4 (m, 2H); ESI-MS, m/z : 299.1 $[\text{M}+\text{H}]^+$.

3.2. Molecular Docking

Molecular docking studies were performed utilizing SY-BYL-X 1.2 drug discovery suite, comprising Surflex dock-Geom program; installed on Dell Precision T-1500 workstation [Intel(R) Core(TM) i7 CPU 860 @ 2.80 GHz, 12.0 GB RAM and 1 TB Hard disk]. Crystal structure of Hsp90, PDB ID: 1YET (resolution 1.90 Å) was utilized for carrying out docking studies [30]. The protein containing chain 'A' was prepared by removal of water molecules, ligand sub-structure extraction and analyzed by addition of H-atoms, fixing of side chain amides and finally, energy minimized by conjugate minimization methodology of Powell [31]. A hypothetical ligand based active site in the protein called 'Protomol' was generated, defined by default parameters (threshold of 0.5 Å and bloat of 0 Å) and an altered bloat value for radicicol, to maximize 'protomol' size. Chemical structures of the lead 'RD' and 'SY series' were saved as .mol files and converted to combined 'SD' format, later prepared by 'Lig-prep' tool of Maestro (Schrodinger suite) to generate 20 best conformations for each ligand. The prepared ligand structures were docked at the generated 'protomol' active site by Surflex dock-Geom program.

3.3. Assessment of Chemical Similarity of Hsp90 Inhibitors

Chem Axon's tools were utilized for defining and analyzing the 2D descriptors for the designed chemical library of molecules. The protocol followed for the assessment of chemical similarity was comparing and analyzing the variety of physico-chemical 2D descriptors of the lead compounds with the data of reported compounds [32]. Twenty-five molecular descriptors for heterocyclic purine (PU) analogues with an IC_{50} threshold of 1 mM (89 structures derived from database) and pyrazole-isoxazole (PY-IS) analogues with an IC_{50} threshold of 10 mM (87 structures derived from database) were defined and a comparative study was done for the designed library of SY series [32].

3.4. Biological Assays***3.4.1. Cell Proliferative Assay by Resazurin Reduction Method [33]***

Briefly, cancer cells (A375, SKMEL-28, MDA-MB-468) (1×10^4 cells/well) were plated into black flat bottomed 96-well plates and treated with or without Tween 20 (3 %), DMSO (0.5 %), SY1-SY3 (3.12-100 μM) and 17-AAG (0.031-1 μM) for 72 h. After this period, resazurin salt solution (10 $\mu\text{g}/100 \text{mL}$) was added per well. Fluorescence was

read after 4 h in a microplate reader (SpectraMax M5/M5e - Molecular Devices) with $\lambda_{exc} = 555$ nm, $\lambda_{em} = 585$ nm. IC_{50} values were calculated by one way Anova using Graph-Pad Prism (Version 5.02, GraphPad software).

3.4.2. Hsp90-Small Molecule Inhibitor Drug Affinity Responsive Target Stability (DARTS) Assay Using Whole Cell Lysate [34]

A375 cells were lysed with lysis buffer [1mM $NaVO_3$, 50 mM HEPES (pH 7.4), 100 mM NaCl, 0.5% NP40, 1 mM EDTA, 1 mM EGTA, 50 μ G/mL RNase, 1% Triton X-100, 1% deoxycholic acid, 1 μ G/ μ L leupeptin or Roche protease inhibitor mixture and 1x protease mixture] for 15 minutes at RT. After centrifugation (14,000 rpm using Eppendorf micro-centrifuge 5415D, 10 min), protein concentration of the lysate was measured using MicroBCA™ protein assay kit. 25 μ G of protein cell lysate was incubated with 1 mM compound, and binding buffer [50 mM Tris HCL pH 8.0, 50 mM NaCl, 10 mM $CaCl_2$] to 20 μ L final volume for 2 h at 25°C. After compound treatment, samples were digested with 200 nG (5 μ L) thermolysin (T) (Roche) at 25°C. The reactions were stopped at different time period of 10/20/30 minutes; by the addition of 5 μ L of 5x SDS loading dye and immediately boiling samples at 95°C for 5 min. Samples were run in 4-15% gradient SDS-PAGE gels at 150 V for 60 minutes by silver stain or western blot. The proteins were transferred from SDS-PAGE gel onto a polyvinylidene difluoride (PVDF) membrane in 1x transfer buffer (191 mM glycine, 25 mM Tris) by electroblotting at 100 V for 30 min on ice using a mini Trans-blot electrophoretic transfer cell (Bio-Rad). The PVDF membrane was incubated with blocking solution (PBS, 0.1% Tween 20, and 2% milk) for 1 h at 25 °C and further incubated with anti-Hsp90 primary antibody (mAb, 2D11B9; Enzo life sciences) diluted in PBST [1:5000] for 18 h at 4°C. The membrane was washed thrice with PBST for 10 min and incubated with secondary antibody (anti-mouse IgG-HRP GE Healthcare) in PBST [1:5,000] for 1 h at 25°C. Western blot developed was exposed to fluorescence detection at emission 526 Excitation 488 (Blue) with normal sensitivity using GE Healthcare Typhoon Trio+.

CONCLUSION

The drug design studies identified **SY1-SY3** as lead molecules based on binding interactions with N-terminal ATP binding site of Hsp90. Compound 2-(4-(4-fluorobenzoyloxy)-benzylidene)-5-chloro-6-hydroxybenzofuran-3(2H)-one (**SY3**) emerged as a promising analogue having significant cell proliferation inhibitory activity against human melanoma cells A375 (IC_{50} 18.46 μ M) and breast cancer cells MDA-MB-468 (22.3 μ M) in comparison with IC_{50} values of 5.20 μ M and 1.33 μ M of 17-AAG against melanoma and breast cancer cells respectively. Further, demonstration by DARTS proteomic analysis on cancer cell lysate confirms the binding interaction with Hsp90 oncoprotein; added to which the designed **SY3** compound, occupied the similar chemical space defined by existing Hsp90 inhibitors (PU, PY-IS series), based on chemical similarity of reported Hsp90 inhibitors. In view of all these results, we propose compound **SY3** as the promising molecule and have scope for further lead optimi-

zation to improve anticancer activity through Hsp90 antagonism.

ETHICS APPROVAL AND CONSENT TO PARTICIPATE

Not applicable.

HUMAN AND ANIMAL RIGHTS

No Animals/Humans were used for studies that are base of this research.

CONSENT FOR PUBLICATION

Not applicable.

CONFLICT OF INTEREST

The authors declare no conflict of interest, financial or otherwise.

ACKNOWLEDGEMENTS

We are thankful to DST (SR/FT/CS-079/2009) and DHR (DHR/HRD Fellow/start up project/6/2013) for providing molecular modeling softwares for this project. This work is also supported by CAPES/Fiocruz, Rio de Janeiro, Brasil. We also thank Dr. Vincent Jo Davison and Mr. Raymond Fatig of MCMP Department, Purdue University, USA for their constructive suggestions and laboratory support throughout the project.

SUPPLEMENTARY MATERIAL

Supplementary material is available on the publisher's website along with the published article.

REFERENCES

- [1] Pratt, W.B. The hsp90-based chaperone system: involvement in signal transduction from a variety of hormone and growth factor receptors. *Proc. Soc. Exp. Biol. Med.*, **1998**, *217*, 420-434.
- [2] Xu, W.; Neckers, L. Targeting the molecular chaperone heat shock protein 90 provides a multifaceted effect on diverse cell signaling pathways of cancer cells. *Clin. Cancer Res.*, **2007**, *13*, 1625-1629.
- [3] Workman, P. Combinatorial attack on multistep oncogenesis by inhibiting the Hsp90 molecular chaperone. *Cancer. Lett.*, **2004**, *206*, 149-157.
- [4] Schulte, T.W.; Blagosklonny, M.V.; Ingui, C.; Neckers, L. Disruption of Raf-1-Hsp90 molecular complex results in destabilization of Raf-1 and loss of Raf-1-Ras association. *J. Biol. Chem.*, **1995**, *270*, 24585-24588.
- [5] Murakai, Y.; Mizuno, S.; Uehara, Y. Accelerated degradation of 160 kDa epidermal growth factor (EGF) receptor precursor by the tyrosine kinase inhibitor herbimycin A in the endoplasmic reticulum of A431 human epidermoid carcinoma cells. *Biochem. J.*, **1994**, *301*, 63-68.
- [6] Sepp-Lorenzino, L.; Ma, Z.; Leibold, D.E.; Vinitzky, A.; Rosen, N. Herbimycin A induces the 20 S proteasome- and ubiquitin-dependent degradation of receptor tyrosine kinases. *J. Biol. Chem.*, **1995**, *270*, 16580-16587.
- [7] Kamal, A.; Thao, L.; Sensintaffar, J.; Zhang, L.; Boehm, M.F.; Fritz, L.C.; Burrows, F.J. A high-affinity conformation of Hsp90 confers tumour selectivity on Hsp90 inhibitors. *Nature.*, **2003**, *425*, 407-410.
- [8] Glaze, E.R.; Smith, A.C.; Johnson, D.W.; McCormick, D.L.; Brown, A.B.; Levin, B.S.; Krishnaraj, R.; Lyubimov, A.; Egorin,

- M.J.; Tomaszewski, J. E. Dose range-finding toxicity studies of 17-DMAG. *Proc. Am. Assoc. Cancer Res.*, **2003**, *44*, 162-163.
- [9] Eiseman, J.L.; Lan, J.; Lagatutta, T.F.; Hamburger, D.R.; Joseph, E.; Covey, J.M.; Egorin, M.J. Pharmacokinetics and pharmacodynamics of 17-demethoxy 17-[[[(2-dimethylamino)ethyl]amino]geldanamycin (17DMAG, NSC 707545) in CB-17 SCID mice bearing MDA-MB-231 human breast cancer xenografts. *Cancer. Chemother. Pharmacol.*, **2005**, *55*, 21-32.
- [10] Soga, S.; Neckers, L.; Schulte, T.W.; Shiotsu, Y.; Akasaka, K.; Narumi, H.; Agatsuma, T.; Ikuina, Y.; Murakata, C.; Tamaoki, T.; Akinaga, S. KF25706, a novel oxime derivative of radicicol, exhibits *in vivo* antitumor activity via selective depletion of hsp90 binding signaling molecules. *Cancer. Res.*, **1999**, *59*, 2931-2938.
- [11] Agatsuma, T.; Ogawa, H.; Akasaka, K.; Asai, A.; Yamashita, Y.; Mizukami, T.; Akinaga, S.; Saitoh, Y. Halohydrin and oxime derivatives of radicicol: synthesis and antitumor activities. *Bioorg. Med. Chem. Lett.*, **2002**, *10*, 3445-3454.
- [12] Chiosis, G.; Lucas, B.; Shtil, A.; Huezo, H.; Rosena, H. Development of a purine-scaffold novel class of hsp90 binders that inhibit the proliferation of cancer cells and induce the degradation of her2 tyrosine kinase. *Bioorg. Med. Chem.*, **2002**, *10*, 3555-3564.
- [13] Ikuina, Y.; Amishiro, N.; Miyata, M.; Narumi, H.; Ogawa, H.; Akiyama, T.; Shiotsu, Y.; Akinaga, S.; Murakata, C. Synthesis and antitumor activity of novel o-carbamoyl methyl oxime derivatives of radicicol. *J. Med. Chem.*, **2003**, *46*, 2534-2541.
- [14] Yang, Z.Q.; Geng, X.; Solit, D.; Pratilas, C.A.; Rosen, N.; Danishefsky, S.J. New efficient synthesis of resorcinylic macrolides via ynolides: establishment of cycloproparadicicol as synthetic feasible preclinical anticancer agent based on Hsp90 as the target. *J. Am. Chem. Soc.*, **2004**, *126*, 7881-7889.
- [15] Maddocks, K.; Hertlein, E.; Chen, T.L.; Wagner, A.J.; Ling, Y.; Flynn, J.; Phelps, M.; Johnson, A.J.; Byrd, J.C.; Jones, J.A. A phase I trial of the intravenous Hsp90 inhibitor alvespimycin (17-DMAG) in patients with relapsed chronic lymphocytic leukemia/small lymphocytic lymphoma. *Leuk. Lymphoma*, **2016**, *57*, 2212-2215.
- [16] Liu, Y.F.; Zhong, J.J.; Lin, L.; Liu, J.J.; Wang, Y.G.; He, W.Q.; Yang, Z.Y. New C-19-modified geldanamycin derivatives: synthesis, antitumor activities, and physical properties study. *J. Asian. Nat. Prod. Res.*, **2016**, *18*, 752-764.
- [17] Chene, P. ATPases as drug targets: learning from their structure. *Nat. Rev. Drug. Discov.*, **2002**, *1*, 665-673.
- [18] Immormino, R.M.; Kang, Y.; Chiosis, G.; Gewirth, D.T. Structural and quantum chemical studies of 8-aryl-sulfanyl adenine class Hsp90 inhibitors. *J. Med. Chem.*, **2006**, *49*, 4953-4960.
- [19] Vilenchik, M.; Solit, D. Basso, A.; Huezo, H.; Lucas, B.; He, H.; Rosen, N.; Spampinato, C.; Modrich, P.; Chiosis, G. Targeting wide-range oncogenic transformation via pu24fcl, a specific inhibitor of tumor Hsp90. *Chem. Biol.*, **2004**, *11*, 787-797.
- [20] Dymock, B.W.; Barril, X.; Brough, P.A.; Cansfield, J.E.; Massey, A.; McDonald, E.; Hubbard, R.E.; Surgenor, A.; Roughley, S.D.; Webb, P.; Workman, P.; Wright, L.; Drysdale, M.J. Novel, potent small-molecule inhibitors of the molecular chaperone hsp90 discovered through structure-based design. *J. Med. Chem.*, **2005**, *48*, 4212-4215.
- [21] Sharp, S.Y.; Prodromou, C.; Boxall, K.; Powers, M.V.; Holmes, J.L.; Box, G.; Matthews, T.P.; Cheung, K.M.J.; Kalusa, A.; James, K.; Hayes, A.; Hardcastle, A.; Dymock, B.W.; Brough, P.A.; Barril, X.; Cansfield, J.E.; Wright, L.; Surgenor, A.; Folepp, N.; Hubbard, R.E.; Aherne, W.; Pearl, L.; Jones, K.; McDonald, E.; Raynaud, F.; Eccles, S.; Drysdale, M. J.; Workman, P. Inhibition of the heat shock protein 90 molecular chaperone *in vitro* and *in vivo* by novel, synthetic, potent resorcinylicpyrazole/isoxazole amide analogues. *Mol. Cancer. Ther.*, **2007**, *6*, 198-211.
- [22] Smyth, T.; Looy, T.V.; Curry, J.E.; Rodriguez-Lopez, A.M.; Wozniak, A.; Zhu, M.; Donsky, R.; Morgan, J.G.; Mayeda, M.; Fletcher, J.A.; Schoffski, P.; Lyons, J.; Thompson, N.T.; Wallis, N.G. The HSP90 Inhibitor, AT13387, Is effective against imatinib-sensitive and -resistant gastrointestinal stromal tumor models. *Mol. Cancer. Ther.*, **2012**, *11*, 1799-1808.
- [23] Gupta, S.D.; Bommaka, M.K.; Mazaira, G.I.; Galigniana, M.D.; Subrahmanyam, C.V.S.; Gowrishankar, N.L.; Raghavendra, N.M. Molecular docking study, synthesis and biological evaluation of Mannich bases as Hsp90 inhibitors. *Int. J. Biol. Macromol.*, **2015**, *80*, 253-259.
- [24] Gupta, S.D.; Revathi, B.; Mazaira, G.I.; Galigniana, M.D.; Subrahmanyam, C.V.S.; Gowrishankar, N.L.; Raghavendra, N.M. 2,4-Dihydroxy benzaldehyde derived Schiff bases as small molecule Hsp90 inhibitors: Rational identification of a new anticancer lead. *Bioorg. Chem.*, **2015**, *5*, 97-105.
- [25] Gupta, S.D.; Snigdha, D.; Mazaira, G.I.; Galigniana, M.D.; Subrahmanyam, C.V.S.; Gowrishankar, N.L.; Raghavendra, N.M. Molecular docking study, synthesis and biological evaluation of Schiff bases as Hsp90 inhibitors. *Biomed. Pharmacother.*, **2014**, *68*, 369-376.
- [26] Zimmermann, H.E.; Ahranjian, L. Overlap control of carbanionoid reactions. II. ¹ the stereochemistry of the perkin reaction and related condensation reactions. *J. Am. Chem. Soc.*, **1959**, *81*, 2086-2091.
- [27] Dewar, M.J.S.; Zoebisch, E.G.; Eamonn, F.H.; James, J.P.S. The development and use of quantum mechanical molecular models. 76. AM1: a new general purpose quantum mechanical molecular model. *J. Am. Chem. Soc.*, **1985**, *107*, 3902-3909.
- [28] Atta-ur-Rahman.; Choudhary, M.I.; Hayat, S.; Khan, A.M.; Ahmed, A. Two new aurones from marine brown alga *Spatoglossum variabile*. *Chem. Pharm. Bull. (Tokyo)*, **2001**, *49*, 105-107.
- [29] Makoto, Y.; Masamichi, N.; Junji, N.; Shouji, N. Benzofuranone derivatives and a method for producing them. U.S. Patent 6143779 November 07, **2000**.
- [30] Stebbins, C.E.; Russo, A.A.; Schneider, C.; Rosen, N.; Hart, F.U.; Pavletich, N.P. Crystal structure of an Hsp90-geldanamycin complex: targeting of a protein chaperone by an antitumor agent. *Cell*, **1997**, *89*, 239-250.
- [31] Wang, R.; Lu, Y.; Wang, S. Comparative evaluation of 11 scoring functions for molecular docking. *J. Med. Chem.*, **2003**, *46*, 2287-2303.
- [32] Audisio, D.; Messaoudi, S.; Ijjaali, I.; Dubus, E.; Petitet, F.; Peyrat, J.F.; Brion, J.D.; Alami, M. Assessing the chemical diversity of an hsp90 database. *Eur. J. Med. Chem.*, **2010**, *45*, 2000-2009.
- [33] Anoopkumar-Dukie, S.; Carey, J.B.; Conere, T.; O'sullivan, E.; van Pelt, F.N.; Allshire, A. Resazurin assay of radiation response in cultured cells. *Br. J. Radiol.*, **2005**, *934*, 945-947.
- [34] Lomenick, B.; Rui, H.; Nao, J.; Randall, M. C.; Mariam, A.; Sarah, W.; Jianing, W.; Raymond, P.W.; Fernando, G.; Joseph, A. L.; James, A.W.; Thomas, M.V.; Jerry, P.; Harvey, R.H.; Jon, C.; Catherine, F.C.; Jing, H. Target identification using drug affinity responsive target stability (DARTS). *Proc. Natl. Acad. Sci. U.S.A.*, **2009**, *106*, 21984-21989.

NOVEL METHOD FOR CHROMATOGRAPHIC DETERMINATION OF SETRALINE AND DOXOFYLLINE IN FORMULATION BY USING RP-HPLC

Usha Kondla* and E. Esther Rani

Gynana Jyothi Collage of Pharmacy, Uppal Depot.

Article Received on
04 Feb 2016,

Revised on 26 Feb 2016,
Accepted on 17 March 2016

DOI: 10.20959/wjpr20164-5165

*Correspondence for
Author

Usha Kondla

Gynana Jyothi Collage of
Pharmacy, Uppal Depot.

ABSTRACT

A simple, rapid, selective, sensitive, linear, precise and accurate NOVALMETHOD FOR CHOMATOGRAPHIC DETERMINATION OF SETRALLINE AND DOXOFYLLINE. Tablet dosage form separation of drug was achieved on a reversed phase symmetry C18 column (150mm x 4.6mm) phosphate buffer was pH 3.5 & the mobile phase was optimized with consist of Acetonitrile, phosphate buffer mixed in the ratio of 30:70% v/v. The solution w3as chromatographed at constant flow rate of 1.0 ml / min. The UV detection wavelength was 234nm & 10 µm of sample was injected. Te linearity ranges of SERTRALINE & DOXOFYLINE were found to be 0.58µm from

1.77µg/ml of SERTRALINE & DOXOFYLINE 0.27 & 0.82µg/ml. Linear regression coefficient was more than 99-100% the value RSD is ranged from 0.37-0.53% indicating accuracy & precision of the method. LOD & LOQ were found to be within limit. The was validated as per ICH guidelines for its sensitivity, linearity, accuracy & precision. The method was successfully employed for routine quality control analysis SERTRALINE & DOXOFYLINE in its pharmaceutical formulations.

Keywords: Novalmethod for Chomatographic Determination of Setralline and Doxofylline.

INTRODUCTION

Pharmaceutical analysis plays a vital role in the Quality Assurance and Quality control of bulk drugs.^[1] Analytical chemistry involves separating, identifying, and determining the relative amounts of components in a sample matrix. Pharmaceutical analysis is a specialized branch of analytical chemistry. Pharmaceutical analysis derives its principles from various branches of sciences like physics, microbiology, nuclear science and electronics etc.

Qualitative analysis reveals the chemical identity of the sample. Quantitative analysis establishes the relative amount of one or more of these species or analytes in numerical terms. Qualitative analysis is required before a quantitative analysis can be undertaken. A separation step is usually a necessary part of both qualitative and quantitative analysis. The results of typical quantitative analysis can be computed from two measurements. One is the mass or volume of sample to be analyzed and second is the measurement of some quantity that is proportional to the amount of analyte in that sample and normally completes the analysis.

CHROMATOGRAPHY

Chromatography^[3] is a separation of mixture into individual components using a stationary phase and a mobile phase. This may be regarded as an analytical technique employed for the purification and separation of organic and inorganic substances. There are various advanced chromatographic techniques, widely used for the estimation of multicomponent drugs in their formulations. The various chromatographic techniques are

- High Performance Liquid Chromatography.
- High Performance Thin Layer Chromatography.
- Gas Chromatography.

1.1.1. HIGH PERFORMANCE LIQUID CHROMATOGRAPHY (HPLC)

HPLC is a type of liquid chromatography that employs a liquid mobile phase and a very finely divided stationary phase. The technique of high performance liquid chromatography is so called because of its improved performance when compared to column chromatography. Advances in column technology, high-pressure pumping system and sensitive detectors have transformed liquid column chromatography into high speed, efficient, accurate and highly resolved method of separation.

The HPLC is the method of choice in the field of analytical chemistry, since this method is specific, robust, linear, precise and accurate and the limit of detection is low and also it offers the following advantages.

- ❖ Greater sensitivity (various detectors can be employed).
- ❖ Improved resolution (wide variety of stationary phases).
- ❖ Reusable columns (expensive columns but can be used for many analysis).
- ❖ Ideal for the substances of low viscosity.
- ❖ Easy sample recovery, handling and maintenance.

- ❖ Instrumentation leads itself to automation and quantification (less time and less labour).
- ❖ Precise and reproducible.
- ❖ Integrator itself does calculations.

Based on Modes of Chromatography

- Normal phase chromatography.
- Reverse phase chromatography.

EXPERIMENTAL AND RESULTS AND DISCUSSION

INSTRUMENTS USED

Sr. no.	Name of Instrument	Instrument Model	Name of manufacturer
1	UV-Visible double beam spectrophotometer	UV 1800	Elico India
2	HPLC	1575	Hitachi LaChrome
3	Ultra sonicator	-----	Entrech electronics limited
4	Melting point apparatus	-----	

CHEMICALS / REAGENTS USED

S.N.	Name	Specifications		Manufacturer/Supplier
		Purity	Grade	
1.	Doubled distilled water	----	----	Sd fine-Chem ltd; Mumbai
2.	Methanol	99.9%	A.R.	Loba Chem; Mumbai.
3.	Dipotassium hydrogen phosphate	96%	L.R.	Sd fine-Chem ltd; Mumbai
4.	Acetonitrile	99.9%	HPLC	Loba Chem; Mumbai.
5.	Potassium dihydrogen orthophosphate	99.9	L.R.	Sd fine-Chem ltd; Mumbai
6.	orthophosphoric acid	99.9	L.R.	Sd fine-Chem ltd; Mumbai

CHARACTERIZATION OF SERTRALINE & DOXOFYLLINE

Solubility of Sertraline

The solubility of drug sample was determined according to I.P. 1996.^[38]

Two 10 ml and one 250 ml volumetric flasks were taken.

Flask 1: 10 mg of Sertraline was accurately weighed and transferred to 10 ml volumetric flask. 0.1 ml of water was added into it. The contents were mixed for one minute. The drug was slightly dissolved. Again 0.1 ml of water was added into the volumetric flask. The contents were mixed for one minute. The solubility state was noted.

Flask 2: 10mg of Sertraline was accurately weighed and transferred to 10 ml volumetric flask. 0.1 ml of methanol was added into it. The contents were mixed for one minute. The drug was slightly dissolved. Again 0.1 ml of methanol was added into the volumetric flask. The contents were mixed for one minute. The solubility state was noted.

Flask 3: Accurately weighed Sertraline (10 mg) was transferred to 250 ml volumetric flask. Added 10 ml of acetonitrile to it. Mixed the solution for one minute. The drug could not dissolve. Added more 90 ml of acetonitrile to the volumetric flask. Mixed the solution for two minutes. The drug could not dissolve. Added more 100 ml of water to the volumetric flask. Mixed the solution for two minutes. The solubility state was noted.

Solubility of Doxofylline

The solubility of drug sample was determined according to I.P. 1996.^[38]

Two 10 ml volumetric flasks were taken.

Flask 1: Accurately weighed Doxofylline (10 mg) was transferred to 10 ml volumetric flask. Added 0.1 ml of water to it. Mixed the solution for one minute. The drug could not dissolve. Added more 0.4 ml of water to the volumetric flask. Mixed the solution for two minutes. The solubility state was noted.

Flask 2: Accurately weighed Doxofylline (10 mg) was transferred to 10 ml volumetric flask. 0.1 ml of methanol was added into it. The contents were mixed for one minute. The drug was slightly dissolved. Again 0.1 ml of methanol was added into the volumetric flask. The contents were mixed for one minute. The solubility state was noted.

RESULT AND DISCUSSION

Sertraline was found to be freely soluble in water and soluble in acetonitrile & methanol.

Doxofylline was found to be soluble in water and soluble in methanol & acetonitrile.

METHOD DEVELOPMENT AND ITS VALIDATION FOR SIMULTANEOUS ESTIMATION OF SERTRALINE & DOXOFYLLINE BY RP-HPLC IN COMBINATION TABLET DOSAGE FORM

Selection of wavelength

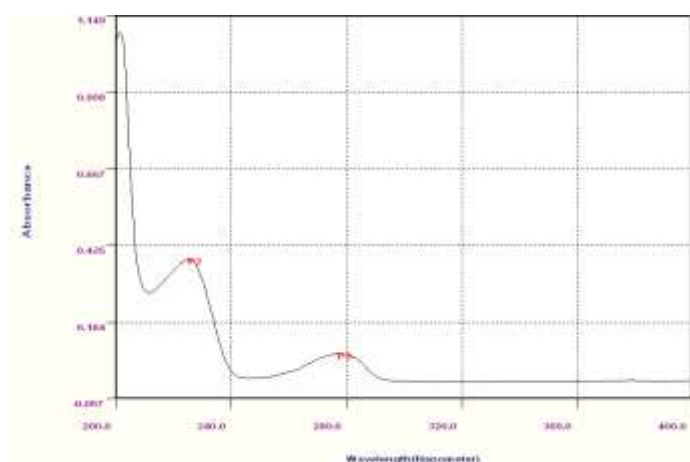
The λ_{\max} of the two ingredients i.e. Sertraline & Doxofylline, were found to be 222 nm and 273 nm respectively in methanol as solvent system. the isobestic point for the drugs were found at 273 nm.

4.6.2 Preparation of standard solution of Sertraline

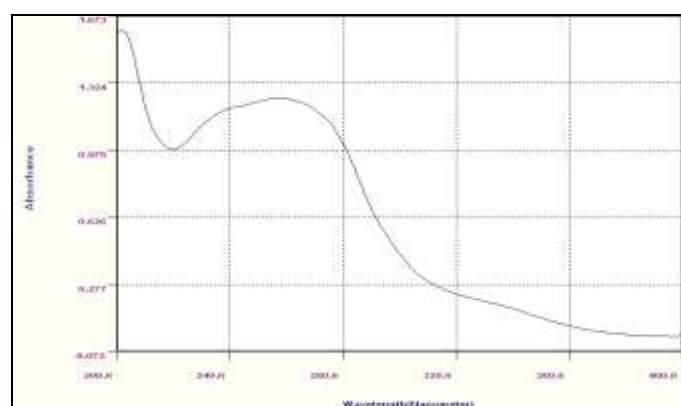
10 mg of Sertraline was weighed accurately and transferred into 100 ml volumetric flask. About 10 ml of HPLC grade methanol was added and sonicated to dissolve. The volume was made up to the mark with same solvent. The final solution contained about 100 µg/ml of Sertraline.

4.6.3 Preparation of standard solution of Doxofylline

10 mg of Doxofylline was weighed accurately and transferred into 100 ml volumetric flask. About 10 ml of HPLC grade methanol was added and sonicated to dissolve. The volume was made up to the mark with same solvent. The final solution contained about 100 µg/ml of Doxofylline.



Sertraline



Doxofylline

Preparation of mix. Standard solution of Sertraline & Doxofylline

Accurately weighed 100 mg of Sertraline and 100 mg of Doxofylline were transferred to two different 100 ml volumetric flask. About 40 ml of mobile phase was added and sonicated to

dissolve. The volume was made up to mark with same solvent. Then 0.5, the detection limit (LOD) and quantitation limit (LOQ) may be expressed as:

$$\text{L.O.D.} = 3.3(\text{SD}/\text{S}).$$

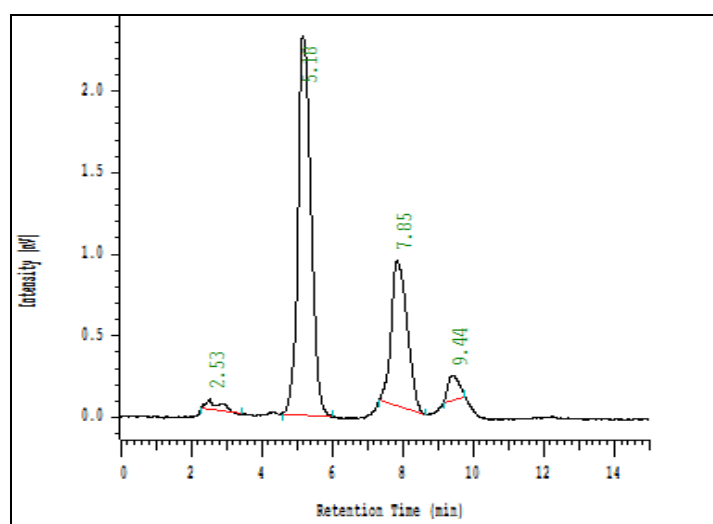
$$\text{L.O.Q.} = 10(\text{SD}/\text{S})$$

Where, SD = Standard deviation of the response

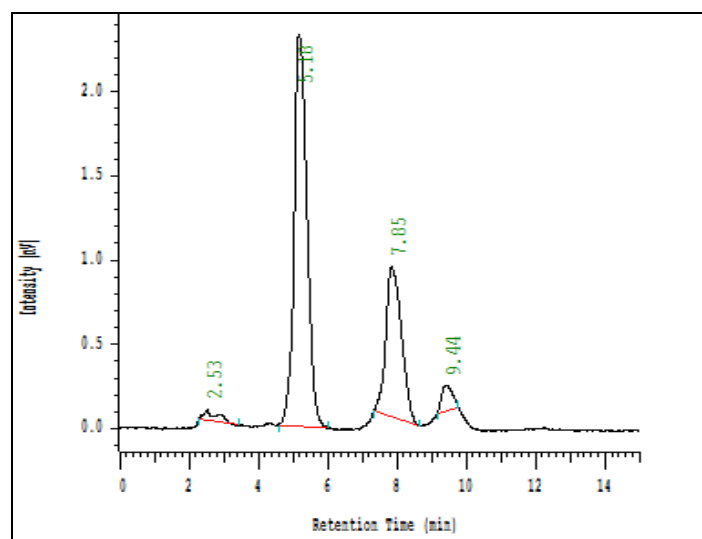
S = Slope of the calibration curve

RESULT AND DISCUSSION

The LOD was found to be 0.32 $\mu\text{g}/\text{ml}$ and 1.44 $\mu\text{g}/\text{ml}$ and LOQ was found to be 0.96 $\mu\text{g}/\text{ml}$ and 4.32 $\mu\text{g}/\text{ml}$ for Sertraline & Doxofylline respectively which represents that sensitivity of the method is high.



Chromatograms for LOD



Chromatograms for LOQ

6 System Suitability Parameter

System suitability testing is an integral part of many analytical procedures. The tests are based on the concept that the equipment, electronics, analytical operations and samples to be analyzed constitute an integral system that can be evaluated as such. Following system suitability test parameters were established. The data are shown in Table 39.

Table 39: Data of System Suitability Parameter.

S.No.	Parameter	Limit	Result
1	Resolution	$R_s > 2$	3.15
2	Asymmetry	$T \leq 2$	Sertraline =0.14 Doxofylline =0.19
3	Theoretical plate	$N > 2000$	Sertraline =3971 Doxofylline= 4861

ASSAY OF SERTRALINE & DOXOFYLLINE IN DOSAGE FORM

Assay was performed as described in previous chapter. Results obtained are tabulated below:

Assay of SERTRALINE & DOXOFYLLINE tablets.

Brand name of tablets	Labeled amount of Drug (mg) Sertraline & Doxofylline	Mean (\pm SD) amount (mg) found by the proposed method (n=6)	Mean (\pm SD) Assay (n = 6)
Doxoder (Wonder Healthcare)	50, 400	50.04 (\pm 0.13) 400.53 (\pm 0.09)	100.08 (\pm 0.39) 100.1325 (\pm 0.42)

The assay of Doxoder tablets containing Sertraline was found to be 100.08% Doxofylline was found to be 100.1325%.

RESULT AND DISCUSSION

To develop a precise, linear, specific RP-HPLC method for analysis of Sertraline & Doxofylline different chromatographic conditions were applied & the results observed are presented in the thesis.

Isocratic elution is simple, requires only one pump & flat baseline separation for easy and reproducible results. So, it was preferred for the current study over gradient elution.

In case of RP-HPLC various columns are available, but here develop Sil, C-18, V size (150mm*4.6mm \varnothing) column was preferred because using this column peak shape, resolution and absorbance were good.

Mobile phase & diluent for preparation of various samples were finalized after studying the solubility of API in different solvents of our disposal (methanol, acetonitrile, dichloromethane, water, 0.1N NaOH, 0.1NHCl). Sertraline was found to be soluble in water and soluble in acetonitrile & methanol. Doxofylline was found to be insoluble in water and soluble in methanol & acetonitrile.

Detection wavelength was selected after scanning the standard solution of drug over 200 to 800nm. From the U.V spectrum of Doxofylline & Sertraline it is evident that most of the HPLC work can be accomplished in the wavelength range of 215-290 nm conveniently. Further, a flow rate of 1.0 ml/min & an injection volume of 20 µl were found to be the best analysis.

The result shows the developed method is yet another suitable method for assay which can help in the analysis of Doxofylline & Sertraline in different formulations.

CONCLUSION

A sensitive & selective stability indicating RP-HPLC method has been developed & validated for the analysis of Sertraline & Doxofylline API.

Based on peak purity results, obtained from the analysis of samples using described method, it can be concluded that the absence of co-eluting peak along with the main peak of Sertraline & Doxofylline indicated that the developed method is specific for the estimation of Sertraline & Doxofylline.

Further the proposed RP-HPLC method has excellent sensitivity, precision and reproducibility.

REFERENCE

1. Beckett H., Stenlake J.B., "Practical Pharmaceutical Chemistry.", C.B.S. Publications, 4th edition, 1.
2. Vijay Malik, "Drugs and Cosmetics Act.", Eastern Book Company Lucknow, 16th edition, 5.
3. Willard H. H., Merit L.L., Dean F.A., and Settle F.A., "Instrumental Methods of Analysis.", C.B. S. Publishers, New Delhi, 7th edition, 2002; 580-613.
4. Skoog D.A., Holler F.J., Nieman T.A., "Principles of Instrumental Analysis.", 5th edition, 2005; 733-738.

5. Sharma B.K., "Instrumental Methods of Chemical Analysis.", Goel Publishing House, Meerut, 24th edition, 2005; C-210-215.
6. Michael E., Schartz S., Krull., "Analytical Method Development and Validation.", 2004; 25-46.
7. Lloyd R. Snyder., Joseph J. Kirkland., Joseph L. Glajesh., "Practical HPLC Method Development.", 2nd edition, 1997; 1-14.
8. CIMS –Current index of medical specialities, 2006; 172 – 174.
9. Alfred Goodman Gilman, Joel G. Hardaman, Lee E. Limbird, Goodman Gilman's The Pharmacological bases of Therapeutics 10th Edn., 2001; 994 – 995.
10. Manoj, Shanmugapandiyam. P and Anbazhagan. S, Indian Drugs., 2004; 41: 284 – 289.
11. T. Radhakrishna, D. Sreenivas Rao^a and G. Om Reddyre, Determination of pioglitazone hydrochloride in bulk and pharmaceutical formulations by HPLC and MEKC methods, S sayad, RP-HPLC method development for determination of pioglitazone hydrochloride from tablets.
12. R.T. Sane, Simultaneous Determination of Pioglitazone and Glimepiride by High-Performance Liquid Chromatography D. Srinivasulu, Development and validation of pioglitazon in dosage form, International journal of chemistry research, 2009; 1(1).
13. D. Boopathy, B. Praveen kumar reddy, Method development and validation of simultaneous determination of pioglitazon and glimepiride by RP-HPLC Ching-Ling Cheng. D, Determination of metformin by HPLC with spectrophotometer detection.
14. Arayne MS, Sultana N, Zuberi MH, Development and validation of RP_HPLC method for analysis of metformin, Pak J Pharm Sci., 2006 Jul; 19(3): 231-5.
15. Parisa Gazerani¹ et, Determination of metformin in human plasma by HPLC.
16. Ceren Yardımcı, Method development and validation for the simultaneous determination of rosiglitazone and metformin in pharmaceutical preparations by capillary zone electrophoresis.

MOUTH-DISSOLVING TABLETS: AN INNOVATIVE AND CONVENIENT DOSAGE FORM FOR PATIENTS WITH SWALLOWING DIFFICULTIES - AN OVERVIEW

Dr. Kokkula Satyanarayana

Professor, Department of Pharmacognosy, Princeton College of Pharmacy, Hyderabad,
Telangana, India

Sunitha Chintala

Asso. Professor, Department of Pharmacognosy, Princeton College of Pharmacy, Hyderabad,
Telangana, India

Abstract- In the design of an oral drug delivery system, which continues to be the preferred method of drug delivery despite a number of drawbacks, ease of administration and increased patient compliance are important considerations. In the novel drug delivery system, "mouth dissolving tablets" (MDTs) can be made that dissolve quickly in the mouth without water in a matter of seconds thanks to the action of a superdisintegrant or by maximizing the pore structure in the formulation. Tablets that dissolve in the mouth are beneficial, especially for children, the elderly, and mentally ill patients who have trouble swallowing traditional tablets and capsules. In addition to various excipients, evaluation tests, marketed formulation, and drugs utilized in this research area, the review discusses the various formulation aspects, superdisintegrants used, and technologies developed for MDTs.

1 INTRODUCTION

Due to its compactness, ease of manufacturing, and self-administration convenience, the tablet is currently the most widely used dosage form. However, conventional tablets are difficult to swallow for elderly, pediatric, and mentally ill patients, resulting in poor patient compliance. Mouth dissolving/disintegrating tablets (MDTs) are a novel drug delivery system developed by scientists to address these issues. These are novel tablets that dissolve, disintegrate, and disperse in saliva without water in a matter of seconds. As per European pharmacopeia, these MDTs ought to break up/deteriorate in under three minutes. The formulation is more beneficial to bedridden individuals and swallowing-impaired patients. MDTs are popular as a preferred dosage form in the current market due to their benefits of improved patient compliance, rapid onset of action, increased bioavailability, and good stability.

Orodispersible tablets, fast disintegrating tablets, orally disintegrating tablets, fast disintegrating tablets, rapid disintegrating tablets, porous tablets, quick melt tablets, and rapid melt tablets are other names for mouth dissolving tablets. However, the United States Pharmacopoeia (USP) recognized these dosage forms as ODTs out of all of the aforementioned terms. US Food and Medication Organization (FDA) characterized ODTs as "A strong dose structure containing restorative substances or dynamic fixings which crumbles quickly inside a couple of moments when put up on tongue".

First, super disintegrants like crosscarmellose sodium, sodium starch glycolate, and crosspovidone are used to make mouth-dissolving tablets. The tablets can also be maximized in terms of their pore structure by freeze drying and vacuum drying. Some drugs may have a greater bioavailability as a result of their oral absorption and the pregastric absorption of dispersed drugs in saliva



before they reach the stomach. Additionally, compared to standard tablets, the amount of drug subjected to first pass metabolism is reduced.

1.1 Requirements of Mouth Dissolving Tablets: Ideal MDTs should 8:

- Dissolve, disperse, and disintegrate in the mouth in a matter of seconds despite requiring no water for oral administration.
- Provide a pleasant mouthfeel
- Possess sufficient taste-masking properties.
- Be less friable and harder
- Leave little or no residue in the mouth after administration

1.2 Advantages of MDTs

It is simple to administer to patients who are unable to swallow, such as the elderly, bedridden, and children, geriatric, and mentally retarded patients.

- The risk of choking or suffocation during oral administration of conventional formulation due to physical obstruction is avoided, thereby providing improved safety
- This is beneficial for traveling patients and busy people, who do not have easy access to water.
- The bioavailability of drug that is absorbed through pregastric absorption of drugs from mouth, pharynx, and esophagus is increased
- Rapid drug therapy intervention
- Bitter taste can be masked by use of flavor and sweetener to produce
- Increased patient adherence

1.3 Challenges to develop MDTs:

- Rapid disintegration and sufficient mechanical strength of the tablet
- Avoid increase in tablet size
- Effective taste masking of bitter drugs
- Minimum or no residue in mouth

- Good package design and protect from moisture
- Has a pleasant mouth feel
- Sensitivity to environmental condition
- Formulate with low cost

1.4 Salient Features of MDTs:

- No need for water to swallow the dosage form, which is a highly convenient feature for patients who are traveling and do not have immediate access to water
- The good mouth feel property of MDTs helps to change the basic view of medication as a bitter pill, particularly for pediatric patients
- Rapid dissolution of drug and absorption, which may produce rapid onset of action
- Some drugs are absorbed from the mouth, pharynx, and esophagus as the saliva passes down into the stomach; The drugs' bioavailability is improved in these situations.

2 LIMITATIONS FOR MDTs:

- It is difficult to formulate medications into MDTs, such as ciprofloxacin, an antibiotic whose adult dose tablet contains approximately 500 milligrams.
- Patients who are taking anticholinergic medications at the same time might not be a good candidate for MDTs, and conditions like Sjogren's syndrome or dry mouth caused by less saliva may not be a good candidate for these tablet formulations.

Technologies with no patents: Whether

to lyophilize or freeze-dry: When making MDTs, the freeze-drying process makes use of the porous product's formation. Lyophilization is a cycle, which incorporates the expulsion of dissolvable from a frozen suspension or arrangement of medication with structure-shaping



added substances. The drug and its additives are freeze-dried, resulting in a highly porous and lightweight product with a glossy amorphous structure. When swallowed, the resulting tablet quickly dissolves and disintegrates, and the freeze-dried unit immediately dissolves to release the medication.

Molding: In this method, water-soluble ingredients are used to prepare molded tablets so that they dissolve completely and quickly. A hydro-alcoholic solvent is used to moisten the powder mixture before molding it into tablets under a pressure that is lower than that used for traditional tablet compression. After that, the solvent is removed by air-drying the tablets. Molded tablets are significantly less compact than compressed ones. These have a porous structure that makes them break down 25 times faster.

How cotton candy is made: This method gets its name from the fact that it makes use of a novel spinning mechanism to produce crystalline structures that look like floss and resemble cotton candy. The cotton candy process involves spinning and flash melting simultaneously to form a matrix of polysaccharides or saccharides. In order to increase the matrix's compressibility and flow properties, it is partially recrystallized. After that, the candy floss matrix is milled, combined with the active ingredients and excipients, and compressed into MDTs.

Spraying dry: As the processing solvent evaporates during the process, this technology results in extremely porous and fine powders. Hydrolyzed and non-hydrolyzed gelatin were used as a supporting matrix, mannitol was used as a bulking agent, and sodium starch glycolate or crosscarmellose sodium was used as a superdisintegrant in this method of making MDTs. The addition of

acidic substances like citric acid or alkaline substances like sodium bicarbonate further enhanced disintegration and dissolution. This plan procedure gives permeable powder and deterioration time < 20 sec

Mass expulsion: This method involves softening the active blend with a solvent consisting of methanol and water-soluble polyethylene glycol, and then extruding the softened mass through an extruder or syringe to form tablets by cutting the product into even segments with a heated blade. By incorporating a super polystate hydrophilic waxy binder such as PEG-6-stearate, MDTs can be prepared using this method. A waxy substance with an m. pt. is called super polystate. between 33 and 37 °C, and a 9 hydrophilic-lipophilic balance It not only binds tablets together and improves their physical resistance, but it also aids in their disintegration because it dissolves quickly in the mouth and leaves no residue. The melt granulation method, in which the molten form of the material results in the formation of granules, was used to incorporate super polystate into the formulation of MDTs.

Method of phase transition: Kuno et. al. 32 used erythritol to investigate the processes of MDT disintegration by sugar alcohol phase transition (m. pt. 122 °C), and xylitol (m. pt. trehalose (97°C) and mannitol (166°C), respectively. The process of compressing a powder that contained two sugar alcohols with opposing high and low melting points and then heating it at a temperature that was in between them led to the production of tablets. Due to their low compatibility, the tablets lack sufficient hardness prior to the heating process. The phase transition of lower melting point sugar alcohol increased the bonding surface area in the tablets, resulting in an increase in tablet hardness following the heating process.



Sublimation: The most important factor in MDTs' rapid disintegration is the tablet matrix's highly porous structure. Due to their low porosity, conventional tablets frequently fail to dissolve rapidly despite having ingredients that are highly water-soluble. During the tableting process, volatile substances like camphor can be sublimated from the formed tablet 33 to increase the porosity. formulated MDTs with camphor, a subliming substance extracted from compressed tablets containing mannitol and camphor. After the tablets were made, camphor was sublimated for 30 minutes in a vacuum at 80°C.

Methods of direct compression: Due to the small number of processing steps, low manufacturing costs, and ability to accommodate high doses, this method is an easy way to make MDTs. The final tablet weight can easily exceed that of another production method 34. Disintegrant, water-soluble excipients, and effervescent agents have a single or combined effect on the disintegration and dissolution of directly compressed tablets. Tablet size and hardness have a significant impact on the efficacy of the disintegrant. Breaking down properties can be improved by medium or low tablet size, low hardness and low actual obstruction .It is fundamental to pick a reasonable and an ideal grouping of disintegrant to guarantee quick deterioration and high disintegration rates.[6,34,35,52] The expansion of water dissolvable excipients or bubbly specialist can additionally build disintegration or crumbling properties. Due to the formulation's combination of swelling and water absorption, super disintegrants break down quickly.

Patient counseling in effective use of MDTs: As pharmacists are ideal persons to know about the recent technologies,

thus have opportunity to educate the patients for effective treatment.

Counseling of patients about this dosage form can avoid any confusion and misunderstanding in taking MDTs. Patient information that needs to be provided include:

Storage of this dosage form as some of MDTs developed may not have sufficient mechanical strength, which needs to be handled carefully.

- Patients with Sjogren's syndrome or dryness of mouth or who take anticholinergic drugs may not be suitable candidates for administering MDTs. Although no water is required to allow drug to disperse quickly and efficiently but decreased volume of saliva may slow the rate of disintegration/dissolution and may reduce the bioavailability of the product.
- Patients need to be clearly told about the difference between effervescent and MDTs. Some of technologies use effervescence, which experience a pleasing tingling Effect on the tongue.
- Although chewable tablets are available in market and patient need to be counseled about differences between chewable and MDTs tablets. These MDTs can be used easily in children who have lost their primary teeth and in geriatric patients who have lost their teeth permanently.

With the pharmacists counseling, intervention and assistance about MDTs, all patients receiving this novel dosage form could be more properly and effectively treated with greater convenience.

3 CONCLUSIONS

The MDTs enjoy expected upper hands over traditional measurement structures, with their superior patient consistence, comfort, bioavailability and fast beginning



of activity had drawn the consideration of many makes more than 10 years. Some of these technologies have produced MDT formulations that have sufficient mechanical strength and dissolve quickly in water.

Children who have lost all of their primary teeth as well as elderly patients who have lost all of their teeth permanently can use these MDTs easily. They transform into a liquid within a few seconds of administration and remain solid during storage, enhancing the stability of dosage forms. MDTs may soon be developed for the majority of drugs currently on the market due to their significant advantages as both solid and liquid dosage forms.

REFERENCES

- Cheng R, Guo X, Burusid B, Couch RA. review of fast dissolving tablets. Pharm Tech, (North America). June, 2000; 52-58.
- Bi Y, Sunada H, Yonezawa Y, Dayo K, Otsuka A, Iida K. Preparation and evaluation of compressed tablet rapidly disintegrating in oral cavity. Chem Pharm Bull (Tokyo) 1996; 44: 2121-2127.
- Quick dissolving tablets. <http://www.biospace.com>. 27 May, 2001.
- Fu Y, Yang S, Jeong SH, Kimura S, Park K. Orally fast disintegrating tablets: Developments, technologies, taste-masking and clinical studies. Crit Rev Ther Drug Carrier Sys 2004; 21: 433-76.
- Suresh Bandari, Rajendar kumar Mitta palli, Ramesh Gannu, Yamsani Madhusudan Rao. Orodispersible tablets: An overview. Asian Journal of pharmaceuticals. Jan 2008.
- Gohel M, Patel M, Amin A, Agarwal R, Dave R, Bariya N. Formulation design and optimization of mouth dissolving tablets of nimesulide using vacuum drying technique. AAPS Pharm Sci Tech 2004; 5: Article 36.
- Panigrahi D, Baghel S, Mishra B. Mouth dissolving tablet: An overview of preparation techniques, evaluation and patented technologies. Journal of pharmaceutical research. July 2005, vol. 4, no. 3: 33-38.
- Bradoo, R., Fast Dissolving Drug Delivery Systems, JAMA India, 2001, 4(10), 27-31.
- Kuchekar, B. S., Atul, Badhan, C. Mahajan, H.S., Mouth dissolving tablets: A novel drug delivery system, Pharma Times, 2003, 35, 7-9.
- Behnke K, Sogaard J, Martin S, Bauml J, Ravindran AV, Agren H, et al. Mirtazapine orally disintegrating tablet versus sertraline: A prospective onset of action study. J Clin Psychopharmacol 2003; 23: 358-64.
- Dollo G, Chevanne F, Le Corre P, Chemtob C, Le Verge R. Bioavailability of phloroglucinol in man. J Pharm Belg 1999; 54: 75-82.
- Gafitanu E, Dumistracel I, Antochi S. Formulations and bioavailability of propyphenazone in lyophilized tablets. Rev Med Chir Soc Med Nat Iasi 1991; 95: 127-8.
- Clarke A, Brewer F, Johnson ES, Mallard N, Hartig F, Taylor S, et al. A new formulation of selegiline: Improved bioavailability and selectivity for MAO-B inhibition. J Neural Transm 2003; 110: 124-5.
- Shimuzu T, Sugaya M, Nakano Y, Izutsu D, Mizukami Y, Okochi K, et al. Formulation study for lansoprazole fast-disintegrating tablet: III, Design of rapidly disintegrating tablets. Chem Pharm Bull 2003; 51: 1121-7.
- Ahmed IS, Nafadi MM, Fatahallaf A. Formulation of a fast-dissolving ketoprofen tablet using freeze-drying in blisters technique. Drug Dev Ind Pharm 2006; 32: 437-442.
- Cilurzo F, Selmin F, Minghetti P, Rimoldi I, Demartin F, Montanari L. Fast dissolving mucoadhesive microparticulate delivery system containing piroxicam. Eur J Pharm Sci 2005; 24: 355-61.
- Sammour OA, Hammad MA, Megrab NA, Zidan AS. Formulation and Optimization of Mouth Dissolve Tablets Containing Rofecoxib Solid Dispersion. AAPS PharmSciTech 2006; 7: Article 55.
- Schiermeier S, Schmidt PC. Fast dispersible ibuprofen tablets. Eur J Pharm Sci 2002; 15: 295-305.
- Chaudhari PD, Chaudhari SP, Kolhe SR, Dave KV, More DM. Formulation and evaluation of fast dissolving tablets of famotidine. Indian Drugs 2005; 42: 641-9.
- Nandgude TD, Saifee M, Bhise KS. Formulation and evaluation of fast disintegrating tablets of diphenhydramine tannate. Asian J Pharma 2006; 1: 1.
- Khan S, Kataria P, Nakhath P, Yeole P. Taste Masking of Ondansetron Hydrochloride by Polymer Carrier System and Formulation of Rapid- Disintegrating Tablets. AAPS PharmSciTech 2007; 8: Article 46.
- Bogner RH, Wilkosz MF. Fast Dissolving tablets: New dosage convenience for patients. US Pharmacist 2002; 27: 34-43.
- Habib W, Khankari RK, Hontz J. Fast-dissolve drug delivery systems. Crit Rev Ther Drug Carrier Sys 2000; 17: 61-72.
- Dobetti L. Fast-melting tablets: Developments and technologies. Pharm Technol N Am 2001; 44-50.



UGC APPROVED JOURNALS NO. 48708

25. Van Scoik KG. Solid Pharmaceutical dosage in tablet triturates form and method of producing the same. US Patent 5,082,667.
26. Meyers GL, Battist GE, Fuisz RC. Process and apparatus for making rapidly dissolving dosage units and product there form. PCT Patent WC 95/34293-A1; 1995.
27. Allen LV, Wang B. Process for making a particulate support matrix for making a rapidly dissolving dosage form. US Patent 6,207,199; 2001.
28. Allen LV, Wang B. Process for making a particulate support matrix for making a rapidly dissolving tablet. US Patent 5,587,180; 1996.
29. Allen LV, Wang B, Davis LD. Rapidly dissolving tablet. US Patent 5,807,576; 1998.
30. Bhaskaran S, Narmada GV. Rapid Dissolving tablet A Novel dosage form Indian Pharmacist 2002; 1:9-12.
31. Abdelbary G, Prinderre P, Eouani C, Joachim J, Reynier JP, Piccerelle P. The preparation of orally disintegrating tablets using a hydrophilic waxy binder. Int J Pharm 2004; 278:423-33.
32. Kuno Y, Kojima M, Ando S, Nakagami H. Evaluation of rapidly disintegrating tablets manufactured by phase transition of sugar alcohols. J Control Release 2005; 105:16-22.
33. Koizumi K, Watanabe Y, Morita K, Utoguchi N, Matsumoto M. New method of preparing high-porosity rapidly saliva soluble compressed tablets using mannitol with camphor: A subliming material. Int J Pharm 1997; 152:127-31.
34. Rishi RK, The pharma review 2004;2:32
35. Makino T, Yamad M, Kikutaj, et al US Patent 1998; 5,939,091.
36. Bolhuis KG, Zuurman, Wrierikte PHG etal Eru.J.Pharm 1997; 5:63.
37. Kintsch KN, Hagen A, Manz E . US Patent 1979; 4,134,943.
38. Heinemann Hand Rotte W. US Patent 1976; 3,885,026.
39. Seager H. Drug-delivery products and the Zydis fast-dissolving dosage form. J Pharm Pharmacol 1998; 50:375-82.
40. Gregory GK, Ho DS. Pharmaceutical dosage form packages. US Patent 4, 305, 502; 1981.



A THOROUGH OVERVIEW OF TRANSDERMAL DRUG DELIVERY SYSTEMS: THE ROLE OF TRANSDERMAL PATCHES**Sangu Jyothi**Asst. Professor, Department of Pharmaceutical Chemistry, Princeton College of Pharmacy,
Hyderabad, Telangana, India**Roopani Madhu**Asst. Professor, Department of Pharmaceutical Chemistry, Princeton College of Pharmacy,
Hyderabad, Telangana, India

Abstract - Today, approximately 70% of medications are taken orally and are found to be ineffective. A transdermal drug delivery system was developed to improve these characters. In contrast to conventional topical drug delivery, the transdermal drug delivery system (TDDS) offers a means of maintaining drug release while simultaneously reducing the intensity of action. As a result, it reduces the side effects associated with oral therapy. The Transdermal Drug Delivery System is the method by which the drug's active ingredients are delivered through the skin. Limiting hepatic first pass metabolism, increasing therapeutic efficacy, and maintaining a constant drug level in the plasma are all significant advantages of transdermal drug delivery. Transdermal patches of various kinds are used to get the active ingredients into the bloodstream through the skin. This review article provides a concise overview of the principles of transdermal permeation, the various patch components, patch approaches, and transdermal system evaluation, application, and limitations.

Keywords: Microneedle, patch, transdermal delivery, preparation method, and evaluation parameter

1 INTRODUCTION

Transdermal medications come in a separate, discrete dosage form. The transdermal drug delivery system is one in which the drug's active ingredients are delivered through the skin. The drug is effectively absorbed through the skin before entering the circulatory system. It is thought that delivering medication to the skin's general circulation is a better option than taking it orally. By passing through the gastrointestinal system, it would avoid liver activation at the first pass and avoid the frequent GI irritation. Additionally, the blood level fluctuations caused by oral dosage forms are usually preferable to the drug's steady absorption over hours or days.

In 1981, the FDA granted approval to the first transdermal patch. Nitroglycerine was used to prevent coronary artery disease-associated angina pectoris and scopolamine was used to prevent motion sickness through controlled systemic absorption through

these delivery systems. These dosage forms have recently undergone development and modification in an effort to improve the skin's permeability and the driving force of drug diffusion. Prodrugs, liposomes, supersaturated systems, penetration enhancers, and other vesicles are among these methods. In the United States, the nicotine patch, which releases nicotine to assist with tobacco smoking cessation, was the transdermal patch that sold the most. Over the course of sixteen hours, the nicotine patch suppresses the smoker's desire for a cigarette. By avoiding first-pass metabolism and increasing patient compliance, transdermal delivery outperforms oral and injectable methods. Transdermal delivery not only eliminates pulsed entry into systemic circulation, which frequently results in undesirable side effects, but it also permits continuous, controlled administration of drugs with short biological half-lives. Currently regarded as



a mature technology, transdermal drug delivery (TDD) relies primarily on occlusive patches. Due to poor oral bioavailability, side effects associated with high peaks, or poor compliance due to the requirement for frequent administration, this method is capable of delivering drugs, but its application would be limited. However, skin irritation, relatively high manufacturing costs, and a less-than-ideal cosmetic appearance are among the TDDs' drawbacks.

1.1 Advantages

- Evasion of first pass digestion
- Evasion of gastro digestive contradiction
- Unsurprising and expanded term of action
- Furnishes use of medications with short natural half lives
- Thin remedial window
- Working on physiological and pharmacological reaction
- Keeping away from the variance in drug levels
- Entomb and intra patient varieties
- Keep up with plasma convergence of intense medications
- End of treatment is simple anytime of time
- More prominent patient consistence because of disposal of different dosing profile
- Capacity to convey drug all the more specifically to a particular site
- Give appropriateness to self organization
- Improve helpful adequacy

1.2 Disadvantages

- The drug must have some desirable physicochemical properties for penetration through stratum corneum.
- The transdermal delivery will be very difficult, if the drug dose required is more than 10 mg/day for their therapeutic application.
- Only relatively potent drugs are suitable candidates for TDDS.

- The barrier function of the skin changes from one site to another on the same person, from person to person and with age.

2 THE SKIN

In addition to being the largest organ in the human body, the skin (cutis) is an excellent biological barrier. The skin is 102–104 times less permeable than a blood capillary wall and contributes approximately 4% of a person's body weight, despite being typically less than 2 mm thick. In humans, the epidermis, or outer skin layer, is typically 0.02–0.2 mm thick. Skin surface PH is also affected by gender and body location. Dermis refers to the area below the epidermis. Both the outer papillary dermis and the inner reticular dermis are typically five to twenty times thicker than the epidermis when taken as a whole. This organ with its many layers protects the body from the outside world and is an effective barrier against exogenous molecules' penetration. The stratum corneum (SC), the skin's uppermost strata, is where the majority of the barrier properties are located. Corneocytes, differentiated non-nucleated cells that are embedded in the lipid domain and filled with keratins, make up this highly hydrophobic layer. Its effective elastic modulus is between 107 and 108 Pa, but it decreases as temperature and moisture content increase. A typical adult's skin absorbs approximately one third of the body's blood and has a surface area of approximately two square meters. Only 0.1 percent of the surface of the human skin is occupied by skin appendages. Nevertheless, the foreign agents may be able to penetrate the skin faster than the stratum corneum through these skin appendages. A compound's extent of skin penetration may be affected by its absorption route. There are three pathways which can be associated with the transdermal saturation of synthetic substances:

- (1) Through SC's lipid domains between cells;
- (2) Appendages that enter the skin; and
- (3) Through the bundles of keratin in SC.



3 BASIC COMPONENTS OF TRANSDERMAL PATCH:

3.1 Polymer Matrix/Drug Reservoir:

A transdermal drug delivery system is built on polymers as its foundation. A drug reservoir or a drug-polymer matrix is sandwiched between two polymeric layers in multilayered polymeric laminates used for transdermal delivery systems:

an inner polymeric layer that serves as an adhesive and/or rate-controlling membrane, and an outer impervious backing layer that prevents drug loss through the backing surface.

3.2 Drug

The best drug candidates for passive adhesive transdermal patches should comply following criteria:

- Should be Non ionic
- Should have Low molecular weight (less than 500 Daltons)
- Should have adequate solubility in oil and water (log P in the range of 1-3)
- Should have low melting point (less than 200°C)
- Should be potent (dose in mg per day).

Drugs like rivastigmine for alzheimer's and Parkinson dementia, rotigotine for parkinson, methylphenidate for attention deficit hyperactive disorder and selegiline for depression are recently approved as TDDS.

3.3 Permeation Enhancers

Enhancers interact with structural stratum corneum components, such as proteins or lipids, to increase stratum corneum permeability for higher therapeutic drug levels. Chemical enhancers may have partially leached epidermal lipids, enhancing the skin's conditions for wetting and transepidermal and transfollicular penetration, resulting in an increase in oil-soluble drug absorption.

3.4 Chemical Enhancers

- Increasing the drug permeability through the skin by causing reversible damage to the SC.
- Increasing (and optimizing) thermodynamic activity of the drug when functioning as co-solvent.
- Increasing the partition coefficient of the drug to promote its release from the vehicle into the skin.
- Conditioning the SC to promote drug diffusion.
- Promoting penetration and establish drug reservoir in the SC.

3.5 Pressure Sensitive Adhesives (PSA)

A PSA keeps the patch in close contact with the skin's surface. It should be aggressively and permanently tacky, adhere with no more than finger pressure, and exert a strong holding force. For instance polyacrylates, polyisobutylene and silicon based glues. PSA should not alter drug release and should be physicochemically and biologically compatible. The public service announcement can be situated on the essence of the gadget (as in supply framework) or toward the rear of the gadget and broadening incidentally (as in the event of lattice framework).

3.6 Backing Laminate

While planning a support layer, the thought of synthetic opposition of the material is generally significant. The compatibility of the excipients with the backing layer should also be taken into consideration because prolonged contact between the excipients and the backing layer may result in additives leaching out of the backing layer or in the diffusion of excipients, drugs, or penetration enhancers through the layer. However, excessive emphasis on chemical resistance may result in patches that lift and may irritate the skin over time due to their high occlusiveness to air and moisture. The backing with the lowest



modulus—also known as high flexibility—good oxygen transmission and a high rate of moisture vapor transmission will be the most comfortable. Vinyl, polyethylene, and polyester films are just a few examples of backing materials.

4 SYNERGISTIC MIXTURES OF CHEMICAL ENHANCER

The mixture's individual chemicals may self-assemble into distinct, intricate secondary structures that permeabilize the skin. Alternately, the chemicals might each affect the structure of the skin on their own.

These systems may increase transdermal flux through one or more of the following mechanisms:

Specific interaction with the stratum corneum, either by altering the various transport pathways (i.e., the polar and nonpolar pathways) in the stratum corneum or by increasing the drug solubility in the stratum corneum (i.e., facilitate partitioning of drug from the vehicle into the skin).

(a) Change in the thermodynamic activity (e.g., by increasing the degree of saturation in the solvent and, consequently, increasing the escaping tendency).

5 FUTURE TECHNOLOGIES AND APPROACHES

- Thermal poration is the process of forming aqueous pathways across the stratum corneum using pulsed heat. This method has been used to deliver conventional drugs and extract glucose from human intestinal fluid.
- Jet injectors are getting more attention these days, which is making it possible to design better devices that can inject drug solutions controlled and without a needle across the skin and into deeper tissue.
- Using a micro infusion pump contained within a large patch that is affixed to the skin, a small needle

is inserted a few millimeters into the skin, and drug solution is flowed through the needle at controlled rates. Morphine has been administered to humans using this method.

- During the past ten years, a number of theories have been proposed regarding chemical-iontophoresis combinations; electroporation and chemicals; synthetics and ultrasound; ultrasonography and iontophoresis; electroporation and iontophoresis; and ultrasound and electroporation.

6 CONCLUSION

The transdermal drug delivery systems and the specifics of their evaluation process are covered in depth in the TDDS review articles, which serve as a handy reference for TDDS-related researchers. Additionally, it provides important information regarding the TDDS application of nanoparticles. Utilizing various enhancers, it aids in the optimization of permeability and includes future injector modification considerations. The fundamental understanding of device design parameters and how they influence device interaction with skin has also significantly improved over the past ten years, as this review demonstrates.

REFERENCES

1. Claudia Valenta, Barbara G. Auner, "The use of polymers for dermal and transdermal delivery", *European Journal of Pharmaceutics and Biopharmaceutics*, 2004, 58, 279–289.
2. Pankaj Karande, Samir Mitragotri, "Enhancement of transdermal drug delivery via synergistic action of chemicals", *Biochimica et Biophysica Acta*, 2009, 1788, 2362–2373.
3. Sara Farahmand, Howard I. Maibach, "Transdermal drug pharmacokinetics in man: Interindividual variability and partial prediction", *International Journal of Pharmaceutics*, 2009, 367, 1–15.
4. Jim E. Riviere, Mark G. Papich, "Potential and problems of developing transdermal patches for veterinary applications,"



UGC APPROVED JOURNALS NO. 48708

- Advanced Drug Delivery Reviews, 2001, 50, 175-203.
5. J. Klimes, J. Sochor, P. Dolezal, J. Korner, "HPLC evaluation of diclofenac in transdermal therapeutic preparations", International Journal of Pharmaceutics, 2001, 217, 153-160.
 6. Changshun Ren, Liang Fang, Lei Ling, Qiang Wang, Sihai Liu, LiGang Zhao, Zhonggui He, "Design and *in vivo* evaluation of an indapamide transdermal patch", International Journal of Pharmaceutics, 2009, 370, 129-135.
 7. Anna M. Wokovich, Suneela Prodduturi, William H. Doub, Ajaz S. Hussain, Lucinda F. Buhse. "Transdermal drug delivery system (TDDS) adhesion as a critical safety, efficacy and quality attribute", European Journal of Pharmaceutics and Biopharmaceutics, 2006, 64, 1-8.
 8. Michael H. Qvist, Ulla Hoeck, Bo Kreilgaard, Flemming Madsen, Sven Frokjaer, "Release of chemical permeation enhancers from drug-in-adhesive transdermal patches", International Journal of Pharmaceutics, 2002, 231, 253-263.
 9. Amit Misra, Pramod Upadhyay. "Apparatus for preparing adhesive dispersion transdermal patches on a laboratory scale", International Journal of Pharmaceutics, 1996, 132, 267-270.
 10. Biswajit Mukherjee, Sushmita Mahapatra, Ritu Guptab, Balaram Patra, Amit Tiwarib, Priyanka Arora. "A comparison between povidone-ethylcellulose and povidone-eudragit transdermal dexamethasone matrix patches based on *in vitro* skin permeation", European Journal of Pharmaceutics and Biopharmaceutics, 2005, 59, 475-483.
 11. Beverley J. Thomas and Barrie C. Finnin, "The transdermal revolution", DDT, 2004, 9(16)
 12. Biana Godin, Elka Touitou. "Transdermal skin delivery: Predictions for humans from *in vivo*, *ex vivo* and animal models", Advanced Drug Delivery Reviews, 2007, 59, 1152-1161.
 13. Anubhav Arora, Mark R. Prausnitz, Samir Mitragotri. "Micro-scale devices for transdermal drug delivery", International Journal of Pharmaceutics, 2008, 364, 227-236.
 14. Gregor Cevc, Ulrich Vierl. "Nanotechnology and the transdermal route A state of the art review and critical appraisal," Journal of Controlled Release, 2010, 141, 277-299.
 15. A.Arunachalam, M.Karthikeyan, D.Vinay Kumar, Prathap. M, S. Sethuraman, S.Ashutoshkumar, S.Manidipa. "Transdermal Drug Delivery System: A Review", Current Pharma Research, 2010, 1.
 16. Kamal Saroha, Bhavna Yadav, Benika Sharma. "Transdermal Patch: A Discrete Dosage Form," International Journal of Current Pharmaceutical Research, 2011, 3(3).
 17. Jitendra Banweer, Subhash Pandey, A. K. Pathak. "Formulation, Optimization and Evaluation of Matrix type Transdermal system of Lisinopril Dihydrate Using Permeation Enhancers." Drug Invention Today, 2010,2(2),134-137.
 18. Divyesh Patel, Nirav Patel, Meghal Parmar, Navpreet Kaur. "Transdermal Drug Delivery System: Review", International Journal Of Biopharmaceutics & Toxicological Research, 2011, 1(1).
 19. Jain, N. K., Controlled and Novel Drug Delivery, CBS Publishers, and Distributors, 2002, 107.
 20. Brahmankar.D.M, Jaiswal.S.B, "Biopharmaceutics and pharmacokinetics A Teatise", Vallabh Prakashan, Delhi,1995, 335-371.
 21. Aulton.M.E, Pharmaceutics; "The science of dosage form design", second edition, Churchill Livingstone, Harcourt publishers-2002.
 22. Ansel.H.C, Loyd.A.V, Popovich.N.G, "Pharmaceutical dosage forms and drug delivery systems", Seventh edition, Lippincott Williams and Willkins publication.
 23. Banker, G. S and Rhodes, C. T Modern pharmaceutics, third edition, New York, Marcel Dekker, Inc, 1990.
 24. Bhowmik D,Chiranjib ,Margret C,Jayakar B, Sampath K P. "Recent Advances in Transdermal Drug Delivery System". Int.J. PharmTech Res. 2010; 2 (1): 68-77.
 25. Shah S. "Transdermal Drug Delivery Technology Revisited: Recent Advances". Pharmainfo.net. 2008; 6(5).
 26. C. W. Yie, "Transdermal Controlled Systemic Medications", Marcel & Dekker Inc., New York, 1982: 125.
 27. Gattani S.G., Gaud R.S. and Chaturvedi S.C., "Formulation and evaluation of transdermal films of chlorpheniramine maleate", Indian drug 44 (1), 2007, 27-33.
 28. Dey B.K, Nath L.K, mohanti B, Bhowmik B.B., "Development and evaluation of propranolol Hydrochloride transdermal patches by using Hydrophilic and Hydrophobic polymer", Indian Journal of pharmaceutical education & Research, 41 (4), 2007, 388-393.
 29. Udhumansha ubaidulla, molugu V.S.Reddy, "transdermal therapeutic system of carvedilol; effect of Hydrophilic and Hydrophobic metrics on *In Vitro* and *In vivo* characteristics", AAPS pharmscitech, 2007; 8(1).
 30. Jain.N.K, "Controlled and novel drug delivery", first edition, CBS publishers and distributors, New Delhi.1997.



ORAL MUCOSAL DRUG DELIVERY SYSTEMS: A COMPREHENSIVE REVIEW**Vaishnavi Munnangi**Asst. Professor, Department of Pharmacology Princeton College of Pharmacy, Hyderabad,
Telangana, India**Sooramagari Sunayana**Asst. Professor, Department of Pharmacology Princeton College of Pharmacy, Hyderabad,
Telangana, India

Abstract - Despite significant advancements in drug delivery, the oral route remains the most important method for systemic drug administration. For self-medication, the parenteral route is rarely utilized. For centuries, it has been known that drug solute administered buccally or sublingually is rapidly absorbed into the reticulated vein beneath the oral mucosa. The oral mucosa has rich blood supply and it is moderately porous. The buccal mucosa is four to one thousand times more permeable than skin. The buccal route has several advantages over the oral route, including QWICK ACTION, avoiding first-pass metabolism, the drug not being exposed to stomach acid, and improved patient compliance, particularly in pediatric and geriatric patients. The purpose of this article is to discuss briefly the structural characteristics of oral mucosal drug delivery, including buccoadhesive film and tablet, medicated chew gum, fast dissolving tablet, film, and capsule, and others.

1 INTRODUCTION

To achieve a systemic pharmacological effect, a drug can be administered in a variety of ways. The oral route, in which the drug is swallowed and primarily enters the systemic circulation through the small intestine membrane, is the most common method of drug administration. The most crucial method of drug administration for systemic effect is oral administration. Self-medication is not typically administered via parenteral route.

It is likely that oral administration accounts for at least 90% of all drugs used to produce systemic effects. After being taken orally, drugs may be absorbed at a variety of body locations between the mouth and the rectum. In most cases, it is desirable for a drug to have a faster rate of action the higher up along the alimentary tract it is absorbed. When taken orally, a drug must withstand significant pH changes as it moves through the gastrointestinal tract, as well as the assault of enzymes that

break down food and the metabolism of the microflora that live there.

It is assessed that 25% of the populace finds it hard to swallow tablets and containers and hence don't accept their medicine as recommended by their specialist bringing about high frequency of resistance and ineffectual treatment. Trouble is knowledgeable about specific by pediatrics and geriatric patients, yet it likewise applies to individuals who are sick incapacitated and to those dynamic working patient who are occupied or voyaging, particularly the people who have no admittance to water. In these instances, oral mucosal drug delivery is the method of choice.

It has been known for centuries that drug solutes administered sublingually and buccally are swiftly absorbed into the reticulated vein, which is beneath the oral mucosa. They then travel through the facial veins, internal jugular vein, and brachiocephalic vein before draining into the systemic circulation. As a result, the hepatic first-pass elimination



of drugs can be avoided by using the buccal and sublingual administration routes. The buccal region of the oral mucosal cavity provides an appealing route of administration for systemic drug delivery. The mucosa is relatively permeable and has a lot of blood. Patients are very happy with the oral cavity because the mucosa is relatively permeable and has a lot of blood, and the oral mucosa is tolerant of potential allergens because it doesn't have any langerhans cells.

2 ORAL MUCOSA'S STRUCTURAL FEATURES INCLUDE:

The mouth's mucosa is distinct from the rest of the gastrointestinal tract and has a more skin-like morphology. An outer layer of stratified squamous epithelium makes up the oral mucosa. Below this is a basement membrane called the lamina propria, and the sub mucosa is the innermost layer. There are three distinct types of oral mucosa. I. e. masticatory, lining and concentrated mucosa. The gingiva and hard palate are covered by the masticatory mucosa. It can withstand the abrasion and shearing forces of the masticatory process because it has a keratinized epithelium that is strongly attached to the underlying tissues by collagenous connective tissue. Other than the tongue's dorsal surface, the lining mucosa covers all other areas.

The drug delivery's design and location are significantly influenced by the permeability characteristics resulting from regional differences in morphology. In general, the epithelia of the oral mucosa are somewhat leaky and lie somewhere in between the epidermis and the intestinal mucosa. The buccal mucosa is thought to be four to four thousand times more permeable than the skin. The blood course through a tissue is significant for accomplishing great medication retention. The primary blood supply to the oral tissues comes from the

external carotid artery. It branches into the lingual, maxillary, and facial arteries. Three principal veins collect blood from the capillary beds and feed the internal jugular vein. It is believed that blood flow through human oral mucosa is sufficiently rapid to not limit drug absorption even during disease.

3 ADVANTAGE AND LIMITATION:

The buccal route of drug administration has a number of advantages over oral administration, including:

- The drug is not exposed to the stomach's harmful acidic environment.
- The drug's therapeutic serum concentration can be achieved more quickly.
- The drug does not first pass through the liver before entering the general circulation.
- The mucosal permeability and local environment can be controlled and manipulated to accommodate drug permeation with the appropriate dosage form design and formulation.
- If necessary, delivery can also be stopped quickly.

Presystemic metabolism plays a significant barrier role for some medications. The buccal mucosa has relatively low enzymatic activity, and drug inactivation is neither rapid nor extensive. However, some drugs, particularly those that are peptide or protein-based, may be degraded by oral enzymes. The administration of bile salts and enzyme inhibitors like aprotinin, bestatin, puromycin, and bile salts together decreases the activity of proteolytic enzymes, resulting in a change in the peptide drug's conformation or the formation of micelles, and/or making the drug less susceptible to enzymatic degradation. The principal deterrents that medications meet when controlled by means of the buccal course get from the restricted ingestion region and the



boundary properties of the mucosa. Although the drug's diffusion through mucus is not a rate-limiting step unless it specifically binds to the mucin or are large molecules, the mucin film may serve as a barrier. The rapid removal of the conventional delivery system, primarily through a lot of salivary flow, is another obvious obstacle that prevents this route from being used effectively. The issue of removal can be resolved with bioadhesive polymer.

4 ORAL MUCOSAL DOSAGE FORMS

There are a variety of drug delivery systems that use the oral mucosa as a drug delivery site, such as chewing gum, fast-dissolving tablets, orodissolving films, and fast caps.

a) Tablet that Dissolves Quickly (FDT):

As a new drug delivery method, fast dissolving systems have recently begun to gain acceptance due to their ease of administration and improved patient compliance. They can also be used as a line extension for already-existing commercial products because they provide unique product differentiation. Direct compression, sublimation, melt granulation, molding, volatilization, and freeze drying are some of the methods that can be used to prepare FDTs. Zydis, orasolve, durasolv, flash dose, wowtab, flash tab, and others are examples of patented technologies. Some drugs that are hard to dissolve in water and have variable bioavailability and bioequivalence because they are hard to dissolve in water. Cogranelation with beta-cyclodextrin increased the drug's solubility in various ways to create a fast-dissolving tablet similar to the solid dispersion technique.

Because fast-dissolving systems dissolve or disintegrate in the mouth of the patient, the active ingredients compete with the patient's taste buds, making taste masking essential to patient

compliance. Taste masking can be accomplished in a variety of ways, such as by adding sweeteners or by mass extruding eudragit E100. There have been a number of recent comparison studies between conventional and fast-dissolving formulations. If given the option, 93% of allergic patients would choose FDT formulations, according to an acceptance survey.

(b) Films with a Quick Dissolve: Despite their short dissolution/disintegration time, certain patient populations continue to be afraid of taking solid tablets and run the risk of choking. By developing a convenient dosage form for administration, recent advancements in novel drug delivery systems aim to enhance the safety and efficacy of drug molecules. One such methodology is quickly dissolving film. It consists of a very thin oral strip that immediately releases the active ingredient once it is taken up by the mouth. Rapid film combines the advantages of liquid dosage forms (easy swallowing, rapid bioavailability) with those of tablets (precise dosage, simple application).

The conveyance framework is basically put on a patient's tongue or any oral mucosal tissue. The film, which is immediately soaked in saliva, quickly hydrates and dissolves to release the medication for oral mucosal absorption. Hot melt extrusion, solid dispersion extrusion, rolling, semisolid casting, and solvent casting are all possible methods. Pullulan, a water-soluble film-forming agent, was discovered in oral consumable films by Spence S.H. et al. A film is likewise fostered that might convey rotavirus immunization to newborn children in ad libbed region. Using PVA as a polymer, Mashru R. C. et al. also created a salbutamol sulphate film that dissolves quickly. Renuka Sharma et al. created a taste-masked film. Utilizing HPMC and Eudragit EPO. Additionally, a



number of patents have been assigned to oral water-soluble films.

(c) Fast Caps. On the basis of gelatine capsules, a brand-new type of fast-dissolving drug delivery system was developed. Fast capsules, in contrast to conventional hard capsules, include various additives and gelation of low bloom strength to enhance the capsule shell's mechanical and dissolution properties. High drug loading, the possibility of solid and liquid filling, the absence of compression of coated taste-masked or extended release drug particles/pellets, good mechanical properties, simple manufacturing, mechanical stability, and the need for special packaging are all advantages of these rapidly disintegrating capsules.

d) Bucco adhesive Tablets and Film: There has been a growing interest in the creation of novel muco- adhesive buccal dosage forms in recent years. These are useful for both local drug targeting to a specific part of the body and systemic drug delivery. Due to their susceptibility to "dose dumping phenomena," water-soluble drugs are thought to be difficult to deliver in the form of sustained or controlled release preparations. Mucoadhesive polymers have been used to try to control their release so that they can only be taken once per day.

e) Medicated Chewing Gums: A number of advantages make medicated chewing gum a desirable alternative for drug delivery, including ease of administration, individually controlled active substance release, and efficient buccal drug administration for the treatment of local oral disease and systemic action. To provide a promising controlled release drug delivery system, chewing gum is primarily used.

Sedated biting gums are presently accessible for help with discomfort,

smoking end, travel sickness and renewing of breath. Chewing gum was made with a gum that repels water. Additionally, a brand-new chewing gum device known as 3Tab gum has been developed. Chewing gum in vitro release studies necessitate specialized instruments and equipment.

5 CONCLUSION

Close to conveyance medication to the body, a medication conveyance framework with a plan to work on persistent consistence and comfort are more significant. In order to meet the growing demand from patients for more convenient dosage forms, significant effort is being put into the development of novel dosage forms these days. These dosage forms are expected to gain popularity more quickly. Oral mucosal delivery is a convenient way to give medication to people who have trouble swallowing and to the general population. They also offer a chance to expand the product line in the market and extend the innovator's patent term.

REFERENCE

1. Swarbrick J, Boylan JC: Encyclopedia of pharmaceutical technology, Second edition, marcel dekker Inc. 2: 800-808.
2. Lachman L, Lieberman HA, Kanig JL: The Theory and practice of industrial pharmacy, Third edition, Varghese publishing house; 171.
3. Banker G S, Rhodes C T: Morden pharmaceuticals, edition-4, Marcel deker inc, 2002; 2: 667.
4. Ansel HC, Allen LV: Pharmaceutical dosage form and drug delivery systems: Eight Editions. 2005; 228.
5. Rathbone JM, Michale SR: Modified release drug delivery technology, marcel dekker inc; 126: 191-200.
6. Scherer DDS, Blagrove, Wiltshire UK: Drug-delivery product and the zydis fast dissolving dosage forms: journal of pharm. Pharmacol. 1998; 50(4): 375-82.
7. Chien YW: "Novel drug delivery systems" , 2nd edition, Marcel Dekker, Inc. New York, 50; 139.
8. Shojaei AH: Buccal mucosa as a route for systemic drug delivery: a review, Journal of pharmaceutical sciences, 1998; 1(1):15-30.



UGC APPROVED JOURNALS NO. 48708

9. Oliver AS, Wolff A, Schumacher A, Libew IN, and vetter T: Drug delivery from the oral cavity, Focus on a novel mechatronic delivery device, *Drug discovery today*, 2008; 13(5-6):247-251.
10. Rossi SR, Sondri G, and Carmella CM: Buccal drug delivery, a challenge already won? *Drug discovery today technology*, 2005; 2(1): 59-65.
11. Gandhi RB, Robison JR: Oral cavity as a site for bioadhesive drug delivery, *Advance drug delivery reviews*, 1994; 13(1-2): 43-74.
12. Reddy LH, Ghosh B. and Rajneesh: Fast dissolving drug delivery systems, a review of the literature, *Indian Journal of pharmaceutical Sciences* 2002; 64(4): 331-336.
14. Liang AC, Chen LH: Fast dissolving drug delivery system, *Expert Opinion on therapeutic patents.*, 2001; 11(6):981-986.
15. Bi YX, Sunada H, Danjo K: Evaluation of Rapidly disintegrating tablet prepared by direct compression method, *Drug Development and Industrial Pharmacy*, 1999; 25(5):571-581.
16. Ishikawa T, Mukai B, Shiraishi S, Fuzi M, and Watanabe Y: Preparation of rapidly disintegrating tablet using new type of microcrystalline cellulose (PH-M Series) and low substituted Hydroxy propyl cellulose or spherical sugar granule by direct compression method, *Chemical Pharm. Bull.*, 2001; 49(2): 134-139.
17. Mahajan HS, Patil SB, and Gattani SG : Evaluation of rapidly disintegrating tablets for elderly patients, *The pharma review*, Oct.2005 ; 49-51.
18. Nayak SM and Gopalkumar P: Design and optimization of fast dissolving tablet for promethazine theoclate, *Indian drugs*, 2004; 41(9): 554-556.
19. Desai S.A, Kharade SV, and Petkar K.C: Orodissolving tablets of Promethazine HCl, *Indian journal of education research*, (2006); 40(3): 172-174.
20. Kaushik D, Saini TR, Dureja H: Development of melt in mouth tablet by sublimation Technique, *Journal of pharmaceutical research*, 2004; 3(2):35-37.
21. Gohel M, Patel M, Amin A, Agarwal R, Dave R, Bariya N: Formulation design and optimization of mouth dissolve tablets of nimuslide using vacume drying technique, *aaps pharm. sci. tech.*, 2004; 3(5):1-6.
22. Perissutti B, Rubessa F, Moneghini M and Voinovich D: Formulation design of carbamazepine fast- release tablet prepared by melt granulation technique. *International journal of pharmaceutics* 2003; 256: 53-63.
23. Panigrahi D, Beghel S, Mishra B: Mouth dissolving tablets: An overview of preparation techniques, evaluation and patented technologies, *journal of pharmaceutical research*, 2005; 4(3): 33-38.
24. Valleri M, Mura P, Maestrelli F, Cirri M, Ballerini R: Development and evaluation of glyburide fast dissolving tablets using solid dispersion technique, *Drug development and industrial pharmacy*, 2004; 30 (5): 525-534.
25. Cirri m, maestrelli F, Corti G, Mura P and valleri M: Fast dissolving tablets of glyburide based on ternary solid dispersion with PEG 6000 and surfactants, *drug delivery*, 2007; 14(4): 247-255.
26. Ghorab MK and Adeyeye MC: Enhanced bioavailability of process-induced fast dissolving ibuprofen co-granulated with beta-cyclodextrin, *journal of pharmaceutical science*, 2003; 92(8):1690-1707.
27. Dandagi PM, Sreenivas SA, Manvi FV and Patil MB : Taste masked ofloxacin mouth disintegrating tablets, *Indian drugs*, 2005 ; 42(1):52-55.
28. Chaudhari PD, Chaudhari SP, Kolhe SR, Dave KV and more DM: Formulation and evaluation of fast-dissolving tablets of famotidine, *Indian drugs*, 2005; 42 (10): 641-649.
29. Ahmed IS and Fatahalla FA, Pilot study of relative bioavailability of two oral formulations of ketoprofen 25 mg in healthy subjects. A fast-dissolving lyophilized tablet as compared to immediate release tablet, *Drug development and industrial pharmacy*, 2007; 33(5): 505-511.
30. Behnke K, Søgaard J, Martin S, Bäuml J, Ravindran AV, Agren H, Vester-Blokland ED: Mirtazapine orally disintegrating tablet versus sertraline: a prospective onset of action study, *Journal of Clinical Psychopharmacology*, 2003; 23(4): 358-364.
31. Van SEA, Lechat P, Remmerie BM, Ko G, Lasseter KC, Mannaert E: Pharmacokinetic comparison of fast-disintegrating and conventional tablet formulations of risperidone in healthy volunteers. *Clinical Therapeutics*, 2003; 25(6): 1687-1699.
32. Johannessen J, and Kristensen P: On-demand therapy in gastroesophageal reflux disease: a comparison of the early effects of single doses of fast-dissolving famotidine wafers and ranitidine tablets, *Clinical Therapeutics*, 1997; 19(1): 73-81.
33. Van SCA, lechat p, remmerie BM, Ko G, Lasseter KC, Mannaert E: Pharmaceutical comparison of fast disintegrating and conventional tablet formulation of risperidone in healthy volunteers., *clinical therapeutics* , 2003; 25(6):1687-1699.
34. Roger RA, Plazas Fernández MJ, Galván Cervera J, Heras Navarro J, Artés Ferragud M and Gabarrón Hortal E: Acceptance survey of a fast dissolving tablet pharmaceutical formulation in allergic patients. Satisfaction



UGC APPROVED JOURNALS NO. 48708

- and expectancies, *Allergol Immunopathol* (PubMed), 2006; 34 (3):107-112.
35. Diez-Ortego I, Cruz M, Largo R, Navarro A, Palacios I, Solans A, Sanchez-Pernaute O and Egido J: Studies of piroxicam absorption by oral mucosa, *Arzneimittelforschung*. (PubMed); 2002; 52(5):385-387.
 36. Vollmer, Paolo Galfetti RapidFilm: Oral Thin Films (OTF) as an Innovative Drug Delivery System and Dosage Form, technology overviews <http://www.labtec-pharma.com>; Accessed on sept 2007.
 37. Pavankumar GV, Ramakrishna V, William GJ and Konde A: Formulation and Evaluation of buccal films of salbutamole sulphate, *Indian Journal of pharmaceutical Sciences*, 2005; 67 (2): 160-164.
 38. Yang N, wang G and Zhang X: Release kinetic of catechins from chewing gum, *Journal of pharmaceutical Sciences*, 2003; 9(2): 293-299.
 39. Pandit A.P, and Joshi S.B: Formulation development of chewing gum as novel drug delivery system for Dltiazem hydrochloride, *Indian drug*, 2006 ; 43(9):725-772.
 40. Maggi L, segale L, conti S and Salini A: Preparation and evaluation of release characteristics of 3 TabGum, a novel chewing device, *European Journal of pharmaceutical Sciences*, 2004; 24: 487-493.



EXPLORING THE MECHANISM OF PROTOCATECHUIC ACID-MEDIATED HYPOLIPIDEMIC ACTIVITY IN ATHEROGENIC DIET-INDUCED HYPERLIPIDEMIC RATS

Gaddam Swetha Reddy

Asst. Professor, Department of Pharmaceutical Chemistry, Princeton College of
Pharmacy, Hyderabad, Telangana, India

Ajmeera Rajya Laxmi

Asst. Professor, Department of Pharmaceutical Chemistry, Princeton College of
Pharmacy, Hyderabad, Telangana, India

Abstract - An abnormally high blood level of fatty substances known as lipids, most commonly cholesterol and triglycerides, is called hyperlipidemia. Protocatechuic acid's hypolipidemic effects in atherogenic diet-induced hyperlipidemia were the goal of this study. The rats treated with Protocatechuic acid at doses of 25 and 50 mg/kg showed significant reductions in total cholesterol, triglyceride, total protein, and high density lipoprotein cholesterol in an atherogenic diet-induced hyperlipidemic model. Therefore, taking into account the effects that were observed in this model, it has been hypothesized that protocatechuic acid had significant hypolipidemic activity. This could be because it increased reverse cholesterol transport or increased cholesterol metabolism by activating lipoprotein lipase.

Keywords: Cholesterol, an atherogenic diet, protocatechuic acid, hyperlipidemia, and hypolipidemic activity

1 INTRODUCTION

Disorders of lipid metabolism, or hyperlipidemia, have been identified as one of the most significant risk factors for the occurrence and severity of atherosclerosis, stroke, and coronary heart disease^{1,2}. Hyperlipidemia is described by raised serum all out cholesterol, low thickness lipoprotein, extremely low-thickness lipoprotein (LDL, VLDL) cholesterol and diminished high-thickness lipoprotein (HDL) levels. The accumulation of fatty substances within the blood vessel lining is referred to as atherosclerosis. In the arterial wall, lipids undergo peroxidative change, eventually causing tissue damage. It is characterized by hardening and

thickening of the arterial walls and vascular areas with mononuclear and proliferating smooth muscle cells³.

One of the main risk factors is a high level of cholesterol, especially LDL-cholesterol. Atherosclerosis-related coronary heart disease remains a leading cause of death worldwide, both in developed and developing nations⁴. Atherosclerosis-related clinical syndromes include myocardial and cerebral infarctions, which are the leading causes of death worldwide. In the treatment of hyperlipidemia, lipid-lowering medications like fibrates, statins, and bile acid sequestrants can have harmful side effects. As a result, a less harmful lipid-lowering medication



is urgently required. Patients with hyperlipidemia and related complications are managed with a variety of herbal treatments⁸.

In Thailand, Hibiscus sabdariffa L. (roselle), also known as Krachiap daeng, it is widely grown. The primary component, which has a sour flavor and is utilized as a beverage and food colorant, is its red persistent calyx⁹. It is said to be a traditional Thai treatment for kidney stones. Additionally, it is used as an antifungal, antibacterial, hypocholesterolemic, diuretic, uricosuric, mild laxative, and antihypertensive¹⁰

The dried calyx extracts of these plants are currently prepared for sale as health food products in the form of granules and tea. They are advertised as being diuretic, hypocholesterolemic, and antihypertensive.

Since Hibiscus sabdariffa L. has hypocholesterolemic activity, the purpose of this study is to assess the hypolipidemic activity of its active component, protocatechuic acid, in rats subjected to hyperlipidemia caused by an atherogenic diet.

2 MATERIALS AND METHODS

Sigma Aldrich in the United States provided the protocatechuic acid. All

other chemicals were locally sourced and of analytical grade. The HDL-C and cholesterol kits came from Biolabs diagnostics MH. The Triglycerides Kit was purchased from India's Erba Diagnostics MH.

3 ANIMALS

Adult male Wistar albino rats weighing 200 to 220 grams were selected and kept in polypropylene cages in a room with a comfortable temperature of 27°C ± 1°C and 12-hour light and dark cycles.

The animals were fed a standard pellet diet and free access to water for seven days to help them adjust to their new surroundings. The creation of atherogenic diet utilized during the review was as given in Table-1. Every one of these treatment bunches comprised of six creatures /bunch. The Institutional Animal Ethics Committee (IAEC), which is part of the Committee for the Purpose of Control and Supervision of Experiments on Animals (CPCSEA), approved the study's protocol.

4 DOSE SELECTION AND ADMINISTRATION

According to reported activities, Protocatechuic acid at the doses of 25 and 50 mg/kg p.o. /day¹¹ was selected for the study.

Table 1 Composition of normal and atherogenic diet

Composition	Normal diet (%)	Atherogenic diet (%)
Protein (Milk powder)	12	10
Carbohydrates (Wheat flour)	71	61
Sugar	05	05
Fat (Butter)	05	16
Salts	04	04
Vitamins	01	02



UGC APPROVED JOURNALS NO. 48708

Fibers	02	01
Cholesterol	-	01
Total Weight	100g	100g

5 EXPERIMENTAL INDUCTION OF HYPERLIPIDEMIA

In order to induce hyperlipidemia, the method reported by Bopanna et al.¹² was followed. The animals were divided into four groups of six rats each and they received the following diets with or without treatment for 45 days orally:

Group I: Normal diet

Group II: Atherogenic diet containing 1% cholesterol.

Group III: Atherogenic diet + Protocatechuic acid (25 mg/kg/day).

Group IV: Atherogenic diet + Protocatechuic acid (50 mg/kg/day).

At the end of the treatment the rats were fasted overnight, blood was drawn from retro orbital plexus as per CPCSEA guidelines. Serum was separated and stored in refrigerator until assay.

6 MEASUREMENT OF SERUM LIPID PROFILE

Biochemical estimation kits (Biolabs diagnostics MH) were used for the photometric estimation of Total cholesterol (TC), total triglyceride (TG), total protein (TP) and total high density lipoprotein (HDL). The atherogenic index was calculated by using the following formula¹³.

Atherogenic index = Total serum cholesterol/ Total serum HDL - Cholesterol

7 CONCLUSION

In rats subjected to atherogenic diet-induced hyperlipidemia, treatment with protocatechuic acid resulted in a

significant decrease in the serum level of lipids. Therefore, taking into consideration the effects that are depicted in this model, the potential mechanism of Protocatechuic acid may involve an increase in HDL-cholesterol. This is because the Lecithin Cholesterol O-acyltransferase (LCAT) enzyme mobilizes cholesterol from peripheral cells to the liver¹⁵. The transesterification of cholesterol, HDL maturation, and cholesterol flux from cell membranes into HDL are all mediated by the LCAT enzyme. Therefore, we can conclude from the preceding findings that protocatechuic acid has hypolipidemic activity.

REFERENCES

1. Grundy S.M, "Cholesterol and coronary heart disease: A new era", J. Am. Med. Assoc, 1986, 256, pp. 2849.
2. Saravanan R, Rajendra P. N, Pugalandi KV, "Effect of *Piper beetle* leaf extract on alcoholic toxicity in the rat brain", J. Med. Food, 2003, 6, pp. 261.
3. Wick G, Romen M, Amberger A, Metzler B, Mayr M, "Atherosclerosis, autoimmunity, and vascular-associated lymphoid tissue", FASEBJ, 1997, 11, pp. 1199.
4. Davey SG, "Cholesterol lowering and mortality: The importance of considering initial level of risk", Int. Med. J, 1993, 306, pp. 1367.
5. Fuster V, Badimon L, Badimon JJ, "The pathogenesis of coronary artery disease and atherosclerosis", Circulation, 1994, 89, pp. 36.
6. Chattopadhyaya R, Pathak D, and Jindal DP, Indian Drugs, 1996, 33, pp. 85-97.
7. Jain S, Kathiravan M, Somania R, Shishooc C, "The biology and chemistry of hyperlipidemia.



UGC APPROVED JOURNALS NO. 48708

- Bioorganic & Medicinal Chemistry”, 2007, 15, pp. 4674–4699.
8. Dahanukar SA, Kulkarni RA, Rege NN, “Pharmacology of medicinal plants and natural products”, Indian J Pharmacol, 2000, 32, pp. S81-S118.
 9. Mahadevan N, Shivali and Kamboj P, “Hibiscus sabdariffa Linn.–An overview”. Natural Product Radiance, 2009, 8(1), pp. 77-83.
 10. Farnworth NR and Bunyapraphatsara N, “Thai Medicinal Plants”, Prachachon Press, Bangkok, 1992, pp. 163–166.
 11. Harini R and Pugalendi KV, “Antioxidant and antihyperlipidaemic activity of protocatechuic acid on streptozotocin-diabetic rats”, Redox report communications in free radical research, 2010, 15(2), pp. 71-80.
 12. Bopanna KN, Bhagyalakshmi N, Rathod SP, Balaraman R, Kannan J, “Cell culture derived *Hemidesmus indicus* in the prevention of hypercholesterolemia in normal and hyperlipidemic rats”, Indian J Pharmacol, 1997, 29, pp. 105.
 13. Gill PI, Rathgeb KA, Robinson CS, “Regulation of acyl Co A: cholesterol acyl transferase activity in normal and atherosclerotic rabbit aortas: role of a cholesterol substrate pool”, Experimental and Molecular Pathology, 1986, 44, pp. 320–339.
 14. Kulkarni SK & Kaur G, “Obesity: an insight into its neurochemical basis and treatment”, Indian. J. Pharmacol, 1999, 31, pp. 388.
 15. Tamura A, Fukushima M, Shimada K, Han KH, Sekikawa M, Watanabe S, Nakano M, Matsumoto M, Chiji H, “Cholesterol metabolism in rat is affected by protocatechuic acid”, J. Nutr. Sci, Vitaminol, 2004, 50(1), pp. 13-18.



ENHANCING THE SOLUBILITY AND BIOAVAILABILITY OF POORLY SOLUBLE DRUGS WITH SOLID DISPERSION: A COMPREHENSIVE REVIEW OF A PROMISING STRATEGY

Thandu Rajini

Asst. Professor, Department of Pharmaceutics, Princeton College of Pharmacy,
Hyderabad, Telangana, India

Malothu Suresh

Asst. Professor, Department of Pharmaceutics, Princeton College of Pharmacy,
Hyderabad, Telangana, India

Abstract- Due to issues with the solubility of poorly water-soluble drugs, improving oral bioavailability of drugs remains one of the most difficult aspects of formulation development. The majority of new chemical entities (NCEs) are poorly soluble in water and poorly absorbed when taken orally. Improved solubility and, consequently, oral bioavailability of BCS class II drugs can be achieved through solid dispersion technologies. Solid dispersion methods have caught on because they make it easier to dissolve highly lipophilic drugs and make them more bioavailable. This article audits on characterization, different readiness techniques, benefits and inconveniences of strong scattering.

Keywords: Carrier, Poorly water-soluble drug, Biopharmaceutical Classification, Solubility Enhancement, and Bioavailability Enhancement.

1 INTRODUCTION

A drug must be in solution for it to enter the systemic circulation and have a therapeutic effect, but relatively insoluble and poorly water-soluble drugs cause problems. As a result, formulation scientists continue to face difficulties in enhancing solubility and, consequently, oral bioavailability.

The most common and most effective method of drug administration is via oral route. The majority of new chemical entities (NCEs) that are intended for use as solid dosage forms exhibit an effective and reproducible in vivo plasma concentration upon oral administration. This is due to the advantages of the oral route, such as ease of production, smaller bulk, precise dosage, and greater stability.

After being taken orally, the drug first dissolves in the fluids of the stomach and/or intestines before permeating the GI tract's membranes and entering the systemic circulation.

As a result, a drug with a low aqueous solubility and a high membrane permeability will exhibit limited absorption rates at the dissolution rate and permeation rate, respectively. In order to increase the active pharmaceutical ingredient's (API) oral bioavailability, pharmaceutical research focuses on two aspects: i) boosting the solubility and rate of dissolution of drugs that are difficult to dissolve in water and ii) boosting the permeability of drugs that are difficult to penetrate³. BCS class II drugs are the focus of the majority of the solid dispersion



research reported. Drugs that have a high membrane permeability and low aqueous solubility are categorized as Class II drugs in the Biopharmaceutical Classification System (BCS). It is possible to increase their bioavailability and lessen side effects⁵⁻¹⁰ by enhancing these medications' drug release profiles. The modified Noyes-Whitney equation reveals some ways to increase the dissolution rate of even very poorly soluble compounds to lessen the barriers to oral bioavailability.

$$dC / dt = AD (C_s - C) / h$$

Where,

dC/dt = the rate of dissolution of drug,

A = the surface area available for dissolution,

D = the diffusion coefficient of the compound,

C_s = the solubility of the compound in the dissolution medium,

C = the concentration of drug in the medium at time t,

h = the thickness of the diffusion boundary layer adjacent to the surface of the dissolving compound.

2 SOLID SOLUTION

Similar to liquid solutions, solid solutions only have one phase regardless of the number of components. Medication's molecule size has been decreased to its outright least viz. the carrier's dissolution rate determines both the molecular dimensions¹⁶ and the dissolution rate. Their miscibility (continuous versus discontinuous solid solutions) or the manner in which the solvate molecules are distributed in the

solventum (substitutional, interstitial, or amorphous) are the criteria for their classification.

3 CONTINUOUS SOLID SOLUTIONS

The fact that the components are miscible in all proportions in a continuous solid solution indicates that the bonding strength between the two components is greater than the bonding strength between the molecules of each component individually. The pharmaceutical literature has not yet reported any continuous solid solutions.

3.1 Spray-Drying

In this technique the medication and transporter is broken down or suspended and afterward showering it into a surge of hot wind current to dissipate the dissolvable. Van Drooge and others by spraying a solution of povidone and diazepam into liquid nitrogen and forming a suspension that was then lyophilized, an alternative solid dispersion was prepared.

3.2 Freeze-Drying

The freeze-drying procedure involves submerging the drug and carrier in a common solvent until they are completely frozen. After that, more lyophilization is done on the frozen solution. The drug is subjected to minimal thermal stress during the formation of the solid dispersion and the risk of phase separation is minimized when freeze drying, both of which are significant advantages.

3.3 Supercritical Fluid Method

Using this method, CO₂ is simultaneously introduced into a



particle formation vessel through a nozzle while the drug and carrier are dissolved in a common solvent. The solid dispersion particles are precipitated as a result of the SCF rapidly extracting the solvent during spraying.

3.4 Co-Precipitation Method

In this technique non dissolvable is added drop wise to the medication and transporter arrangement, under consistent blending. So the medication and transporter are coprecipitated to form miniature particles. The microparticle suspension is then dried and filtered.

3.5 Dropping Method

It is a new procedure in that a solid dispersion of a melted drug carrier mixture is pipetted and then dropped onto a plate, where it solidifies into round particles. This method also avoids the pulverization, sifting and compressibility difficulties.

3.6 Advantages of Solid Dispersions

Carriers with surface activity, such as cholic acid and bile salts, when used, can significantly increase the wettability properties of drugs.

A high surface area is formed, resulting in an increased dissolution rate and, consequently, improved bioavailability.

Solid dispersions containing linear polymers produce larger and more porous particles than those containing reticular polymers and, therefore, result in a higher dissolution rate.

Presenting drugs in amorphous form increase the solubility of the particles.

3.7 Disadvantages of Solid Dispersions

Problems with solid dispersion's commercial application, including (a) its method of preparation, (b) the reproducibility of its physicochemical properties, (c) its formulation into dosage forms, (d) the scaling up of manufacturing processes, and (e) the drug's and vehicle's physical and chemical stability. Stage partition, precious stone development or transformation of an item to more steady construction from metastable translucent structure during capacity are significant impediments as they bring about diminished solvency and hence disintegration rate.

4 CONCLUSION

Improve the solubility and oral bioavailability of poorly water-soluble drugs with solid dispersion. The drug is released as fine colloidal particles when the solid dispersion is exposed to aqueous media, dissolving the carrier. Because the carriers can either speed up or slow down drug release, this technology has a lot of potential for controlled release dosage forms.

REFERENCES

1. Ikegami K, "Bioavailability and in vivo release behavior of controlled release multiple-unit theophylline dosage forms in beagle dogs, cynomolgus monkeys, and gottingen minipigs". *J. Pharm. Sci.*, 2006, 95, 1888-1895.
2. Charman SA and Charman WN, Oral modified-release delivery systems. In *Modified-Release Drug Delivery Technology* (Rathbone, M.J. et al. eds), Marcel Dekker, 2003, 1-10.
3. Lewis K, Dhirendra K, Udupan N, Atin K, Manipal College of Pharmaceutical Sciences, Manipal, Karnataka, India, *Pak J. Pharm. Sci.*, 22, 2009, 234-246.



UGC APPROVED JOURNALS NO. 48708

4. Amidon GL, Lennernas H, Shah VP, Crison JR, "Theoretical basis for a biopharmaceutical drug classification: the correlation of in vitro drug product dissolution and in vivo bioavailability", *Pharm Res*, 1995, 2(3), 413-420.
5. Van Drooge DJ, "Characterization of the molecular distribution of drugs in glassy solid dispersions at the nano-meter scale, using differential scanning calorimetry and gravimetric water vapour sorption techniques", *Int. J. Pharm.*, 2006, 310, 220-229.
6. Streubel A, "Drug delivery to the upper small intestine window using gastroretentive technologies", *Curr. Opin. Pharmacol.* 2006, 6, 501-508.
7. Tanaka N, "Development of novel sustained-release system, disintegrationcontrolled matrix tablet (DCsMT) with solid dispersion granules of nilvadipine (II): In vivo evaluation", *J. Contr. Release*, 112, 51-56.
8. Leuner C, Dressman J, "Improving drug solubility for oral delivery using solid dispersions", *Eur. J. Pharm. Biopharm.*, 2000, 50, 47-60.
9. Majerik V, "Bioavailability enhancement of an active substance by supercritical antisolvent precipitation", *J. Supercrit. Fluids*, 2007, 40, 101-110.
10. Prabhu S, "Novel lipid-based formulations enhancing the in vitro dissolution and permeability characteristics of a poorly water-soluble model drug, Piroxicam". *Int. J. Pharm.*, 2005, 301, 209-216.
11. Noyes A, Whitney WR, "The rate of solution of solid substances in their own solutions", *J. Am. Chem. Soc.*, 1897, 19, 930-934.
12. Sekiguchi K, Obi N, "Studies on Absorption of Eutectic Mixture. I. A comparison of the behaviour of eutectic mixture of sulfathiazole and that of ordinary sulfathiazole in man", *Chem. Pharm. Bull*, 9, 1961, 866-872.
13. Goldberg AH, Gibaldi M, Kanig JL, "Increasing dissolution rates and gastrointestinal absorption of drugs via solid solutions and eutectic mixtures II - experimental evaluation of a eutectic mixture: urea-acetaminophen system", *J. Pharm. Sci.*, 55, 1966, 482-487.
14. Castellan GW, *Physical Chemistry*, Addison-Wesley, Menlo Park, CA, 1983, 324-336.
15. Swarbrick J, *Encyclopedia of Pharmaceutical Technology*, 3, 2006, 775- 777.
16. Goldberg AH, Gibaldi M, Kanig JL, "Increasing dissolution rates and gastrointestinal absorption of drugs via solid solutions and eutectic mixtures. I. Theoretical considerations and discussion of the literature", *J. Pharm. Sci*, 1965, 54(8), 1145-1148.
17. Hume-Rotherly W, Raynor GV, *The Structure of Metals and Alloys*, Institute of Metals, London, 1954.
18. Chiou WL, Riegelman S, "Pharmaceutical applications of solid dispersion systems", *J. Pharm. Sci*, 1971, 60, 1281-1302.
19. Reed-Hill RE, *Physical Metallurgy Principles*, Van-Nostrand, Princetown, NJ, 1964.
20. Chiou WL, Riegelman S, "Preparation and dissolution characteristics of several fastrelease solid dispersions of griseofulvin", *J. Pharm. Sci.* 1969, 58, 1505-1510.
21. Kreuter J, Dispersionen F, in: Kreuter J, Herzfeldt CD (Eds.), *Grundlagen der Arzneiformenlehre Galenik*, 2, Springer, Frankfurt am Main, 1999, 262-274.
22. Vilhelmsen T, "Effect of a melt agglomeration process on agglomerates containing solid dispersions", *Int. J. Pharm.*, 303, 2005, 132-142.
23. Mooter G, "Evaluation of Inutec SP as a new carrier in the formulation of solid dispersions for poorly soluble drugs", *Int. J. Pharm*, 2006, 316, 1-6.
24. Won DH, "Improved physicochemical characteristics of felodipine solid dispersion particles by supercritical antisolvent precipitation process", *Int. J. Pharm*, 2005, 301, 199-208.
25. Pokharkar VB, "Development, characterization and stabilization of amorphous form of a low Tg drug", *Powder Technol*, 2006, 167, 20-25.



A REVIEW OF NIOSOMES AS A VIABLE DRUG DELIVERY SYSTEM

Dr. Harikiran Lingabathula

Asso. Professor, Department of Pharmacology Princeton College of Pharmacy,
Hyderabad, Telangana, India

Soorammagari Sunayana

Asst. Professor, Department of Pharmacology Princeton College of Pharmacy,
Hyderabad, Telangana, India

Abstract - A novel method for delivering drugs, niosomes contain the medication within a vesicle. The term "Niosomes" refers to the bilayer of non-ionic surface active agents that make up the vesicle. The niosomes are extremely small, typically measured in microns. The nanometric scale describes their size. They have a number of advantages over liposomes despite being structurally similar to them. Since it has recently been demonstrated that niosomes can be used for both targeted drug delivery and transdermal drug delivery, further research into these structures may lead to the development of novel drug delivery strategies.

Keywords: Diclofenac sodium, Niosome, Methotrexate, Cholesterol, Dicetyl phosphate, Maltodextrin, Doxorubicin.

1 INTRODUCTION

Niosomes are vesicles of a non-ionic surfactant that are produced when synthetic non-ionic surfactants are hydrated, either with or without cholesterol or other lipids added. They look like liposomes. That can serve as carriers for drugs that are lipophilic and amphiphilic. By limiting the drug's action to the target cells, it is less toxic and increases its therapeutic index. Niosomes are tiny, lamellar structures produced by combining cholesterol with a non-ionic surfactant of the alkyl or dialkyl polyglycerol ether class and then hydrating the mixture in aqueous media.

The properties of the vesicles can be changed by shifting the synthesis of the vesicles, size, lamellarity, tapped volume, surface charge and focus.

Within the vesicle, a variety of forces operate, such as van der Waals forces between surfactant molecules,

repulsive forces resulting from electrostatic interactions between charged groups of surfactant molecules, entropic repulsive forces of surfactant head groups, short-acting repulsive forces, etc. The vesicular structure of niosomes is maintained by these forces. In any case, the dependability of niosomes are impacted by kind of surfactant, nature of epitomized drug, capacity temperature, cleansers, utilization of layer spreading over lipids, the interfacial polymerization of surfactant monomers in situ, consideration of charged atom.

Niosomes may release the drug in a controlled manner as a depot. By preventing the drug from entering the biological environment and limiting its effects to target cells, delayed clearance from the circulation can also improve the herapeutic performance of the drug molecules.

Niosomes resemble liposomes in that they entrap solute. They are osmotically active, stable on their own, and they also improve the entrapped drugs' stability. Surfactants do not require any special conditions for handling or storage. Due to their infrastructure of hydrophilic and hydrophobic moieties working together, niosomes are able to accommodate drug molecules of varying solubilities. They can be designed to suit the desired situation and have structural characteristics like composition, fluidity, and size that are flexible. Niosomes enhance drug penetration through the skin and increase the oral bioavailability of poorly absorbed drugs⁸. They can be administered orally (niosomes are better absorbed than liposomes because phospholipids have been replaced by nonionic surfactants, making niosomes less susceptible to the action of bile salts), parenterally⁹, or topically. By incorporating hydrophilic groups such as poly (ethylene glycol), concanavalin A, and polysaccharide into the non-ionic surfactant, they function as stealth or long-circulating niosomes and make it possible for hydrophilic moieties to attach to their surface and cause changes in vivo. To control the rate of drug delivery, niosomal dispersion in the aqueous phase can be emulsified in the non-aqueous phase and administered to normal vesicles in the extended non-aqueous phase.

2 NIOSOMES Vs. LIPOSOMES

Niosomes are vesicles of a non-ionic surfactant that are produced when synthetic non-ionic surfactants are hydrated, either with or without cholesterol or other lipids added. They

look like liposomes. That can serve as carriers for drugs that are lipophilic and amphiphilic. By limiting the drug's action to the target cells, it is less toxic and increases its therapeutic index. Niosomes are tiny, lamellar structures produced by combining cholesterol with a non-ionic surfactant of the alkyl or dialkyl polyglycerol ether class and then hydrating the mixture in aqueous media.

The properties of the vesicles can be changed by shifting the synthesis of the vesicles, size, lamellarity, tapped volume, surface charge and focus.

Within the vesicle, a variety of forces operate, such as van der Waals forces between surfactant molecules, repulsive forces resulting from electrostatic interactions between charged groups of surfactant molecules, entropic repulsive forces of surfactant head groups, short-acting repulsive forces, etc. The vesicular structure of niosomes is maintained by these forces. In any case, the dependability of niosomes are impacted by kind of surfactant, nature of epitomized drug, capacity temperature, cleansers, utilization of layer spreading over lipids, the interfacial polymerization of surfactant monomers in situ, consideration of charged atom.

Niosomes may release the drug in a controlled manner as a depot. By preventing the drug from entering the biological environment and limiting its effects to target cells, delayed clearance from the circulation can also improve the herapeutic performance of the drug molecules.

Niosomes resemble liposomes in that they entrap solute. They are

osmotically active, stable on their own, and they also improve the entrapped drugs' stability. Surfactants do not require any special conditions for handling or storage. Due to their infrastructure of hydrophilic and hydrophobic moieties working together, niosomes are able to accommodate drug molecules of varying solubilities⁶. They can be designed to suit the desired situation⁷ and have structural characteristics like composition, fluidity, and size that are flexible. Niosomes enhance drug penetration through the skin and increase the oral bioavailability of poorly absorbed drugs. They can be administered orally (niosomes are better absorbed than liposomes because phospholipids have been replaced by nonionic surfactants, making niosomes less susceptible to the action of bile salts), parenterally⁹, or topically. By incorporating hydrophilic groups such as poly (ethylene glycol), concanavalin A, and polysaccharide into the non-ionic surfactant, they function as stealth or long-circulating niosomes and make it possible for hydrophilic moieties to attach to their surface and cause changes in vivo. To control the rate of drug delivery, niosomal dispersion in the aqueous phase can be emulsified in the non-aqueous phase and administered to normal vesicles in the extended non-aqueous phase.

3 METHOD OF PREPARATION

A. The ether injection method This technique makes niosomes by slowly introducing a surfactant solution dissolved in diethyl ether into warm, 60°C water. A 14-gauge needle is used to inject the ether-surfactant mixture into an aqueous material solution.

Vesicles with one layer are formed when ether is vaporized. The vesicle's diameter can range anywhere from 50 to 1000 nm depending on the conditions that were used.

B. Hand shaking (Thin film hydration technique)

In a round bottom flask, the mixture of vesicle-forming ingredients like cholesterol and surfactant is dissolved in a volatile organic solvent like diethyl ether, chloroform, or methanol. Using a rotary evaporator, the organic solvent is evaporated at room temperature (20°C), leaving behind a thin layer of solid mixture on the flask's wall. At temperatures between 0 and 60 °C, the dried surfactant film can be gently rehydrated with aqueous phase. The typical multilamellar niosome is produced by this process. By evaporating the organic solvent at 60°C and leaving a thin layer of lipid on the wall of the rotary flash evaporator, thermosensitive niosomes were made. The drug-containing aqueous phase was slowly added by intermittently shaking the flask at room temperature and then by sonication.

4 APPLICATIONS

1) Neoplasia

Doxorubicin, the anthracyclic antibiotic with broad spectrum anti tumor activity, shows a dose dependant irreversible cardio toxic effect. Niosomal delivery of this drug to mice bearing S-180 tumor increased their life span and decreased the rate of proliferation of sarcoma. Niosomal entrapment increased the half-life of the drug, prolonged its circulation and altered its metabolism. Intravenous

administration of methotrexate entrapped in niosomes to S-180 tumor bearing mice resulted in total regression of tumor and also higher plasma level and slower elimination.

2) Targeting of bioactive agents

a) To reticulo-endothelial system (RES)

The cells of RES preferentially take up the vesicles. The uptake of niosomes by the cells is also by circulating serum factors known as opsonins, which mark them for clearance. Such localized drug accumulation has, however, been exploited in treatment of animal tumors known to metastasize to the liver and spleen and in parasitic infestation of liver.

(b) To organs other than RES

It has been suggested that carrier system can be directed to specific sites in the body by use of antibodies. Immunoglobulins seem to bind quite readily to the lipid surface, thus offering a convenient means for targeting of drug carrier. Many cells possess the intrinsic ability to recognize and bind particular carbohydrate determinants and this can be exploited to direct carriers system to particular cells.

3) Leishmaniasis

Niosomes can be used for targeting of drug in the treatment of diseases in which the infecting organism resides in the organ of reticuloendothelial system. Leishmaniasis is such a disease in which parasite invades cells of liver and spleen. The commonly prescribed drugs are antimonials, which are related to arsenic, and at high concentration

they damage the heart, liver and kidney.

5 NIOSOMES AS DRUG CARRIERS

Muramic acid and triglycerol surfaces on doxorubicin niosomes were not significantly absorbed by the liver. Muramic acid vesicles and triglycerol niosomes accumulated in the tumor and spleen, respectively. The polyoxyethylene-coated vesicles were rapidly absorbed by the liver and less extensively accumulated in the tumor.

Methotrexate-loaded niosomes were prepared and administered to mice via oral and intravenous routes by Azmin et al.⁸. When compared to the free drug solution, they observed a significant increase in Methotrexate uptake in the liver from niosomes and a significant prolongation of plasma levels.

By incorporating polyethylene alkyl ether into the bilayered structure of niosomes, Cable et al.³⁵ altered the surface of the particles. They looked at the delivery example and plasma level of Doxorubicin in niosomes and Doxorubicin blended in with void niosomes and noticed a maintained and higher plasma level of doxorubicin from niosomes in mice.

The anti-inflammatory properties of niosome-encapsulated Diclofenac sodium in arthritic rats were documented by Raja Naresh et al.¹⁹. It was discovered that the niosomal formulation made by mixing Tween 85 in a 1:1 ratio produced a more consistent anti-inflammatory effect that lasted for more than 72 hours after a single dose was taken.

Namdeo et al announced the definition and assessment of Indomethacin stacked niosomes and showed that helpful adequacy

expanded and all the while poisonous aftereffect decreased as contrasted and free Indomethacin in pawoedema bearing rodents. Methotrexate niosome formation and pharmacokinetic evaluation in tumor-bearing mice were documented by Chandraprakash.

6 CONCLUSION

The use of liposomes or niosomes allows for improved drug targeting at the appropriate tissue. Niosomes are a magical module for the delivery of drugs. Niosomes are thought to be better candidates for drug delivery than liposomes due to various factors such as cost, stability, and so on because they have a structure that is similar to that of a liposome. As a result, they can represent alternative vesicular systems in comparison to liposomes. Niosomes can be used for targeting, ophthalmic, topical, parenteral, and other forms of drug delivery. Because it is a promising targeted drug delivery system, research is ongoing to develop a suitable technology for large-scale production. Niosomes are an alternative to liposomes that are biodegradable, relatively nontoxic, and more stable.

REFERENCES

1. Breimer DD, Speiser R, "Topics in pharmaceutical Sciences", Elsevier Science Publishers, New York, USA, 1985, 291.
2. Udupa N, Jain NK, Niosomes as drug carriers. Controlled and novel drug delivery. 1st ed.
3. Baillie AJ, Florence AT, Hume LR, Muirhead GT, Rogerson A, "The preparation and properties of niosomes - non-ionic surfactant vesicles", J Pharm Pharmacol, 1985, 37, 863-8.
4. Rogerson A, Cummings J, Willmott N, Florence AT, "Niosome as control drug delivery system", J. Pharm. Pharmacol., 1988, 40, 337.
5. Baille AJ, Florence AT, Hume LR, Muirhead GT, Rogerscon A, "Non-ionic surfactant vesicles for targeted drug delivery system", J. Pharm. Pharmacol. (suppl.), 1984, 36, 48.
6. Udupa N, Pillai GK, "Niosome as a nonionic surfactant", Pharmag, 1991, 3, 45.
7. Chitnis MP, Menon RS, Gede RP, "Pharmacokinetic parameter of niosome". Tumori, 1984, 70, 313.
8. Azmi MN, Florence AT, Handjani-vila RM, Stuart JF, Vanlerberghe G, Whittaker JS. "Niosome use as cancer therapy", J. Pharm. Pharmacol, 1985, 37, 237.
9. Ruckmani K, Jayakar B, Ghosal SK, "Drug in niosome for magical delivery". Drug Develop. Ind. Pharm., 2000, 26, 217.
10. Dufes C, Schatzlein AG, Tetley L, Gray AI, Watson DG, Olivier JC, Couet W, Uchegbu IF, "Liposome as a novel drug delivery". Pharm. Res., 2000, 17, 1250.
11. Buckton G, Harwood, "Interfacial phenomena in Drug Delivery and Targeting", Academic Publishers, Switzerland, 1995, 154-155.
12. Don A, Van H, Joke AB, Hans E, Ph.D. thesis, "Nonionic surfactant vesicles containing estradiol for topical application", Centre for drug research. 1997, 330-339.
13. Handjani-Vila R.M, Ribier A, Rondot B, Vanlerberghe G. "Dispersions of lamellar phases of non-ionic lipids in cosmetic products", Int. J. Cosmetic Sci. 1979, 1, 303-314.
14. McCormack B, Gregordias G., "Drugs- α -cyclodextrins- in-liposomes: an approach to controlling the fate of water insoluble drugs in vivo", Int. J. Pharm. 1998, 162, 59-69.
15. Baillie AJ, Florence AT, Hume LR, Rogerson A, Muirhead GT, "The preparation and properties of niosomes-nonionic surfactant vesicles", J. Pharm Pharmacol., 1985, 37(12), 863-868.
16. Chandraprakash KS, Udupa N, Umadevi P, Pillai GK, "Pharmacokinetic evaluation of surfactant vesicles containing methotrexate in tumor bearing mice", Int. J. Pharma, 1990, R1-R3, 61.

17. Rogerson A, Cummings J, Willmott N, Florence AT, "The distribution of doxorubicin in mice following administration in niosomes", *J Pharm Pharmacol.*, 1988, 40(5), 337-342.
18. Baillie AJ, Coombs GH, Dolan TF, "Nonionic surfactant vesicles, niosomes, as delivery system for the anti-leishmanial drug, sodium stibogluconate", *J. Pharm. Pharmacol.* 1986, 38, 502-505.
19. Raja Naresh RA, Chandrashekhara G, Pillai GK, Udupa N, "Anti-inflammatory activity of Niosome encapsulated diclofenac sodium with Tween-85 in Arthritic rats", *Ind. J. Pharmacol*, 1994, 26, 46-48.
20. Khandare JN, Madhavi G, Tamhankar BM, "Niosomes novel drug delivery system", *The Eastern Pharmacist*, 1994, 37, 61-64.

A CRITIQUE OF THE POLYMERS EMPLOYED IN IN-SITU GEL DRUG DELIVERY SYSTEMS

Dr. P. Raja Sridhar Rao

Asst. Professor, Department of Pharmaceutics, Princeton College of Pharmacy,
Hyderabad, Telangana, India

G Satheesh

Asst. Professor, Department of Pharmaceutics, Princeton College of Pharmacy,
Hyderabad, Telangana, India

Abstract - Before being administered to the body, in situ gel drug delivery systems are used in sol form; however, once administered, they undergo gelation in situ to form a gel. The changes in temperature, pH, the presence of ions and ultraviolet irradiation, electrical sensitivity, and enzyme sensitivity all play a role in the formation of the gel, which is where the drug is released in a controlled and sustained manner. Hydrogels used in biomedical applications typically have aqueous solutions that are typically liquid at room temperature and gel at physiological temperature. When compared to conventional drug delivery systems, the in situ gel-forming polymeric formulations offer a number of advantages, including sustained and prolonged action. From a manufacturing perspective, the investment and manufacturing costs are lower because these devices are produced with less complexity. The use of natural and synthetic polymers as polymers is the focus of this review.

Keywords: In-situ drug delivery, transformation from sol to gel, natural and synthetic polymers.

1 INTRODUCTION

The development of drug administration vehicles that are technologically superior is a major objective of pharmaceutical technology. Imaginative cycles permitted an upgrade in the organoleptic properties of the arrangements and the amplification of the solidness and bioavailability. The low solubility of approximately fifty percent of the approved active molecules in the physiological aqueous environment, which results in limited gastrointestinal absorption and poor bioavailability, is still a drawback. Although parenteral and even topical formulations face challenges due to limited solubility, oral administration of therapeutic

agents is the method of choice for ensuring patient compliance.

because higher bioavailability typically correlates well with improved solubility. To ensure the proper drug solubilization, a number of nanotechnological strategies are being pursued⁴. Nanoparticle engineering is one worth mentioning among them.

Hydrogels are polymeric organizations that can ingest and hold a lot of water and natural liquids and swell, actually keeping up with their three-layered structure. The hydrogel structure is created when these polymeric networks' hydrophilic domains are hydrated in an aqueous environment. The presence of cross-links that prevent the hydrophilic

polymer from dissolving in an aqueous medium is referred to as a network. Hydrogels outperform other drug delivery systems thanks to their biocompatibility and superior mechanical and optical properties. Hydrogel degradation products are typically less toxic or nontoxic. Protein adsorption and cell adhesion on the hydrogel's surface are minimized by a lower interfacial tension between the hydrogel's surface and the physiological fluid. When used as in vivo implants, the soft, rubbery nature of hydrogels can also reduce mechanical irritation. There are currently two distinct categories of hydrogels: preformed and in situ-forming gels. Preformed hydro gels are straightforward, viscous solutions that do not change after being administered. Formulations applied as solutions, sols, or suspensions that undergo gelation following instillation due to stomach-specific physicochemical changes are known as in situ gels.

1.1 In-Situ Gel Delivery Systems

After the composition or formulation has been applied to the application site, a process known as in-situ gelation occurs. The terms "sites of application" and "injection sites," "topical application sites," and "surgical sites," respectively, all refer to locations in human and animal medicine where the agents come into contact with tissues or bodily fluids. As a medication conveyance specialist, the in-situ gel enjoys a benefit connected with the gel or polymer network being shaped in-situ giving supported arrival of the medication. Simultaneously, it allows the medication to be conveyed in a

fluid structure. The Latin word "in situ" means "in the place."

U.S. Pat. reveals the compositions for in-situ gelation made with ionic polysaccharides. No. 5,958,443, which reveals compositions that include a drug, a film-forming polymer, and an ionic polysaccharide that forms a gel (like alginate). These compositions utilized two independently applied components: a solution of cross-linking cations is applied to the site, and a second liquid component, which consists of the drug, a film-forming polymer, and an ionic polysaccharide, reacts with the cross-linking ions to form a gel. Starches and modified celluloses, gellan, chitosan, hyaluronic acids, pectins, and other similar polymers have also been used in drug delivery formulations that may or may not have formed cross-linked gels.

2 NATURAL POLYMERS AND DERIVATIVES

Many natural polymers have been shown to exhibit gelation upon temperature change. Researchers have used them alone or in combination with synthetic polymers to fabricate thermally responsive hydrogels with desired properties.

3 POLYSACCHARIDES CELLULOSE DERIVATIVES

Natural polymers can be used to make thermoreversible gels. When the temperature of the majority of natural polymer aqueous solutions is decreased, a gel phase develops. Gelatin and carrageenan are classic examples of natural polymers that transition from sol to gel. In solution, these polymers take on a random coil

shape at high temperatures. Partially helix formation results in the formation of a continuous network upon cooling. This gelation mechanism is not applicable to all cellulose derivatives. Their aqueous solutions are liquid at low temperatures at low concentrations (1–10%wt), but they gel when heated. Examples of such polymers include hydroxypropyl methylcellulose (HPMC) and methylcellulose (methylcellulose). HPMC undergoes a phase transition between 75 and 90 °C, whereas methylcellulose solutions turn opaque gels between 40 and 50 °C. These phase transition temperatures can be lowered through chemical or physical modifications. Gelation of methylcellulose or HPMC solutions is primarily caused by the hydrophobic interaction between molecules containing methoxy substitution. For instance, NaCl lowers the transition temperature of methylcellulose solutions to 32–34 °C, while reducing the hydroxypropyl molar substitution of HPMC lowers its transition temperature to 40 °C. The macromolecules are hydrated at low temperatures, and the only interaction between polymers is simple entanglement. The polymers gradually lose their water of hydration as the temperature rises, as evidenced by a decrease in relative viscosity.

4 GELLAN GUM

Gellan gum is a commercially available exocellular polysaccharide that is linear, anionic, and deacetylated. It is produced by the microbe *Sphingomonas paucimobilis*, which was formerly known as *Pseudomonas elodea*. It has a tetrasaccharide repeating unit that

consists of one -L-rhamnose, one -D-glucuronic acid, and two - The temperature-dependent and cation-induced gelation that results in the formation of double-helical junction zones and the aggregation of the double-helical segments into a three-dimensional network through complexation with cations and hydrogen bonding with water is its distinctive property. Gelrite w or Kelcogel w (Kelco division of Merck and Co., USA) are the names given to the acetylated form. Deacetylated gellan gum is approved for use as a gelling, stabilizing, and suspending agent in food products in both the US and the EU. The presence of monovalent or divalent ions like Na⁺ and Ca²⁺ causes the sol-gel transition. The temperature of the preparation, the polysaccharide concentration, and the nature and concentration of cations are some additional parameters that have an impact on the phase transition.

When it came to promoting the gellation of the polysaccharide, it was determined that divalent ions like calcium or magnesium performed better than monovalent cations did. Deacetylated gellan gum has been extensively studied for use as an in situ gelling agent in ocular formulations due to its capacity to form strong, clear gels at physiological ion concentrations. It has been accounted for to give an essentially drawn out corneal contact time in correlation with customary arrangements and is as of now promoted in the controlled-discharge timolol plan Blocadren Warehouse (Timoptic-XEw). Gellan gum has also been proposed as a promising polymer for nasal formulations.

However, to our knowledge, it has only been included in one study on this topic, in which it was demonstrated to moderately enhance the local and serum antibody response in mice following viral antigen administration via nasal route. On the other hand, temperature and pH-responsive gels and other in situ gelling systems that have been shown to increase residence time and enhance drug absorption have appeared more frequently in nasal drug delivery studies. This material's use in ophthalmic drug delivery has received the most attention in the pharmaceutical industry; Due to the temperature and ionic conditions in the tear fluid, aqueous gellan solutions dropped into the eye change into a gel. However, accidental gelation does not occur during storage like it does with thermo reversible gels because the presence of lachrymal fluid is required to elicit gel formation. However, the concentration of sodium chloride that is sufficient to elicit gelation is between 2 and 6 g/l.

5 SODIUM ALGINATE

Alginic acid is a linear block copolymer polysaccharide that is linked by a 1,4-glycosidic link between the residues -D-mannuronic acid (M) and -L-guluronic acid (G). The algal source determines how each block is distributed and how it is arranged along the molecule. When di- and trivalent metal ions are added to diluted aqueous solutions of alginates, a co-operative process involving consecutive guluronic residues in the G blocks of the alginate chain results in firm gels. This property has been widely used to

create vehicles, usually as matrix devices, for the long-term delivery of bioactive molecules. It comprises predominantly of sodium salt of Alginic corrosive; Each unit of a polyuronic acid has a free - D-mannuronic acid carboxyl group, and the glycosidic linkage protects the aldehyde group.

Alginates have only been mentioned in a few reports when they are used in oral sustained release liquid preparations. Zatz and Woodford created a sodium alginate-containing suspension of theophylline that gelled upon contact with simulated gastric fluid. For the purpose of eliminating *Helicobacter pylori*, a liquid sustained release formulation containing sodium alginate was presented by another author. In this formulation, in situ gelling was achieved by administering a calcium salt solution orally immediately following the sodium alginate solution. Similar to the above-mentioned method for gellan in situ gelation, a different approach to achieving in situ gelation of sodium alginate solutions has been reported. Through complexation of the Ca^{2+} ions with sodium citrate, gelation of a sodium alginate solution containing Ca^{2+} ions is delayed until the preparation reaches the stomach's acidic environment. Despite the fact that the aforementioned commercial preparations contain sodium alginate, they do not include a metal ion source. Naturally, these commercial preparations do not intend for the alginate to form a gel matrix in the stomach, as in the formulations discussed, but rather to form a raft on the surface, thereby reducing acid regurgitation.

6 CONCLUSION

The decision of a specific hydrogel relies upon its natural properties and imagined helpful use. When ophthalmic applications are taken into consideration, for instance, the formation of a transparent gel is of particular significance. Gels that are not biodegradable may be useful for administration methods other than parenteral. Perhaps the most extensively studied systems are poloxamer hydrogels. However, despite their clinical acceptance as solubilizers and thickeners, poloxamers have not lived up to initial expectations as biomedical implants. This is primarily due to the fact that these polymers are not biodegradable and cannot provide sustained drug delivery for more than a few days. In most cases, polysaccharides have good biocompatibility and/or biodegradability, and their solutions, even at low polymeric concentrations, are thermosensitive. Due to their large, water-filled pores, these systems may not be suitable for the sustained release of hydrophilic, low molecular weight drugs. On the other hand, they provide sufficient scaffolds for tissue repair and cell growth. One of the thermoresponsive systems that has received the most research is poly(N-isopropylacrylamide) and its copolymers with other polymers, whether they are synthetic or natural. The intrinsic shortcomings of pNiPAAm, such as its non-biodegradability and mechanical properties, can be mitigated with the proper copolymerization.

For pharmaceutical purposes, PEO/PLGA hydrogel systems are particularly appealing. They generally have a favorable safety profile and are

biodegradable. After parenteral extravascular administration, their composition can be tailored to provide drug delivery for several weeks or months. The use of in-situ gels with a thermosensitive sol-gel behavior as cell carriers for tissue regeneration has recently been reported.

REFERENCES

1. Francis MF, Cristea M, Winnik FM, "Polymeric micelles for oral drug delivery: Why and how", *Pure Applied Chemistry*, 2004, 76(7-8), 1321- 1335.
2. Amidon GL, Lennernas H, Shah VP, Crison JR, "A theoretical basis for a biopharmaceutical drug classification: the correlation of in vitro drug product dissolution and in vivo bioavailability", *Pharmaceutical Research*, 1995, 12(3), 413-420.
3. Lipinski C, "Poor aqueous solubility – an industry wide problem in drug delivery", *American Pharma Review*, 2002, 5, 82-85.
4. Hasirci V, Vrana E, Zorlutuna P, Ndreu A, Yilgor P, Basmanay FB, Aydin E, "Nanobiomaterials: a review of the existing science and technology, and new approaches", *Journal of Biomaterial Science and Polymer*, 2006, 17(11), 1241-1268.
5. Hu J, Johnston KP, Williams III RO, "Nanoparticle engineering processes for enhancing the dissolution rates of poorly water soluble drugs, *Drug Delivery*". *Indian Pharmacy*, 2004, 30(3), 233-245.
6. Overhoffa KA, Engstrom JD, Chenc B, Scherzerd BD, Milnerc TE, Johnston KP, Williams III RO, "Novel ultra-rapid freezing particle engineering process for enhancement of dissolution rates of poorly water-soluble drugs", *European Journal of Pharmacy and Biopharmaceutics*, 2007, 65(1), 57-67.
7. Muller RH, Jacobs C, Kayser O, "Nanosuspensions as particulate drug formulations in therapy rational for drug development and what we can expect for the future", *Advanced Drug Delivery Review*, 2001, 47(1), 3-19.
8. Kipp JE, "The role of nanoparticle technology in the parenteral delivery of poorly water-soluble drugs",

- International Journal of Pharmacy, 2004, 284(1-2), 109-122.
9. Saraswat R, Bhan CS, Gaur A, "A review on polymers used in in-situ gel drug delivery systems", International Journal of Pharmaceutical Innovations, 2011, 1(2), 111-118.
 10. Guenet JM, "Thermoreversible Gelation of Polymers and Biopolymers", Academic Press, London, 1992, 287.
 11. Finch CA, "Chemistry and technology of water-soluble polymers", Plenum Press, New York, 1983, 118.
 12. Harrington WF, Von Hippel PH, "The structure of collagen and gelatin", Advances in Protein Chemistry, 1961, 16, 1-138.
 13. Anderson NS, Campbell JW, Harding MM, Rees DA, Samuel JW, "X-ray diffraction studies of polysaccharide sulphates: double helix models for k- and i-carrageenans", Journal of Molecular Biology, 1969, 45(1), 85-99.
 14. Heymann E, "Studies on sol-gel transformations, I: The inverse sol-gel transformation of methylcellulose in water", Transaction of Faraday Society, 1935, 31, 846-864.
 15. Sarkar N, "Thermal gelation properties of methyl and hydroxypropyl methylcellulose", Journal of Applied Polymer Science, 1979, 24(4), 1073-1087.
 16. Tate MC, Shear DA, Hoffman SW, Stein DG, LaPlaca MC, "Biocompatibility of methylcellulose-based constructs designed for intracerebral gelation following experimental traumatic brain injury", Biomaterials, 2001, 22(10), 1113-1123.
 17. Carlsson A, Karlstrom G, Lindman B, Stenberg O, "Interaction between ethyl (hydroxyethyl) cellulose and sodium dodecyl sulphate in aqueous solution", Colloid Polymer Science, 1988, 266(11), 1031-1036.
 18. Carlsson A, Karlstrom G, Lindman B, "Thermal gelation of nonionic cellulose ethers and ionic surfactants in water", Colloids and Surfaces, 1990, 47, 147-165.
 19. Nystrom B, Walderhaug H, Hansen FK, "Rheological behavior during thermoreversible gelation of aqueous mixtures of ethyl(hydroxyethyl) cellulose and surfactants", Langmuir, 1995, 11(3), 750-757.
 20. Carlsson A, Lindman B, Watanabe T, Shirahama K, "Polymersurfactant interactions. Binding of Ntetradecylpyridinium bromide to ethyl (hydroxyethyl) cellulose", Langmuir, 1989, 5, 1250-1252.
 21. Lindman B, Carlsson A, Karlstrom G, Malmsten M, "Nonionic polymers and surfactants—some anomalies in temperature dependence and in interactions with ionic surfactants", Advances in Colloid and Interface Science, 1990, 32(2-3), 183-203.
 22. Shirakawa M, Yamotoya K, Nishinari K, "Tailoring of xyloglucan properties using an enzyme", Food Hydrocolloid, 1998, 12(1), 25-28.
 23. Ruel-Gariepy E, Leroux JC, "In situ forming hydrogels-review of temperature-sensitive systems", European Journal of Pharmacy and Biopharmaceutics, 2004, 58(2), 409-426.
 24. Nisbet DR, Crompton KE, Hamilton SD, Shirakawa S, Prankerd RJ, Finkelstein DI, Horne MK, Forsythe JS, "Morphology and gelation of thermosensitive xyloglucan hydrogels", Biophysics Chemistry, 2006, 121(1), 14-20.
 25. Miyazaki S, Suisha F, Kawasaki N, Shirakawa M, Yamatoya K, Attwood D, "Thermally reversible xyloglucan gels as vehicles for rectal drug delivery", Journal of Controlled Release, 1998, 56(1-3), 75-83.
 26. Suisha F, Kawasaki N, Miyazaki S, Shirakawa M, Yamatoya K, Sasaki M, Attwood D, "Xyloglucan gels as sustained release vehicles for the intraperitoneal administration of mitomycin C", International Journal of Pharmacy, 1998, 172(1-2), 27-32.
 27. Kawasaki N, Ohkura R, Miyazaki S, Uno Y, Sugimoto S, Attwood D, "Thermally reversible xyloglucan gels as vehicles for oral drug delivery", International Journal of Pharmacy, 1999, 181(2), 227-234.
 28. Miyazaki S, Kawasaki N, Endo K, Attwood D, "Oral sustained delivery of theophylline from thermally reversible xyloglucan gels in rabbits", Journal of Pharmacy and Pharmacology. 2001, 53(9), 1185-1191.

MICROBUBBLES ARE UTILIZED AS BOTH A THERAPEUTIC AND DIAGNOSTIC TOOL

Hariprasad Kadiyam

Asso. Professor, Department of Pharmaceutical Chemistry, Princeton College of Pharmacy,
Hyderabad, Telangana, India

G Lavanya

Asst. Professor, Department of Pharmaceutical Chemistry, Princeton College of Pharmacy,
Hyderabad, Telangana, India

Abstract - Gas filled microbubbles are notable as ultrasound contrast specialists for clinical ultrasound imaging and for painless conveyance of medications and qualities to various tissues. The term "microbubbles" refers to air- or gas-filled microspheres that are suspended in a liquid carrier phase after being introduced. Surfactants control the bubble's stability and surface properties in the liquid phase. Microbubbles are made from biocompatible materials, so they can be infused intravenously. Because their average size is less than that of red blood cells (RBCs), microbubbles are able to penetrate even the tiniest blood capillaries and release drugs or genes embedded on their surface when ultrasound is applied. The radiation that is used in ultrasound is safe. Due to its low cost and speed, the majority of doctors today prefer ultrasound imaging with microbubbles to other diagnostic methods. The target organs and tissues can be pinpointed by focusing the ultrasonic field; As a result, the treatment's selectivity can be enhanced, reducing undesirable side effects. Targeting ligands have recently been attached to the surface of microbubbles, and they have been widely used in the diagnosis and treatment of cancer, the cardiovascular system, and other tumors. The characteristics of microbubbles that give them therapeutic properties and some important ultrasound parameters that are known to influence microbubble-mediated drug delivery are the primary topics of this review. Additionally, new therapeutic applications of microbubbles are the subject of current research.

Keywords: Ultrasound, a contrast agent, a microbubble, and targeted drug delivery.

1 INTRODUCTION

The primary objective of using microbubbles for drug delivery and targeting is to lessen unwanted side effects like toxicity in healthy tissues and increase drug efficacy in the area where disease cells are formed. Various external energy fields, such as light (photodynamic therapy), neutron beam (boron neutron capture therapy), magnetic field (targeted accumulation of magnetic drug carrier in tissues close to the magnet), or mechanical energy, are utilized for the drug's action and/or deposition in the targeted region. We used mechanical energy in the form of ultrasound irradiation to enhance drug action. Drug delivery into tissue and cells is improved by ultrasound.

For ultrasound (US) diagnostics and imaging of the presence of ultrasound energy deposition foci in the tissues,

microbubbles are referred to as contrast agents. By disrupting cell membranes, they make cells more permeable. Recently, it is anticipated that microbubbles will find additional

applications in therapy as effective and secure targeted drug and gene carriers. The intrinsic compressibility of microbubbles is approximately 17,000 times greater than that of water, and their size range is 100 nm to 100 μ m. Microbubbles are colloidal particles filled with gas. They are also known as ultrasound contrast agents because they scatter ultrasound very strongly.³ Gas-filled microbubbles that are injected into the bloodstream can act as cavitation nuclei. Therefore, they can be used for a wide range of ultrasound-mediated drug delivery applications⁴. The primary use of ultrasound and microbubbles is for the

targeted delivery of drugs and genes to a particular area of the disease. These targeted microbubbles would carry a drug or gene to a specific area of interest when exposed to sufficiently high-amplitude ultrasound. After that, ultrasound is used to burst the microbubbles, resulting in site-specific delivery of the bioactive material.

1.1 Gas Phase

a gas core that is encased in a protein (albumin), lipid, surfactant, or biocompatible polymer shell that is more or less pliable. Medical ultrasound imaging commonly uses encapsulated gas microbubbles as contrast agents. The primary goal of encapsulation is to increase the material's resistance to gas loss, dissolution, and microbubble coalescence. By reducing the surface tension of the microbubble to values that are close to zero, a surfactant layer extends the microbubble's half-life.

In gas phases, a single gas or a combination of gases is typically used. By generating gas osmotic pressure, combination gases are used to stabilize the microbubbles by causing a difference in partial pressure.

Two kinds of gases are involved in a combination:

1. The primary modifier gas, or first gas, is one. Eg. Nitrogen 2, air Second gas, also known as gas osmotic agent; which is less permeable than the modifier gas through the surface of the microbubble. As long as it has a sufficient partial vapour pressure at the temperature of use to produce the desired osmotic effect, a gas osmotic agent can typically be either a liquid or a gas at room temperature. Eg. Perfluorocarbons and sulfur hexafluoride are examples of heavy gases.
2. The gas center is the main piece of the ultrasound contrast microbubble in light of the fact that

it decides the echogenicity. In contrast-enhanced ultrasound, the strong and distinctive sonogram is produced by gas bubbles compressing, oscillating, and reflecting in an ultrasonic frequency field. Weighty gases are less water-dissolvable so they are less inclined to spill out from the microbubble to weaken echogenicity. As a result, microbubbles with dense gas cores are more likely to circulate for longer. Because they are smaller than red blood cells, they are able to flow through the tiny blood capillaries and release drugs and genes when an ultrasound field is applied.

2.2 Shell Material

The composition of the shell and the microbubbles' resistance to rupture in the ultrasound pressure field determine their stiffness. The gas phase is encased by the shell material. Its major role in the microbubble's mechanical properties and gas diffusion out of the bubble. The shell material also affects microbubbles' elasticity or compressibility. The immune system's ability to absorb the microbubble depends on the shell material that is chosen. Because the shell material is more elastic, it needs more acoustic energy to withstand before bursting or breaking up, which increases the bubbles' stay in the body. The body easily absorbs shell material that is more hydrophilic, which reduces the bubbles' residence time in the body. The time available for contrast imaging is shortened as a result. Eg: carbohydrates like galactose, phospholipids like phosphatidylcholine, and proteins like albumin, among others

2.3. Aqueous or Liquid Phase

The outer, persistent fluid stage contains a surfactant or frothing specialist. Surfactants reasonable for use remember any compound or creation that guides for the development and support of the microbubble film by shaping a layer at the

interphase. The frothing specialist or surfactant might contain a solitary part or any mix of mixtures, like on account of co-surfactants.

Eg: Polyoxypropylene, polyoxyethylene, sugar esters, fatty alcohols, aliphatic amine oxides, hyaluronic acid esters and salts, dodecylpoly (ethyleneoxy) ethanol, and so on are examples of block copolymers. Surfactants with no ions: Copolymers of polyoxyethylene and polyoxypropylene, like Pluronic F-68, polyoxyethylene stearates, polyoxyethylene greasy liquor ethers, polyoxyethylated sorbitan unsaturated fat esters, glycerol polyethylene glycol ricinoleate and so on.

2.4. Other Components

Osmotic agents, stabilizers, chelators, buffers, viscosity modulators, air solubility modifiers, salts, and sugars can all be added to the formulation to fine-tune the microbubble suspensions for maximum shelf life and contrast enhancement.

It is possible for the oxygen- or air-most microbubbles to remain suspended in water for an extended period of time. Air filled the first generation of microbubbles, like Albunex®. As a result of the great solvency of air in blood and a slight (10-15 nm) protein shell coat that was not a decent obstruction against gas dispersion, these microbubbles vanished from the circulation system inside the space of seconds after organization. Second- and third-generation contrast agents make use of inert, high-molecular-weight gases like sulfur hexafluoride or perfluorocarbons. The lifespan of microbubbles in the circulation is extended by their low diffusion coefficient and low solubility.

3 CHARACTERISATION OF MICRO-BUBBLE

1. Microbubble Diameter & Size Distribution: Measure by Laser light Scattering, Scanning Electron

Microscopy and Transmission Electron Microscopy.

2. Shell Thickness: By the coating the microbubbles with the fluorescent dye using Fluorescent Microscopy against a dark background.
3. Microbubble Concentration: Measure by counting the number of microbubbles per ml by using the Coulter Counter Machine.

Air Content by densitometry: The content of air encapsulated within the microbubbles in the suspension samples is measured by oscillation U-tube densitometry with a DMA-58.

4 METHODS TO PREPARE MICROBUBBLES

The various approaches that can be utilized to make these microbubbles, such as cross-linking polymerization, emulsion solvent evaporation, atomization and reconstitution, and sonication.

1. Cross Linking Polymerization: This method involves vigorously stirring a polymeric solution (2% PVA in water) to produce a fine foam of the polymer that serves as a colloidal stabilizer and a bubble coating agent. Microbubbles float on the surface of the mixture following the cross-linking of the polymer. Dialyzed microbubbles that are floating are extensively separated. The cross-linking reaction is stopped by neutralizing the mixture when HCl or H₂SO₄ is added as a catalyst, and microbubbles are then separated.)

2. Emulsion Solvent Evaporation This method produces two solutions: one is an aqueous solution with the right surfactant, which could be an amphiphilic biopolymer like gelatine, collagen, albumin, or globulins. The emulsion system's outer continuous phase is created by this. The second is made by dissolving a wall-forming polymer in a mixture of two organic liquids that are insoluble in water. For the polymer, one of the organic liquids is a relatively volatile solvent, while the other is a relatively nonvolatile nonsolvent. To create an

emulsion, the polymer solution is agitatedly added to the aqueous solution. The step of emulsification continues until the inner phase droplets reach the desired size. The microbubble's size will be determined by the size of the droplet.

3. Atomization and Reconstitution To create a spray-dried surfactant solution, a surfactant solution is atomized into a heated gas, resulting in the formation of porous spheres containing the primary modifier gas. After that, these spheres with holes are put in a vial; The second gas or gas osmotic agent is then added to the vial's headspace. After being sealed, the vial is reconstituted with a sterile saline solution when it is used. Upon reconstitution the essential modifier gas diffuses out and the auxiliary gas diffuses in, bringing about size decrease. The resulting microbubbles are then given to the patient and remain suspended in the saline solution.

Sonication is preferred for the formation of microbubbles, either by penetrating a septum with an ultrasound probe that includes an ultrasonically vibrating hypodermic needle or by transmitting ultrasound through a transmitting septum. There are numerous methods for sonication, such as Through a thin membrane, a vial with a surfactant solution and gas in the headspace can be sonicated. An ultrasonic probe or a focused ultrasound "beam" can be used to contact or even depress the membrane for sonication. The microbubble solution can be taken out of the vial and given to the patient following successful sonication. A low-power ultrasonically vibrated aspirating assembly on the syringe can also be used for sonication inside the syringe.

5 APPLICATIONS

5.1. Imaging Application

The presence of microbubbles is extremely detectable by ultrasound. Actually, cavitation imaging and other methods can detect a single microbubble. At the moment, ultrasonography is the

diagnostic imaging technique that is used the most frequently. It uses portable, real-time imaging equipment and is non-invasive and relatively inexpensive. Additionally, it keeps out harmful ionizing radiation. The interfaces between various body tissues or structures partially reflect or scatter ultrasound pressure wave pulses that are broadcast by an ultrasound transducer placed on the skin or inside the body. A portion of the dissipated sound waves return to the transducer. These signals are digitized and transformed into electrical pulses by the imaging system. The tissue's sound speed and the time intervals between pulse transmission and reception are known. As a result, it is possible to generate an image based on scattered sound signals. In any case, blood a fluid stage material with low compressibility, disperses ultrasound ineffectively. Contrast agents, which increase the scattering and reflection of ultrasonic waves, can be used to improve ultrasound images of blood.

6 CONCLUSION

We discussed the most pressing issues in contrast agent development in this article. To begin, microbubbles' unique acoustic and biological properties make them a promising vehicle for drug and gene delivery. The designated microbubbles have an extraordinary use in future. Microbubbles can be used for diagnostic imaging of thrombo-embolic or inflammatory processes because they have been shown to bind to leukocyte and blood clot receptors. These microbubbles can be used as a vehicle for drugs or genes, and ultrasound can be used to destroy them for local delivery. Intravascular microbubbles can further develop drug infiltration into tissues when joined with centered ultrasound treatment, for example, through the blood-cerebrum hindrance. Drug substances, including plasmid DNA, can be connected to or consolidated in the microbubble particles for ultrasound-set

off discharge in the insonated organs and tissues. In general, microbubble contrast agents and ultrasound-assisted drug delivery will contribute to the treatment of debilitating diseases.

REFERENCES

1. Kassan, DG, Lynch AM, Stiller MJ, "Physical enhancement of dermatologic drug delivery: iontophoresis and phonophoresis", *Journal of the American Academy Dermatology*, 1996, 34, 657-666.
2. Kurup N, Naik P, "Microbubbles: A novel delivery system", *Asian Journal of Pharmaceutical Research and Health care*, 2(3), 228-234.
3. Majumdar S, Chowdhury S, "Novel Therapeutic Application of Microbubbles for Targeted Drug Delivery", *International Journal of Pharma and Bio Sciences*, 2010, 1(3), 1-9.
4. Sophie HB, Alexander LK, "Microbubbles in ultrasound-triggered drug and gene delivery", *Advanced Drug Delivery*, 2008, 60, 1153-1166.
5. Patel R, "Microbubble: An ultrasound contrast agent in molecular imaging", *Pharma Times*, 2008, 40, 15-16.
6. Maliwal D, "Microbubble contrast agents using ultrasound", *Research Journal of Pharmacy and Techonology*, 2008, 1(3).
7. Eniola AO, Hammer DA, "*In vitro* characterization of leukocyte mimetic for targeting therapeutics to the endothelium using two receptors", *Biomaterials*, 2005, 26, 7136-7144.
8. Eniola AO, Willcox PJ, Hammer DA, "Interplay between rolling and firm adhesion elucidated with a cell-free system engineered with two distinct receptor-ligand pairs", *Biophysical Journal*, 2003, 85, 2720-2731.
9. Bjercknes K, Sontaum PC, "Preparation of polymeric microbubbles: formulation studies & product characterisation", *International Journal of Pharmaceutics*, 1997, 158, 129-130.
10. Yiyao Liua BC, Hirokazu Miyoshib, Michihiro Nakamurac, "Encapsulated ultrasound microbubbles: Therapeutic application in drug/gene delivery", *Journal of Controlled Release*, 2006, 114, 89-99.
11. Klibanov AV, Rychak JJ, Yang WC, Alikhani S, Acton S, Lindner SR, "Targeted ultrasound contrast agent for molecular imaging of inflammation in higher shear flow contrast media", *Molecular Imaging*, 2006, 1, 259-266.
12. Lentacker I, Geers B, Demeester J, Smedt SC, Standers NN, "Design and evaluation of doxorubicin containing microbubble for ultrasound triggered doxorubicin delivery", *Cytotoxicity and Mechanism involved Molecular Theory*, 2010, 18, 101-108.
13. Martin JK, Jennifer CC, Evan CU, Mark JM, David OC, "Microbubble contrast agents: a new era in ultrasound", *Clinical review, Science, medicine and the future*, 2001, 1222-1225.
14. Klibanov AL, "Targeted delivery of gas filled microspheres, contrast agents for ultrasound imaging", *Advanced Drug Delivery Review*, 1999, 37 139-157.
15. Klibanov AL, "Ligand carrying gas filled microbubble: Ultrasound contrast agents for targeted molecular imaging", *Bioconjugate Chemistry*, 2005, 16, 9-17.
16. Lindner JR, "Microbubbles in medical imaging: Current applications and future directions", *Nature Reviews Drug Discovery*, 2004, 3, 527-32.
17. McCulloch MC, Gresser S, Moos J, "Ultrasound contrast physics: A series on contrast echocardiography", *Journal of the American Society Echocardiography*, 13, 959-967.
18. Annemieke van Wamel, Klazina Kooimam, "Vibrating microbubbles poking individual cells: Drug transfer into cells via sonoporation", *Journal of Controlled Release*, 2006, 112, 149-150.
19. Ka-Yun Ng & Terry O.Matsunga, "Ultrasound Mediated drug delivery"; *Wiley Publications*.
20. Lindner JR, Klibanov AL, Ley K, "Targeting inflammation, In: Biomedical aspects of drug targeting", 2002; 149-172.
21. Ying-Zheng Zhao E Cui-Tao Lu, "Factors that affect the efficiency of antisenseoligodeoxyribonucleotide transfection by insonated gas-filled lipid microbubbles", *Journal of Nanoparticle Research*, 2008, 10, 449-454.
22. Brisken AF, Francis SE, Cumberland DC, Crossman DC, Newman CM, "Microbubble-enhanced ultrasound for vascular gene delivery & gene therapy", 2000, 7, 2023-2027.
23. Bjorn TG, "Multimodal imaging and ultrasound microbubble drug delivery in targeted cancer therapy", *Institute of Medicine*, 2002, 16(11), 292-301.
24. E.Unger, Matsunaga TO, Schumann PA, R. Zutshi, "Microbubbles in molecular imaging and therapy", *MEDICAMUNDI*, 2003, 58-65.
25. Frauscher F, Klauser A, Halpern EJ, Horninger W, Bartsch G, "Detection of Prostate cancer with a microbubble ultrasound contrast agent", *The Lancet*, 357(9271), 2001, 49-50.
27. Dialekti Vlaskou, Olga Mykhaylyk, Riccardo Giunta, Iva Neshkova, Nicole Hellwig, Florian Kroetz, Christian Bergemann, Christian Plank, "Magnetic Microbubbles: New Carriers for Localized Gene and Drug Delivery", *Molecular Therapy*, 2006, 13, 290-291.

UNDERSTANDING OSMOTIC-CONTROLLED DRUG DELIVERY SYSTEMS: AN OVERVIEW

Korna Devamani

Asst. Professor, Asst. Professor, Department of Pharmaceutical Analysis, Princeton College of Pharmacy, Hyderabad, Telangana, India

Kurma Kirankumar

Asst. Professor, Department of Pharmaceutical Analysis, Princeton College of Pharmacy, Hyderabad, Telangana, India

Abstract - Utilizing osmotic principles for controlled drug release from the formulation, this paper examines constructed drug delivery systems. The most promising strategy-based systems for controlled drug delivery are osmotic devices, which are tablets coated with walls of controlled porosity. These pumps, in contrast to standard tablets, provide a constant (zero order) rate of drug release. Low levels of a water-soluble additive are leached from the polymeric material, which is the semipermeable membrane, when these systems are exposed to water, and the drug releases in a controlled manner over a long period of time. The vitally clinical advantages of oral osmotic medication conveyance framework are their capacity to further develop treatment decency and patient consistence. The ability to deliver drugs continuously, regardless of the drug's chemical properties, the patient's physiological factors, or subsequent food intake, is primarily responsible for these benefits. The theoretical idea of drug delivery, as well as the history, benefits and drawbacks of various delivery systems, various oral osmotic drug delivery systems, factors affecting the drug delivery system, and products on the market, are discussed in this review.

Keywords: Zero-order release, oral osmotic systems, and osmotic pressure are all synonyms for osmosis.

1 INTRODUCTION

The effective concentration at the target site is virtually uncontrollable with conventional drug delivery systems, which have very little control over drug release. Plasma concentrations may fluctuate frequently and be unpredictably as a result of this kind of dosing pattern. The controlled or modified release drug delivery systems enable controlled drug delivery over an extended period of time. They include injectable and implantable systems as well as oral and transdermal dosage forms. The oral route continues to be the most suitable method of

administration for the majority of drugs. Due to restrictions on their solubility or permeability, some molecules may not be as bioavailable when taken orally. The development of a dosage form with an extended release also necessitates adequate absorption throughout the gastrointestinal tract (GIT). The most suitable method for increasing these drugs' bioavailability is the creation of an osmotic drug delivery system. Osmotic medication conveyance frameworks discharge the medication with the zero request energy which

doesn't rely upon the underlying focus and the physiological elements of GIT.

1.1 Osmosis The term "osmosis" refers to the movement of solvent molecules across a semipermeable membrane from a lower concentration to a higher concentration.

1.2 Osmotic pressure An osmotic property of a solution is one in which the magnitude of the solution's osmotic pressure is independent of the number of distinct solute entities present in the solution. The drug's delivery from the osmotic device is controlled by the osmotic pressure that is brought into the dosage form by the imbibition of fluid from the external environment. The osmotic pressure created by the osmogen's imbibition of fluids is directly proportional to the rate of drug delivery from the osmotic pump.

2 HISTORICAL BACKGROUND

The osmosis principle was first applied to the design of drug delivery systems approximately 75 years after it was discovered⁶. Osmotic drug delivery was initiated by Australian scientists Rose and Nelson. In 1955, they created a pump that could be inserted into the body. It had three chambers: a chamber for drugs, a salt chamber with too much solid salt in it, and a water chamber. A rigid, semipermeable membrane separates the drug and water chambers. Water moves into the salt chamber from the water chamber due to the difference in osmotic pressure across the membrane. This water flow makes the salt chamber bigger. It also spreads the latex diaphragm that separates the drug and salt chambers and

pumps drugs out of the device. This pump's design and mechanism are comparable to those of a modern push-pull osmotic pump. The water chamber, which must be charged prior to use, was the primary drawback of this pump. The equation indicates this push-pull pump's pumping rate.

$$dM/dt = dV/dt \times c$$

This equation generally applies to all other kinds of osmotic systems, with or without some modifications. Alza Corporation made a number of Rose-Nelson pump simplifications in the early 1970s. Rose Nelson's modified version is the Higuchi-Leeper pump. The device is activated by water absorbed from the surrounding environment and does not contain a water chamber. When it is swallowed or inserted into the body, the pump kicks in. The semipermeable membrane is supported by a perforated frame in this pump's rigid housing. A fluid solution containing excess solid salt is contained in its salt chamber. The Higuchi-Leeper pump was recently modified to allow for pulsatile drug delivery. By creating a critical pressure at which the delivery orifice opens and releases the drug, the pulsatile release was achieved. Higuchi and Theeuwes developed a further simplified version of the Rose-Nelson pump. The outer semipermeable membrane of this pump is rigid and controls the pump's rate. It surrounds a solid layer of salt that is coated on the inside by an elastic diaphragm and on the outside by the membrane. When in use, the salt chamber draws water osmotically, forcing the drug out of the drug chamber.

2.1 Advantages & Disadvantages of Osmotic Controlled Drug Delivery Systems Advantages

- They typically give a zero order release profile after an initial lag.
- Deliveries may be delayed or pulsed if desired.
- Drug release is independent of gastric pH and hydrodynamic condition.
- They are well characterized and understood.
- The release mechanisms are not dependent on drug.
- A high degree of in-vitro and in-vivo correlation (ivivc) is obtained in osmotic systems.
- The rationale for this approach is that the presence of water in git is relatively constant, at least in terms of the amount required for activation and controlling osmotically base technologies.
- Higher release rates are possible with osmotic systems compared with conventional diffusion-controlled drug delivery systems.
- The release from osmotic systems is minimally affected by the presence of food in gastrointestinal tract.
- The release rate of osmotic systems is highly predictable and can be programmed by modulating the release control parameters.

3 HYDROPHILIC AND HYDROPHOBIC POLYMERS

These polymers are utilized in the plan improvement of osmotic frameworks for making drug containing grid center. The moderately water-soluble compounds can be co-entrapped in hydrophilic matrices to achieve more controlled

release, while the highly water-soluble compounds can be co-entrapped in hydrophobic matrices. In most cases, osmotic pumps for water-soluble drugs have been made with combinations of hydrophilic and hydrophobic polymers. The decision is made based on the drug's solubility as well as the pump's release rate and quantity. The polymers can expand or contract in any direction. Pumps that contain drugs that are moderately soluble in water typically make use of swellable polymers. Since they increment the hydrostatic tension inside the siphon because of their enlarging nature, the non swellable polymers are utilized in the event of profoundly water-dissolvable drugs². Due to their osmogenic nature, ionic hydrogels like sodium carboxymethyl cellulose are preferred. By incorporating these polymers into the formulations, a more precise controlled release of the drug scan can be achieved.

3.1 Wicking Agents

A material that can draw water into the porous network of a delivery device is known as a wicking agent. The wicking agents are those that help the drug's contact surface area with the incoming water increase. The application of the wicking agent contributes to an increase in the rate of drug release from the drug's orifice. There are two types of wicking agents: swellable and non-swellable. They are distinguished by their capacity for physisorption in water. Through Van der Waals interactions between the surface of the wicking agent and the adsorbed molecule, physisorption is a type of absorption in which the solvent molecules can loosely adhere

to the surfaces of the wicking agent. The wicking agent's job is to carry water to surfaces inside the tablet's core, resulting in channels or a network with more surface area. PVP, colloidal silicon dioxide, and sodium lauryl sulfate are examples.

4 CONCLUSION

In recent years, the development of oral osmotic controlled drug delivery systems has been very active due to the emergence of new products and technologies. The oral osmotic controlled drug delivery systems S is poised to expand their market within oral modified-release dosage forms due to the expiration of their primary patents and the growing demand from health authorities for improved patient treatment compliance and tolerability.

Oral osmotic controlled drug delivery systems were created as a platform for delivering drugs regardless of their physicochemical properties. They are used in early clinical phases (including early-stage exploration of pharmacokinetics), the development of novel dosage forms, and product life-cycle management. The ability of oral osmotic controlled drug delivery systems to deliver a drug at a predetermined rate, independent of physiological parameters like food intake or patient age, is primarily responsible for the clinical benefits they provide. These days, the enormous assortment of oral osmotic controlled drug conveyance frameworks advancements accessible permits an intriguing transformation of the framework to the medication properties and measurements strength. The reported clinical

benefits have opened up new perspectives for the development of drugs as oral osmotically driven systems in spite of the controversy surrounding their safety when administered.

REFERENCES

1. Gupta BP, Thakur N, Jain N, Banweer J, Jain S, Osmotically Controlled Drug Delivery System with Associated Drugs, *J Pharm Pharmaceut Sci.* 2010, 13(3), 571–588.
2. Dong L, Shafi K, Wan J, Wong PA. Novel osmotic delivery system: L-OROS Soft cap, in *Proceedings of the International Symposium on controlled Release of Bioactive Materials*, Paris, France, 2000.
3. Pfefer WEP. *Osmotische Untersuchungen*, Leipzig. 1877, 232.
4. Li X, Jasti BR. Osmotic controlled drug delivery systems, In: *Design of controlled release of drug delivery systems*, McGraw Hill. 2006, 203-229.
5. Rastogi SK, Vaya N, Mishra B, Osmotic pump: A novel concept in rate controlled oral drug delivery, *Eastern pharmacist.* 1995, (38), 79-82.
6. Rose S, Nelson JF. A continuous long-term injector, *Aust J Exp Biol.* 1955, 33, 415.
7. Higuchi T, Leeper HM. Improved osmotic dispenser employing magnesium sulfate and magnesium chloride. US Patent 3760804, 1973.
8. Higuchi T, Leeper HM. Osmotic dispenser with means for dispensing active agent responsive to osmotic gradient. US Patent 3995631, 1976.
9. Fix J. In: *Encyclopedia of controlled drug delivery*. Edmathiowitz, vol-2, John Wiley and sons, Inc 700.
10. Kaushal AM, Garg S. An update on osmotic drug delivery patents, *Pharm Tech.* Aug 2003, 38-44.
11. Parmar NS, Vyas SK, Jain NK. In: *Advanced in controlled and novel drug delivery*. CBS publisher, 2008, 22-31.
12. Kaushal AM, Garg S. An update on osmotic drug delivery patents, *Pharm Tech.* 2003, 27, 38-44.
13. Bhatt PP. Osmotic drug delivery systems for poorly soluble drug, the drug delivery companies report autumn/winter. 2004.

15. Parmar NS, Vyas SK, Jain NK. Advances in controlled and novel drug delivery. CBS publisher & distributors, New Delhi, 2001, 18-39.
16. Eckenhoff, Yum SI. The osmotic pump: novel research tool for optimizing drug regimen, *Biomaterials*. 1981, 2, 89-97.
17. Ade RN, Lavande JP, Dukale SV, Jaiswal SB, Sheaikh SS, Chandewar AV, Osmotically controlled drug delivery system: an updated review, *International Journal of Universal Pharmacy and Bio Sciences*, 2013, 2(2), 183-206.
18. Lindstedt B, Ragnarsson G, Hjartstam J. Osmotic pumping as a release mechanism for membrane-coated drug formulations, *International Journal of Pharmaceutics*. 1989, 56(3), 261-268.
19. Seminoff LA, Zentner GM, Cellulosic coating, US Patent 5,126,146, 1992.
20. Jensen JL, Appel LE, Clair JH, Zentner GM. Variables that affect the mechanism of drug release from osmotic pumps coated with acrylate/methacrylate copolymer latexes, *Journal of Pharmaceutical Sciences*. 1995, 84(5), 530-533.
21. Theeuwes F. Elementary osmotic pump, *Journal of Pharmaceutical Sciences*. 1975, 64(12), 1987-1991.
22. 21. Zentner GM, Rork GS, Himmelstein KJ. The controlled porosity osmotic pump," *Journal of Controlled Release*. 1985, 1(4), 269-282.
23. 22. Ghosh T, Ghosh A. Drug delivery through osmotic systems -an overview, *Journal of Applied Pharmaceutical Science*. 2011, 1(2), 01 (02), 38-49.
24. 23. E. M. Rudnic, B. A. Burnside, H. H. Flanner et al., Patent 6,110,498, 2000.
25. 24. McClelland GA, Sutton SC, Engle K, Zentner GM. The solubility-modulated osmotic pump: in vitro/in vivo release of diltiazem hydrochloride, *Pharmaceutical Research*. 1991, 8(1), 88-92.
26. 25. Jerzewski RL, Chien YW. Osmotic drug delivery: in *Treatise on Controlled Drug Delivery: Fundamentals, Optimization, Application*. Marcel Dekker, New York, NY, USA, 1992, 225-253.
27. 26. Kelbert M, Bechard SR. Evaluation of a cellulose acetate (CA) latex as coating material for controlled release products, *Drug Development and Industrial Pharmacy*. 1992 18(5), 519-538.
28. 27. Kaushal M, AG Sanjay. An Update on Osmotic Drug Delivery Patents: *Pharmaceutical Technology*, 2003, 12-23.
29. 28. Guo JH. Effects of plasticizers on water permeation and mechanical properties of cellulose acetate: antiplasticization in slightly plasticized polymer. *Drug Development and Industrial Pharmacy*. 1993, 19(13), 1541-1555.
30. 29. Bindschaedler C, Gurny R, Doelker E. Mechanically strong films produced from cellulose acetate latexes, *Journal of Pharmacy and Pharmacology*. 1987, 39(5), 335-338.
31. 30. Guo JH. An investigation into the formation of plasticizer channels in plasticized polymer films, *Drug Development and Industrial Pharmacy*, 1994, 20(11), 1883-1893.

IMPURITY PROFILING: IMPORTANCE, TECHNIQUES, AND GUIDELINES FOR DRUG DEVELOPMENT AND QUALITY CONTROL

Surendar Angothu

Asst. Professor, Department of Pharmacognosy, Princeton College of Pharmacy,
Hyderabad, Telangana, India

Boggula Ratnakumari

Asst. Professor, Department of Pharmacognosy, Princeton College of Pharmacy,
Hyderabad, Telangana, India

Abstract - The process of collecting and analyzing data to determine an impurity's biological safety is known as impurity profiling. Any organic material that, in addition to the drug substance or its ingredients, arises from synthesis or contains unwanted chemicals that remain in APIs is considered an impurity. The pharmaceutical industry faces a pressing problem right now: keeping impurities under control. Guidelines for controlling impurities were formulated by the International Conference on Harmonization (ICH). The requirements for purity and the detection of impurities in Active Pharmaceutical Ingredients (APIs) are being emphasized by a number of regulatory agencies, including the ICH, the US Food and Drug Administration, and the Canadian Drug and Health Agency. TLC and HPLC are the methods used to identify impurities. The development of hyphenated techniques has revolutionized impurity profiling by separating and structurally elucidating impurities at the same time. For drug impurity profiling, LC-MS-MS, LC-NMR, LC-NMRMS, GC-MS, and LC-MS are the most frequently used methods.

Keywords: Hyphenated Methods, HPLC, impurity profiling, and ICH guidelines.

1 INTRODUCTION

Impurities are defined by ICH as pharmaceutical products; Impurities are substances that are present in the product but are not the API or the excipients that were used to make it. Thus, impurities are undesirable chemicals that remain in trace quantities within the API or formulation¹. It is impossible to avoid the drug substance's trace presence of impurities. They can be brought down or change the pharmacological adequacy of dynamic drug fixings (Programming interface). Impurities can occasionally have teratogenic, mutagenic, or carcinogenic effects. As a result, this may be harmful to human health in fetuses; controlling and monitoring impurities in API/pharmaceutical products is becoming increasingly popular. As a result, API impurity profiling is necessary.

The identity and quantity of impurities in pharmaceuticals, or impurity profiling, are currently receiving significant and critical attention from regulatory authorities. The various pharmacopoeias, including BP and USP. The US Food and Medication Organization (FDA) have embraced the direction arranged under the sponsorship of the ICH. The debasement profile of drugs is of expanding significance as medication security gets increasingly more consideration from people in general and from the media. This topic is covered in a number of recent books and journal reviews, and US and international authorities provide guidelines.

Unless the potential impurities are anticipated to be unusually potent or toxic, it is not considered

necessary, according to ICH guidelines on impurities in new drug products, to identify impurities below the 0.1% level. Impurities should always be classified⁴. Mass spectrometry (MS), nuclear magnetic resonance (NMR), high-performance liquid chromatography (HPLC), and tandem mass spectrometry have all been used to isolate and identify process-related impurities and degradation products in a number of articles for pharmaceutical substances. As a result, an essential component of drug development and regulatory evaluation is the identification, quantification, and control of impurities in the drug substance and drug product.

The various impurities that can be found in APIs, methods for identifying them, and potential ways to deal with the resulting interferences are discussed in this article.

1.1 Portrayal Strategies

Profoundly refined instrumentation, for example, MS joined to a GC or HPLC, are unavoidable devices in the distinguishing proof of minor parts (drugs, contaminations, debasement items, metabolites) in different grids. Different methods are used to characterize impurities: which include these:

1.2 Nuclear Magnetic Resonance

(NMR):¹² NMR is a powerful analytical tool for structural elucidation because it can reveal the specific bonding structure and stereochemistry of pharmaceutically relevant molecules. In comparison to MS, which only requires a sample of less than 1 mg, conventional NMR sample requirements are around 10 mg.

1.3 Mass Spectroscopy (MS) Over the past few decades, it has had a growing impact on the pharmaceutical development process. New opportunities for monitoring, characterization, and quantification of drug-related substances in active pharmaceutical ingredients and pharmaceutical formulations have been provided by advancements in the design and efficacy of interfaces that directly connect Mass Spectrometers with separation techniques.

2 VALIDATION OF ANALYTICAL PROCEDURES

The process of confirming that the HPLC procedure used for a particular test is appropriate for its intended use is known as HPLC method validation. Method validation is an important part of good analytical practice because it can be used to evaluate HPLC results' quality, dependability, and consistency. Strategy approval has gotten extensive consideration in writing and from modern boards of trustees and administrative organizations.

Specificity: The ability to evaluate the analyte without ambiguity in the presence of expected components is known as specificity. Impurities, degradants, matrix, and other topics are frequently examined. It is not always possible to show that an analytical method is unique to a specific analyte (complete discrimination).

Precision: The degree to which the value that is accepted as either an acceptable reference value or a conventional true value is in agreement with the value that is found is what is meant by the accuracy of an analytical procedure. Accuracy can be evaluated using spiked samples containing known quantities of impurities, and it should

be reported as a percentage of recovery (percent recovery is the area obtained by spike the impurity in the sample).

Accuracy: The closeness of agreement between a series of measurements obtained from multiple samplings of the same homogeneous sample under the specified conditions is how an analytical procedure's precision is expressed. The variance, standard deviation, or coefficient of variation of a series of measurements typically represent an analytical procedure's precision.

Continuity: intraassay precision also describes the precision achieved over a brief time period under the same operating conditions.

Advanced precision: demonstrates with laboratory variations: various days, various analysts, various pieces of equipment, etc.

Compatibility: demonstrates the precision between laboratories (collaborative studies, typically used for methodology standardization).

The detection limit: The smallest amount of analyte in a sample that can be detected but not necessarily quantified to an exact value is the limit of detection for a particular analytical method. As far as not entirely set in stone by the examination of tests with known groupings of analyte and by laying out the base level at which the analyte can be dependably recognized. Based on Signal-to-Noise b. Based on Response Standard Deviation and Slope

Quantity Limit or Quantity Limit: The lowest amount of analyte in a sample that can be quantitatively determined with sufficient precision and accuracy is the limit of quantitation for a particular analytical method. Linearity: The ability of an analytical procedure to yield test

results that are directly proportional to the concentration (quantity) of analyte in the sample within a specified range is known as its linearity.

Sturdiness: An analytical procedure's robustness is a measure of its ability to withstand subtle but deliberate variations in method parameters and indicates its dependability in everyday use.

3 APPLICATIONS

Numerous applications have been sought in the areas of drug designing and in monitoring quality, stability, and safety of pharmaceutical compounds, whether produced synthetically, extracted from natural products or produced by recombinant methods.

4 CONCLUSION

The requirements for purity and the detection of impurities in Active Pharmaceutical Ingredients (APIs) are being emphasized by a number of regulatory agencies, including the ICH, the USFDA, and the Canadian Drug and Health Agency. The process of collecting and evaluating data to determine an impurity's biological safety is known as "qualification of the impurities." thus demonstrating the significance and necessity of drug impurity profiling in pharmaceutical research. Chromatographic and spectroscopic methods can be used by themselves or in conjunction with other methods to identify impurities. TLC, HPLC, HPTLC, AAS, and other techniques can be used to identify and characterize impurities in a variety of ways. In the field of impurity profiling, conventional liquid chromatography, particularly HPLC, has been extensively utilized; Its numerous applications are due to its sensitivity, cost-effective separation,

and wide range of detectors and stationary phases. One of the most popular methods for locating residual solvents is headspace GC. Impurity profiling has been transformed by hyphenated techniques, which not only separate impurities but also identify them structurally. Among all joined strategies, the most taken advantage of procedures, for debasement profiling of medications are LC MS, LCNMR, LC-NMR-MS, GC-MS, and LC-MS. The impurity profiling process is made simple by the precise method development and procedure validation. The concept of quality assurance is vast. This idea brings us to the subject of IMPURITY PROFILING. A substance under investigation's impurity profile gives as much information as possible about its impurities. Manufacturers now have quality standards to meet thanks to the establishment of guidelines for the levels of impurity in drugs and products. The qualification of the impurity profile of a new chemical entity is essential. The pharmaceutical analyst must carefully consider their analytical technology because high dose compounds have a qualification threshold of less than 1%. The development scientists are aware of the significance of qualifying impurity profiles in order to guarantee that the impurities in the batches used in safety studies are taken into account. This field of impurity identification and quantification has advanced from limit tests for impurities. utilizing more recent methods like NMR, GCIR (Gas Chromatography- Infrared Spectrometry), UV spectroscopy with diode array detection, and HPLC. The purpose of this article is to try to comprehend the concept of an impurity profile as well as various

aspects and methods associated with it.

REFERENCES

1. Ahuja Satinder. Impurities Evaluation of Pharmaceuticals. Ed. By New York, Marcel Dekker, 1998, 15-18
2. Indian Journal of Pharmaceutical Education and Research, 44(3), 2010.
3. S. Lakshmana Prabu, Suriyaprakash TNK, 3(2), 2010, 68- 69.
4. International Conferences on Harmonization, Draft revised Guidance on Impurities in new drug Substances. Q3A®. Federal Register. 2000.
5. Alsante KM, Hatajik TD, Lohr LL, Sharp TR, "Isolation and Identification of Process Related Impurities and Degradation Products from Pharmaceutical Drug Candidates. Part 1", American Pharmaceutical Review, 2001, 4(1), 70.
6. Lohr LL, Sharp TR, Alsante KM, Hatajik TD, "Isolation and Identification of Process Related Impurities and Degradation Products from Pharmaceutical Drug Candidates. Part II: The Roles of NMR and Mass Spectrometry", American Pharmaceutical Review, 2001.
7. Winger BE, Kemp CA, "Characterization of Pharmaceutical Compounds and Related Substances by using FTICR-MS and Tandem Mass Spectrometry", American Pharmaceutical Review, 2001.
8. Handbook of isolation and characterization of impurities in pharmaceuticals. Volume 5 of separation science and technology a reference series edited by Satinder Ahuja, 4-6.
9. Handbook of isolation and characterization of impurities in pharmaceuticals. Volume 5 of separation science and technology a reference series edited by Satinder Ahuja, 95.
10. Handbook of isolation and characterization of impurities in pharmaceuticals. Volume 5 of separation science and technology a reference series edited by Satinder Ahuja, 29.
11. Rao NR, Mani Kiran SS, Prasanthi NL, Indian J. Pharm. Educ. Res, 2010, 44(3), 302-306.
12. Bari SB, Kadam BR, Jaiswal YS, Shirkhedkar AA, Impurity profile: Significance in Active Pharmaceutical

- Ingredient. Eurasian Journal of Analytical Chemistry Volume 2, Number 1, and 2007 1306-3057 pg no. 33, 43-46.
13. ICH Harmonised Tripartite Guideline Validation of Analytical Procedures: text and methodology Q2 (R1).
 14. British Pharmacopoeia the Department of Health, Social Services and Public Safety, 2004.
 15. Indian Pharmacopoeia Government of India, Ministry of Health and Family Welfare. Published by the Controller of Publications, Delhi, 1996.
 16. Krishna Reddy KVSR, Moses Babu J, Vijayvitthal TM, Eswaraiah S, Satyanarayana Reddy M, Dubey PK, Vyas K, "Impurity profile study of repaglinide". J Pharm Biomed Anal, 2003, 32, 461.
 17. Dams R, Benijts T, Lambert W, Massart D and De Leenheer a Heroin impurity profiling: trends throughout a decade of experimenting- Review. Forensic Science International, 2001, 121, 81.
 18. Horvath P, Balogh G, Brlik J, Csehi A, Dravec F, Halmos Z, Lauko A, Renyei M, Varga K and Gorog S, "Estimation of impurity profile of drugs and related materials Part 16: identification of the sideproducts of the ethinylation step in the synthesis of contraceptive gestogens". J Pharm Biomed Anal, 1997, 15, 1343.